

https://dspace.org/

Inflammatory dependent bioresponsive smart transdermal delivery system incorporating susppended nanofibrous mats as a platform for wound healing

Mayet, Naeema

2016-10-25
http://hdl.handle.net/10539/21260

Downloaded from a DSpace repository. https://dspace.org/

INFLAMMATORY DEPENDENT BIORESPONSIVE SMART TRANSDERMAL DELIVERY SYSTEM INCORPORATING SUSPENDED NANOFIBROUS MATS AS A PLATFORM FOR WOUND HEALING

NAEEMA MAYET

A thesis submitted to the Faculty of Health Sciences, University of the Witwatersrand,
in
fulfilment of the requirements for the degree of
Doctor of Philosophy

Supervisor:
Professor Viness Pillay
Department of Pharmacy and Pharmacology, Faculty of Health Sciences, University of the
Witwatersrand, South Africa

Co-Supervisors:
Professor Yahya E. Choonara
Dr Lisa C. du Toit
Mr Pradeep Kumar
Department of Pharmacy and Pharmacology, Faculty of Health Sciences,
University of the Witwatersrand, South Africa

Johannesburg
2016

DECLARATION

I, Naeema Mayet, declare that this thesis is my own work. It has been submitted for the degree of Doctor of Philosophy in the Faculty of Health Sciences at the University of Witwatersrand, Johannesburg, South Africa. Prior to this, this thesis has not been submitted for the attainment of any degree or examination at this or any other university.

.....

Signed this day ..... February 2016

PUBLICATIONS

Naeema Mayet, Yahya E. Choonara, Pradeep Kumar, Lomas K.Tomar, Charu Tyagi, Lisa C. du Toit, and Viness Pillay. A Comprehensive Review of Advanced Biopolymeric Wound Healing Systems. Journal of Pharmaceutical Sciences. 2014. 103:2211-2230. Doi: 10.1002/ jps.24068 ***(Top 10 Most Downloaded Article)***

Naeema Mayet, Pradeep Kumar, Yahya E. Choonara, Lomas K. Tomar, Charu Tyagi, Lisa C. DuToit and Viness Pillay. Synthesis of a Semi-Interpenetrating Polymer Network as a Bioactive Curcumin Film. American Association of Pharmaceutical Scientist (AAPS) PharmSciTech. 2014. 15:6. DOI: 10.1208/s12249-014-0170-3 1530-9932/14/0600-1476/0

Naeema Mayet, Pradeep Kumar, Lisa C. du Toit, Yahya E. Choonara and Viness Pillay. Crosslinked Electrospun Chitosan Nanofibre Mats as a Potential Application for Wound Healing: exposition of the Physicomechanical and Physicochemical Nature of Electrospun Mats. (To be Submitted: *Journal of Biomedical Materials Research. Part A*)

Naeema Mayet, Pradeep Kumar, Lisa C. du Toit, Yahya E. Choonara and Viness Pillay. Advanced and Accelerated In Vivo Full Thickness Wound Healing by the Development of Crosslinked Nanofibrous Wound Healing Mat. (To be Submitted: *American Association of Pharmaceutical Sciences. AAPS PharmSciTech*)

APPENDIX 11.1

RESEARCH PRESENTATIONS

Naeema Mayet, Pradeep Kumar, Yahya E. Choonara, Lisa C.du Toit and Viness Pillay. Synthesis of a Semi-Interpenetrating Polymer Network as a Bioactive Curcumin Film for Wound Healing. ***(Abstract Publication).*** *Boehringer Ingelheim Young Scientist Competition, 35TH Conference of the Academy of Pharmaceutical Sciences.* Nelson Mandela Metropolitan University (NMMU). Port Elizabeth, South Africa, 2014.

Naeema Mayet, Viness Pillay, Yahya Choonara, Pradeep Kumar, Lisa C. du Toit. An Inflammatory Bioresponsive Transdermal Delivery System as an Application for Wound Healing. ***(Podium Presentation).*** *School of Therapeutic Sciences Research Day.* University of the Witwatersrand, Johannesburg, South Africa, 2015.

Naeema Mayet, Viness Pillay, Yahya E. Choonara, Pradeep Kumar, Lisa C. du Toit. Synthesis of a bioactive nanofibrous mat as an application for wound healing. ***(Podium Presentation).*** *Conference of the Academy of Pharmaceutical Sciences, APSSA/SAAPI conference, "Today's Solutions for Tomorrow's Needs".* University of the Witwatersrand, Johannesburg, South Africa, 2015.

Naeema Mayet, Lisa C.du Toit, Pradeep Kumar, Yahya E. Choonara and Viness Pillay. A Bioresponsive Transdermal Delivery System (BTDS) for Wound Healing. ***(Poster Presentation).*** *American Association of Pharmaceutical Sciences (AAPS) Annual Meeting and Exposition.* Orange County Convention Centre, Orlando, Florida, USA, 2015.

APPENDIX 11.2

PATENT FILED

Bioresorbable Wound Dressings. Naeema Mayet, Viness Pillay, Yahya E. Choonara, Pradeep Kumar, Lisa C.du Toit. SA Patent Application. PCT Filed

ACKNOWLEDGEMENTS

On reaching the finishing point of this challenging task I would like to extend my heartfelt gratitude to all those who have made it possible for achievement of this goal.

First and Foremost to the Almighty, the Most-Great for all the guidance and countless blessings he has showered upon me. To my parents, Yusuf Ahmed and Sherina who I am forever indebted to for all their sacrifices, encouragement, inspiration, unconditional love and care. It is only through their guidance, support and prayers, I am where I am today. I am truly privileged beyond comprehension to be blessed with them in my life for pushing me to my full potential in every aspect of life. I can only hope and pray that I make them proud. To my siblings, Aasief Ahmed, Zaakirah and Muhammed Zaakir Mayet for their constant moral support and encouragement and lastly to my fiancé, my best friend Muhammed Patel for his motivation through the final straws of this venture.

In particular, I would like to thank my closest of friends, Famida Ghulam Hoosain who has been my “partner in crime”throughout this journey and every step of the way. The moments we shared, laughter’s, jokes, comments, lab moments and everything else are definitely cherished moments and made this journey a whole lot easier. I would also like to express my gratitude to Bibi Fatima Choonara, Poornima Ramburrun and Karmani Murugun for their inspiration, encouraging chats and enchanting company who have definitely made this venture a whole lot more enjoyable.

To my Supervisor, Prof Viness Pillay for making the achievement of this goal possible, for the support, advice and exemplary mentorship and guidance he has given through the course of this research.

To my co-supervisors, Prof Yayha E Choonara and Dr Lisa C du Toit, thank you for the effort, time, and commitment endowed in guiding me and ensuring the successful completion of this research. A momentous thank you to Mr Pradeep Kumar who has been a noteworthy co-supervisor and mentor to me and for structuring the skills I have in the pharmaceutical field. I greatly appreciate the assistance, knowledge and enthusiasm he has imparted on me throughout the years.

To Dr Charu Tyagi for her words of motivation, in particularly for the encouragement and inspiration she provided me with to undertake a degree in Doctor of Philosophy.
A special thanks to Felix Mashingaidze and Mpho Ngoepe for the assistance, advice and direction they always provided willingly in the laboratory.

To my colleagues Steven Mufamadi, Nonhlanhla Masina, Ahmed Seedat, Angus Hibbins, Tasneem Rajan, Khadija Rhoda, Thiresen Govender, Teboho Kgesa, Martina Manyikana, Kealeboga Mokolobate, Khadija Rhoda, Zamanzima Mazibuko, Jonathan Pantshwa, Pierre Kondiah, Mershan Govender, Sunanina Indermun, Olufemi Akilo, Khuphukile Madida, Sichuan Hayiyana, Margaret Siyawamwaya and Mduduzi Sithole for their companionship and support.

To Mr Sello Ramarumo, Ms Pride Mothobi, Mr Kleinbooi Mohlabi and Mr Bafana Temba for their vital assistance with running of the laboratories.

I would also like to thank the team at the Central Animal Service (CAS) of the University of Witwatersrand for their assistance and guidance on carrying out the *in vivo* expect of this research as well as Doctor Chetan Patel for providing me with a central method for undertaking the *in vivo* procedure.

I would also like to acknowledge Professor Paul Dankwerts and the rest of the staff of the Department of Pharmacy and Pharmacology, Mr David Bayever, Ms Nompumelelo Damane, Mrs Neelaveni Padayachee and Mrs Rubina Sheikh.

This research would not be made possible without the financial assistance of the National Research Foundation (NRF) of South Africa, their support is sincerely appreciated.

ABSTRACT

The perception of wound healing within the current decade goes beyond the straightforward assertion of the three phases assembling the wound healing cascade. Healing of wounds is a complex process that involves a dynamic series of interactions and reactions and requires a collaboration of the many cell pedigrees, mediators and different tissues. The skin is the largest organ of the body and serves as a protective barrier against foreign objects therefore a loss in its veracity may lead to a decrease quality of life or even death.

The primary goal for wound care and treatment is an aesthetically pleasing scar with close to complete functionality at the wound site and rapid wound closure. Attainment of these features requires incorporation of various characteristics such as a moisture retention, absorption and debridgement amongst others. A huge variety of wound dressings are available however not all of these meet the specific requirements of an ideal wound healing device to cover every aspect within the wound healing cascade. Highlighted within this thesis is the design and development of a Bioresponsive transdermal delivery system (BTDS) for wound healing that aims at the incorporation of the significant characteristics for optimal wound management and treatment.

Nanobiotechnology is an interdisciplinary field that combines many avenues to revolutionise the development of drug delivery systems specific to wound healing. Delivery systems produced on the nanoscale can encourage the promotion of biologically active new molecular entities that were previously considered underdeveloped by the enhancement of the therapeutic efficacy of wound healing materials. Recent research interest has focused on the development of smart biomaterials. Combining biomaterials that are crucial for wound healing will provide opportunities to synthesize matrices that are inductive to cells and that stimulate and trigger target cell responses crucial to the wound healing process. Stimuli responsive systems provides an attractive, novel and alternate approach to the process of healing by offering an advanced alternative to simple wound dressings as they have the ability to adapt to the surrounding wound environment and regulate the healing process by thermal, chemical, biochemical, electrical and mechanical means on exposure to an external stimulus that triggers the effect.

The research focused on the development and characteristic analysis of a complete prototyped device for wound healing incorporating a nanofibrous mat as well as a bioresponsive component to inflammation which could be the first novel prototype developed as an inflammation bioresponsive device for superior wound healing incorporating a nanofibrous mat. The BTDS was synthesized by the attainment of a statistically derived Box-

Behnken Design Template, whereby 15 formulations were generated to fabricate a wound healing nanofibrous mats as well as a lyophilized inflammatory dependent matrix. The technique entailed the process of electrospinning for nanofiber formation as well as blending and lyophilization for the inflammatory responsive component. Elucidation of the various polymeric and crosslinker concentrations greatly influenced the properties and characteristics of the system. An endorsement in intensity and conjugation is noted by the FTIR spectra whereby greater shifts in wavelengths from 3260.11cm^{-1} to 3278.79cm^{-1} is noted when enhancements in crosslinking bridges is undertaken. Structural morphological analysis revealed the synthesis of smooth, cylindrical, uniformly aligned nanofibres without the presence of nanobeads as well as the formation of a lyophilized matrix having a tough backbone structure at higher concentrations. Upon nanotensile mapping, variation in Young's Modulus was observed at 4.25MPa providing flexibility whereas a higher Young's Modulus provides rigidity and stiffness to the structure. Determination of the bioresponsive nature was carried out in a stimulated inflammatory environment by utilisation of the Fentons reaction: $Fe^{2+} + H_2O_2 \rightarrow Fe^{3+} + OH\cdot + OH^-$. Results amongst the experimentally derived formulations revealed the reliance of bioactive release on the hyaluronic acid concentration and degradation by hydroxyl radicals present. MDT results obtained depicted a value at 42.39 at a higher hyaluronic concentration and degree of crosslinkage whereas at lower concentrations, MDT values at 33.21 and 35.76 were depicted. In vivo histological examination revealed the healing progression whereby the presence of the nanofibrous mat illucidated a close to complete re-epithelisation and remodelling of the wound site represented by thick, vascular granulation tissue dominated by fibroblasts and extensive collagen deposition.

The approach of introducing a topical device for wound management containing both nanotechnology and stimuli responsive techniques provide an innovative and encouraging proposal for wound care to the pharmaceutical industry.

DEDICATION

This thesis is dedicated to my pillars of strength, my motivation, my parents, Yusuf Ahmed and Sherina Mayet for whom without, I would not be where I am today.

TABLE OF CONTENTS

DECLARATION.....i
PUBLICATIONS.....ii
RESEARCH PRESENTATIONS.....iii
PATENT FILED.....iv
ACKNOWLEDGEMENTS.....v
ABSTRACT.....vii
DEDICATION.....ix
LIST OF ABBREVIATIONS.....xxvi
LIST OF EQUATIONS.....xxviii
LIST OF FIGURES.....xxix
LIST OF TABLES.....xxxvii

CHAPTER 1

INTRODUCTION AND RATIONALE OF THE STUDY

1.1. Background to the Study……1

1.2. Rationale and Motivation of the Study…….4

1.3. The Mechanism of Action of the Combined Bioresponsive Topical Delivery System (BTDS) ……6

1.4. Novelty of the Study……..9

1.5. Possible Therapeutic Applications of the Study…….10

1.6. Aim and Objectives of the Study……...10

1.7. Overview of the Thesis……11

1.8. Concluding Remarks……...15

CHAPTER 2

A COMPREHENSIVE REVIEW OF ADVANCED BIOPOLYMERIC WOUND HEALING SYSTEMS

2.1. Introduction……..……..…..16

2.2. Physiology and Mechanism of Action of the Native Skin…….……....16

2.3. Wound Types and the Wound Healing Cascade……...18

2.4. Wound Care and Management Aids……...……....21

2.5. Components of Wound Management Aids…….……25

2.5.1. Polymers…….……....……26

2.5.1.1. Natural Polymers……....…...26

2.5.1.2. Synthetic Polymers……..…..……..……....27

2.5.1.3. Interpolymer Complexes…….....……....27

2.5.2. Hydrocolloids……..……..……..…..28

2.5.3. Bioactives and Drugs…….…….....29

2.6. Employment of Cell Based Therapies for Wound Healing……..…….....….33

2.6.1. Gene Therapy in Cutaneous Wound Healing…….…….....33

2.6.2. Stem Cells and Wound Healing……..…….……..35

2.6.3. Gap Junction and Connexin 43 Mimetic Peptides in Wound Healing…….....35

2.7. Classification of Wound Dressings…….……..….36

2.7.1. Traditional Wound Dressings……....…….37

2.7.2. Lyophilised Wafers and Drug Incorporation……....……...38

2.7.3. Hydrogels……..…….……..…….38

2.7.4. Wound Healing Films……..……....…..…39

2.7.5. Wound Healing Foams……..……..……...40

2.7.6. Multi-Layered Wound Dressings……..……..……...41

2.7.7. Nanofibrous Scaffolds and Mats for Wound Healing……..…….....…....42

2.8. Recent Research Focus: Healing from a Molecular and Structural Perspective.....43

2.9. Nanotechnology……...……....44

2.9.1. Nanoparticle-Based Delivery Systems for Wound Healing…..…….…….....…44

2.9.2. Nanohealing: Techniques Employed…….…….……..45

2.10. Concluding Remarks……..…….…...……..47

CHAPTER 3

DESIGN, CHARACTERIZATION AND OPTIMIZATION OF THE BIOACTIVE CURCUMIN FILM SYNTHESIZED BY THE INTERPENETRATING POLYMER NETWORK TECHNIQUE EMPLOYING AN EXPERIMENTAL DESIGN STRATEGY

3.1. Introduction……..……..50

3.2. Biopolymeric Components employed in the Synthesis of an s-IPN Bioactive Film……51

3.3. Part 1: Preliminary Investigation of the Biopolymeric Films……..……..…....54

3.3.1. Determining the Upper and Lower Variables for Formulation Preparation required for Input into Box-Behnken Design…….……..…….....……54

3.3.2. The Influence of Crosslinking with Genipin on Film Formation and the Effect of Variable Polymer Concentrations……..……...…….....…...54

3.4. Part B: Experimental Synthesis and Statistical Optimization of the Films for Wound Healing…….....……60

3.4.1. Materials and Methods……..…….....60

3.4.1.1. Materials……...……..….60

3.4.1.2. Synthesis of a Semi-Interpenetrating Network Polymer Film……..…...….60

3.4.1.3. Chemical Structure Analysis by Fourier Transform Infrared Spectroscopy……..…….....61

3.4.1.4. Thermodynamic Property Analysis by Differential Scanning Calorimetry Studies……...……...62

3.4.1.5. Surface Morphological Analysis by Scanning Electron Microscopy Imaging…….....62

3.4.1.6. Determination of the Physicomechanical Properties of the Films by Textural Profile Analysis…….....62

3.4.1.7. Durability Testing of the Films by Nano-Tensile Mapping…….....63

3.4.1.8. Determination of the Swelling Capacity and Equilibrium Water Content…….…....63

3.4.1.9. Analysis of the Water Vapor Transmission Rate into the Semi-IPN Films.....64

3.4.1.10. Measurement of the Rheological Properties of the Semi-IPN Polymer Blends…...64

3.4.1.11. In Vitro release of Bioactive……..……64

3.4.1.12. Ex Vivo Permeation Studies through the Sprague Dawley Rat Skin Model…..65

3.5. Results and Discussion…….……...66

3.5.1. Chemical Structure Stability and Vibration Transitional Analysis……66

3.5.2. Assessment of the Thermodynamic Behaviour of the Semi-IPN Films…….....68

3.5.3. Structural Morphological Analysis of the Semi-IPN Films……..…….....70

3.5.4. Textural Profile Analysis and Young's Modulus Determination of the Semi-IPN Films……..…..72

3.5.5. Swelling Capacity and Equilibrium Water Content Analysis of the Semi-IPN Films…….……72

3.5.6. Water Vapour Transmission Rate Analysis……....76

3.5.7. Rheological Characterization of the Semi-IPN Film Polymer Blends……..…....78

3.5.8. Bioevaluation of the Curcumin-loaded Semi-IPN Film…….....79

3.6. Concluding Remarks…….……..81

CHAPTER 4

FABRICATION AND CHARACTERISATION OF THE CROSSLINKED NANOFIBROUS MAT AS A WOUND HEALING DELIVERY SYSTEM

4.1. Introduction……...……....83

4.2. The Technique of Electrospinning……....84

4.3. Limitations Pertaining to the Degree of Successful Nanofibre Formation utilizing then Bioactive Polymeric Solution……...……..…….……...86

4.4. Selection of Optimal Parameters for Advantageous Nanofibre Formation…….....…..89

4.5. Materials and Methods……..……..…...90

4.5.1. Materials……....90

4.5.2. Preparation of Crosslinked Nanofibrous Mats…….……..…....90

4.5.3. Strategic employment of the Box-Behnken Experimental Design for Optimization of the Nanofibrous System…….……....91

4.5.4. Determination of the Molecular Vibrational Transitions of the Nanofibrous Mats by Fourier Transform Infrared Spectroscopy……..…….…....92

4.5.5. Surface Morphology and Nanofibre Density by Scanning Electron Microscopy……..……..……..92

4.5.6. Determination of the Thermal Analysis by Advanced Differential Scanning Calorimetry…….……..…92

4.5.7. Determination of the Tensile Properties of Nanofibrous Mats by the application of Texture Analysis…….…….....……...93

4.5.8. Determination of Young's Modulus and Tensile Properties by the Application of Nano Tensile Analysis……..……..93

4.5.9. Determination of Young's Modulus and Tensile Properties by the Application of Nano Tensile Analysis……..…….....94

4.5.10. Bioevaluation of Nanofibrous Mats as a Wound Healing Platform…...……..….95

4.5.10.1. In vitro Release of Bioactive…….95

4.5.10.2. Ex Vivo Bioadhesivity Testing of the Nanofibrous Mats……..……....95

4.6. Results and Discussion…….....96

4.6.1. Chemical Vibrational Analysis of the Nanofibrous Mats……..……..97

4.6.2. Determination of Surface Morphology and Network Density of Polymeric Nanofibrous Mats……...……..….99

4.6.3. Thermodynamic Evaluation of the Nanofibrous Mat……..……...……...102

4.6.4. Young's Modulus Analysis of Nanofibrous Mats to determine Mechanical Characteristics…….....104

4.6.5. Rheological Characterisation of the Nanofibrous Mats…….…....108

4.6.6. *In Vitro* Release Kinetics of Curcumin……...……....…...112

4.7. Mucoadhesive Characteristics of the Nanofibrous Mats……..……....…..114

4.8. Concluding Remarks……..…115

CHAPTER 5

STATISTICAL OPTIMIZATION OF THE CROSSLINKED NANOFIBROUS MAT AND THE INFLUENCE OF CROSSLINKING ON DYNAMIC CHARACTERISTICS OF THE SYSTEM AS A CONSTITUENT OF A MULTI-COMPONENT STIMULI RESPONSIVE PROTOTYPE DEVICE

5.1. Introduction……..……..116

5.2. Materials and Methods……..……..117

5.2.1. Materials……..……..117

5.2.2. Fabrication of the Optimized Nanofibrous Mat…….....117

5.2.3. Characteristics of the Optimized Nanofibrous Mat…….……..119

5.2.3.1. Evaluation of the Polymeric Vibrational Frequency and Structural Properties…….……..119

5.2.3.2. Evaluation of Surface Morphology and Topography…….…….....119

5.2.3.3. Evaluation of Thermodynamic Transitions occurring over a Specified Heating Range……..……..…….119

5.2.3.4. Determination of the Young's Modulus and Tensile Properties of the Crosslinked and Uncrosslinked Fibres…….…….....120

5.2.3.5. Analysis of the Pertinent Rheological Properties of the Polymeric Formulations……..……..……..……..…..120

5.2.3.6. Determination of the Degree of Crystallinity by X-Ray Diffraction…….....121

5.2.3.7. *Determination of In vitro Bioactive Release and the Effect of Crosslinking on Release Kinetics*…….……..…….....121

5.2.3.8. Release Kinetics by Ex Vivo Studies using a Franz Diffusion Cell Type Apparatus……..……..…...…...121

5.3. Results and Discussion…….……..…..…122

5.3.1. Characteristic Analysis of the Optimized Nanofibrous Mat…….……..…...122

5.3.1.1. Attainment of an Optimized Nanofibrous Wound Healing System by Residual Analysis and Surface Plot Evaluation…….…….....122

5.3.1.2. Response Optimization……...…...……...129

5.3.2. Stability Analysis in Terms of Chemical Structural Transitions by Fourier Transform Infrared Spectroscopy……..…….....130

5.3.3. Surface Topographical and Morphological Evaluation by Scanning Electron Microscopy……...……....131

5.3.4. Thermodynamic Behaviour of the Nanofibrous Mats in terms of Differential Scanning Calorimetry……..……...134

5.3.5. Determination of the Young's Modulus and Tensile Properties of the Crosslinked and Uncrosslinked fibres…….....…135

5.3.6. Analysis of the Pertinent Rheological Properties of the Polymeric Formulations……..……....136

5.3.7. Determination of the Degree of Crystallinity by X-Ray Diffraction…….…..….137

5.3.8. Evaluation of *In Vitro and Ex Vivo* Bioactive Release Kinetics……...…….....138

5.4. Concluding Remarks……..…….……....139

CHAPTER 6

DESIGN OF THE LYOPHILIZED INFLAMMATORY DEPENDENT MATRIX OF THE MULTICOMPONENT STIMULI RESPONSIVE PROTOTYPE DEVICE

6.1.1. Introduction of Advancements to the Bioactive Delivery System……..……140

6.1.2. Inflammation as a Stimulus Employed for Controlled Topical Bioactive Delivery…….……..…...141

6.1.3. Polymeric Components of the Lyophilized Matrix……..…….....142

6.2. Materials and Methods…….…….....145

6.2.1. Materials…….…….....145

6.2.2. Preparation of Bioresponsive Lyophilized Matrix Component of the BTDS……...……145

6.2.3. Formation of a Stimuli Responsive Topical Delivery System (BTDS) incorporating the Nanofibrous Mat……...……..…...146

6.2.4. Chemical Transitional Analysis through Fourier Transform Infrared Spectroscopy…….....147

6.2.5. Thermodynamic Analysis through Differential Scanning Calorimetry…….....147

6.2.6. Analysis of Physicomechanical Properties by Textural Profiling…….....147

6.2.7. Determination of Young's Modulus by Nano Tensile Analysis……..……...148

6.2.8. Determination of Water Content and Erosion by Analysis using a Kaarl Fisher Volumetric Tritrator……..……..…….....148

6.2.9. Identification of Surface Topographical Structure and Morphology Employing Scanning Electron Microscopy……..……...…….....149

6.2.10. Measurement of the Transient Rheological Characteristics of the Bioresponsive transdermal delivery system…….....149

6.2.11. Evaluation of the Stimuli Responsiveness of the Bioresponsive Topical Delivery Device to an Inflammatory Stimulus through *In Vitro* Release Studies……...149

6.3. Results and Discussion……..…….150

6.3.1. Determination of the Chemical Stability and Transitions of the Lyophilized Component……..…….…..….150

6.3.2. Identification of the Thermodynamic Properties of the Bioresponsive Topical Delivery Device……..…...153

6.3.3. Determination of Tensile Strength and Young's Modulus by Textural Profiles…….……...154

6.3.4. Water Content Determination of the Bioresponsive Topical Delivery Device……...…….....158

6.3.5. Identification of Surface Topographical Structure and Morphology employing Scanning Electron Microscopy……....159

6.3.6. Measurement of Transient Rheological Characteristics of the Bioresponsive Topical Delivery Device……....162

6.3.7. Evaluation of the Stimuli Responsiveness of the Bioresponsive Topical Delivery System to an Inflammatory Stimulus through *In Vitro* Release Studies……..……...163

6.4. Concluding Remarks……...…….……....167

CHAPTER 7

CONCEPTUALIZATION AND STATISTICAL OPTIMIZATION OF THE SMART INFLAMMATORY RESPONSIVE MATRIX AS A COMPONENT OF THE PROTOTYPE DEVICE

7.1.1. Introduction……..……..168

7.1.2. Formation of the Polyelectrolyte Complex……..…..……....170

7.1.3. The Employment of Mucoadhesion to Promote Effective, Targeted and Convenient Topical Bioactive Delivery……...……..……171

7.1.4. Optimization of the Lyophilized Matrix in terms of its Inflammatory Responsive Nature of the BTDS…….……...……..…172

7.2. Materials and Methods……..……...173

7.2.1. Materials……..……173

7.2.2. Synthesis and Formation of a Backing Layer to serve as a Component of the Prototype Device……...……...…….…….173

7.2.3. Formulation of the Crosslinked Bioresponsive Lyophilized Matrix incorporating the Entrapped Nanofibres…….....173

7.2.4. Optimization of the Formulary Components…….……....174

7.2.5. Evaluation of the *In Vitro* Bioresponsive Bioactive Release Behaviour by employing the Fenton's Reaction……..……..……..….....174

7.2.6. Characterisation in terms of the Hydration Dynamics Behaviour…….……..……..175

7.2.7. *Ex Vivo* determination of Mucoadhesive Properties through Textural Profiling……...……..……..…..175

7.2.8. Characterisation in terms of Chemical and Vibrational Transitions…….....…..176

7.2.9. Evaluation of the Thermodynamic Behaviour of the Matrix…….....176

7.2.10. Surface Structure and Morphological Analysis……..…….....176

7.2.11. Determination of Young's Modulus by Nanotensile Mapping……..……....176

7.2.12. Physicomechanical Characterisation by Textural Profiling……..……....177

7.2.13. Evaluation of the Transient Rheological Properties……...……...177

7.3. Results and Discussion……..…….……178

7.3.1. Optimization of the Lyophilized Component of the BTDS…….……..…...181

7.3.1.1. Response Surface Plot Analysis for Formulary Optimization……..……190

7.3.1.2. Response Optimization of the Bioresponsive transdermal delivery system…….....185

7.3.2. Inflammatory Responsive Bioactive Release Behaviour…….....186

7.3.3. Water Content Analysis of the Bioresponsive transdermal delivery system…….....188

7.3.4. Evaluation of the Degree of Mucoadhesion of the Prototype Device…..……..……189

7.3.5. Vibrational Transitional Analysis to determine the Molecular Transitions of the crosslinked structures……..…….…….....191

7.3.6. Thermodynamic Evaluation of the Optimized BTDS Device……..……...…...193

7.3.7. Topographical and Morphological determination of the Bioresponsive Topical Delivery Device…….....194

7.3.8. Evaluation of the Tensile Strength and Young's Modulus of the Optimized System……...…….....195

7.3.9. Rheological Elucidation of the Stimuli Responsive and Non Stimuli Responsive Systems…….....198

7.4. Concluding Remarks…….....200

CHAPTER 8

IN VIVO ANALYSIS OF THE MULTI-COMPONENT INFLAMMATORY RESPONSIVE BIOACTIVE DELIVERY DEVICE

8.1. Introduction……201

8.2. Materials and Methods……203

8.2.1. Materials……203

8.2.2. Animal Husbandry……203

8.2.3. *In Vivo* Experimental Design……203

8.2.4. Preparation of the Wound Area……204

8.2.5. *In vivo* Surgical Procedure: Full thickness Wound Model……204

8.2.6. Macroscopic Determination by Percentage Wound Closure Evaluation……205

8.2.7. Visual Comparative Analysis……206

8.2.8. Histomorphological Examination to assess the Degree of Healing with the BTDS device……206

8.2.9. Scores of Wound Healing Establishment as a Function of Time……206

8.3. Results and Discussion……207

8.3.1. Gross Observation of Wound by Photographic Analysis……207

8.3.2. Wound Size Reduction Analysis by Wound Closure……209

8.3.3. Histopathological Evaluation of the Wound Site……211

8.3.3.1. Ulceration and Wound Healing of the Tested Sample Specimens……211

8.3.3.2. Inflammation and Granulation of the investigated Specimens……213

8.3.3.3. Epithelisation and Remodelling at the Wound Site over the 20 Day Period……215

8.3.4. Wound Healing Scores……217

8.4. Concluding Remarks……219

CHAPTER 9

CONCLUSIONS, RECOMMENDATIONS AND FUTURE OUTLOOK

9.1. Conclusions……221

9.2. Recommendations…….……...222

9.3. Future Outlook……223

10. References……224

11. Appendices……...…..…....255

11.1. Publications……...……255

11.1.1. Review Paper 1……...……..255

11.1.2. Research Paper 1……...…..256

11.1.3. Research Paper 2.....257

11.1.3. Research Paper 3.....258

11.2. Research Presentations…….....……...259

11.3. Animal Ethics Clearance Certificate……...……..….263

LIST OF ABBREVIATIONS

ADH- Adipic Acid Dihydrazide

AESC- Animal Ethics Screening Committee

B-B- Box Behnken

BTDS- Bioresponsive transdermal delivery system

CAS- Central Animal Services

CS- Chitosan

CX43- Connexin 43

DoE- Design of Experiments

DSC- Differential Scanning Calorimetry

ECM- Extra Cellular Matrix

EGF- Epidermal Growth factor

FDC- Franz Diffusion Cell

FGF- Fibroblast Growth Factor

FTIR- Fourier Transform Infrared Spectroscopy

GAG- Glycosaminoglycan

H&E- Haematoxylin and Eosin

HA- Hyaluronic Acid

I.P- Intraperitoneally

IGF- Interleukin Growth factor

IPN- Interpenetrating Polymer Network

LMWP- Low Molecular Weight Protoamine

M_w- Molecular Weight

NA- Nanotensile Analysis

PBS- Phosphate Buffer Solution

PDGF- Platelet Derived Growth Factor

PEC- Polyelectrolyte Complex

PEO- Polyethylene Glycol

PGA- Polyglycolic Acid

PU- Polyurethane

PVA- Polyvinyl Alcohol

SEM- Scanning Electron Microscopy

s-IPN- Semi Interpenetrating Polymer Network

TGF- Transforming Growth Factor

WVTR- Water Vapour Transmission Rate

XRD- X-Ray Diffraction

LIST OF EQUATIONS

Equation 3.1: Determination of the Young's Modulus…….62

Equation 3.2: The Determination of the Percentage Swelling Capacity…….63

Equation 3.3: The Determination of the Percentage Equilibrium Water Content……..63

Equation 3.4: The Determination of the Water Vapour Transmission Rate…….64

Equation 3.5: Computation of the Drug Flux for Permeation across Membranes…….65

Equation 4.1: Measurement of the Work of Mucoadhesion……...96

Equation 5.1a: Regression Equations generated for Young's Modulus…….123

Equation 5.1b: Regression Equation generated for Water Vapour Transmission Rate…...123

Equation 5.1c: Regression Equation generated for Percentage Swelling Capacity……...123

Equation 5.1d: Regression Equation generated for Ultimate Strength……...123

Equation 6.1: Determination of the Tensile Strength and Young's Modulus……147

Equation 6.2: Equation for the Determination of the Equilibrium Swelling ratio……..148

Equation 6.3: Employment of the Fenton's Reaction for *In Vitro* Bioactive Release Studies……...……..……...149

Equation 7.1: Determination of the Work of Mucoadhesion…….……175

Equation 7.2: Generation of the Complete Regression Equation for Stimuli Responsive Bioactive Release……..179

Equation 7.3: Generation of the Complete Regression Equation for Young's Modulus…..179

Equation 7.4: Generation of the Complete Regression Equation for Viscosity……...179

Equation 8.1: Equation for the Determination of Percentage Wound Closure…….....206

LIST OF FIGURES

Figure 1.1: Structure and function of the native skin……..……2

Figure 1.2: Mechanism of action of the BTDS on exposure to inflammation at a wounded skin site……..……..…...5

Figure 1.3: Technology applied in the development of the BTDS to ensure bioresponsive release of nanofibrous mats……..…….……...…..….6

Figure 1.4: Schematic conceptualisation of bioresponsive stimulization of the BTDS showing a response on exposure to an inflammatory stimulus…….……....7

Figure 1.5: Schematic conceptualisation depicting the integration of the Bioresponsive transdermal delivery system (BTDS) with the nanofibrous mat and release of the various biopolymeric components upon degradation……..…….……....8

Figure 1.6: Schematic of the breakdown of each chapter in this thesis…….…….....14

Figure 2.1: Image displaying the cross section of the skin……..…..17

Figure 2.2: Classification of wound types…….……18

Figure 2.3: Infiltration of various factors for the process of wound healing……..……....19

Figure 2.4: The major stages undertaken by the body's defence mechanism during the process of wound healing…….……..20

Figure 2.5: Cell mediators interactions at the wound site to promote proliferation and remodelling of skin tissue……...……...21

Figure 2.6: Functions and desirable characteristics of wound dressings and devices related to treatment clinical significance…….....24

Figure 2.7: Nanofibres fabricated by electrospinning, elucidating different nanofibres diameters…….…....47

Figure 2.8: Different forms of polymeric scaffolds for tissue engineering and repair…….....48

Figure 3.1: Proposed mechanism for the formation of an s-IPN…….……..51

F**igure 3.2:** Illustration of the crosslinked reaction between genipin and chitosan……..…..55

Figure 3.3: Chitosan films crosslinked with genipin at various concentrations. (a): 0.1%$^{w}/_{v}$, (b): 0.2%$^{w}/_{v}$, (c): 0.3%$^{w}/_{v}$, (d): 0.4%$^{w}/_{v}$, (e): 0.5%$^{w}/_{v}$…….……..….....56

Figure 3.4: Crosslinked film constituting of high crosslinker and polymer concentration…...57

Figure 3.5: Chemical transitions depicted by the FTIR spectra in (a): genipin crosslinked chitosan films, (b): Uncrosslinked chitosan films…….....58

Figure 3.6: Image displaying the texture analysis process when a strain is applied to the films to determine its tensile strength……..….....59

Figure 3.7: Graph depicting the influence of varying concentrations of genipin on the tensile strength of films……..….....59

Figure 3.8: Fourier transform infrared spectroscopy of semi-IPN films: a: film 1, b: film 2, c: film 5, d: film 9, and e: film 10……..……..…….....68

Figure 3.9: Differential scanning calorimetry of semi-IPN films: (a): film 1, (b): film 9, (c): film 2, (d): film 10, and (e): film 6…….....70

Figure 3.10: Scanning electron micrographs of semi-IPN films: (a), (b): optimized film, (c): film 1, (d): film 2, (e): film 5, (f): film 9, and (g): film 10…….....72

Figure 3.11: Tensile strength (N.mm^{2}) of the various semi-IPN Films……...…..…..73

Figure 3.12: Young modulus E(MPa) for various film formulations via nano-tensile Analysis…….....…….....74

Figure 3.13: Stress–strain nano-Tensile profile and Young's modulus……..…….....74

Figure 3.14: Profile of swelling capacity of the semi-IPN films 1–14 and the optimized Film…….....…….....76

Figure 3.15: Profile of the rate of water vapour transmission within the semi-IPN films 1–14 and the optimized formulation……..….77

Figure 3.16: (a): Drug release profile of curcumin-loaded semi-IPN films and (b): drug release permeation through the Sprague-Dawley rat skin……..……..…….....81

Figure 4.1: (a) The electrospinning apparatus with significant elements to fabricate the (b) nanofibrous mat…….……...85

Figure 4.2: Schematic representation of mounted nanofibres secured on

template for nanotensile mapping……..……..……..94

Figure 4.3: Fourier Transform Infrared Spectroscopy of Nanofibrous mat (a) F6, (b) F15, (c) F2, (d) F4, (e) F9, (f) F5……...……...99

Figure 4.4: Scanning electron microscopic profiles of (a) F3, (b) F2, (c) F4, (d) F5, (e) F9, (f) F6 and (g) F15……..……...……..…101

Figure 4.5: Differential Scanning Calorimetry profiles of nanofibrous mats (a): F4, (b): F5, (c): F15, (d): F9, (e): F6……..……..……103

Figure 4.6: Stress-Strain relationship profile of nanofibrous mats where (a) is the linear portion of the slope from which Young's Modulus can be derived and (b) represents the fracture point of the sample…….....…...……..105

Figure 4.7: Force versus distance curve whereby the tensile strength can be derived. Area A resembles the resilience and Area A+B the toughness of measured samples…….....106

Figure 4.8: Vertical Bar outlining the variations between nanofibrous mats of (a) Tensile Strength (N.mm^2), (*b*) Young's modulus (*E*; MPa), (*c*) yield stress (*σy*; MPa), (*d*) ultimate strength (*σu*; MPa), (*e*) ultimate strain (*εu*) and (*f*) toughness (*uf*; J cm−3) of nanofibrous mats 1–7 (where 1: F2, 2:F3, 3:F4, 4:F5,5:F9,6:F6,7:F15)…….....……..107

Figure 4.9: Dynamic Modulus G' and G" of [crosslinked] (a) F1, (b)F2, (c) F5, (d) F6, (e) F8; [uncrosslinked] (a) F1, (b) F2, (c) F5, (d) F6, (e) F8……..……...…....111

Figure 4.10: Release profile of curcumin of the various nanofibrous mats, **(**a): F2-5, (b): F6, 9, 15……...……113

Figure 4.11: Force-distance textural profile employed to compute work of adhesion and the peak adhesion force…….……114

Figure 5.1: Schematic conceptualization of nanofibre production comprising of s-IPN formation and electrospinning…….……...118

Figure 5.2: Schematic illustrating the textural analysis procedure employed to cause a break or fracture in the nanofibrous strip so that a force against distance plot could be generated to determine the tensile strength……..……...120

Figure 5.3: Summary of Residual plots for Young's Modulus, Ultimate Strength, Swelling Capacity and Water Vapour Transmission Rate……..……..125

Figure 5.4: Contour and Response Surface Plots depicting the interactions between polymers and crosslinker on mechanical characteristics resembled by Young's Modulus.....126

Figure 5.5: Contour and Response Surface Plots depicting the interactions between polymers and crosslinker on mechanical characteristics resembled by Ultimate Strength…….....127

Figure 5.6: Response surface and contour plots depicting the effects of chitosan, hypromellose and genipin on swelling……..……..128

Figure 5.7: Surface and contour plot analysis depicting the influence of swelling and water vapour transmission……..……..……..…….....129

Figure 5.8: Optimization plot for the definition of the optimum nanofibrous system…….....130

Figure 5.9: FTIR spectra of (a): Crosslinked nanofibrous mat and (b): Uncrosslinked nanofibrous mat……..……..……..131

Figure 5.10: Morphological representation of(a), (b), (c): Uncrosslinked nanofibres; (d), (e), (f): Crosslinked Nanofibres……...…….……....133

Figure 5.11: Differential Scanning Calorimetry Thermograms of (a): Crosslinked nanofibrous mat, (b): Uncrosslinked nanofibrous mat……...…….....135

Figure 5.12: Nanotensile mapping depicting comparisons in mechanical strength of (a): Uncrosslinked nanofibrous mat, (b): Crosslinked nanofibrous mat [a: Linear portion depicting Young's Modulus, b: Fracture point]…….…….....……...…....136

Figure 5.13: Depiction of pertinent rheological parameters affecting nanofibres formation **(**a): Crosslinked hydrogel, (b): uncrosslinked hydrogel……..…….……137

Figure 5.14: XRD profiles of **(**a): Crosslinked nanofibrous mat, (b): uncrosslinked nanofibrous mat…….....……..…..138

Figure 5.15: *in vitro* bioactive release and *ex vivo* permeated release profile of the optimum nanofibrous mat……...……...……139

Figure 6.1: Illustration revealing influx of infiltrate mediators to the wound site that will serve as an inflammatory stimulus for the delivery system…….……142

Figure 6.2: Functionalisation of HA with amino groups by the use of ADH…….....145

Figure 6.3: Chemical vibrational transitions of (a): Hyaluronic Acid, (b): F2, (c): F5, (d): F8, (e): F10, (f): F14……..…….....153

Figure 6.4: DSC analysis illustrating the thermal behaviours of the various formulations: (a): F7, (b): F5, (c): F15, (d): F13, (e): F2…….....….....154

Figure 6.5: Stress-Strain relationship profile of the lyophilized matrix where (a) is the linear portion of the slope from which Young's Modulus can be derived and b resembles the fracture point of the sample…….…….....156

Figure 6.6: Vertical bar charts outlining the variations in mechanical properties amongst the various formulations where (a): Young's modulus (*E*; MPa); (b): yield stress (*σy*; MPa); (c): ultimate strength (*σu*; MPa); (d): ultimate strain (*εu*) and (e): Tensile Strength ($N.mm^2$)….....157

Figure 6.7: Percentage water content analysis of formulation 1-15……....……...159

Figure 6.8: Topographical imagery by scanning electron microscopy of (a): F15, (b): F3, (c): F2, (d): F8, (e): F9, (f): F11, (g): F12…….....…..161

Figure 6.9: Depiction of flow behaviour of a crosslinked HA hydrogel upon an applied shear stress over time……....…….…..163

Figure 6.10: Bioactive release profiles based on an inflammatory stimulus of (a): F1-3, (b): F4-6, (c): F7-9, (d): F10-12, (e): F13-15…….……..…166

Figure 7.1: Mechanism of action of the prototype device……..……170

Figure 7.2: Residual plots of (a) stimuli responsive bioactive release; (b) Young's Modulus (c) Viscosity…….……...181

Figure 7.3: Contour and Surface Plots of the stimuli responsive bioactive release (MDT) in relation to amendment in concentration of polymer and crosslinker……...183

Figure 7.4: Surface and Contour Plots depicting the effect of varying polymeric and crosslinker concentration on the Young's Modulus and tensile strength...184

Figure 7.5: Response surface and contour plots depicting the effect of varying concentrations on the viscosity of the formulation……....185

Figure 7.6: Desirability plots representing the levels of Alginate, Hyaluronic Acid and Adipic Acid Dihydrazide required to synthesis the optimized formulation……...186

Figure 7.7: Comparative bioactive release profiles for the stimuli responsive

(optimized) formulation and non stimuli responsive (Control) under inflammatory (F) and normal conditions (N)……..……..188

Figure 7.8: Area under the curve for the work of mucoadhesion of the prototype device where (a): Backing Layer, (b): Lyophilized matrix with incorporated nanofibrous mat……..191

Figure 7.9: Molecular vibrational transitions of a: the stimuli responsive system and b: the non stimuli responsive system……..…….....192

Figure 7.10: Thermographic profiles of a: the stimuli responsive system, b: the non stimuli responsive system……..…….....194

Figure 7.11: Surface topographical imagery of (a): Non stimuli responsive system and (b): Stimuli responsive system……...……...……...….195

Figure 7.12: Nanomapping profiles revealing Young's Modulus (a) and fracture points (b) of A: Stimuli responsive system, B: Non stimuli responsive system, C: Backing Layer.....197

Figure 7.13: Characteristic tensile strength profile…….……...……....198

Figure 7.14: Pertinent rheological properties in terms of the G' and G" Modulus of a: Stimuli responsive system, b: non stimuli responsive system……....…..199

Figure 8.1: Schematic overview of the componential architecture and formulation of the BTDS……...202

Figure 8.2: Photographic images pertaining to the administration of the various delivery systems whereby A is the inflammatory responsive device, B: nanofibrous mat, C: films loaded with curcumin, D: application of the conventional system, E: topical administration of non-medicated gauze and simple bandage and F: non inflammatory responsive device.....204

Figure 8.3: Surgical and preparatory procedure undertaken for burn wound induction…….205

Figure 8.4: Summary of the preparation and *in vivo* surgical procedure for wound induction followed by methods undertaken to determine wound healing evaluation.....207

Figure 8.5: Photographic appearance of wounds (i) Group A: nanofibrous mat, Group B: Curcumin loaded film, Group C: Conventional system, Group D: Control, (ii) Group E: Stimuli

responsive device, Group F: Non-stimuli responsive device…….....209

Figure 8.6: Percentage wound closure profile over the treatment 20 Day profile for Group A: Nanofibrous mat, Group B: curcumin loaded film, Group C: Conventional system, Group D: Control, Group E: Stimuli responsive system, Group F: Non-stimuli responsive system.….....211

Figure 8.7: Histopathological characteristics in terms of ulcerative dermatitis of **(**a) Control Day 0, (b) control Day 20, (c) nanofibrous mat Day 0, (d) Film Day 0, (e) Film Day 20, (f) conventional Day 0, (g) Conventional Day 20, (h) non-stimuli responsive Day 20, (i) stimuli responsive Day 1, (j) and (k) non-stimuli responsive Day 1…….....213

Figure 8.8: Histopathological analysis depicting inflammation in **(**a) nanofibrous mat Day 5; (b) nanofibrous mat Day 10; (c) Film Day 5; (d) conventional Day 5; (e) conventional Day 10; (f) Control Day 5, (g) stimuli responsive device Day 1, (h) stimuli responsive device Day 15, (i) non-stimuli responsive device Day 15…….....215

Figure 8.9: Histogram revealing rate of epithelisation and remodelling in **(**a) nanofibrous mat Day 20; (b) nanofibrous mat Day 15; (c) films Day 15; (d) films Day 10; (e)conventional Day 15; (f)control Day 15; (g) control Day 10; (h) stimuli responsive device Day 15; (i) stimuli responsive device Day 20; (j) stimuli responsive device Day 20; (k) stimuli responsive device Day 20; (l) non-stimuli responsive device Day 20…….....217

LIST OF TABLES

Table 1.1: Categories of wounds……3

Table 1.2: Wound healing characteristics of the various biopolymers……9

Table 2.1: Classification of various wound dressings and their properties……..49

Table 3.1: Template exhibiting Upper and lower limits derived from preformulation experimentation……....54

Table 3.2: Box-Behnken design template for statistically derived semi-IPN film Formulations……..61

Table 3.3: Parameters employed for textural analysis……63

Table 3.4: Resistance and conductivity of skin preparations to determine skin integrity before and after *ex vivo* permeation studies……65

Table 3.5: Effects of various concentrations of polymer and crosslinker on the formulation viscosity and yield stress……...79

Table 4.1: Parameters pertaining to limitation occurrence during the electrospinning Process……..88

Table 4.2: Box-Behnken Design Template for statistically derived s-IPN Nanofibrous Mats……92

Table 4.3: Parameters employed to carry out varies rheological analysis on polymer solutions for electrospinning……..95

Table 4.4: Parameters pertaining to optimal nanofibres formation……97

Table 4.5: Representation of nanofibre fabrication from the Box-Behnken experimental design……...97

Table 4.6: Viscosity and Yield Stress of the various hydrogel formulations for nanofibre synthesis……....110

Table 5.1: Statistically derived superlative concentrations for crosslinked and uncrosslinked nanofibres……...118

Table 5.2: Depicting parameters and properties related to nanofibre solution and electrospinning……..……119

Table 5.3: Resistance and conductivity of skin preparations to determine skin integrity before and after *ex vivo* permeation studies…….....……122

Table 5.4: ANOVA analysis of the measured responses…….……..…....124

Table 5.5: Experimental values obtained from the nanotensile mapping of crosslinked and uncrosslinked nanofibrous mats……....136

Table 6.1: Box-Behnken Design Template of the 15 statistically derived formulations for the design of an inflammatory responsive lyophilized matrix of the BTDS……...…….146

Table 6.2: Depiction of upper and lower limits of independent variables: polymer and crosslinker concentration…….....146

Table 6.3: Parameters employed for Texture Analysis…….....148

Table 6.4: Viscosity and Yield Stress values of the various formulations…….....163

Table 6.5: MDT bioactive release profiles of formulation 1-15……...…..167

Table 7.1: Statistically derived superlative concentrations of the bioresponsive and non-bioresponsive component……....174

Table 7.2: Parameters employed for Texture Analysis…….....177

Table 7.3: ANOVA analysis of the measured responses…….....179

Table 7.4: Physicomechanical analysis revealing the various values for evaluation in terms of mechanical characteristics…….....197

Table 8.1: Wound healing scores of the various groups where (i): Group A and B, (ii): Group B and C, (iii) Group D and E represented throughout the wound healing cascade…….....218

CHAPTER 1

INTRODUCTION AND RATIONALE OF THE STUDY

"The measurement of greatness in a scientific idea is the extent to which it stimulates thought and opens up new lines of research"

- 'Paul A.M Dirac'

1.1. Background to the study

The perceptive understanding of cutaneous burns and wound healing requires thorough comprehension and knowledge with regards to the function of the skin, its anatomy and physiology (Mihm et al., 1976). The skin serves as the largest organ of the body portraying many physiological functions thus playing a pivotal role in the maintenance of normal body function and homeostasis. Primarily the skin is structured by three main layers namely the epidermis, dermis and hypodermis as indicated in Figure 1.1. The skin serves as the bodies' first line of defence against foreign obstacles in that it is in direct contact with the outside environment. It serves protection as a physical barrier mostly owing to the presence of the epidermis and its rich availability of keratinocytes arranged in a scaffold-like lattice and a lipid-rich matrix that serves as a robust and waterproof barrier. Furthermore mechanical, sensory, metabolic and structural functions are maintained by the skin under physiological conditions and stresses (Venus et al., 2010)

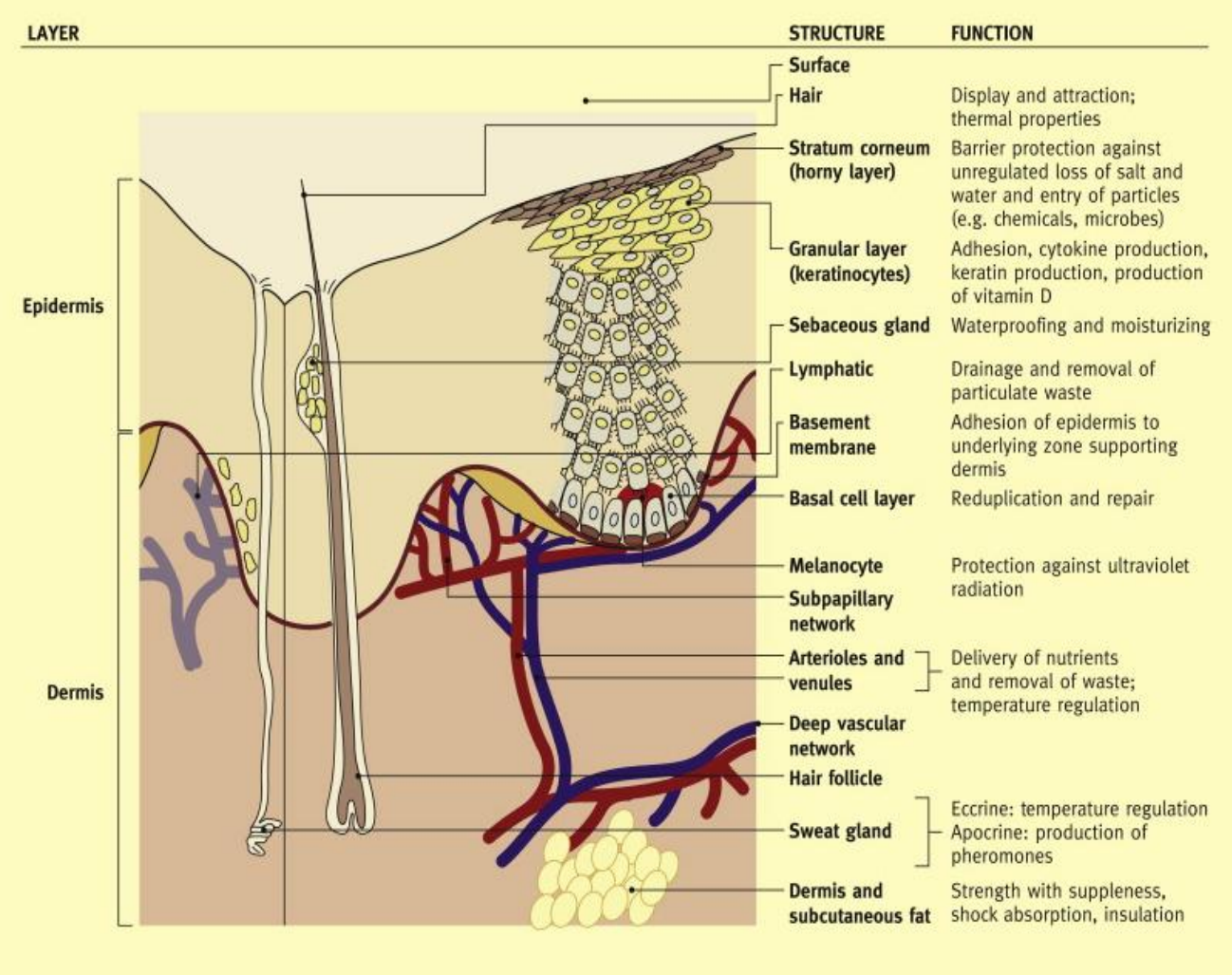

Figure 1.1: Structure and function of the skin (obtained from Venus et al., 2010)

A wound can be described as a break or defect in the skin tissue whereby its integrity may be compromised due to physical, thermal or chemical factors (Boatang et al., 2008). They can be classified as traumatic, surgical and pathological malignancies whereby these injuries may result in a declined function of the skins native physiological functions. There are seven major categories of wounds of interest, distinct from each other, by the manner in which the skin or tissue is broken and its general appearance as described in Table 1.1. Of significant interest to this research are burn wounds and the healing process of burns. Burn wounds may be described as injury to the skin caused by thermal, chemical, and electrical sources that may be distinguished by the appearance and burn depth of the skin layers. Thermal burns such as scalds tend to cause superficial dermal burns whereas flame burns and contact burns cause deep dermal injury to the full thickness of the skin. Electrical burns are caused by tangenial exposure of skin tissue to varying degrees of current. Chemical burns are caused by both alkali and acidic sources. These wounds tend to be deep, as corrosive agents may cause coagulative necrosis until the full thickness of the skin is removed. Table 1.1 provides a depiction of the various wound types and their occurrence as follows: (Hettiaratchy and Dziemulsky, 2004; Mallefet and Dweck, 2008).

Table 1.1: Categories of wounds

Wound Category	Description
Abrasions	Caused by rubbing or scraping of the skin
Incisions	Clean cut wounds which tend to bleed freely
Lacerations	Ragged wounds with irregular edges and masses of torn tissue beneath
Punctures	Created when sharp objects enter the skin and penetrate the tissue leaving a small surface opening
Avulsions	Tearing of tissue from a body part with heavy bleeding
Contusions/closed wounds (bruises)	Result of forceful trauma that injures an internal structure without breaking the skin
Burns: 1. Themal 2. Chemical 3. Electrical	Distinguished by the appearance and burn depth of the skin layers: Scalds: superficial dermal burns, flame burns/contact burns, deep dermal injury to the full thickness of the skin, Deep corrosive with coagulative necrosis caused by alkali and acidic sources, Tangenial exposure of skin tissue to varying degrees of current

Wound treatment and management has proven to be challenging due to the fact that various extrinsic and intrinsic factors govern significant roles during the healing process (Gethin, 2007). Wounds occur on a daily basis and can result in a declined quality of life depending on the severity. Wound healing involves three interlapping and dynamic phases that work hand in hand; namely the inflammatory, proliferation and remodelling phases. Thus an advanced delivery system is required to ensure adequate and optimal treatment (Li et al., 2012). Numerous wound dressings have been marketed in the past. However, the majority of these systems lack the necessary therapeutic effects required to target all factors associated with the process of adequate healing. These include natural and synthetic bandages, cotton wool, lint and gauzes with varying degree of absorbency and efficiency (Lock et al., 1980).

Many of the available systems lack the adequate fundamentals for effective wound healing such as poor fluid absorption capabilities, low gas transmission and water vapour rates as well as poor tensile strength (Archana et al., 2013). An effective wound healing device should

possess both desirable clinical and pharmaceutical properties for optimal treatment such as a moist wound environment, which allows for rehydration of desiccated tissue which enhances angiogenesis and connective tissue proliferation, debridement for the removal of necrotic tissue and foreign bodies which have the ability to promote the inflammatory phase and serve as a medium for microbial growth. Absorption promotes the removal of excess exudates which hinders cell activity and proliferation. Gaseous exchange allows management of the healing process stimulating fibroblasts and promoting angiogenesis. Minimal adherence to the wound site will ensure convenient removal as well as minimal tissue damage and pain affliction to the user. Microbials produce an unpleasant wound odour and tend to induce tissue damage thus the ideal wound healing device would prevent this and promote collagen synthesis and tissue repair. Extended usage features and a low frequency of dressing change ensure cost effectiveness (Boateng et al., 2008). In addition, durability, tensile strength and the desired film thickness need to be considered.

1.2. Rationale and Motivation of the study

A single assembled device that has the ability to incorporate the many required features as discussed, of an advanced wound healing delivery system that will have the potential to advance drug delivery with regards to afflicted burns and wound healing. This research focuses on overcoming the many challenges associated with effective wound healing, by the development of a smart device composed of various components that have the potential to stimulate advanced wound healing synergistically when incorporated as a single system.

Burn wounds in particular occur at varying levels and can be termed as 1st, 2nd and 3rd degree depending on the severity. First degree burns are associated to burn wounds occurring only on the epidermal surface with no blister formation, 2nd degree burns involve partial thickness of the skin such as the epidermis and superficial dermal layers whereas 3rd degree burns involve the full thickness of the skin giving it a white leathery look. The device described aspires to effectively target and ensure healing of burn wounds at all wound depths associated with burns. To accomplish this efficiently the single assembled device will incorporate an intelligent crosslinked nanofibrous system that has the ability to mimick the extracellular structures of the native skin thereby forming ‘pseudoskin’ accelerating the healing process with regards to regeneration, proliferation, epithelisation, and furthermore resulting in a scarless healing artefact together with a stimuli (inflammatory) responsive component ensuring prolonged and targeted release. The emergence of applications surrounding stimuli-responsive technology in drug delivery may provide as a promising technique for wound healing allowing responses to specific chemical or physical changes at the wound site such as that of inflammation, improving the therapeutic response and ensuring targeted and prolonged bioactive release. Challenges that are currently faced which

include factors such as drug accumulated toxicity and side effects, indefinite delivery as well as unpredictable release can be overcome by application of these systems (Cabane et al., 2012).

The above mentioned system is a step forward from other wound healing systems in that it combines the innate structures, such as biopolymers presenting with wound healing properties in a nano-based system together with the bioresponsive nature of the natural healing cascade as depicted in Figure 1.2. The device composes of a backing layer, lyophilized inflammatory dependent matrix as well as a nanofibrous mat incorporated into the lyophilized matrix and is termed a 'Bioresponsive transdermal delivery system (BTDS)'. This allows and ensures specified release of the bioactives in correspondence to the inflammatory mediators released through the wound healing cascade ensuring aligned levels of bioactive with the presence or absence of inflammation experienced by any individual person. In addition, the various biopolymers and bioactives will be combined by employing the interpenetrating polymer network (IPN) technique explained in greater detail in Chapter 3, that allows the crosslinking or semi crosslinking of polymers by ionic, covalent or hydrogen bonding thus endowing advantageous properties to the system. The combinatory delivery system will employ the use of various technology strategies as outlined in Figure 1.3 which also depicts the advantageous of each, to develop a single healing device with multiple properties. As a comparison to the device, a bioactive film as described in Chapter 3 is synthesized to determine the efficacy of the device in terms of *in vivo* analysis carried out on a burn wound.

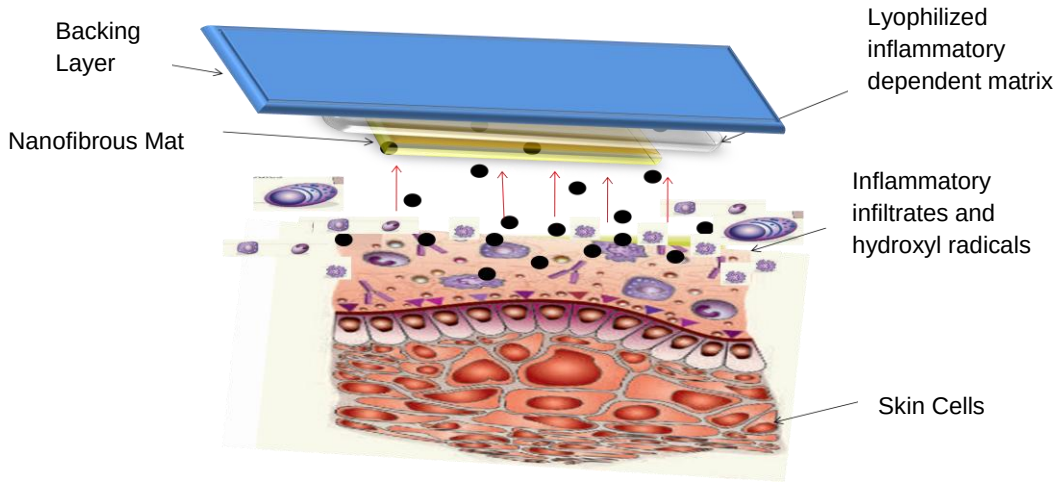

Figure 1.2: Mechanism of action of the BTDS on exposure to inflammation at a wounded skin site.

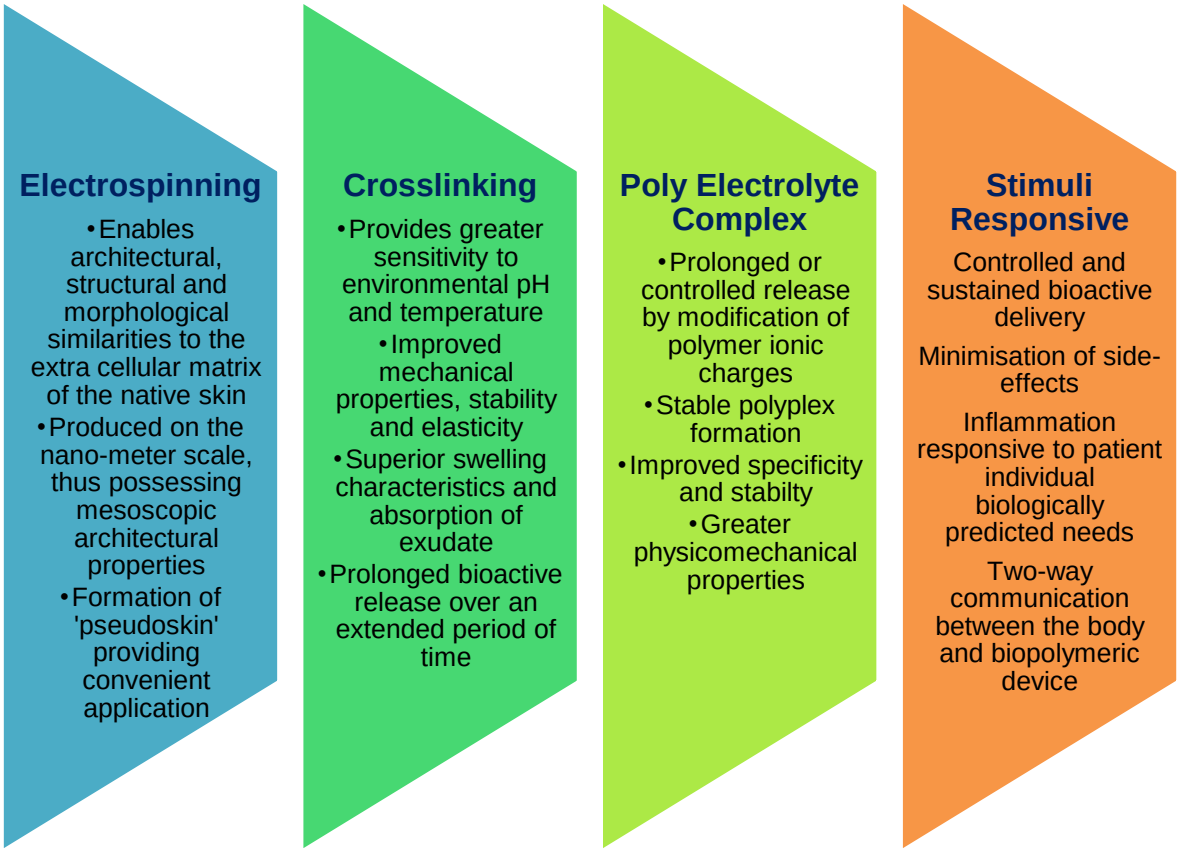

Figure 1.3: Technology applied in the development of the BTDS to ensure bioresponsive release of nanofibrous mats

1.3. The Mechanism of Action of the Combined Bioresponsive Topical Delivery System (BTDS)

The research focuses on the fabrication of a bioresponsive transdermal delivery system (BTDS) that integrates a wound healing system with an inflammation responsive system. This is achieved by the inclusion of a stimuli-responsive system that ensures a two-way communication between the delivery system and the body so that a prompt therapeutic intervention occurs upon recognition of biochemical responses. This is achieved through the targeted release of a nanofibrous polymeric mat designed to mimic the extracellular matrix of the natural skin whilst simultaneously promoting healing in all stages of the healing process (Alvarez-Lorenzo and Concheiro, 2004).

The proposed BTDS composing of smart polymeric materials serves as an application for a smart stimuli-responsive system that has the capability to deliver nanofibrous wound healing mats at controlled therapeutic levels on exposure to inflammation at the pathological wound site as depicted in Figure 1.4. Inflammatory molecules such as neutrophils, macrophages and hydroxyl radicals inherent to the healing process will be the intrinsic factor that the BTDS responds to. The wound healing process comprises of three main phases, namely: the inflammatory, proliferative and remodelling phase. Of particular interest, is the inflammatory phase that occurs immediately post injury to establish homeostasis. During this stage several mediators for wound healing, such as platelet derived growth factors, chemotactic factors,

macrophages and neutrophils are secreted that adhere to the extracellular matrix of the skin to promote metamorphosis and reparative functions (Singer and Clark, 1999). Furthermore, hydroxyl radicals are generated during the inflammatory process (Darzynkiewicz and Balazr, 1971) and thus will serve as the main target of the BTDS to ensure bioresponsive behaviour.

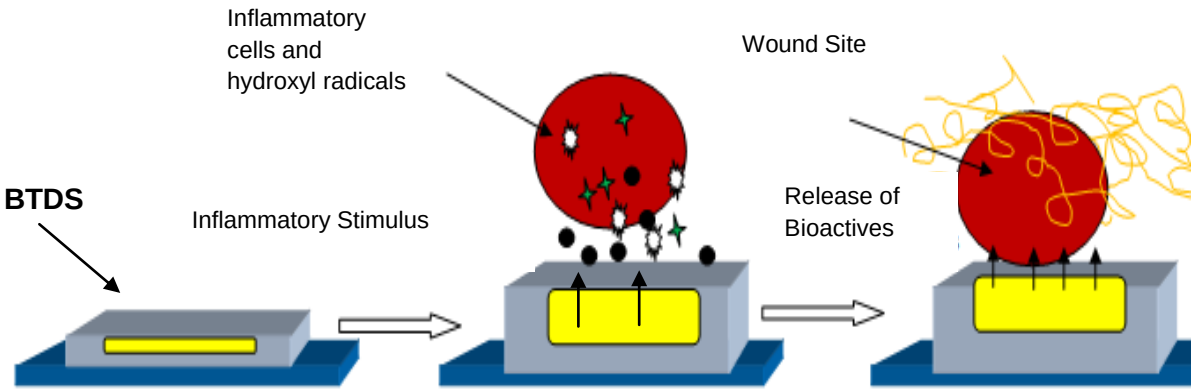

Figure 1.4: Schematic conceptualisation of bioresponsive stimulization of the BTDS showing a response on exposure to an inflammatory stimulus

Incorporated within the BTDS, is a lyophilized matrix that will serve as a drug reservoir, incorporated with a nanofibrous mat comprised of natural polymers that have the capacity to accelerate re-epithelisation and remodelling at the wound site. Advantageous features such as mimicking the ECM of the native skin together with possessing wound healing characteristics that can be additively combined and in addition properties such as biodegradability, biocompatibility, bioadherence and non toxicity can be established within the system thus ensuring minimal to no scarring of tissue at the wound site. These nanofibrous mats enhance healing and are composed of natural polymers such as chitosan and hypromellose crosslinked with a natural crosslinker genipin and in addition include a bioactive curcumin, have been proven to be effective through both *in vitro* and *in vivo* studies in the promotion and enhancement of the healing process throughout all the interlapping phases as shown in Figure 1.5 and described in Table 1.2. The BTDS incorporating the nanofibrous mat will further serve as a delivery platform having the potential to mimic the extracellular matrix as described and deliver selected nanofibrous polymeric material with wound healing properties in a prolonged controlled manner. The formation of a BTDS will enhance this by ensuring prolonged and direct release at the wound site at a specific interphase within the healing process. Inclusion within the BTDS design criteria is the use of biopolymers such as hyaluronic acid and sodium alginate that have the ability to act in a bioresponsive manner to inflammation in addition to having wound healing characteristics.

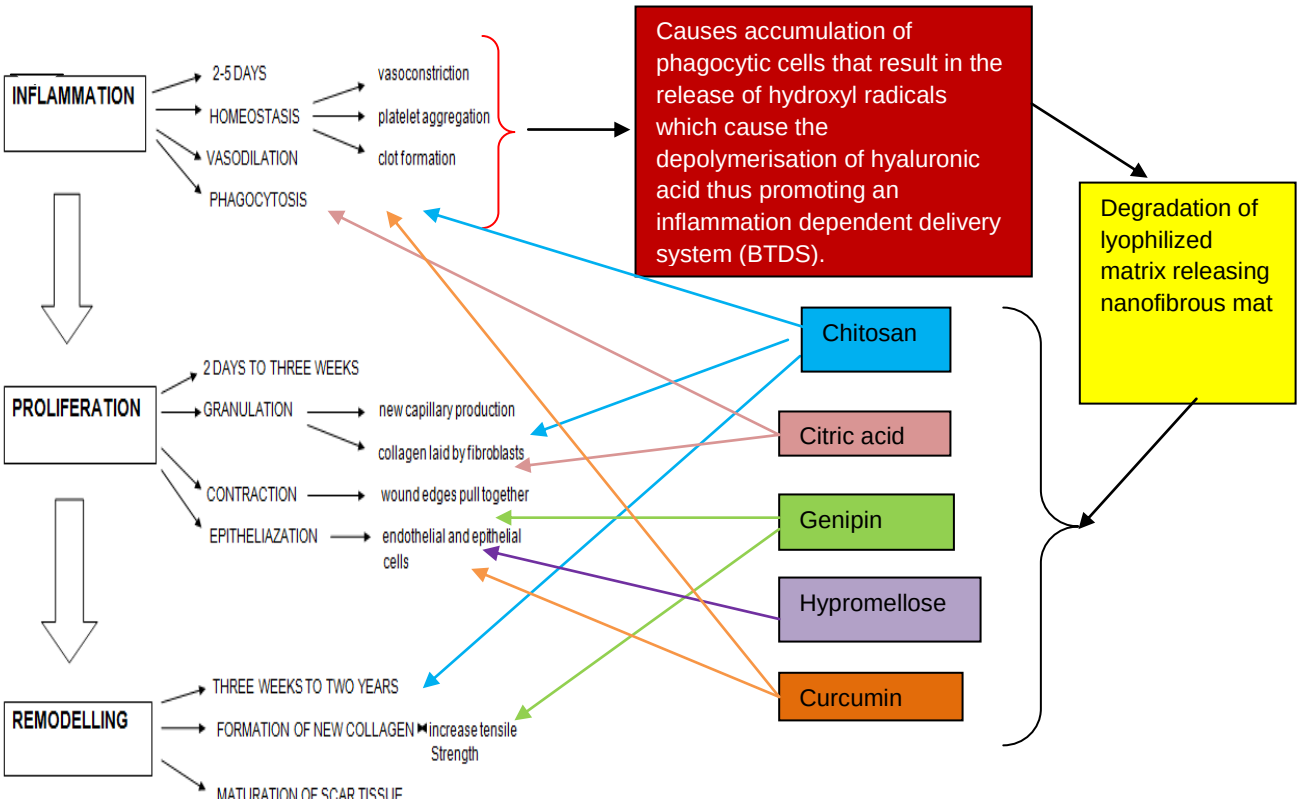

Figure 1.5: Schematic conceptualisation depicting the integration of the Bioresponsive transdermal delivery system (BTDS) with the nanofibrous mat and release of the various biopolymeric components upon degradation.

Table 1.2: Wound healing characteristics of the various biopolymers

Phase	Inflammation	Proliferation	Remodelling	References
Chitosan	Homeostasis	Differentiation, re-epithelisation and fibroplasia during granulation	Decreased hypertrophic scar formation	Howling et al., 2001; Ishihara et al., 2002; Alemdaroglu et al., 2006
Citric Acid	Decreased microbe infestation and exudates excretion	Laying of granulation tissue and epithelisation	___	Naqoba et al., 2011
Genipin	___	Epithelisation and proliferative activity	Promotion of new collagen formation and remodelling	Mi et al., 2002; Muzarelli, 2009
Hypromellose	___	Angiogenesis	___	Braund et al., 2002;Topham, 2002
Curcumin	Anti-inflammatory, anti-oxidant, TGF-β1 formation.	Cellular proliferation, induction of growth factors and granulation tissue formation	___	Pachence, 1996; Gopinath et al., 2004
Hyaluronic Acid (BTDS)	Interaction with hydroxyl radicals, water attracting properties, absorption of exudates	Promotion of proliferation and regeneration.	proteolytic degradation of provisional matrix to increase cell migration and tissue remodelling	Perttila et al., 1990; Anilkumar et al., 2011

1.4. Novelty of the Study

The use of a bioresponsive system comprising of hyaluronic acid, a biological component of the skins natural extracellular matrix, in combination with a nanofibrous mat composed of purely natural polymers having wound healing properties, will result in a synergistic system to enhance wound healing. The concurrence of nanotechnology and stimuli responsive systems serves as a unique technique whereby properties of both systems may be combined to enhance system performance thus accelerating the healing process and promoting scar free closure. Innovative incorporation of the various technologies such as a bioresponsive system ensures effective action of the device only upon recognition of the wound site through distinguished mediators. At the same time incorporation of the nanofibrous mat will ensure the formation of ‘pseudoskin’ whereby the various components of the natural ECM can be

mimicked further advancing the healing process. In addition the employment of the various biopolymers in combination serves as a novel blend for fabrication of the device having wound healing attributes and properties thus providing advantageous characteristics throughout the wound healing cascade.

1.5. Possible Therapeutic Applications of the Study

- Foot ulcers occur in approximately 5-10% of the population and are on the increase in majority of the population affected with diabetes. Lower limb amputation is primarily due to ulcerative wounds and requires appropriate management. The use of an inflammatory responsive topical wound healing system will assist in prevention of infection, bacterial colonisation as well as aid the healing process.
- Wounds and lesions associated with AIDS conditions such as Kaposis Sarcoma, oral and orofacial lesions and contraction of bacterial infections such as *Staphylococcus aureus* and *Salmonella*, can be prevented and maintained by the use of a wound healing device that promotes the healing process and prevents the occurrence of bacterial infestation and disease.
- Enhanced healing therapy through targeted and prolonged delivery of nanofibrous mats will enhance the therapeutic effect of lesions, avulsive wounds, ulcerations, burn wounds and incisions thus promoting scar free and optimal healing.

1.6. Aim and Objectives of the Study

The aim of this research is to develop a device that will efficiently and effectively accelerate the healing process of wounds. This can be undertaken by the fabrication of a device known as the Bioresponsive transdermal delivery system (BTDS) that employs the use of innovative technologies. The device can be set in a componential manner whereby the various components comprises of a nanofibrous mat employing nanotechnology and electrospinning as well as an inflammatory responsive component employing stimuli-responsive techniques, in addition to the use of biopolymers having influential wound healing qualities.

For pragmatic fulfilment of the aim, the following objectives will be undertaken:

1. Identification of potential polymeric biomaterials in terms of their biocompatibility, wound healing significance and stimuli responsive behaviour to inflammation to be used in the synthesis of the BTDS which will consist of the lyophilized matrix, nanofibrous mat and backing layer.
2. Generation of a three factor Box-Behnken Design obtained from preliminary mathematical feasibility studies that involve the procurement of upper and lower limits for synthesis of the device.

3. Optimization of the BTDS acquired from computational collaboration and conceptualisation of the Box-Behnken Design template.
4. Analysis of the BTDS in terms of its physicomechanical and physicochemical characteristics by performance of Fourier Transform Infrared Spectroscopy (FTIR),Nanotensile Analysis (NA), Scanning Electron Microscopy (SEM) and Differential Scanning Calorimetry (DSC) amongst other characterisation tests.
5. *In vitro* analysis for responsiveness to inflammation on exposure to chemical mediators such as hydroxyl radicals.
6. *Ex vivo* analysis to determine the biological characteristics in terms of adhesion and release through biological tissue
7. *In vivo* analysis to determine the biological and preclinical prospection in terms of its wound healing capacity

Successful conclusions of the above objectives, may lead to establishment of the feasibility of the system in humans.

1.7. Overview of the Thesis

Each chapter in this thesis is based on the aim and objectives as outlined in Section 1.6. A summary will be provided whereupon Figure 1.6 will further provide a straightforward and pragmatic overview of the processes undertaken in pursuing the origin of the BTDS system.

Chapter 1 of this thesis provides a background that portrays a brief description of the native skin as well as a general indication of wounds and wound healing. It also describes wound management and the strategies employed in this work to overcome the challenges faced with treatment. A brief synopsis is also provided illustrating the architectural structure of the proposed prototype device. Further a rationale and motivation, novelty of the study is also provided. A list of objectives and an aim is presented.

Chapter 2 of this thesis provides a comprehensive review on delivery systems for wound healing. It ushers in an introduction of wound healing and the mechanisms involved there forth outlining the physiology, mechanism of actions, wound types and wound management. Further revealed in this literature survey, is a detailed depiction that focuses on wound management aids, both advanced and traditional as well as the use of smart polymeric materials, bioactives and biopolymers in wound healing devices. The chapter concludes with an illustration of modern day techniques employed to fabricate wound healing devices.

Chapter 3 of the thesis describes the synthesis of a bioactive film. The role of the various biopolymers and the semi interpenetrating polymer network (s-IPN) technique is depicted.

The synthesis of the films by preparation of the various variants followed by the construction of a 3 factor Box-Behnken design template is discussed. Optimization is then pursued and the applicability of the respective design is analysed. Furthermore, the physicochemical and physicomechanical characteristics are evaluated to determine design feasibility.

Chapter 4 of the thesis introduces the process of electrospinning and the characteristics of nanofibres. The challenges faced during the electrospinning process to optimise the fibres are also included. Following on from the theoretical basis established, novel methodology was accomplished for electrospinning of the nanofibrous mats. The 3 factor Box-Behnken experimental design was used originating from a set of variables whereby upper and lower limits were established. Physicomechanical, physicochemical and *in vitro* characteristics were scrutinised to confer an in-depth acquaintance to system properties and performance.

Chapter 5 of this thesis focuses on the optimization of the nanofibrous mats established via the successful design as described in Chapter 4. The nanofibrous mat optimization is undertaken by employing a Response Surface Methodology. Characterisation of bioactive release kinetics, property dynamics in terms of chemical transitions and mechanical properties were further investigated.

Chapter 6 describes the synthesis of the stimuli responsive component of the BTDS. This chapter focuses on the experimental investigation by employment of the 3 factor Box-Behnken Design template for formulary analysis whereby fifteen formulations are obtained. The selection of responsive polymers and novel methodology for the design is presented.

Chapter 7 of this thesis portrays the optimization of the stimuli responsive component of the BTDS obtained from evaluation of the fifteen formulations described in Chapter 6. Furthermore, the chapter focuses on the assemblance of the prototype device which consist of the backing layer, optimized stimuli responsive lyophilized matrix discussed in greater detail in this chapter and the nanofibrous mat (discussed in Chapter 4 and 5) incorporated within the stimuli responsive lyophilized matrix. Further detailed analysis is characterised on the BTDS followed by *in vitro* and *ex vivo* bioactive release kinetics. Of significant interest is the elucidation of the hydroxyl radical effect on the inflammatory behaviour of the device when a simulated pathological state is created.

Chapter 8 of this thesis demonstrates the *in vivo* performance of the device and provides a comparative analysis between the experimental groups, control, placebo and conventional systems. A detailed description of the methodologies undertaken to inflict a burn wound and the healing progression is presented on the selected Sprague Dawley Rat model. Highlighted

in the chapter are the nanofibrous mat and BTDS compatibility as well as the various intrinsic methods employed for wound healing determination.

Chapter 9 of this dissertation provides an overall conclusion of the inclusive outcome of this research. Future recommendations and outlook is also provided.

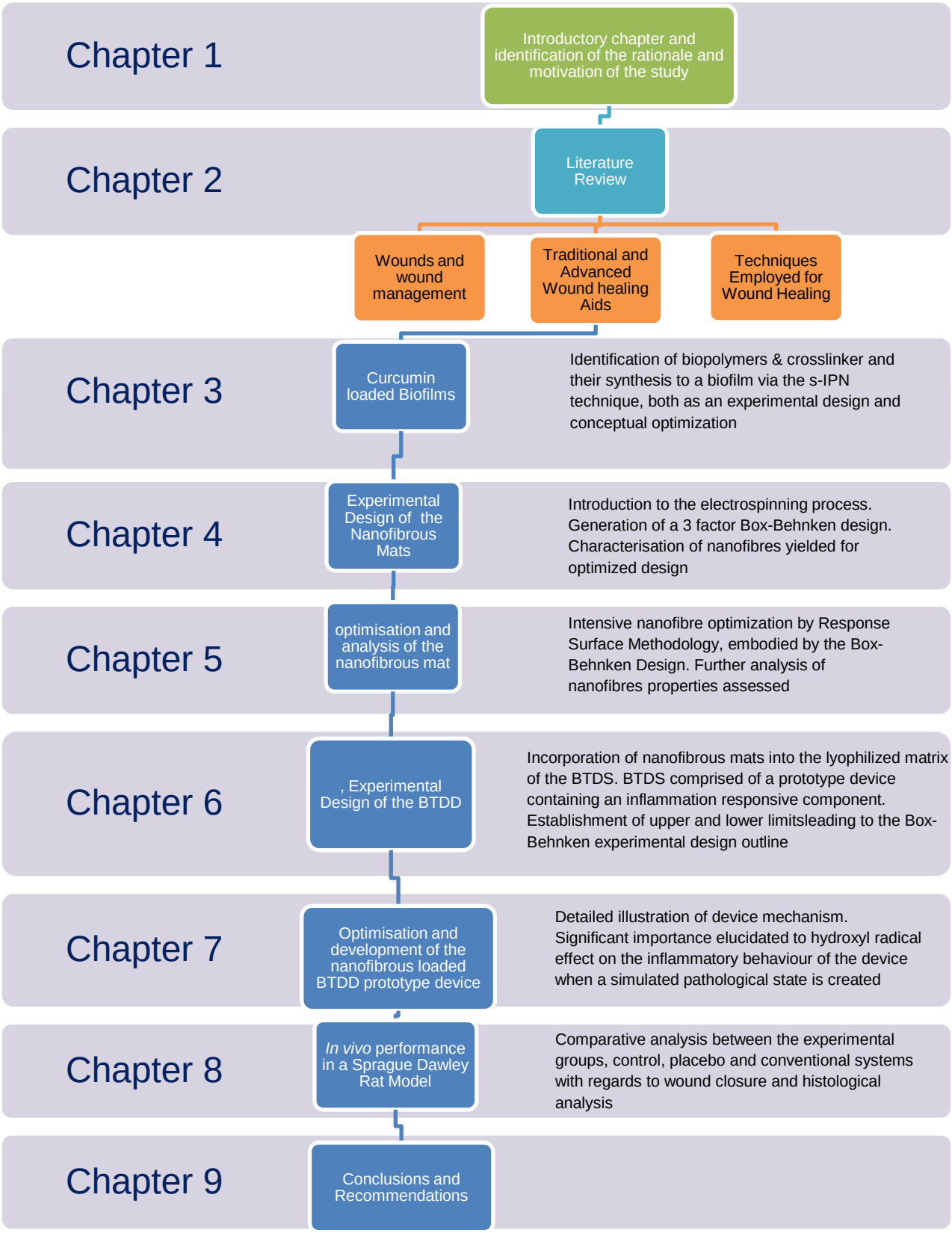

Figure 1.6: Schematic of the breakdown of each chapter in this thesis.

1.8. Concluding Remarks

In this chapter a description of the novel system developed is provided in terms of conceptualisation, structure and functionilisation of the various components of the Bioresponsive Transdermal Delivery System (BTDS). The chapter highlights the fundamentals of wound healing, challenges and difficulties needed to be overcome in order to ensure effective and enhanced healing. The chapter sought to provide a rationale for effective wound dressings and devices whilst the appropriate stimulus was selected for targeting bioactive delivery at the wound site (In particular delivery of the nanofibrous mat). The focus of the chapter was a description of the BTDS, with particular emphasis on the functioning and architectural structure of the various componential layers.

CHAPTER 2
A COMPREHENSIVE REVIEW OF ADVANCED BIOPOLYMERIC WOUND HEALING SYSTEMS

2.1. Introduction

The formation of creative ideas for the use and modification of delivery systems which will influence complex wound healing behaviours, such as proliferation, migration and differentiation of cells will promote novel opportunities for tissue regeneration and repair in the wound healing process. Many agents are pivotal and multifunctional, that is they are potent within the different stages of wound healing to ensure repair and regeneration (Shi et al., 2010) Synthetic polymer delivery systems that can control and sustain release are particularly promising as materials for enhancing tissue regeneration (Biondi et al., 2008) This review discusses the processes involved in skin regeneration and the state of the art in nanotechnology and polymer drug-delivery systems and their potential application for wound healing. The interdisciplinary field of nanobiotechnology, which combines biology, chemistry, engineering and medicine is revolutionising the development of drug-delivery systems and devices. Research in the area of drug delivery, tissue engineering and wound healing has provided unlimited potential to improve human health (Goldberg et al., 2007). Within the field of tissue engineering, drug delivery and wound healing, new dimensions can be envisioned with regards to enhancing the therapeutic effect and at the same time reducing risks and adverse effects. Developments in the field of nanotechnology involving nanomedicine, nanopharmacy, production of nanofibres, nanotubes and nanorods may promote novel opportunities for delivering wound dressings with efficient drug delivery (Broudriot et al., 2006; Patzke et al., 2002). Nanoscale delivery vehicles can enhance the therapeutic efficacy and enable new classes of therapeutics by encouraging the promotion of biologically active new molecular entities that were previously considered underdeveloped (Shi et al., 2010).

2.2. Physiology and Mechanism of Action of the Native Skin

The skin is the largest organ of the body which comprises about 8% of the human body mass and covers the entire external body surface. The surface area varies from person to person because of the variation in weight and height; skin thickness may also range from 1.5 to 4.0 mm (Chong et al., 2007). The skin plays a crucial role in many functions such as sensory detection and fluid homeostasis. It serves as an effective barrier against microbial invasion, and enables formation of a self-repairing and self renewing interface between the body and its environment. It is capable of protecting the body against thermal, chemical, mechanical

and osmotic damage, and has properties which allow for adsorption, selective permeability to chemicals and excretion (Chong et al., 2007).

The main skin components of interest for wound healing comprises of the epidermis, dermis and sub-dermal layers (Figure 2.1). The epidermis has a thin and highly cellular structure that forms the superficial layer of the skin. It is the outermost barrier having high impermeability, thus controlling water loss and serving as a barrier against external harmful stimuli. Underlying and separated from the epidermis by a basement membrane is the dermis. The dermis composes of collagen-rich extracellular matrix (ECM), elastin, fibroblast and glycosaminoglycans (Zhong et al., 2010). It provides flexibility and physical strength to the skin and supports the extensive vasculature, nerve bundles and lymphatic system. Throughout the dermis is a network of nerve fibres that serve a sensory role in the skin and influence immune and inflammatory responses (Chong et al., 2007). The hypodermis is the layer beneath the dermis and contains a large amount of adipose tissue that is well vascularised and contributes to both the thermoregulatory and mechanical properties of the skin (Cohen. 1983).

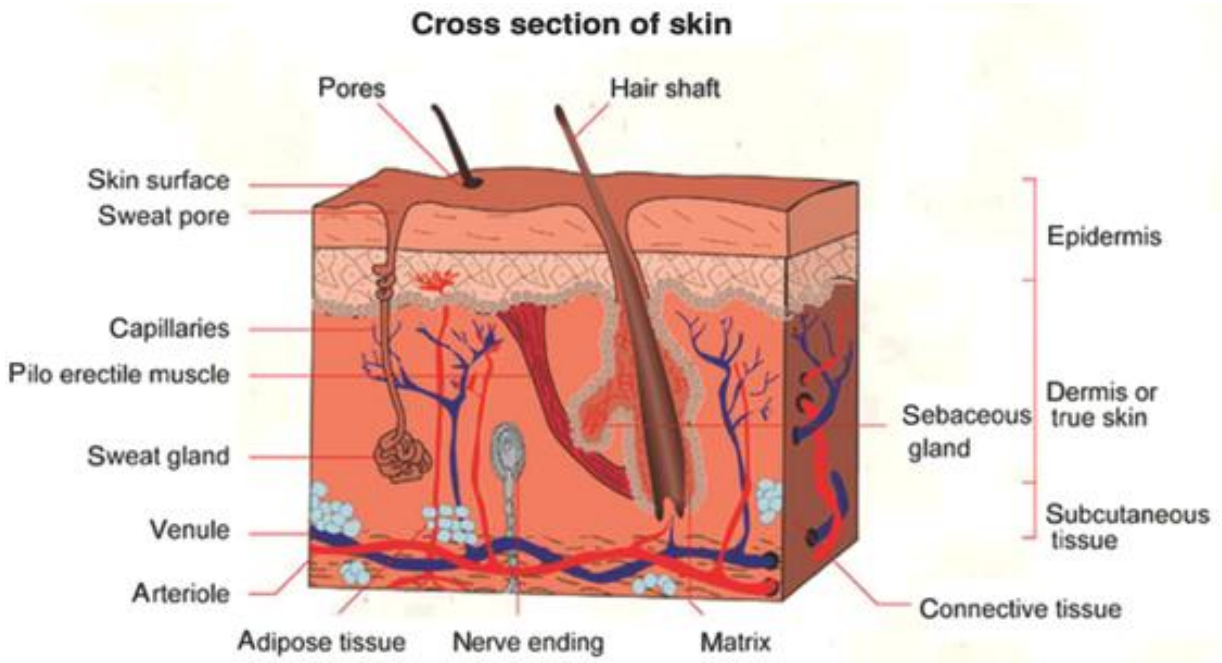

Figure 2.1: Image displaying the cross-section of skin (http://www.infovisual.info/0./0.36-en.html) (Access Date: 04/06/2014)

2.3. Wound Types and the Wound Healing Cascade

A wound can be described as a defect or a break in the skin which could be due to physical, chemical or thermal damage or as a result of an underlying physiological or medical condition which would then result in a disruption of the normal anatomical structure and function of the skin (Boatang et al., 2008). Figure 2.2 classifies the various forms of wound occurrence, furthermore wounds may be classified as acute or chronic on the basis of the wound healing process. Acute wounds are usually healable within a period of time and are caused by traumas that would result in abrasions, avulsions, incisions, contusions and lacerations. These categories of wounds are likely due to by mechanical damage or exposure to extreme heat, irradiation, and electrical shocks or corrosive chemicals. Chronic wounds occur as a result of a specific disease such as diabetes, which could lead to ulcers, severe physiological contaminations and tumours. Unlike acute wounds, these wounds could take a long period of time usually exceeding 12 weeks to heal and reoccurrence is not uncommon (Shanmagasundaram et al., 2005). Trauma to the skin is subsequently followed by the beginning of a regime of an organised and predictable sequence of events that has a cascade effect until the wound is bridged by scar tissue regeneration that binds and holds the wound in stasis (Mallefet and Dweck, 2008). The cascade of events initiated by skin trauma, involves three phases that is immediate and works towards repair as shown in Figure 2.3.

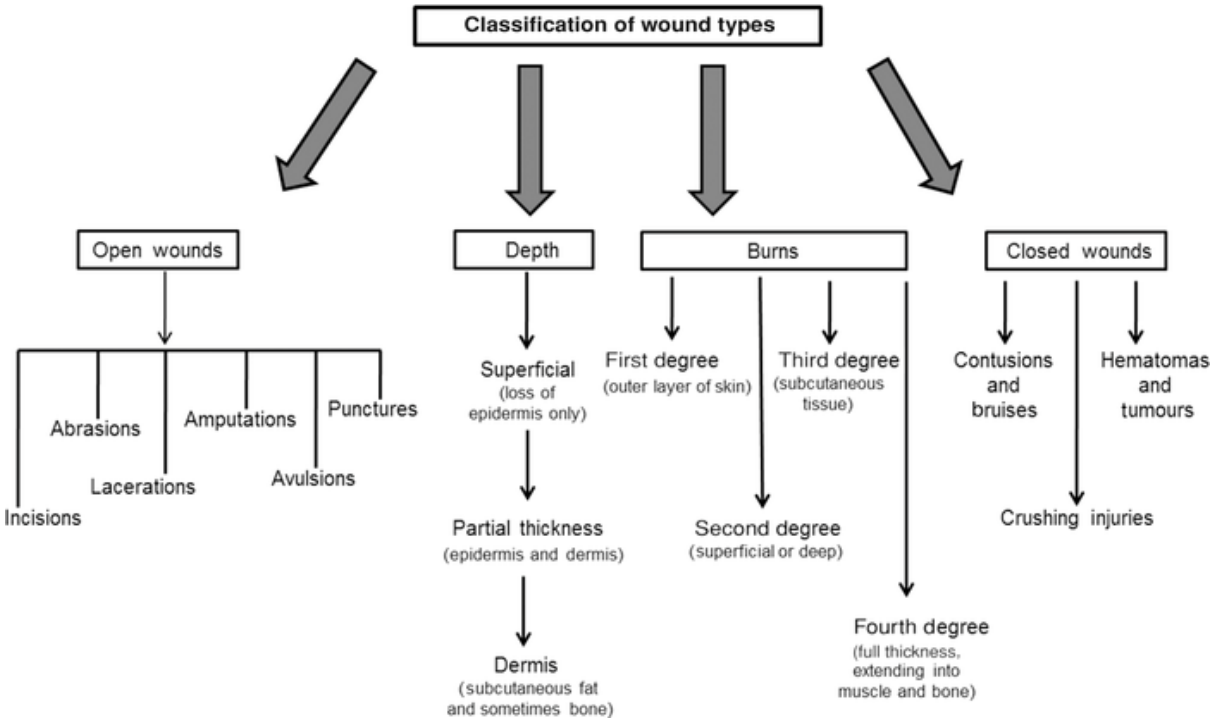

Figure 2.2: Classification of wound types

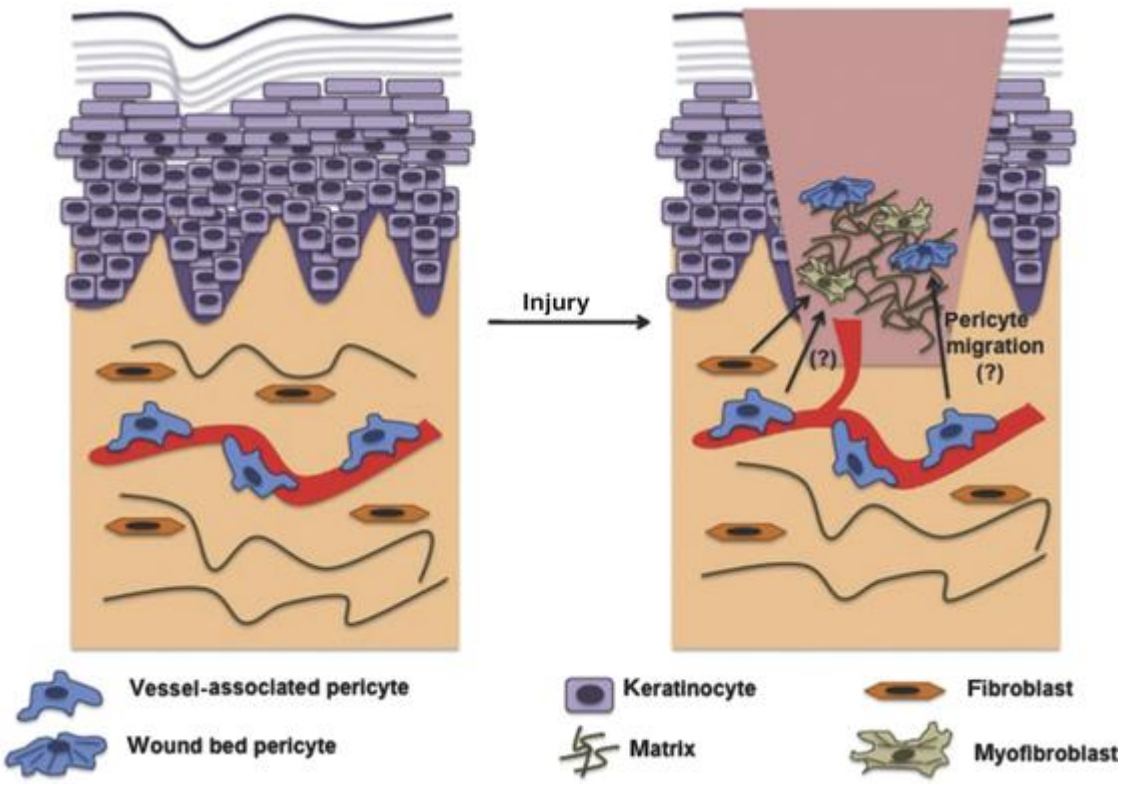

Figure 2.3: Infiltration of various factors for the process of wound healing. Reproduced with permission from Elsevier BV Ltd©_ 2012.16

Wound healing is a dynamic interactive process that involves parenchymal cells, ECM, blood cells and soluble mediators. The three phases involved in wound healing can be classified as the inflammatory, proliferative and the tissue remodelling phase which is outlined in Figure 2.3 (Madhumathi et al., 2010).The healing cascade begins when the inflammatory phase prepares the area of injury for healing by immobilising the wound and causing it to swell and become painful (Mellefet and Dweck. 2008). Bleeding occurs at the injury site to ensure removal of toxic waste and activation of homeostasis begins which is initiated by exudate components. The clotting mechanism is elicited by platelets and this results in coagulation and the formation of a fibrin network. The inflammatory phase also results in vasodilation and phagocytosis whereby histamine and serotonin is released. Phagocytes enter the wound and engulf dead cells and platelets are liberated and form aggregates as part of the clotting mechanism (Boatang et al., 2008).

The proliferative phase involves the proliferation of epidermal cells at the wound margin behind the actively migrating cell (Singer et al., 1999) whereby cells travel about 3 cm from the point of origin in all directions. This process usually occurs 2 days to 3 weeks following injury and results in the formation of granulation tissue at the wound space. Granulation is the effect of fibroblasts and macrophages providing a continuing source of growth factors necessary to stimulate angiogenesis and fibroplasias (Singer et al., 1999). This result in a

bed of collagen that helps fill the defect whereby wound edges pull together and new capillaries are produced. The final stage is known as the remodelling stage and usually begins three weeks post injury up to 2 years. Remodelling of dermal tissue to produce greater tensile strength whereby new collagen is formed is the main aim of this phase. The principle cell involved is the fibroblast. Collagen molecules begin to form whereby it undergoes further modification and molecules begin to form in a characteristic triple helical structure. Collagen is released in the extracellular space whereby stable cross-links are formed. As collagen matures at the wound site more and more intra-molecular and intermolecular cross-links are formed. Cross-linking gives collagen its strength and stability over time; however, the tissue will never regain the properties of uninjured skin (Sibbald et al., 2003) Figures 2.4 and 2.5 briefly illustrate the process of healing associated with the wound healing cascade (Dulmovits et al., 2012; Stein and Kutcher. 2013).

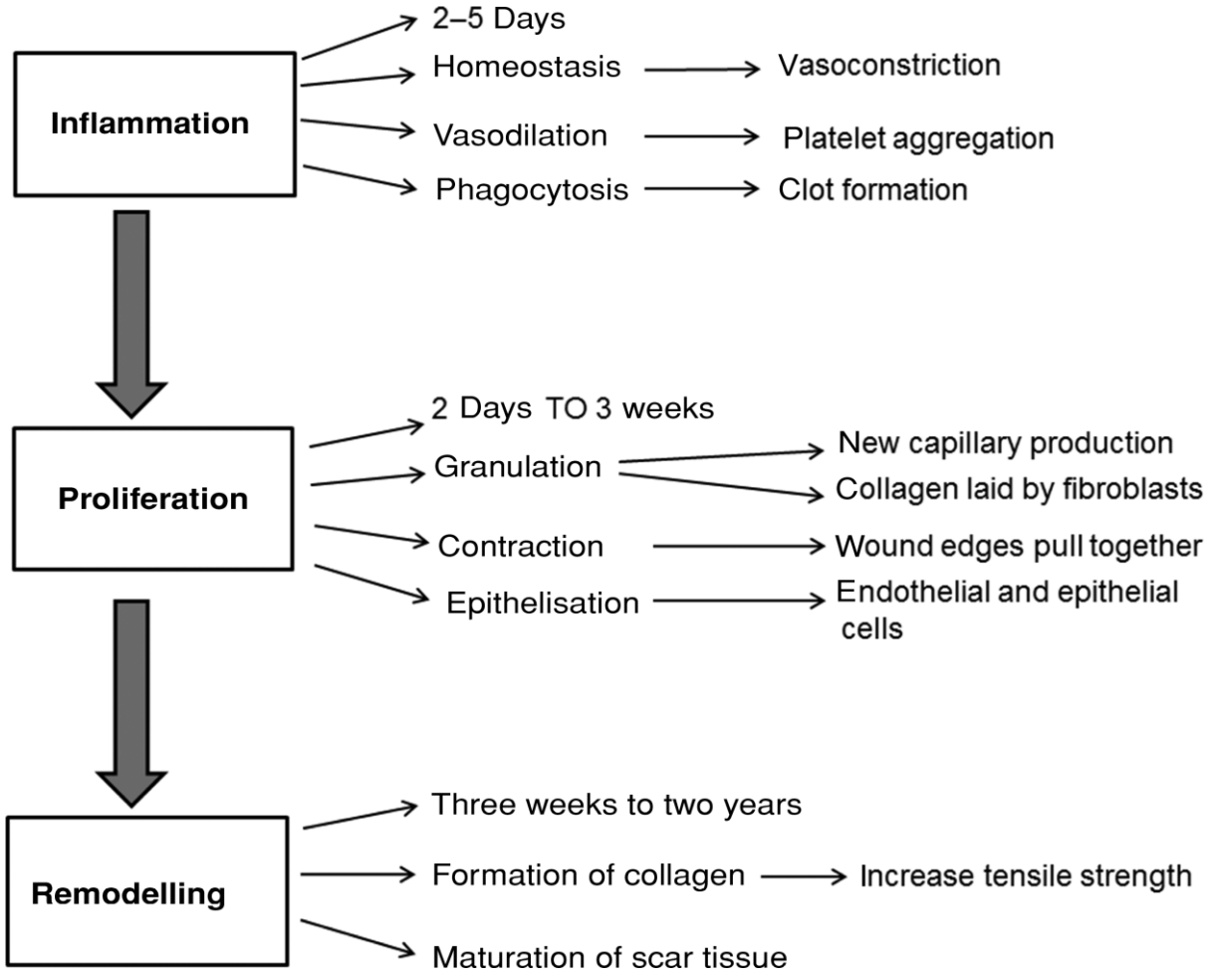

Figure 2.4: The major stages undertaken by the body's defence mechanism during the process of wound healing

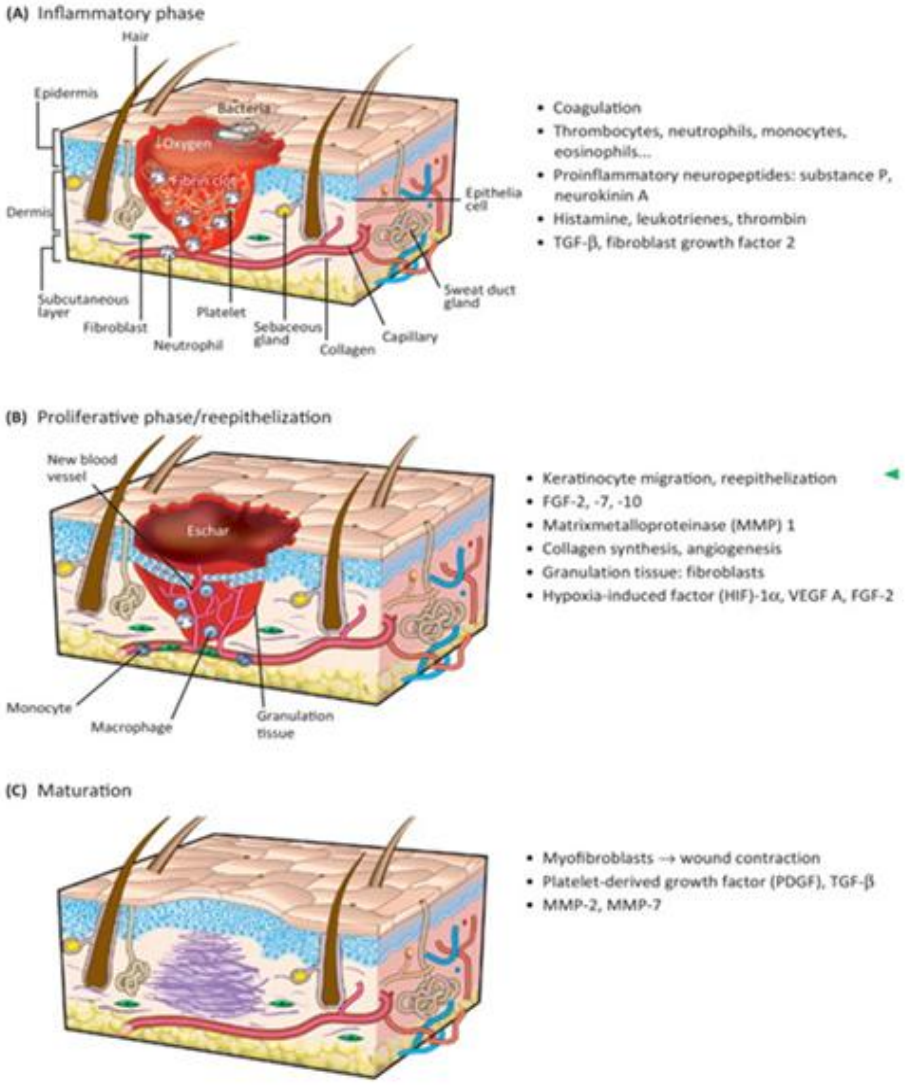

Figure 2.5: Cell mediator's interactions at the wound site to promote proliferation and remodelling of skin tissue. Reproduced with permission from Elsevier BV Ltd© 2013.

2.4. Wound Care and Management Aids

The objective of wound management is to heal the wound in the shortest period of time that is possible with minimum pain, discomfort and scarring to the patient (Jannesari et al., 2011). The successful treatment of a wound should ensure that the formation of scar tissue is minimal, the amount of necrotic tissue produced is reduced and microbial invasion is prevented. In the past, wound management involved simple principles such as 'to cover and conceal'. Materials used for wound management such as simple gauze materials were passive products that did very little to encourage the wound healing process, as limited attention was given towards the requirements of a wound healing environment or the functional performance of wounds. In recent years, the treatment of wounds has been revolutionised because of a greater understanding of the underlying molecular and cellular abnormalities that prevent the wound from healing. An approach to ensure that the pharmacological, mechanical and pharmacokinetic requirements of wound healing are met

will provide a novel approach, to remove these barriers to natural healing and enhance the effects of advanced therapies (Schultz et al., 2009).

The ability of the skin to repair itself after a minor injury is a remarkable process; however, when the damage is severe or occurs in large amount of skin area, appropriate and immediate coverage of the wound area with an optimal device or adequate dressing is essential to protect the wound and accelerate wound healing. Ultimately, immediate wound coverage and protection is the principle goal of wound care management (Bindu et al., 2010). To promote and ensure effective wound management many factors involved in the wound healing process need to be taken into account. The introduction of the 'TIME concept' provides the basis to which appropriate wound management can be effectively understood.

T—deficient and non-viable tissue can physically impede the migration of wound cells across the wound bed and act as a focus for infection.
I—uncontrolled inflammation and infection may perpetuate a cycle of repeated injury and insult to the wound area. This needs to be corrected in order for cellular migration to proceed during the wound healing process.
M—both, excess moisture and wound desiccation may impede the wound healing process. Desiccation may impede cellular migration and wound contraction, whereas excess moisture may result in maceration of the wound bed and surrounding tissue.
E—the formation of a migrating epithelial edge is a visible sign that healing is taking place, whereas a non-migrating edge is a signal showing poor healing properties (Granick et al., 2006).

This concept provides a systemic approach to assessing and treating wounds with the aim of restoring the biochemical environment that stimulates healing and it provides the necessary concepts required for the design of advanced wound healing devices.

Wound management aids are available in a variety of physical forms such as hydrogels, xerogels, tissue engineering, hydrocolloids, skin scaffolds, films, lint and gauzes (Lloyd et al., 1998; Boatang et al., 2008). The various type of wounds require different environments and properties for effective healing thus the physicochemical and clinical properties of various wound healing dressings and devices must be designed in order to suite the requirements of the TIME philosophy mentioned above. The functions and desirable characteristics of wound healing devices and dressings are summarised in Figure 2.6 include debridement of the wound area, as this clears the wound of necrotic tissue and bacteria, to maintain a clean surface that will heal relatively easy. Debridement plays a critical role in wound healing as devitalised, necrotic tissue provides a focus for infection, impedes re-epithelisation, prolongs

the inflammatory phase and mechanically obstructs contraction of the wound surface. Debridement using mechanical methods such as application of the appropriate wound dressing is all that may be required to promote the first step of wound healing as assisted debridement accelerates the wound healing process(Schultz et al., 2003).Clinically the effects of wound healing dressings have a profound effect on the rate of healing. Moisture retentive dressings may accelerate the wound healing process as a moist wound/dressing environment facilitates the recruitment of vital host defences and the necessary cell population, such as macrophages which help promote wound healing. An amazing number of growth factors are elaborated by these cells creating a milieu characterised by increased fibronolysis, accelerated angiogenesis and connective tissue synthesis, prevention of cell desiccation and death, and an accelerated rate of healing which is promoted by the autolytic properties of a moist environment that rejuvenates and rehydrates desiccated skin and tissue. An added benefit of moist wounds and dressings is decreased pain at rest, during ambulation and patient convenience during dressing changes (Parsons et al., 2005). Removal of blood and excess exudates is an important factor affecting wound healing. Absorption of exudates is a significant characteristic of dressings and wound healing devices as excess exudates contain tissue degrading enzymes that block the activity and proliferation of cells and break down extracellular materials and growth factors thus delaying the wound healing process. The body tends to function optimally in an environment that mimics or is similar to its own environmental conditions, thus normal tissue temperature improves the blood flow to the wound bed promoting epidermal migration (Boatang et al., 2008). Insulation characteristics is a significant property of wound management aids, as maintenance of body temperature will be optimised thus accelerating the healing process under normal body conditions.



Figure 2.6: Functions and desirable characteristics of wound dressings and devices related to treatment clinical significance

Wounds often provide a favourable environment for the colonisation of microorganisms (Chambers et al., 1962; Brook. 1996; Adam et al., 1999; Bowler and Davies, 1999). In order to improve the process of wound healing, conditions that are unfavourable for microorganism growth is essential and thus an environment that is favourable for the host repair mechanism must be implemented (Canal et al., 2009). For more than a century, one of the major rationales for the prevention of infection was the application of a dressing to the wound site. Theoretically, dressings can protect the wound from gross microbial contamination and acts as a barrier between the wound and the outside world. The composition and properties of the wound dressing or device itself can play a major role in modifying the wound microenvironment (Falanga, 1988). An infected wound may give of an unpleasant odour and delay collagen synthesis, the inflammatory phase is also prolonged in the presence of microbials and epidermal migration is inhibited which results in further damage to the tissue (Boatang et al., 2008).Oxygen delivery is a critical element for the healing of wounds as the formation of wound granulation tissue is increased, epithelisation and fibroblast formation as well as wound contraction and secondary closure is accelerated (Kallaiinen et al., 2003).

Oxygen is an essential nutrient for cell metabolism, thus under hypoxic conditions wound healing is delayed as a result of reduced granulation and epithelisation processes. Therefore, a desirable characteristic of wound dressings and devices is effective gaseous exchange of both water and air, whereby exudates can be effectively managed by the permeability of wound dressings to water vapour. In addition to the above, wound management aids should also ensure low adherence to the wound site, thus preventing trauma, pain and further injury to the wound site. Adherent dressings can result in further tissue damage at the injury site and can be agonising and difficult on removal. The economical factors also need to be considered, to ensure cost effectiveness and a low frequency of change (Boatang et al., 2008). In addition, an acceptable shelf life, acceptable mechanical properties that are compatible to topical application of dressings and at the same time the variation in degradation should be compatible with the healing process, that is, inflammation, regeneration and remodelling therefore matching the timeline for the healing process. When in contact with the skin surface, the material should not cause a toxic or inflammatory response, should provide permeability, convenience and be able to be easily metabolised and cleared from the body (Lloyd. 2002).

2.5. Components of Wound Management Aids

Wound healing and dermal substitution are areas in medicine where there have been many recent advances. The main component of every wound is the connective tissue matrix, thus there is an overall consensus that in order to effectively heals wounds, it is necessary to ensure the effective substitution of the main component (Ruszczak. 2003). Wound dressings are an essential part of wound management and care to ensure the enhancement of the natural wound healing process, thus new material technologies are evolving in this field. The development of new intelligent dressings is underway, that promise to play an active role in modifying and promoting healing of both acute and chronic wounds (Atiyeh et al., 2002). Wound dressings are usually classified according to their nature of action as: (i) passive products, (ii) interactive products and (iii) bioactive products. Gauze and other traditional dressings such as Tulle are passive products, whereas polymeric films and foams which feature transparency, permeability to water vapour and oxygen and in some cases biodegradability are termed as interactive products. Advanced dressings that have the ability to transport active substances to the wound site by the design of dressings composed of materials having endogenous activity or by the delivery of active substances in wound healing are regarded as bioactive products. These products include collagen, proteoglycans, chitosan and alginates (Paul and Sharma. 2004). There has been transitions from simple wound management aids to advanced specialised devices with specific characteristics, such advanced wound dressings are infused with various components in optimised proportion, which may include polymers and hydrocolloids.

2.5.1. Polymers

When choosing a material for application in treatment of wounds, it must meet specific requirements. Of utmost importance is the biocompatibility of the material, as the material chosen must induce the appropriate response within the host organism. Current research has suggested the incorporation of bioactive materials as opposed to those that are inert, since the bioactive material can interact with the biological environment and influence activities such as the cells function (Paul and Sharma., 2004). A large variety of materials can be used, which may be classified as (i) natural, (ii) synthetic or (iii) hybrid. Within these subdivisions, in particular synthetic materials, one can further delineate materials as degradable and non-degradable materials. The degree of degradability within materials can be controlled by altering parameters such as polymer compositions and variation as well as the ratio of amorphous to crystalline segments (Kim and Park. 2006). Polymers are considered as potential material due to their amenability to chemical modification, resulting in defined chemical composition, potential for defined 3D structures and customised surface functionality (Sill and von Rectum. 2006). Several polymers are clinically used as therapeutics: synthetic polymers such as (poly(ethylene glycol), *N*-(2-hydroxypropyl) and methacrylamide co-polymers, natural polymers such as (dextran (*α*-1,6 polyglucose), dextrin (*α*-1,4 polyglucose), hyaluronic acid and chitosan, others include linear polyamidoamines and pseudosynthetic polymers [(the man-made poly (amino acids) poly(L-lysine), poly(L-glutei acid), poly(malic acid) and poly(aspartamides)] (Duncan. 2003). Polymers are suitable for drug delivery as they offer effective unlimited diversity in topology, dimensions and chemistry (Brocchini and Duncan. 1999). A vast range of polymer architecture is available such as graft, linear, branched, cross-linked, multivalent, dendronised and star-shaped polymers (Goldberg et al., 2007). Within particular interest for the management of wounds, polymers that can be used as skin culture substitutes may be tissue derived or synthetic.

2.5.1.1. Natural Polymers

Natural polymers can be classified as those obtained from natural sources such as animal, microbial and vegetable sources. They usually are of protein or polysaccharide nature (Qiu and Bae. 2006; Moura., 2013). Natural origins of these polymers make them suitable substitutes of the ECM and original cellular environment of the native skin. However, limitations to their applications are improvised as when isolated from animal and vegetable tissues, batch to batch variability and large heterogeneity are seen in addition to their high costs (Tabata. 2009; Sell et al., 2010). Disadvantages associated with the use of natural polymers, such as a high biodegradability can be overcome by modification with synthetic polymers. Natural polymers such as chitosan, collagen and gelatin can be successfully implemented to fabricate wound dressings with desirable properties, as polymers such as chitosan and similar substrates are the principle structural component of natural ECM

(Malafaya et al., 2007). Commonly used natural polymer is collagen that promotes healing by allowing attachment and migration. It is commonly used in medical devices as a coating or an implant. Other important natural biopolymers of increasing interest are hyaluronic acid which assists in providing scarless wound healing (Livesey et al., 1995; Balakrishan et al., 2006). Chitosan is one of the most abundantly found natural polymers suitable for the use in wound dressings as it not only aids the healing process but is biodegradable, biocompatible, non-toxic, bioadhesive, bioactive, non-antigenic, anti-microbial and at the same time possesses haemostatic effects (Duo et al., 2001; Qiu and Bae. 2006; Melcafe and Ferguson. 2007).

2.5.1.2. Synthetic Polymers

Synthetic polymers offer the advantage of overcoming many of the shortcomings seen in natural polymers as they can be synthesised and modified in a controlled manner according to specific requirements needed to produce constant and homogenous physical and chemical properties as well as stability (Zhong et al., 2010). However, they are biologically inert thus do not offer a therapeutic advantage as is seen in natural polymers. Commonly used synthetic polymers for wound dressings include polyvinyl alcohol (PVA), which has the capability of being favourably moulded in many dressing forms such as foams, films, particles, sponges and fibres. Additionally PVA can also provide excellent water absorption, mucoadhesion and oxygen permeability (Bourke et al., 2003; Perez et al., 2012). Other commonly used synthetic polymers include polyethyleneoxide (PEO) and polyethyleneglycol which serve an advantageous purpose in the healing process as they are non-toxic, biocompatible, non-immunogenic, hydrophilic and flexible and can further be used to incorporate mediators such as growth factors to assist the healing process (Lee and Mooney., 2001; Kim et al., 2008; Zhong et al., 2010). Tissue regeneration and wound healing applications can further be promoted with other beneficial synthetic polymers such as polycaprolactone which is biodegradable and compatible and reduces inflammatory infiltrate, polyurethane (PU), poly lactic acid, poly vinyl pyrrolidone polyglycolic acid (PGA), poly(lactic-co-glycolic acid) (Qiu and Bae. 2006).

2.5.1.3. Interpolymer Complexes

Novel polymer combinations can be used to form scaffolds, wound healing meshes and films with improved mechanical, biological and chemical characteristics by hybridising polymers of natural origin with those that are synthetic and biodegradable (Slaughter et al., 2009). Combination of polymers allows for the integration of both polymer types thus exhibiting the advantages of both polymers, as ideally the most important features that polymers and biomaterials possess can be combined in a delivery systems for wound healing. Because of the range and complexity of polymer substances currently used, an ideal system cannot be

considered as one polymeric system. In order to achieve this, a wide range of biodegradable materials with specific and unique characteristics need to be developed (Kim et al., 2001). Current research efforts have focussed on the development of tailor made and custom designed biodegradable materials for specific applications with novel resorbable biomaterials by attempting computational and combinatorial approaches, development of biomimetic polymer structure with unique chemistries thus increasing diversity (Nair and Laurencin., 2007). Tsao and co-workers (2011) reported the use of a polyelectrolyte complex which consists of chitosan and γ-poly (glutamic acid) (γ-PGA) as a wound dressing material. This complex combination allowed the exhibition of good mechanical properties, suitable moisture content and favourable removal without the damage of regenerated tissue. Kim and co-workers (2003) also reported the use of chitosan with polyxamer to form a suitable wound dressing. In addition, a semi-interpenetrating polymer network was further introduced to provide enhanced compatibility and mechanical strength. Novel wound dressing applications have been improvised by novel bioprocesses and advances in organic chemistry, thus enabling the development of novel enhanced smart polymers as candidates for specialised and unique wound dressings that elicit favourable, biological, physical and chemical responses (Nair and Laurencin., 2007).

2.5.2. Hydrocolloids

Hydrocolloid dressings are amongst the most widely used dressings and are based on the modern dressing technology principle of creating and maintaining a moist wound environment. The term ‘hydrocolloid' describes the family of wound management products obtained from colloidal materials that are gel forming agents combined with other materials such as elastomers, gelatine, pectin, carboxymethylcellulose and adhesives. These agents may be bonded together to produce a thin film, sheet or foam with the properties of hydrocolloids, whereby a gel is formed on the wound surface to promote moist wound healing. Hydrocolloids are useful clinically because unlike other wound healing dressings, they adhere to both the moist and dry sites (Boatang et al., 2008). Cross-linkage of materials used in dressings influences the viscosity of the gel formed. Hydrocolloids are virtually impermeable to water vapour and air as they contain an occlusive outer covering that prevents water vapour exchange between the wound and it’s surrounding; however, as the gel forms, they become progressively more permeable to air. Their properties of impermeability made them effective dressings for rehydration and autolytic debridement in the past; however, recent research suggests dressings with good water vapour permeability and gaseous exchange are characteristics for optimal wound healing. Pain associated with wounds may be reduced by the use of hydrocolloid dressings as their barrier and non-adherent properties at the wound site allow patients to bath shower and maintain their daily activities without the risk of wound contamination. Hydrocolloid dressings are also available

as fibres in the form of a non-woven flat sheet that is hydrophilic. On exposure to moist surfaces such as wound exudates, they tend to form a soft coherent gel sheet from the previously dry dressing, thus making them effective dressings for wounds that produce a large amount of exudates. These dressings are referred to as hydrofibre dressings (Jones et al., 2006).

2.5.3. Bioactives and Drugs

Topical wound treatment aids are designed to overcome and rectify both structural and physiological imbalances, thus promoting a homeostatic environment at the wound site. Novel complex biodegradable systems can be modified to incorporate many active compounds to facilitate the provision of homeostasis and these features by incorporating actives agents such as anti-biotics, anti-inflammatories, anti-septics, antibodies and other bioactives. In the treatment of wounds caused by ulcers, Rayment and co-workers (2008) reported the use of tetracycline, doxycycline, bisphosphonate and hydroxamic acid as a protease inhibitor to inhibit high levels of excessive proteolytic activity namely MMP activity found in chronic wound fluid that have a negative impact on the influx of growth factors which positively influence the healing process. Curcumin which is a natural product derived from the rhizomes of *curcuma longa* has widely been used in the treatment of inflammatory conditions for centuries in indigenous medicine. Li and co-workers (2001) have shown the use of curcumin as an anti-oxidant and anti-inflammatory agent loaded into a nanoformulation of methoxy poly (ethylene glycol)-graft-chitosan composite film. Combined therapy which allows the use of drugs with different therapeutic outcomes and pharmacological actions ensures the inflammatory response is to the minimum and optimum allowing rapid healing. Combinational treatment using antibiotic drugs such as streptomycin prevents and treats infection whilst the concurrent administration of anti-inflammatory drugs such as diclofenac can relieve the swelling and pain associated with injuries and wounds by targetting the inflammatory phase of wound healing (Pawar et al., 2013).

Inherent in the process of normal wound healing is the involvement of endogenous growth factors. Insulin-derived growth factors, platelet-derived growth factor (PDGF), epidermal growth factor (EGF) and transforming growth factor (TGF) amongst others contribute to the process of homeostasis regulation, cytokine attraction, restoration and repairment of tissue and remodelling of the wound site (Miller. 2009). To improve the healing outcome, a foundation for therapeutic intervention must be instilled. For successful healing, the cell–matrix and cell–cell interactions are fundamental whereby a balance is maintained by cytokines and growth factors, thus regulating cellular migration, adhesion and proliferation to a large extent (Kiwanuka et al., 2012). Within the clinical practice, growth factors are been employed to accelerate the healing process and to ensure rapid and full recovery that is

clean and scar free (Judith et al., 2010; Bao et al., 2009; Pawar et al., 2013). Growth factors can be integrated in wound healing delivery systems as the healing cascade involves continuous and dynamic processes in a step by step manner. Accelerated or retarded tissue repair can be influenced by various factors and cells. Some of these include growth factors such as epidermal growth factors (EGF), TGFs, fibroblast growth factors (FGFs) and PDGFs. These growth factors play a crucial role as critical modulators that have the capacity to orchestrate all events occurring within the wound healing cascade.

Epidermal growth factors have successfully been used in the process of wound healing by enhancing proliferation, cell motility as well as mesenchymal and epidermal regeneration (Hardwicke et al., 2008). However, with regards to superficial wounds, a limitation exists with the use of EGF in that they have a limited transdermal permeability, which does not allow for further distribution to the stratum corneum and underlying dermal stem cell layers thus compromising optimal healing (Cohen. 1983; Tolino. 2011). This is largely due to their large size and hydrophilic nature. Choi et al (2012) prepared a system by employing recombinant technology whereby a low-molecular-weight protoamine (LMWP) was conjugated to EGF thus allowing enhanced transdermal properties. LMWP is an arginine-rich cell penetrating peptide that has the capacity to deliver large molecules such as proteins and gene products into the cells (Park et al., 2005; Gurther et al., 2008). TGFs and PDGFs display chemotactic and mitogenic properties during the inflammatory phase whereby they mediate chemotaxis of neutrophils, fibroblast and macrophages at the wound site. Both TGF and PDGF can be incorporated into wound dressing systems simultaneously in order to provide an additive therapeutic effect (Pierce et al., 1991; Robson. 1991). To determine the effects of growth factors, a wound model was designed by Mustoe and co-workers (1992) by creating an excisional defect measuring 6 mm on a cartilage of a rabbit. A PDGF-BB system composed of a PDGF-B dimer was applied to the wound area to determine healing progress. The influence of the growth factor system resulted in an increased volume of granulation tissue at the wound site comprising greater deposition of both glycosamine and hyaluronic acid. The addition of TGF showed a further increase in granulation tissue together with the formation of new and increased collagen. Thus, it can be deduced that growth factors such as TGF play an active role in stimulating inflammation and angiogenesis, whereas other factors such as FGFs ensure the presence of fibroblast within the collagen matrix at the wound site to promote homeostasis. In addition, PDGF play a chemotactic role for fibroblast and allow mutagenesis of mesenchymal cells (Cromack et al., 1990; Mustoe et al., 1991).

However, many factors need to be taken into account when designing delivery systems incorporating growth factors as they may significantly affect the therapeutic efficacy. Most growth factors in their native form are susceptible to degradation on administration and have

low membrane permeability. In addition on manipulation, these proteins are easily denatured and may cause multiple side effects if administered in high or multiple doses to reach a desirable therapeutic concentration. Wound healing is a dynamic and complex process whereby many intricate processes involved may overlap. Thus, it is essential to ensure that the precise growth factors are elected when designing a delivery system. Chen and co-workers, 2010 have reported the possible inhibitory effects of growth factors on wound healing when delivered in combination or alone. *In vivo* models on spontaneous bone healing have shown the reduction of bone formation in comparison with controls when treated with TGF-β and BFGF. Thus, the efficacy of recombinant human TGF-β1 delivery can also be challenged as it is found to have proliferative effects only on cells already involved in the osteoblastic lineage. This suggests that inhibitory effects may be induced on osteoblast formation *in vivo*. Combined growth factor delivery such as BMP-2 and IGF-1 has also demonstrated inhibitory effects on bone healing and osteoblast differentiation under *in vivo* and *in vitro* conditions. Thus, it can be seen that critical considerations need to be taken into account when designing a growth factor incorporated delivery system or recombinant delivery systems as these findings are due to adverse combinations. Thus, inappropriate growth factor combinations can lead to undesirable outcomes when erroneous stimulations causing signalling of multiple cascades occur (Chen et al., 2010). Regulation of cutaneous healing has been extensively researched with regards to their cellular and molecular function. However, the cell to cell communication and intracellular systems involved in the effective repair of cutaneous wounds have not been established. Thus, all aspects of the wound healing response cannot be effectively mediated by a single exogenous agent; therefore combinational drug therapy is required.

The platelet is a rich source of a complex group of growth factors. Moreover, they have the ability to assist in clot formation warranting cessation of local lymph and blood loss together with recruiting crucial cytokines and growth factors that induce and accelerate the healing process. Recruitment of growth factors as active healing agents from platelets occurs upon its degeneration caused by proteins (Carter et al., 2003). The use of a platelet gel will infer significant advantages to the process of wound healing. A platelet gel is a hemocomponent that can be obtained by associating cryoprecipitates and activated hyper-concentrated platelets. Within a platelet gel, growth factors can be released to procure clinical healing processes whereby homeostasis and tissue regeneration can be restored (Crovetti et al., 2004). Kazakos and co-workers (2009) have shown a platelet gel to be effective as a drug-delivery system that promotes homeostasis, angiogenesis and remodelling by sensitivity to growth factors. Platelet-rich gels have been reported to be effective in chronic non-healing wounds and acute soft tissue wounds. Patients treated with platelet-rich gels initiated adequate tissue regeneration and faster healing rates (Kazakos et al., 2009).Platelets serve

as specialised secretory cells that have the ability to release a large number of biologically active substances such as growth factors upon activation thus modulating the healing process (Sandri et al., 2011). Growth factors influence many processes involved in tissue repair which include chemotaxis, cellular proliferation, angiogenesis as well as the synthesis of the ECM (Sandri et al., 2013).Of paramount importance is the development of a suitable therapeutic vehicle that will allow the release of growth factors according to the wound healing requirements. This is of great significance as the efficacy of hemoderivate growth factors critically depends on the way they are made available to the injury site. Platelet-rich plasma can be employed to provide a therapeutic effect by activation and preparation of a 'lysate'. This process involves the destruction of platelets by freeze–thawing and the attainment of bioactive molecules, which begins in a platelet-rich plasma sample in the presence of anticoagulant agents. Platelet lysate can be prepared from donors (allogenic) or from the patients themselves (autologous) (Sandri et al., 2013). Clinically, platelet lysate has been shown to be effective in the healing of oral mucositis and occipital decubitus ulcers. Furthermore platelet lysate has been proven capable in promoting the healing process in corneal and buccal lesions (Caramella et al., 2011). Rossi and co-workers (2013) successfully demonstrated the use of a sponge-like dressing to deliver platelet lysate in the treatment of chronic wounds and concluded that platelet-rich preparations have the capacity to release their complete pool of biologically active substances.

Many challenges are faced when designing a delivery system or wound dressing that will ensure adequate and optimal therapeutic effects. These challenges include high viscosities, over adhesion and phase separation. In addition, many physiological factors can impose an undesirable effect when dealing with wound healing. One such factor would be fibrosis and excessive wound contraction of injured skin that may result in a fibroproliferative state causing limited or suboptimal use of the site infected together with the presence of hypercontractile scars. Mast cells, released during the healing process, regulate the healing process; however, when in excessive amounts, can result in hypercontractility, fibrosis and fibrotic scars. Thus, Gallant-Behm and co-workers (2008) introduced the use of a stabiliser known as ketotifen at wound healing sites, thus decreasing the rate of wound contraction and avoiding unwanted fibrosis. Other stabilisers that are shown to be medically useful include Lewis acids such as nitric oxide, sulphur dioxide and boron triflouride (Gallant-Behm et al. 2008). Another class of stabilisers include free radical stabilisers such as catechol, hydroquinone, monomethyl ether hydroquinone, monoethyl ether hydroquinone and nitrhydroquinone. Sulphonic acid and sulphur dioxide have also been shown to display anionic stabilising effects when in combination (Asbill and Mickmack. 2000).

Anti-oxidants, anaesthetics, analgesics and preservatives are other incorporates that can be included in wound healing dressings. The addition of such substances may enhance the overall therapeutic outcome of wound dressing delivery systems. Li and co-workers (2002) have stated the use of anti-oxidants such as alkaloids, triterpenes and flavanoids as an application to prevent oxidative stress that may result in further pathogenesis due to lipid peroxidation and free radical scavenging. Anaesthetics such as lidocaine and bupivacaine can be used at the wound site either incorporated within wound dressings or injected at the injury site to reduce the pain associated with open wounds. Minor dermal lacerations can be treated with an anaesthetic known as tetracaine–epinephrine [adrenalin]–cocaine (TAC) topically. Anti-inflammatory agents such as NSAIDS and corticosteroids can be used in dressings to prevent progressive inflammatory damage thus promoting speedy healing (Shah. 1994).

2.6. Employment of Cell Based Therapies for Wound Healing

2.6.1. Gene Therapy in Cutaneous Wound Healing

Advances in cell biology have led to the identification of various factors such as growth factors and their receptors and genetic therapy. Recent research interest has found the skin to be a significant target for gene therapy. Gene therapy involves the insertion of a gene into the recipient skin cells that acts as a vehicle. Possible application of gene therapy is made simpler by the cultivation and harvesting of fibroblasts and keratinocytes. There are two basic strategies that can be implied for the introduction and expression of foreign DNA and genetic material into host cells. These strategies include genetic medicine whereby short-term expression of a gene product is transformed and permanent insertion of genetic material such as DNA at the target site (Khavari et al., 2002). The delivery of genes can be conducted under either *in vivo* or *ex vivo* conditions. *Ex vivo* delivery involves a technique whereby transplantation of genetic material to the host can be done upon cultivation and isolation of selected cells with their transfection *in vitro*. *In vivo* techniques employ a direct introduction to genes to the target tissue (Sprugel at al., 1987).

Classification of gene delivery systems employs two procedures namely viral or non viral vectors. Viral techniques involve the use of viruses as natural vehicles for gene delivery. The technological strategy involved in this technique is to generate a replication-defective particle by replacement of some viral genes with the gene of interest conveying the desired therapeutic effect (Kootstra and Verma. 2003). ‘Packaging cells' are specialised cell lines which may be engineered to restore recombinant viruses when a viral gene is removed. The development of therapeutical gene vectors can be can be approached by the modification of several types of viruses. These include retroviruses and lenti viruses as non-lytic replicators.

Lytic receptors are also employed such as the herpes simplex virus, adeno-associated viruses and human adeno viruses. Non-lytic replicators leave the host cell relatively intact and are created from the cellular membrane of infected cells, whereas lytic replicators involve the release of a virion upon the collapse of a host cell after infection (Branski et al., 2009). Several authors have described the successful use of viral vectors in cutaneous wound healing. Platelet-derived growth factor B (PDGF-B) was transferred to an adenoviral vector in a chronic wound of a rabbit ear by Liechty and co-workers (1999). Findings showed accelerated and rapid re-epithelisation of the wound site on comparison with control groups (Galeano et al., 2003). Furthermore epithelisation regeneration and neo-angiogenesis can be accelerated by a gene–vector combination of vascular endothelial growth factor A (VEGF-A) and serotype 2 of Adeno-associated viruses as reported by Deodato et al., 2002; Galeano et al., 2003 and Branski et al., 2009. Viral vectors play a significant role in gene therapy as they are the most established and original. Successful applications for cutaneous wound healing have been made possible by the use of viral vectors. However, of particular concern with the use of virus-mediated gene transfer models is the risk of both systemic and local infections and transfection efficacy. The production of viral vectors is also cost and time consuming (Branski et al., 2009).

An alternative approach employed is the use of non-viral vectors whereby genes are injected directly into the skin. However, employment of the native DNA constructs show low transfection efficacy, undergo degradation easily and have limited penetration into cells due to their electrical charge and large size (Vogel. 2000). Advantages of this type of therapy include the delivery of genes to target cells without the repeated exposure to viral vectors and cellular damage. In addition, prevention of recombination with wild-type viruses is also avoided. On a large scale, non-viral vectors are easier to manufacture employing plasmids constructs grown with existing fermentation technology (Ortiz-Urda, 2002). Modification of these vectors are required due to their drawbacks as discussed above, thus techniques such as ‘micro-seeding', ‘gene-gun', extrapolation and the use of cationic liposomes can be employed. ‘Micro-seeding' involves the use of solid needle mounted on a modified tattooing machine to directly transfer the desired gene to the target cell. However, transfection using this method was only observed in superficial layers (Eriksson et al., 1998). The ‘gene-gun' method infers gene propellation into skin cells via the use of tungsten or gold-coated particles. This method has reported successful transfection results whereby significant improvement in wound healing was noted when gene gun particle mediated transfection of different PDGF isomers utilised (Eming et al., 1999). Cationic liposomes are surrounded by negatively charged DNA strands that offer protection. These complexes are synthetically prepared and contain a positively charged surface. Uptake of these complexes occurs by endocytosis when the net positive charge of liposomes binds to the negatively charged cell

surface (Felgner and Ringold. 1989). Thus, genes encapsulated in liposomes may be applied by direct injection or topically. Studies utilising IGF-I cDNA transfected in animals revealed increased basal skin proliferation in wounded tissue (Jeschke et al., 2000). The extrapolation technique utilises electrical field induction with simultaneous administration of growth factors and plasmid DNA. Lee and co-workers (2004) reported the use of electropolation in combination with tissue growth factor β1 in diabetic mouse wound models. An increased rate of re-epithelisation, angiogenesis and collagen formation was reported (Lee et al., 2004; Branski et al., 2009).

2.6.2. Stem Cells and Wound Healing

Wound healing is a dynamic process that integrates complex molecular and biological events during the healing cascade involving inflammation, proliferation and remodelling. The creation of a complex viable skin substitute is of significance, however, is difficult and challenging to reconstitute. A complex structure can be created by the use of stem cells as they have the ability to differentiate into various tissue types by asymmetrical replication. Moreover they can prolong their self-renewal capacity. Stem cells can be isolated from a variety of sources which include the bone marrow, adipose tissue, umbilical and peripheral blood as well as skin and hair follicles (Branski et al., 2009). These cells have the ability to modulate healing responses in both acute and chronic wounds. Stem cells show promising results in cutaneous wound healing as studies have shown the persistence of stem cells originated for eleven months post grafting (Flowers. 1990). Furthermore, these stem cells initiated from male cells show potential effects in female hosts thus suggesting that stem cells have the ability to differentiate in a variety of tissues and exist in all tissues (Cairns. 1975). Furthermore, they have a very long life. Han (2005) have reported the acceleration of wound healing on application of human bone marrow stromal cells *in vitro*. Dermal reconstitution was achieved by the development of new elastic fibres of treated wounds by Falanga (2005) Human autologous bone marrow-derived cultured cells were applied to non-healing and acute wounds. Thus, it can be seen that stem cell therapy has made a significant contribution to the study of the basic mechanisms of cell proliferation, differentiation and remodelling. Stem cells thus offer an alternative approach to reconstitute wounded structures as they have been proven effective in the development of cellular therapy.

2.6.3. Gap Junction and Connexin 43 Mimetic Peptides in Wound Healing

Research and development in drug-based therapies have led to the introduction of diverse pathways with dynamic complex mechanisms that promote the healing processes. Recent studies have indicated that targetting of gap junctional connections in wound healing pathways may provide an unexpected breach to scar free healing. Between cell gap junctions couplings are formed by aggregates of protein that form intercellular channels and

are encoded by the connexion multigene family. A significant aspect influencing cutaneous injury response are intercellular communications mediated by gap junctions. Functions of connexions specific to wound healing include wound closure and scar tissue formation after injury, inflammatory response co-ordination and propagation of injury signals between cells (Wei. 2004). Connexion 43 (CX43) peptides can potentially be targeted at wound sites to influence the healing progression as they have been found to be expressed in both the epidermis and dermal layers (Goliger and Paul. 1995). Throughout the process of wound healing, CX43 communication and expression has been found to decrease transiently in epidermal cells, thus decreasing intercellular coupling and gap junctional communication levels (Richards. 2004). Transient knockdown of the CX43 protein in a wound bed by the employment of an antisense oligodeoxynucleotide shows promising results in the early stages of wound healing. Qiu and co-workers (2003) reported a single application of the antisense dramatically improved the rate of healing and the macroscopic wound appearance in a wound healing model. Another study conducted by Qiu and co-workers (2003) revealed the use of CX43 antisense oligonucleotides reduces infiltration of inflammatory cells and the overall area of granulation tissue formation post injury. Wound healing processes were accelerated as well. Furthermore, it has been shown that CX43 antisense treatment significantly increases the level of TGF-β1 mRNA thus further promoting the wound healing process. It can be deduced that by transiently disrupting one signalling pathway through the knockdown of a specific type of gap junction channel CX43, responses involved in the process of inflammation can be dampened. This allows for enhancements in the rate of re-epithelisation by positively targetting the early stages of wound healing. The mechanism involved with the down regulation of transient CX43 causes a decrease in the recruitment of cytokines such as neutrophils and macrophages subsequently dampening their amplifications and further blocking the exuberant influx of leukocytes that lead to scarring (Kapoor. 2005). In addition, CX43 down regulation can be employed as a safe and effective technique in wound healing therapy approaches as they can further enhance epidermal closure in the early stages of wound healing (Rhett et al., 2008).

2.7. Classification of Wound Dressings

There are many classification criteria used for the classification of wound dressings. These include classification by the physical form of the dressing such as gels, ointments, creams, films and scaffolds (Buyuktimkin. 1997). Further, classification may depend on the function of the dressing in the wound, namely debridgement, adherent, antibacterial, occlusive or absorbent (Morghimi et al., 2009) or by the type of material employed to produce the dressing such as alginate, chitosan, hydrocolloid and collagen (Quintero. 2003). Yet another classification criterion include traditional wound dressings, advanced modern wound dressings, wound healing devices and skin replacement products. Primary and secondary

dressings distinguish between those that make direct contact with the wound surface and those dressings that are used as a cover on primary dressings respectively. In addition, island dressings are those dressings that contain an outer adherent portion with an inner absorbent centre (Bolton and Fattu. 1994; Boateng et al., 2008). The discussion that follows classifies the various wound management aids according to the physical form of the dressings discussed.

2.7.1. Traditional Wound Dressings

Wound dressings have been used widely for at least the past two millennia; however, germ theory and its treatment are only about a century old. Cotton wool, natural and synthetic bandages and gauze were used as absorbent wound dressing material to absorb exudates and provide physical protection (Falabella. 2006). These dressings are dry and do not provide a moist environment. They may be used to perform a specific function in conjunction with other wound dressings such as hydrogels and colloids whereby each dressing component plays a pivotal role in the wound healing process. Traditional dressings are functional as both primary and secondary dressings. These traditional wound healing agents have largely been replaced by modern technologically advanced devices with the ability to provide a moist environment, ensure effective gaseous exchange, prevent bacterial contamination and colonisation as well as prevent maceration of the wound and accumulation of exudates as discussed above. Traditional dressings such as gauze and cotton wool have limited effectiveness with regards to these functions and further have the tendency to become adherent to the wound site as the fluid content diminishes, thus making it painful to remove. Gauze dressings allow evaporation thus causing dehydration of the wound site resulting in a delayed wound healing process (Boateng et al., 2008). In addition, gauze dressings are made of interwoven fibres of cotton and polyester which may become loose and embed within the skin at the wound site causing great patient discomfort. Other traditional agents include topical formulations such as ointments, gels and creams which may be in the liquid-gel phase as well as suspensions, solutions and emulsions in the liquid phase. Many formulations are available that included the following: chlorhexidine, used for the irrigation of wounds as it has antibacterial properties, lack of toxicity and enhancement of the healing phase, povidine iodine, which is available commercially in several formulation forms (solution, cream and ointment) and is used in wound management for its antiseptic properties and wound cleansing thus preventing or treating localised infections. Other agents include hydrogen peroxide for its antiseptic and disinfectant properties as well as cadexomer iodine available as an ointment (Purner and Babu. 2000). Because of the low viscosity of many topical formulations such as those found in the solution form, they have the disadvantage of having a short residence time at the wound surface especially at high exudating wound sites thus limiting their activity as wound management aids. Agents such as

gels and ointments have a longer residence time due to their semi-solid state, however a high degree of exudation and wound fluid will be absorbed when applied to a highly exudating wound. Semi-solid preparations are not very effective as they lose their rheological characteristics and flow easily away from the wound site thus hindering their wound healing capabilities.

2.7.2. Lyophilized Wafers and Drug Incorporation

Lyophilised wafers have potential as drug-delivery systems for suppurating wounds, as they can be applied directly to the wound surface. Freeze dried wafers made from polymeric solutions or gels to yield solid porous structures can be used to incorporate drugs promoting wound healing and applied to the wound surface. Their physical architecture resembles those of foam dressing sheets which are made of PU, sometimes with adhesive borders (Queen et al., 2004). Wafers have the capacity to absorb fluid such as excess exudates and revert to its gel form in order to allow the diffusion of the contained drug. With conventional products such as gels and creams, the amount of drug applied to the wound surface is unpredictable and difficult and there is often a high degree of fluid been discharged from the wound site. The use of dried wafers addresses a major hurdle with regards to drug incorporation, as the wafer relies on the presence of discharge from the wound site to form a viscous gel allowing targeted drug delivery, whereas in contrast gels and other conventional therapies are diluted by discharge, thus reducing its viscosity, causing the gel to run from the target area together with the active drug essential for treatment. Therapeutic agents such as antibiotics and growth factors may be incorporated into lyophilised wafers to ensure sustained release of drug particles (Van Rijswijk.2006).

2.7.3. Hydrogels

Rosiak and co-workers (1989) invented hydrogels as the basic material used for manufacturing of wound dressings in 1989. Since then, many modifications have been undertaken to improve their physical and chemical properties. Hydrogels are hydrophilic, insoluble, and swellable dressings made mostly from synthetic polymers such as polyvinylpyrrolidine and methacrylates. Hydrogels contain water molecules of up to 80%–90%, thus allowing them to maintain a moist environment at the wound site by the donation of water molecules. Unlike hydrocolloids, hydrogels cannot absorb much exudate and are thus not suitable for wounds producing a high amount of exudates. Maceration of the skin may result due to fluid accumulation and poor absorption properties, this may then lead to bacterial proliferation and the production of a foul odour from an infectious wound site. One of the major problems associated with the application of hydrogels, is their poor mechanical strength. The plasticising effect of water held within the polymer network is the underlying cause of their poor tear strength and limited resistance to mechanical deformation. Ironically,

it is this same structural feature that dominates permeability, selectivity and surface properties thus giving hydrogels their interesting and unique properties such as improved transmission of moist vapour and oxygen (Lawrence. 1994). Hydrogels with greater mechanical strength and elastic properties were then thus formulated by the incorporation of hydrofibres and reinforcing agents such as small scale inorganic particles (Cooper. 2005; Matthews et al., 2005; Boatang et al., 2013). Hydrogels rehydrate non-viable tissue thus promoting wound debridement and facilitating the natural autolysis process. In addition, they reduce the pain at the wound site as they are non-adherent and cool the surface of the wound. They are considered as the standard treatment form for the management of necrotic and sloughy wounds. Amorphous gels that usually are in the form of thick, viscous gels are the most commonly used hydrogels (Rosiak., 1989) Properties of hydrogels include:

- Supply moisture to wounds with low to medium exudates
- May cause macerations
- Useful in flat wounds, sinuses and cavities
- Suitable for necrotic and sloughy wounds
- Need secondary dressing
- May stay in place for several days
- Examples include: Aquaform, Intrasite, Granugel, Nu-Gel, Purilon, Sterigel

Gels may also be formed i-situ upon contact the skin surface. A natural polymer alginate is an example whereby application of alginate dressing at the wound site results in the exchange of ion from the alginic fibres with those of the exudate and blood thus forms a protective coating of gel which maintains optimal healing temperature and moisture content. The gelation properties of the alginates are attributed to cross-linking in the presence of calcium ions which help to form a polymeric cross-linked gel with low degradability properties. The formation of cross-linking between calcium ions and the alginic polymer make it the ideal material for scaffold formation for tissue engineering (Corkhill. 1989; Kokabi. 2007). Polymer alginate gels are highly absorbent and need to be changed daily, need secondary dressings, are for all wound types with high exudates and are useful for sinuses, cavities and undermining wounds. Examples of alginate dressings include Tegagen, Urgosorb, Sorbsan SA, Algisite and Algosteril (Rosiak. 1989).

2.7.4. Wound Healing Films

A film may be described as a homogenous structure with uniform properties and may include co-polymers, homopolymers and plasticised polymers (Churochkinaet al., 1998). Films dressings have been used tremendously in the past for the management of wound healing and are currently still used in day-to-day clinical practice. They may be used as a primary or secondary dressing and are also often incorporated into other dressings such as hydrogel

sheets, composite dressings, foams and hydrocolloids (Matthews et al., 2005). These dressings were originally manufactured from nylon derivatives and supported in an adhesive polyethylene frame, thus making it occlusive (Gao et al., 1993; Lansown et al., 2003). However, these dressings did not allow for absorption of exudates thus creating a favourable environment for bacterial contamination. They also contained limited exchange of water vapour and gases which delayed the healing process. Modern films dressings are semi-permeable adhesive sheets made by drying polymeric solutions or gels of acrylic derivatives, nylon (Queen et al., 2004) or natural polymeric materials such as chitosan. They are transparent and may be modified, thus making them permeable to oxygen and moist water vapour yet waterproof. Because of their semi-permeable nature they help maintain a moist wound environment by trapping moisture at the wound surface, they facilitate cellular migration and promote autolysis of the necrotic tissue. They also provide a barrier thus preventing bacterial contamination. Films are used for superficial wounds and wounds with light exudates. They may be also used as a retentive for primary dressings; in addition semi-permeable films are relatively economical (Guncem et al., 2009).

Semi-permeable films are formulated from various individual polymers, biomaterials, copolymers and block polymers but in addition are highly modified to suit the purpose of semi-permeability, thus allowing specified entry and release of gases and moisture. Interpenetrating (IPN) or semi-interpenetrating polymer network (s-IPN) formation serves as a method to produce semi permeability. IPN can be defined as a system comprised of two or more polymers that are combined where one of the polymers is cross-linked or in the immediate presence of the other. A novel property profile is introduced by the advancement in multi-component polymeric systems and these semi-permeable films include the following properties (Van Rijswijk. 2006):

- Promote a moist environment
- Allow visual checks and adhere to healthy skin but not to the wound
- Are suitable for flat shallow wounds with low to medium exudates
- Are not for infected or heavily exudating wounds
- Useful as secondary dressings
- May be left in place several days and provide no cushioning
- Marketed examples include Bioclusive Mefilm, Opsite and Opsite plus, Tegaderm, Flexigrid.

2.7.5. Wound Healing Foams

Foams are structures that contain a large fluid binding capacity and are processed in the form of a sponge or foam (Churochkina. 1998). A sponge may be defined as a solid matrix characterised by the dispersion of gas particles which is usually air. Within the

pharmaceutical and biomedical arena, there has been great interest for the use of sponges and foams for wound dressing applications, controlled drug delivery, and within the tissue engineering field, as a matrix for cell growth (Queen et al., 1987). Advanced pharmaceutical formulations such as foam dressings, scaffolds, hydrogels and films have been designed in order to distribute therapeutic substances to exudating wounds in a controlled release manner. These formulations may contain pain-relieving, anti-bacterial and anti-inflammatory therapeutic agents. Drug-delivery systems such as foam dressings have high exudate absorbing properties and thus can be used effectively for exudate wounds, as it has been shown to have advantages in treating chronic low-to-high exudating wounds in comparison with dressings of poor absorbing properties (Sussman. 2010). The use of natural polymers and polysaccharides have developed unfound interest for the design of foams and sponges due to their favourable characteristics such as low toxicity, biodegradability, favourable mechanical properties and bioresorption ability of the constituent materials. One such example is alginate which is derived from brown algae and is an anionic linear polysaccharide composed of 1,4-linked β-d-mannuronates residues and 1,4-linked α-l-guluronates in varying proportions (Debra and Cheri. 1998). Alginate has widely been used in the medical field as a wound dressing application, scaffolds, surgical and dental impressions as it is hydrophilic, relatively economical and biocompatible (Weller and Sussman, 2006). Its use as dressings for wound treatment stems primarily from the ability to form gels on exposure to wound exudates thus giving them high absorbent properties thus minimising microbial contamination and limits wound secretion. Alginate dressings occur either in the form of freeze dried porous sheets (foams) or as flexible fibres.

2.7.6. Multi-Layered Wound Dressings

Wound healing is an intricate and complex process that requires many favourable biological processes in order to ensure optimal healing. As discussed above some of these characteristics include a moist wound environment, adequate gaseous exchange, absorption of wound exudates and infection prevention. In order to promote all of these characteristics, multi-layered wound dressings can be developed. Lee and co-workers (2012) have discussed the formation of multi-layered wound dressings of various properties such as the combination of an adhesive layer with an absorbent layer for highly exudating wounds. More sophisticated dressings can also be implemented such as the development of a dressing which consists of a transmission layer; a core that is absorbent and a contracting wound layer which limits the lateral extend of exudates in the dressing to the region of the wound (Saltzmann and Olbricht., 2002). Lee and co-workers (2012) further developed a hydrogel multi-layered dressing whereby a base layer was formed to provide mechanical support lined by an absorbent top layer. Optimal healing can be achieved by incorporation of the various characteristics into a multi-layered wound dressing.

2.7.7. Nanofibrous Scaffolds and Mats for Wound Healing

Research in this field include many areas such as biomaterial sciences, design aspects involving engineering for the creation of both 2D and 3D cell expansions and tissue growth, biology whereby cell proliferation and differentiation occur. Other aspects include biomechanical and informatic properties of design. Deep open wounds are unable to regenerate by themselves in some cases thus the creation of a scaffold will promote the natural sequence of healing events by providing mechanical support to the development of neotissue (Lutolf and Hubbell. 2005). A Scaffold is a network that supports and holds together living tissue. They are produced by the body naturally after injury or when a wound occurs, but they may also be engineered as a tissue substitute to speed up the healing process. Synthetic and natural polymers which are biodegradable and compatible have been used for the development of scaffolds for tissue engineering. Scaffolds of optimal activity should mimick the biological function as well as the structure of the bodies ECM, thus regulating cellular activity and maintaining mechanical support (Chung and Park. 2007). Cellular activity may be induced to ensure tissue regeneration by the engineering of scaffolds that provide biological function. Functionalisation of the surface of a 3D scaffold will promote cell adhesion by specific cell matrix interactions (Langer and Vacanti. 1993). In addition, many growth factors and other immunologically active substances may be interdispersed within a scaffold. Growth factors have the ability to signal molecules thus inducing tissue repair, in particular proliferation, differentiation, cell migration and organisation within a functional tissue (Steven. 1996). Biodegradable polymeric scaffolds for tissue engineering promote cellular and tissue growth by providing a spatial and temporal environment. (Hutmatcher. 2000; Kenawy et al., 2002, Khil et al., 2003; Vachon and Yager., 2006). Scaffolds that are formulated by electrospinning from materials such as collagen (Khil et al., 2003), poly ethylene-co-vinyl alcohol (Thakur et al., 2008) PU (Peter et al., 1998) and collagen-PEO (Queen. 1987) may be potential applications in the treatment of wounds, as such substrates have the ability to accommodate high amounts of exudates due to their high void volumes. They may also have the ability to improve the breathability and permeability of the applied wound dressings (Diegelmanns and Evans. 2004). The ideal scaffold requires several chemical and structural features: (i) the desired shape, mechanical strength and volume contained within a three dimensional architectural structure,(Hutmatcher. 2000; Khil et al., 2003) (ii) minimisation and prevention of immune and inflammatory responses by the insurance of a biodegradable and compatible chemical composition of products and at the surface of the wound site, (iii) a well interconnected open pore structure and highly porous scaffold that allows for optimal tissue in-growth and high cell seeding density and (iv) provision of sufficient support to impaired tissue until its full re-growth by a finely tuned in pattern of the degradation rate of polymeric scaffold. (Hutmatcher. 2000; Senet. 2004). Techniques such as the application of nanotechnology will ensure the fabrication of a

biodegradable scaffold for directing a series of tissue regeneration processes in a more active manner promoting faster wound healing.

2.8. Recent Research Focus: Healing from a Molecular and Structural Perspective

The underlying principle for the treatment of wounds is that dissociated cells should have the ability to reassemble into a structure that resembles the original skin infrastructure. Native ECM is a dynamic and hierarchically organised nanocomposite that interacts, promotes and regulates cellular functions such as adhesion, proliferation, migration, morphogenesis and differentiation in addition to providing mechanical support (Mallefet and Dweck., 2008). A stable multifunctional matrix is created by the linkage of supramolecular structures by multiple binding domains. The typical skin structure contains structural protein fibres such as elastin fibres and collagen fibres which naturally have dimensions ranging from 10 to several hundred nanometres. These protein fibres that are nanoscaled entangle with each other in order to form a non-woven mesh that provides the skin with its elasticity and tensile strength. Within the ECM, adhesive proteins that are also nanoscaled such as fibronectin and laminin exist that provide specific binding to ensure cell adhesion. Native ECM contains less than 1% solid material, yet still has the capacity to provide diverse functionality and remain mechanically robust. Thus, it can be observed that nature tends to assemble structures with the minimal amounts of material as necessary and the optimal solution is building hierarchically organised structures from the molecular level up to macroscopic scale. The mechanical properties of biological tissue are modulated by nature by adjustments of the tissues composition with a perceivable alteration to its nanoscale organisation (Goldberg et al., 2007).

The skin has a unique biochemical composition, viscoelastic properties and structural organisation thus an attainment of the understanding of its hierarchical tissue organisation and function from a molecular level to microscopic level will more than likely provide a rational guide for the design of films, scaffolds etc that offer synthetic ECM substitutes. With the use of nanotechnology, biodegradable polymers can be modified to recapitulate the hierarchical organisation of natural ECM thus, artificial substitutes in the form of scaffolds, films etc can be engineered that mimick the morphological features of the skin (Goldberg et al., 2007; Steffensen and Herping. 2008).

2.9. Nanotechnology

The field of nanotechnology relates to structures like nanofibres, nanoparticles, nanorods and nanotubes with unique chemical, mechanical and optical properties. New dimensions can be envisioned for areas such as wound healing and tissue engineering drug delivery with regards to enhancing the therapeutic aspect whilst reducing side effects and risks when

introducing novel concepts such as nanotubes, nanofibres, nanorods and branched nanoobjects (Miyoshi et al., 2006). Several amazing characteristics can be observed, when the diameters of polymer fibre materials are shrunken from micrometers to submicrons or nanometers. These characteristics include a very large surface area to volume ratio, the ratio of a nanofibre in comparison with that of a microfibre may be as much as 10^3 greater. It even provides greater mechanical support relating to functionalities such as tensile strength and stiffness as well as improved flexibility within the topology as compared with any other known form of the same material. A polymer nanofibre is the optimal candidate to promote and ensure effective wound healing due to the outstanding properties mentioned above (Kumar et al., 2014). Based on the requirements for optimal wound healing agents as described above, materials used for wound healing devices formulated via electrospinning is currently the state of art in pharmaceutical wound healing technology. Electrospun nanofibres have been applied in many fields including optical sensor fields, filtration and biomedical sciences. In the field of biomedical sciences, they can be used as a means of drug delivery in wound dressings and in the production of tissue engineering scaffolds and films (Horber and Miles. 2003; Bishop et al., 2010). The useful properties of electrospun nanofibres such as variable pore size distribution, oxygen-permeable high porosity, and morphological similarity to the body's natural ECM thus promoting wound healing processes involving cell adhesion, migration and proliferation (Horber and Miles. 2003). In addition, nanofibres have a high surface to volume ratio thus making it an appropriate agent for the use in wound dressing materials. For wound dressing applications, nanofibres are made from polymers that are biocompatible, biodegradable, have a low toxicity and promote the process of wound healing (Dersch. 2005).

2.9.1. Nanoparticle-Based Delivery Systems for Wound Healing

The process of wound healing consist of three different phases whereby various characteristic progressions occur during each phase to ensure optimal curative therapy thus low changing frequency dressings are of favourable preference (Wolf et al., 2009). Of increased interest is the synthesis of stable nanoparticles, as they have unique physicochemical characteristics such as optical properties, antibacterial properties, catalytic activity and magnetic properties (Bhuveneshwari et al., 2014). Nanoparticles are complex mixtures whereby they may be defined as particulate matter having at least one dimension that is less than 100 nm. The behaviour of nanoparticles differs from that of other matter in that the properties of the different components need to be considered. Nanoparticles have an exceptionally high surface to volume ratio contributing to their unusual properties and behaviour. Furthermore, because of its high surface area, its surface structure will also differ from that of the core. Specific and suitable functional groups can be attached to the surface of a nanoparticle to meet its target such as interactions with biological systems. Thus,

nanoparticles can be modified to suit the purpose intended (Christian et al., 2008). As a therapeutic agent in wound healing and acceleration of the healing process nanoparticles can be utilised as a carrier system for sustainable delivery of therapeutic agents (Losi et al., 2013). Hendi (2011) reported the use of silver as a wound healing therapeutic agent that promotes the therapeutic process and reduces scar appearance, however its use has been restrained due to its many toxic effects. The emergence of silver nanoparticles is a form of nanotechnology that provides a means of reducing the percentage of pure silver thus reducing the rate of potential side effects. Application of nanoparticles allows for the synthesis of particles with varying shape, size, chemical composition and mono-dispersity. Wolf and co-workers (2009) also reported the use of a nanoparticulate carrier system to release opiod analgesics at a wound site thus minimising pain at a wound site (Wolf et al., 2009). Nanoparticles as a delivery system allow the loaded drug to be released in a slow manner and increase its skin penetration by several folds. Various intrinsic factors and characteristics need to be considered when designing a wound healing therapeutic agent, therefore the use of metals provide essential characteristics as antimicrobial agents. Integration of nanotechnology and biology can bring the use of metals such as copper, silver and zinc to the forefront in the form of metallic nanoparticles (Gopal et al., 2014). These agents may serve as excellent antimicrobial agents owing to their large surface area to volume ratio and their nanoscale structure in comparison with their metal bulk form (Wu et al., 2014). Thus, the formation of nanoparticles by the application of nanobiotechnology, combined with the acquaintance to wound healing cellular and subcellular events offers great opportunities for improving wound care (Gopal et al., 2014).

2.9.2. Nanohealing: Techniques Employed

The combined use of two techniques namely electrospraying and spinning is made use of in a highly versatile technique called electrospinning (Wu et al., 2014). Recent years has shown a growing interest in the exploration of electrospinning technology. This technique may be used to produce nanoscale fibres especially so, for the fabrication of nanofibrous scaffolds and films for tissue engineering and wound repair. Non-woven membranes can be produced by the application of the electrospinning technique whereby individual fibre diameters may range from a few nanometres to hundreds of nanometers. In addition the fibres may be modified to form a porous structure that is ideal for gene, drug as well as cell delivery (Huang et al., 2003; Luu et al., 2003; Agarwal et al., 2008). The process of electrospinning utilises a high voltage source to inject charge of a known polarity into a polymer melt or solution, which acts as one of the electrodes. This is then accelerated towards a collector of opposite polarity. A Taylor Cone is formed when the electrostatic attraction between the opposite charges and the electrostatic repulsion between like charges in the liquid become stronger. The formation of continuous fibres occur when a fibre jet travels through the atmosphere

causing the solvent within the polymer solution to evaporate, thus resulting in the deposition of solid polymer fibres on the collecting disk. The process of fibre jet formation occurs when the electric field strength exceeds the surface tension of the liquid. Notably, this technique may be applied to fabricate filaments on the nanometer scale (Yoshimoto et al., 2003; Mattews et al., 2002., Pillay et al., 2013). During the process of electrospinning, many factors may be manipulated in order to produce the optimal filament for healing. These factors include parameters such as the electric field strength, the length and radius of the spinneret, the distance of the electric field generated, solution parameters such as conductivity, viscosity, concentration and ionic strength. In addition the solution flow rate should also be considered (Chow et al., 2002). By the alteration of these parameters, properties such as the kinetic, biological and mechanical may be manipulated in order to produce the desired fabrication. Electrospinning also has the advantage of producing a non-woven nanofibrous structure which has similarities such as morphological, topographical and architectural features that are similar to the natural ECM of the skin, thus enabling it to mimic the natural environment of the body thus playing an important role in proliferation and adhesion of cells during wound healing (Green et al., 1994; Flemming et al., 1999; Chow et al., 2002; Chong et al., 2007). Non-woven fibrous mats composed of nanofibres have the ability to interact with cells as they have a very high fraction of surface available to interact with cells, thus making them ideal candidate for cell attachment. Additionally, they may aid in nutritional support due to the porosity within electrospun mats (Figure 2.7) (Su et al., 2006).

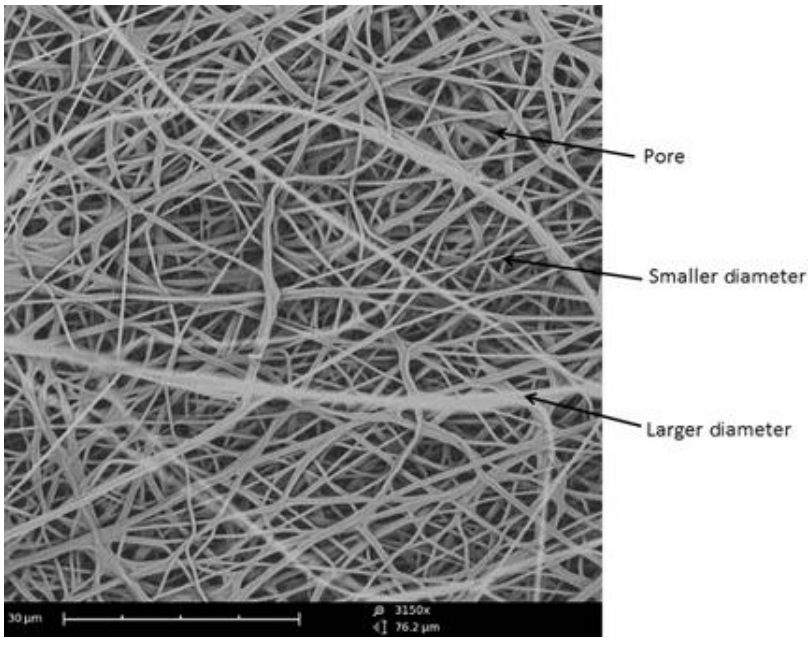

Figure 2.7: Nanofibres fabricated by electrospinning, elucidating different nanofibres diameters

2.10. Concluding Remarks

Considering the variation in the rate of production of wound exudates and the variation in the appearance of the wound surface, no single wound dressing can significantly influence all

wound types, thus the challenge is to develop novel wound healing drug-delivery formulations that have the capacity to positively influence all or most wound types. It thus then seems ideal to fabricate a composite wound healing device that incorporates the different characteristics of all current technologies available thus overcoming challenges that remain with current devices available (Table 2.1 and Figure 2.8). With the advancement and emergence of tissue engineering technologies individual therapy options can be explored in order to target specific wound types and ensure its effective treatment. In addition, the emergence of novel polymers that can be modified to mimic the skin environment, conditions and structure play a pivotal role in the treatment and management of various wound types. Furthermore, the incorporation of active agents, growth factors and drugs can stimulate wound healing responses thus further promoting optimal treatment and management. Such advanced approaches may aid in the treatment of both acute and chronic wounds in a clinically efficient manner. There are many requirements that's need to be ensured when designing and developing a wound healing device and techniques such as electrospinning can be employed to ensure this. This review aimed at providing an insight to the development of an idealised wound healing device that has the capacity to overcome all current challenges.

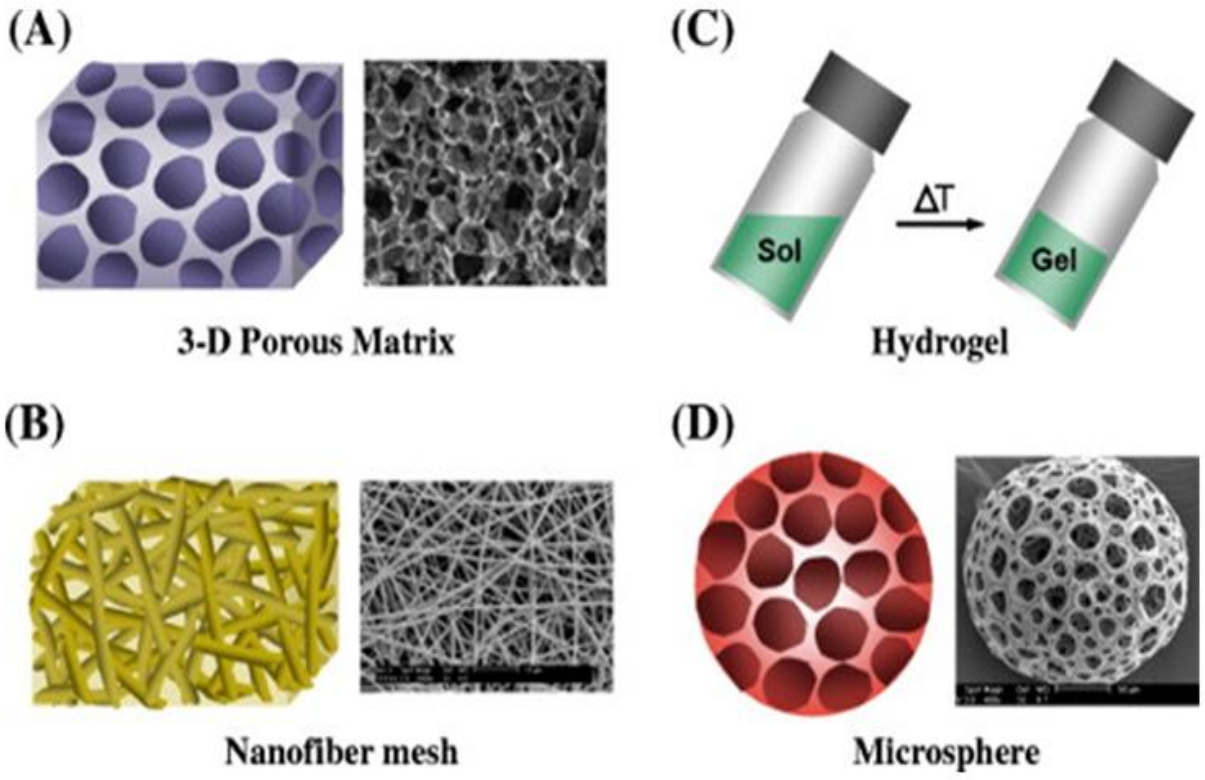

Figure 2.8: Different forms of polymeric scaffolds for tissue engineering and repair. Reproduced with permission from Elsevier BV Ltd©2007.

Table 2.1: Classification of various wound dressings and their properties.

Form	Biomaterials	Bioactives	Application	References
Traditional dressings	Cotton wool, gauze and cotton bandages	Can be used in conjunction with hydrogels and hydrocolloids	Primary and secondary dressings	Asbell and Mickmack. 2000
Lyophilised wafers	Synthetic polymers: Polyurethane	Antibiotics and growth factors	Adhesive and absorptive dressings	Morghimi et al., 2009; Li et al., 2011;
Hydrocolloids	Gel forming agents: elastomers, gelatine, pectin	Active agents such as local anaesthetics	Clinically useful due to adhesion to either moist or dry sites. Provides an optimal moist wound environment	Boatang et al., 2008
Hydrogels	Synthetics and natural polymers: polyvinylpyrrolidine and methacrylates	Anti-inflammatory antimicrobials and local anaesthetics	Primary dressing having swellable and hydrophilic properties	Kootstra and Verma. 2003
Films and semi-permeable films	Co-polymers, homopolymers and plasticized polymers both natural and synthetic	Wound healing bioactive includes growth factors, stabilisers and antimicrobials	Primary and secondary dressings, in conjugation with foams, hydrogels or hydrocolloids. Semi-permeable films promote enhanced gas exchange and moisture	Eming et al., 1999 Rossi et al., 2013
Foams	Natural polymers, polysaccharides, solid matrices with gas particles	Pain relieving, antibacterial and anti-inflammatory agents	Controlled drug delivery and as a matrix for cell growth	Galeano et al., 2003; Quintero. 2003;Falanga. 2005
Multi-layered dressings	Natural and synthetic polymers	Bioactives: local anaesthetics, antimicrobials, anti-inflammatory	Multi-characteristic dressings that provides adhesion, absorption, mechanical support, strength and moisture	Wei. 2004
Electrospun nanofibres mats and scaffolds	Natural, electroconductive and synthetic polymers: chitosan, polyvinylalcohol, surfactants	Bioactives: anti-inflammatory, antibiotics and antiseptics	Primary and secondary dressings mimicking the properties of the skin and may form pseudoskin	Lawrence. 1994;Boatang et al., 2013

CHAPTER 3
DESIGN, CHARACTERIZATION AND OPTIMIZATION OF THE BIOACTIVE CURCUMIN FILM SYNTHESIZED BY THE INTERPENETRATING POLYMER NETWORK TECHNIQUE EMPLOYING AN EXPERIMENTAL DESIGN STRATEGY

3.1. Introduction

This chapter aims at introducing techniques, biomaterials and progressions made in this investigation to overcome the many challenges and complex processes faced during the wound healing cascade. The employment of novel practical ideas and the use of forward-thinking approaches are essential to establish outstanding outcomes in the therapeutic field. The overall outcome of this chapter elaborates on the use of a simple technique demonstrating a significant interest to the use of biomaterials and the semi interpenetrating polymer network (s-IPN) technique.

Currently there are numerous wound healing products available for the treatment of burns, lacerations, incisions, chronic and decubitus ulcers (Suzuki et al., 1997; Tanihara et al., 1998; Kanokpanont et al., 2012). However there is a growing need for novel initiatives in the treatment of burn wounds and excessive skin loss (Kim et al., 2012). Novel wound dressing applications can be produced by the modification and synthesis of biocompatible materials. Biomaterials play a pivotal role in the wound healing process as they are biodegradable, biocompatible, bioadherent and bioabsorbable thus augmenting the healing process. In addition, they contribute inductive, instructive, stimulating and triggering effects to the skin cells and tissues. Numerous synthetic and natural polymers have been used for wound dressing applications: natural polymers include alginate (Hashimoto et al., 2004; Thu et al., 2012), gelatine (Choi et al., 1999; Kanokpanont et al., 2012), collagen (Ma et al., 2003) and chitosan (Muzzarelli et al., 2005; Li et al., 2012) and the synthetic polymers such as poly (ethylene glycol) (Kim et al., 2000), silicone rubber (Crowder and Gooding, 1997) and poly (amino acid) (Hwang and Stupp, 2000) have also shown to be useful for wound healing applications.

Interpenetrating polymer network (IPN) structures can be described at the molecular level as two or more polymer components interlaced in order to form a network that cannot be broken unless the individual entities can be chemically separated and considered a viable option (Zhang et al., 2004; Liu et al., 2006; Yao et al., 2010). The formation of an interpenetrating polymer network (IPN) allowing intermolecular bondage between various components such

as genipin, chitosan and hypromellose, ensures that the components remain interlaced and there is a resistance to phase separation (Saimani et al., 2010).

Considerable interest has been focused on the use of an IPN based drug delivery system as application of this technique will open up new avenues for the combination of natural and synthetic polymers. The use of an s-IPN offers many benefits in that it allows the coalescence of synergistic properties of both polymers, thus avoiding limitations present by the use of single polymer entities. The IPN technique involves the merging of two or more polymers exhibiting diverse characteristics by the process of crosslinking in the presence of the other polymer. Semi-IPN occurs when one polymeric component of the system is left in the linear form whilst the other is crosslinked. (Bhardwaj et al., 2012)

In this study the formation of a semi interpenetrating polymer network was implemented as illustrated in Figure 3.1 in order to form films with the use of natural biopolymers, crosslinkers and bioactives.

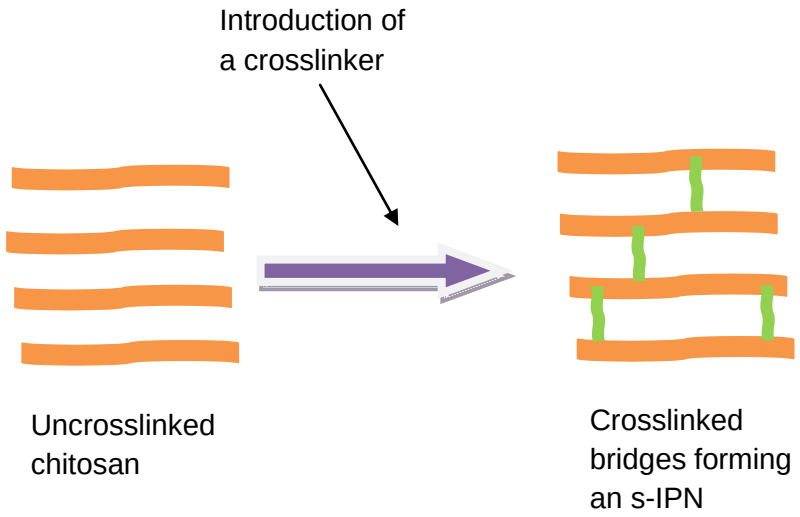

Figure 3.1: Proposed mechanism for the formation of an s-IPN (Adapted from Muzarelli, 2009)

3.2. Biopolymeric Components employed in the Synthesis of an s-IPN Bioactive Film

Selection of biopolymers plays an important role as they should beable to adequately influence the physiological and biological environment of the wound site and cooperate within the electrospinning process with regards to their capabilities and essential potential usage to produce nanofibres as will be discussed in Chapter 4 and 5. Of key importance when selecting a polymer is its profound ability to produce biodegradable, biocompatible, bioresorbable, bioadherent and bioactive activity at the designated site of need (Ishihara et al., 2001; Ueno et al., 2001).

Chitosan (CS) is a natural polymer and a derivative of chitin which has many positive facets in the wound healing process such as biodegradability and excellent biocompatibility properties that are native to the body constituents (Dash M et al., 2011; Li et al., 2012). In addition, it is non toxic and plays an imperative role in the wound healing process due to its versatile biological activity which includes the induction of the healing process within the regenerative and inflammatory phase and its ability to promote tissue growth and differentiation within skin tissue (Datta et al., 2011) thus playing a major role in large wound areas due to its function in granulation and organisation as it has an adaptable property to the wound (Ishihara et al., 2001; Ueno et al., 2001). Howling and co-workers (2001) have found chitosan to be influential during all stages of wound healing when carrying out an *in vivo* study. Homeostatic ability by chitosan has been pronounced within the inflammatory phase whereby re-epithilisation and fibroplasia have been accelerated avoiding further complications by foreign bodies, and at the same time promoting the granulation phase (Howling et al., 2001; Ishihara et al., 2002; Alemdaroglu et al., 2006). Studies carried out in dogs and cats have also shown an advantage of decreased scar formation as excessive hypertrophic scar formation was prevented by the use of chitosan (Ueno et al., 1999). In addition chitosan exhibits gelation and film forming characteristics, is non toxic and biocompatible (Ishihara et al., 2001; Alemdaroglu et al., 2006).

Citric acid, a chemical agent is beneficial in the treatment of wounds as it is convenient, inexpensive, non-toxic and highly effective against organisms thus preventing the development of infection by manifestation of microbes in open wound sores. It has also been found to enhance the wound healing process by promoting the laying of granulation tissue and epithelisation while at the same time exudates excretion is minimised (Naqoba et al., 2011). In studies carried out citric acid was found to be effective in wounds of humans against various bacteria (Nagoba et al., 1998; Nagoba et al., 2010). In addition citric acid serves to create an acidic environment when dissolving chitosan within an aqueous medium.

Hypromellose a natural polymer is known for its advantageous hygroscopic properties thus ensuring lubrication and providing an essential moist wound environment during the wound healing process. Hypromellose also promotes angiogenesis at the wound site, is non-toxic, highly viscous thereby registering sustained release of biopolymers by acting as a viscous barrier and controlling the rate of hydration and diffusion (Topham, 2002).

Throughout the tropical regions such as South East Asia, Africa, India and China, the cultivation of *Curcuma Longa* has been widely established. *C. Longa* also known as turmeric belongs to the *Zingeberace* family and is a perennial herb known to humankind for over 6000 years (Kurrup and Barrios, 2008). Within the biological and medical field, of particular interest

are the phytochemical constituents such as curcuminoids and curcumin for their wide spectrum of biological activities. “Tumeric” or curcumin is a yellow rhizome which is extensively used in the food industry as a colouring and flavouring agent, condiment and spice (Adaramoye et al., 2009). Furthermore, traditional medical practitioners of the tropical regions utilized curcumin to treat inflammation, urinary tract infections, hypertension and eczemas (Dao et al., 2012), in addition to being used as an antioxidant and anticancer agent (Sidhu et al., 1998). Current extensive studies and understanding of the phytochemical constituents of curcumin has lead to the discovery of biological activities associated to appropriate wound healing such as anti-inflammatory and antioxidant properties. Furthermore, studies conducted in various animal models have proven curcumin to be nontoxic at even high doses (Ponnusamy et al., 2012). Curcumin moreover has been shown to play an important role in wound repair by ensuring the induction of TGF-β1 within the wound thus significantly enhancing the healing process (Sidhu et al., 1998; Mani et al., 2002; Li et al., 2012).

Many polymers including the natural polymers have major drawbacks such as poor mechanical properties and rapid degradation which limits their application in the skin and tissue engineering field. Interest in the use of genipin as a crosslinker is on the increase due to the many toxic effects of other chemical crosslinkers such as glutaraldehyde (Beppu et al., 2007), glyoxal (Pauliukaite et al., 2009), epichlorohydrin (Singh et al., 2006), and formaldehyde (Machado et al., 2009). Genipin is extracted from the *Gardenia jasminoides* fruit and is an iridoid glucoside that has been used by the food industry and Chinese traditional medicine as a blue colorant. It can crosslink macromolecules such as polysaccharides and proteins and is a well-known crosslinker of chitosan, a natural polymer consisting of many amino groups. The degree of crosslinking by genipin is mainly dependent on the availability of free amino groups to which it can react under mild conditions and can clearly be noted by the blue colour change that occurs upon crosslinking (Pujana et al., 2013; Gao et al., 2014). In comparison to other potent crosslinkers as mentioned above, genipin can produce crosslinked materials with comparative degradative and mechanical properties (Gao et al., 2014). Within the field of biotechnology and biomaterials, genipin is widely employed in studies related to tissue engineering, regeneration, and fixation. In addition, it has been used in the formation of interpenetrating polymer networks (IPN), nanocomposites, nanoparticles, as well as microspheres and macrogels (Pujana et al., 2013). Furthermore, in a study carried out by Chang and co-workers (2003) it has been shown that genipin exhibits great cell compatibility and wound coverage by epithelisation as this is further enhanced by the presence of genipin as a crosslinker (Bigi et al.,2002). Proliferative activity of cells at wound sites showed greater outcomes in comparison to other crosslinking agents such as

glutaraldehyde thus making it a well suited agent for clinical usage (Sung et al., 2002; Muzarelli, 2009).

A combination of these biopolymers can serve as a potential application throughout the process of healing as collectively they may induce an additive complementary therapeutic effect that has the capability to accelerate the healing process as well as optimize the beneficial effect of each individual entity.

3.3. Part 1: Preliminary Investigation of the Biopolymeric Films

3.3.1. Determining the Upper and Lower Variables for Formulation Preparation required for Input into the Box-Behnken Design

The merit of attempting a preliminary study permits an understanding of the various system characteristics, whereby establishment of an optimized candidate can be achieved. Preliminary studies involve selection and evaluation of the various biopolymers significant to the wound healing process as well as advantageous for film formation. The identification of variables incorporating upper and lower limits is of paramount importance when considering further experimentation and optimization. Various factors in this investigation were considered and include the following (Lloyd et al., 1998):

- Protection of the wound from the outside environment
- Storage conditions and shelf life
- Flexibility and toughness
- Homeostatic, biodegradable, microbial invasion, exudates absorption
- Restoration of normal function and appearance
- Convenient and easy removal, patient compliance

The variable upper and lower levels of the various formulations analysed were as follows:

Table 3.1: Template exhibiting Upper and lower limits derived from preformulation experimentation

Polymer/Active Crosslinker	**Chitosan (%$^{w}/_{v}$)**	**Hypromellose (%$^{w}/_{v}$)**	**Genipin (%$^{w}/_{v}$)**	**Citric acid (%$^{w}/_{v}$)**	**Curcumin (%$^{w}/_{v}$)**
Upper Level	1	0.4	0.1	5	1
Lower Level	3	1.6	0.5	5	1

3.3.2. The Influence of Crosslinking with Genipin on Film Formation and the Effect of Variable Polymer Concentrations

Within this investigation, of interest is the use of genipin as a natural crosslinker to form a semi-interpenetrating polymer network (s-IPN) whereby it also provides further advantageous therapeutic benefits relating to wound healing such as anti-inflammatory properties (Gao et al., 2014). The addition of a cross-linker such as genipin can greatly improve upon or overcome many physicomechanical drawbacks. Furthermore, genipin is nontoxic and biocompatible, thus it has been shown to be an effective crosslinking agent of biomaterials such as chitosan which contains a large amount of amino groups and the natural cellular tissue (Huang et al., 1998; Mi et al., 2002; Yan et al., 2010).

Chitosan is a highly biodegradable polymer thus needs to be crosslinked in order to modulate its properties enhancing bioavailability and mechanical properties. Genipin, a crystalline substance with a highly defined structure serves as a desirable crosslinker due to its natural origin and low cytotoxicity. The mechanism of crosslinking is pH dependent and within an acidic environment the olefinic carbon atom at C3 undergoes a nucleophilic attack by the amino groups of chitosan. This is followed by the opening of the dihydropyran ring whereby an attack occurs by the secondary amino groups on the newly formed aldehyde group. Condensed genipin having short chains perform as crosslinking bridges whereby genipin acts as a dialdehyde (Muzzarelli, 2009). In this manner, the structural composition of chitosan is modified introducing supplementary bonds greatly impacting the physicomechanical properties of the polymer as illustrated in Figure 3.2. According to a study conducted by Mi et al., 2005, chitosan in the presence of genipin undergoes crosslinking at a neutral pH whereby heterocyclic amines are formed associated to crosslinked networks whereby short chains of dimmer, trimer and tetramer bridges are formed.

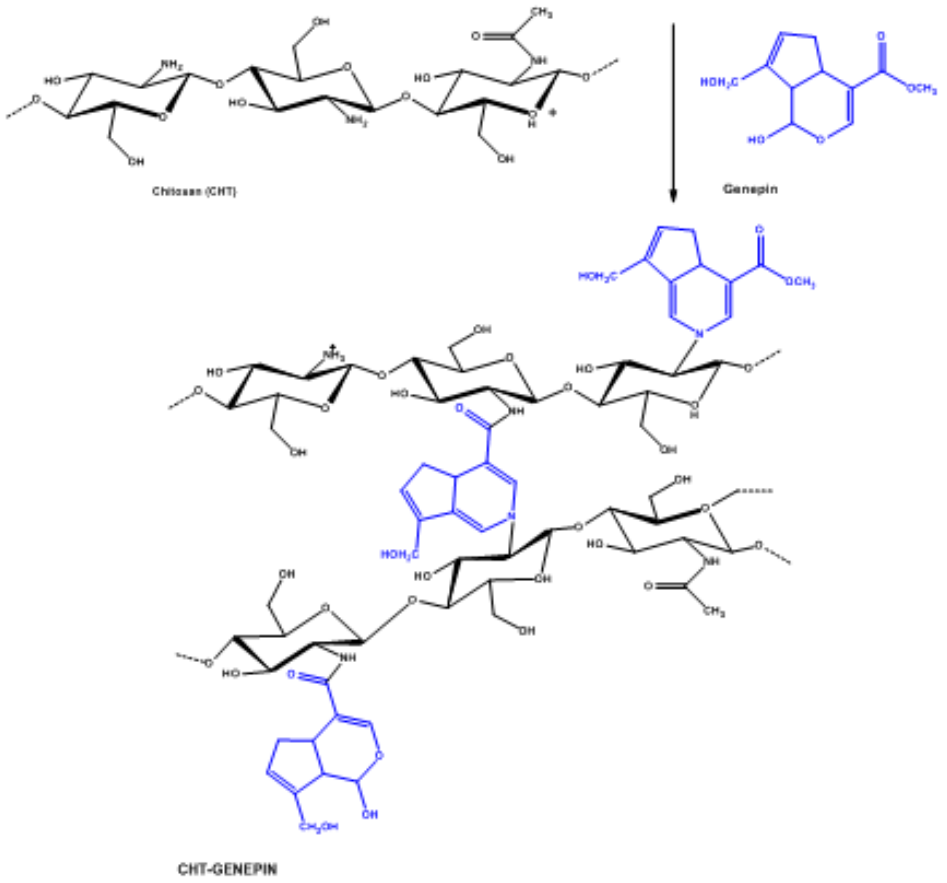

F**igure 3.2:** Illustration of the crosslinked reaction between genipin and chitosan (Chen et al., 2004)

In this investigation, variable concentrations of genipin were introduced to determine the crosslinking potential of chitosan ranging between 0.1%$^{w}/_{v}$ and 0.5%$^{w}/_{v}$. The illustrations in Figure 3.3 depict the crosslinking effects on the chitosan films observed by the colour change. Crosslinking with genipin results in the formation of a blue pigmentation viewed as green in this instance (due to presence of curcumin) formed via the reaction of amino groups with genipin in the presence of oxygen (Butler et al., 2003). As can be noted the films presented with a darker pigmentation as the concentration of genipin was increased thus advocating greater formation of crosslinking bridges. The impact of crosslinking was then determined by analysing various characteristic properties. Furthermore it was observed that when very high concentrations of genipin was used as a crosslinker, the mechanical properties of the films decreased due to elevated molecular bonding making the films brittle and fragile. Additionally using higher concentrations of biopolymers such as chitosan lead to an increase in solution viscosity further diminishing the tensile properties of films and forming films of irregular and uneven textural constitutes as observed in Figure 3.4

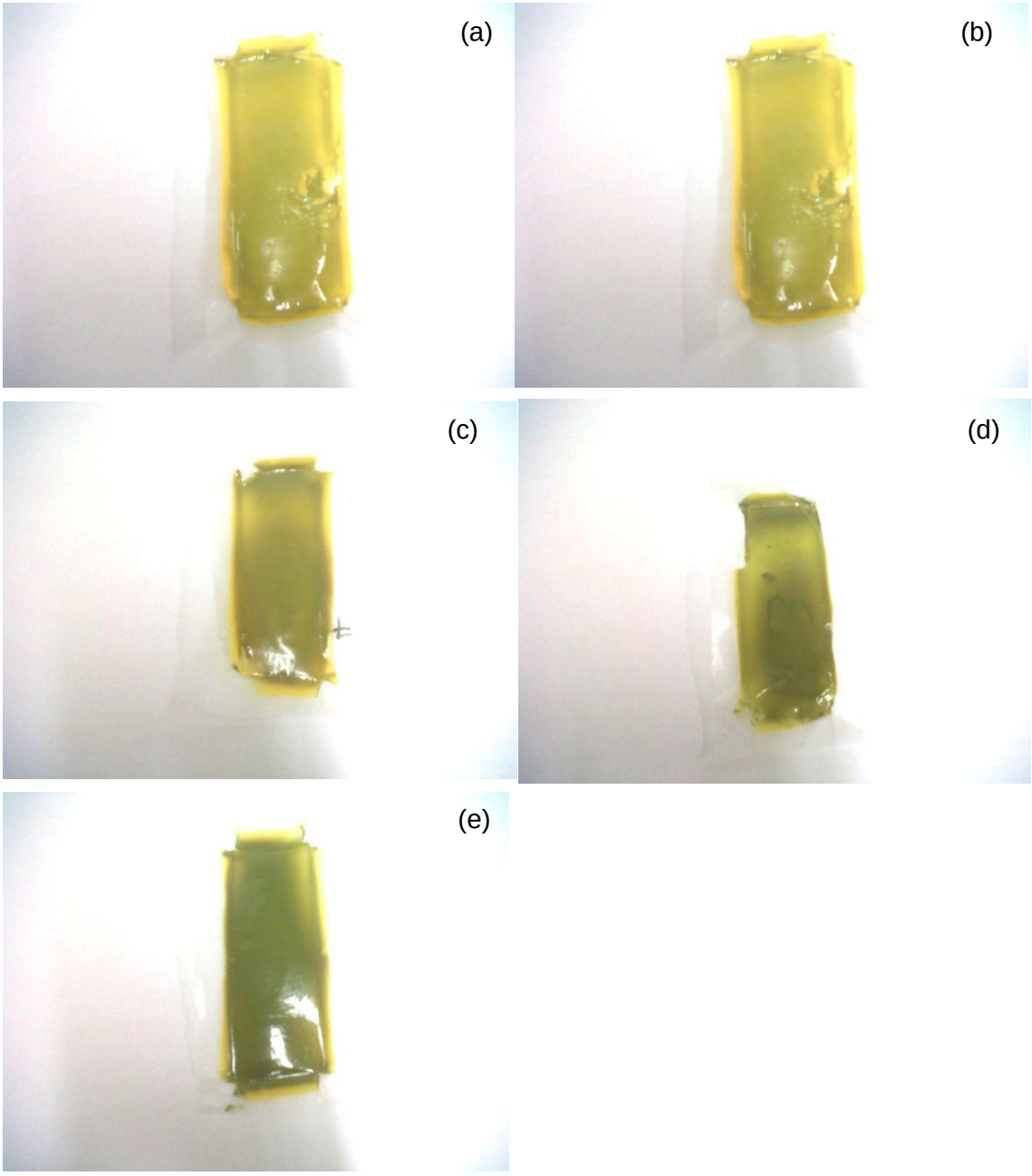

Figure 3.3: Chitosan films crosslinked with genipin at various concentrations. (a): 0.1%$^{w}/_{v}$, (b): 0.2%$^{w}/_{v}$, (c): 0.3%$^{w}/_{v}$, (d): 0.4%$^{w}/_{v}$, (e): 0.5%$^{w}/_{v}$

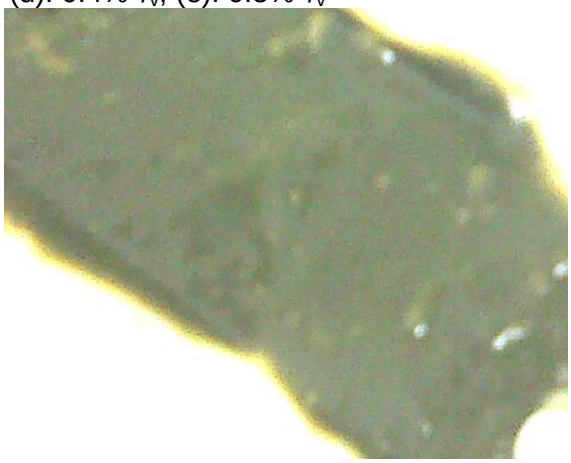

Figure 3.4: Crosslinked film constituting of high crosslinker and polymer concentration

The crosslinking reaction could further be noted by the FTIR spectra analysis. Upon crosslinking a shift in the wavelength to the left is noted from 3260.11cm^{-1} in Figure 3.5b to 3278.79cm^{-1} in Figure 3.5a and 2049.97cm^{-1} in Figure 3.5b to 2164.10cm^{-1} in Figure 3.5a. This strongly suggest an increase in conjugation and bond intensity due to greater intermolecular forces occurring due to the presence of the crosslinker as is illustrated in the FTIR spectra (demarcated in Figure 3.5). A shift in wavelength is seen and absorbance is also further augmented. Wavenumbers at 1634 and 1636cm^{-1} were examined and upon analysis it is seen that that an increase in conjugation and bond intensity is seen at 1636cm^{-1} in Figure 3.5a due to a shift to the left in wavelength from 1634cm^{-1} in Figure 3.5b thus augmenting the crosslinking intermolecular bondage. The slight peak depicted in Figure 3.5 at 2164.10 cm^{-1} and 2049.97 cm^{-1} are representative of an alkyne stretch due to conjugation which is more prevalent in Figure 3.5a.

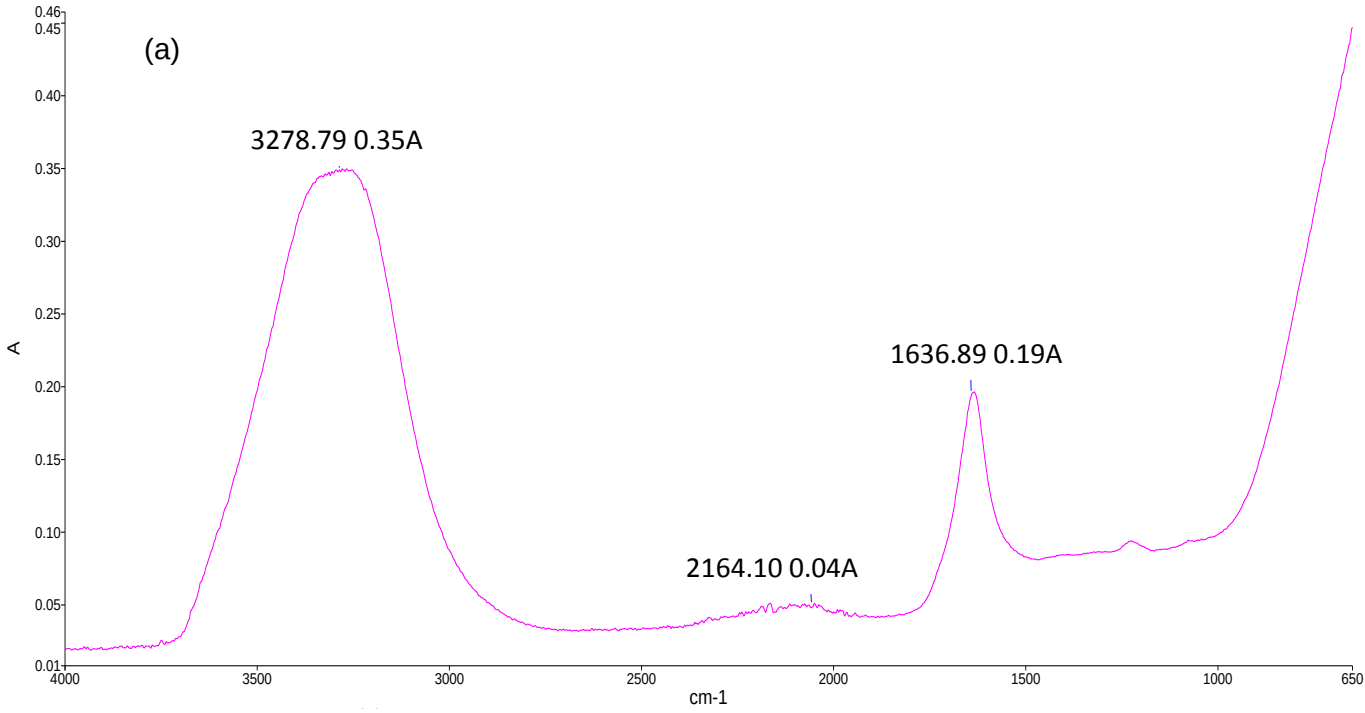

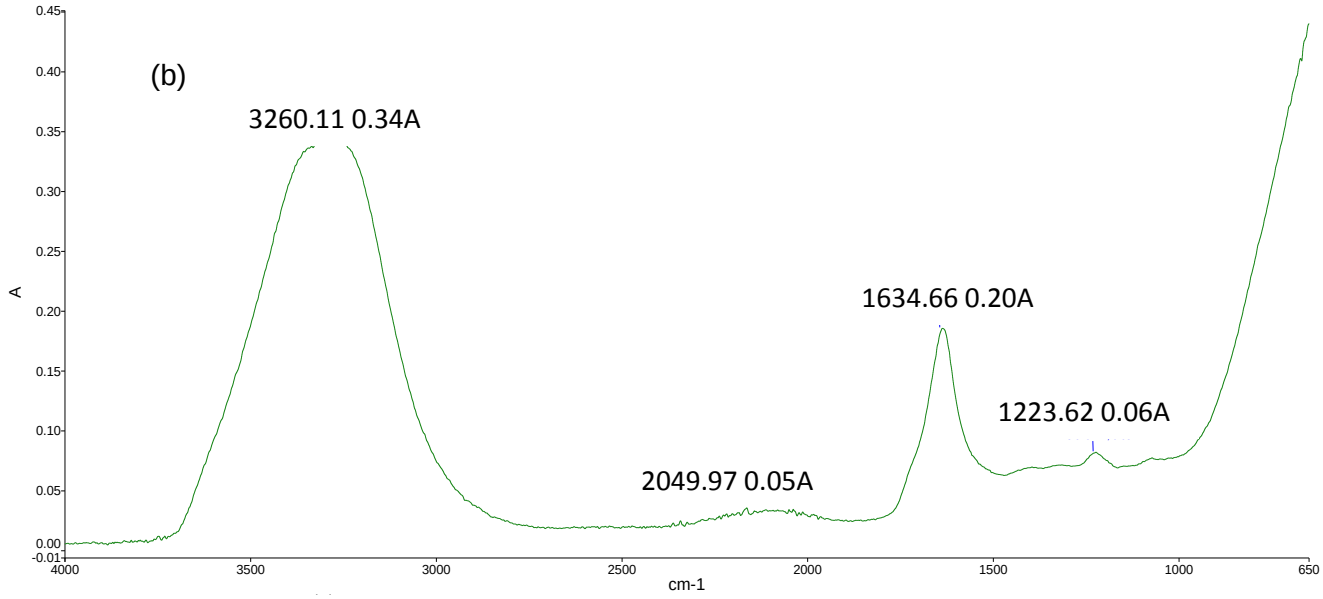

Figure 3.5: Chemical transitions depicted by the FTIR spectra in (a): genipin crosslinked chitosan films, (b): Uncrosslinked chitosan films

Upon formation of films of varying concentrations obtained from the variable data, of paramount interest was the determination of the physicomechanical properties by texture analyses (illustrated in Figure 3.6) to analyse the tensile strength ($N.mm^2$) by varying polymer concentration. Upon close examination it was noted that an increase in tensile strength occurred as the crosslinker genipin concentration was increased up to $0.4\%^{W}/_{V}$ at $0.187N.mm^2$.

A further increase in crosslinking such as $0.5\%^{W}/_{V}$ rendered a decrease in tensile strength as depicted in Figure 3.7 at $0.134N.mm^2$, making the films brittle and more prone to tearing and breakage. This phenomonan can be attributed to the Young's modulus. as the concentration of genipin was increased so to did the mechanical characteristics of the films exhibiting a greater Young's modulus. An increase in the Young's modulus reveal greater strength, toughness and rigidity to the films. However, at higher concentrations the strong intramolecular and intermolecular bonding results in decreased elasticity and flexibility to the films rendering them brittle and easy torn.

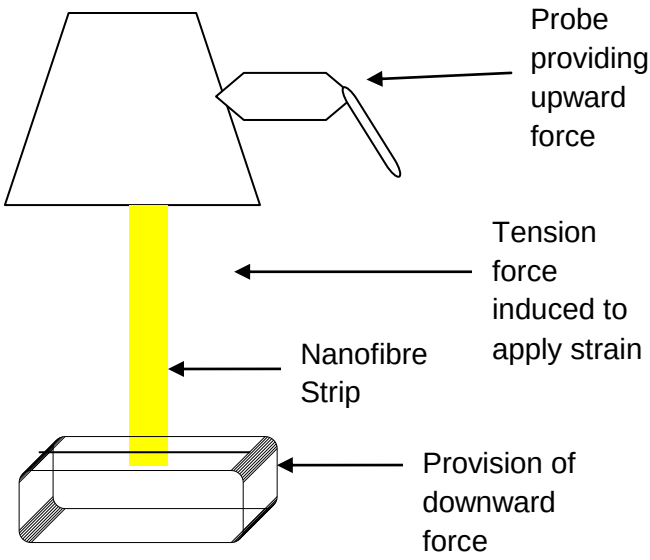

Figure 3.6: Image displaying the texture analysis process when a strain is applied to the films to determine its tensile strength

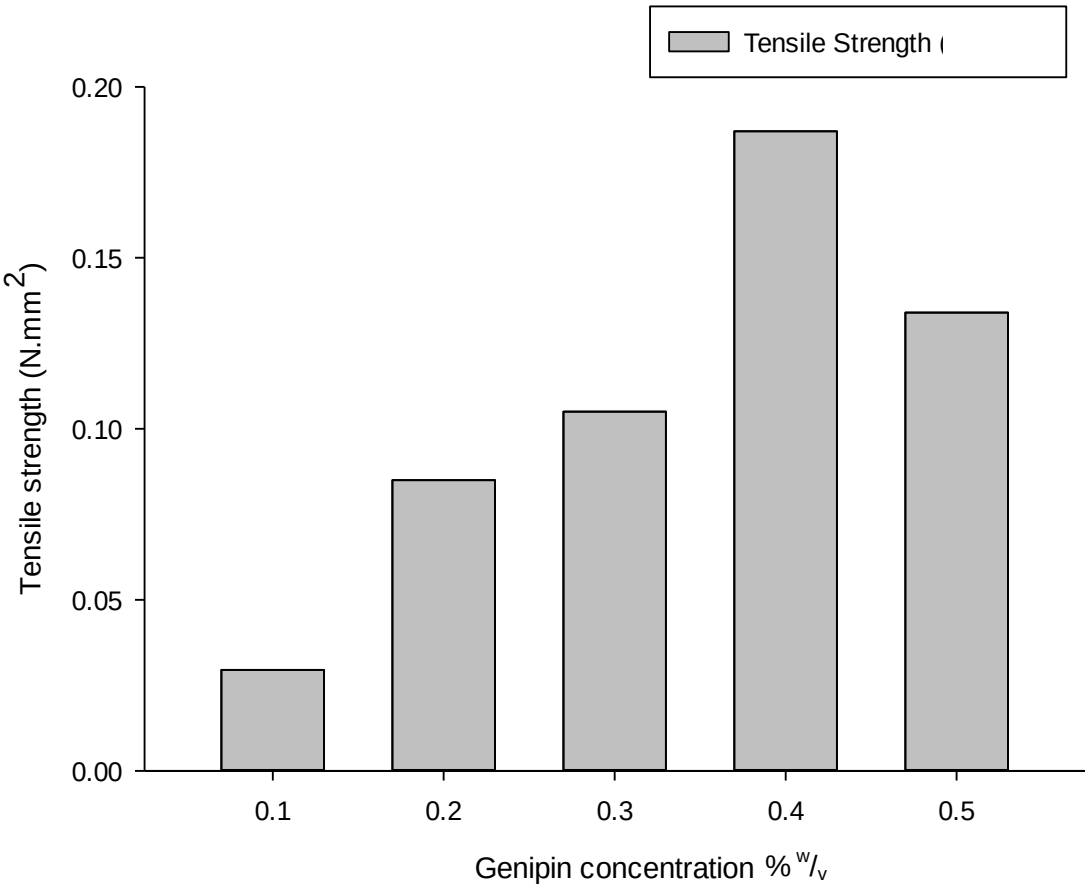

Figure 3.7: Graph depicting the influence of varying concentrations of genipin on the tensile strength of films

Further analysis was conducted to establish the influence of polymeric concentration and crosslinking on the bioavailability and bioactive delivery at the wound site. A swelling test was conducted whereby the various films with differing polymer and crosslinker

concentration was immersed in buffer of neutral pH over a period of 1 hour and the weight was taken before and after immersion to determine the swelling capacity. From the results obtained it was noted that at higher crosslinker concentrations the swelling capacity was lowered, such as 36.16%$^{w}/_{v}$ at 0.2%$^{w}/_{v}$ genipin compared to 8.92%$^{w}/_{v}$ at 0.4%$^{w}/_{v}$ allowing a controlled release of bioactive and greater bioavailability. In addition when the polymeric concentrations of chitosan were increased, the percentage swelling capacity decreased. Addition of 1% $^{w}/_{v}$ chitosan revealed a % swelling capacity of 43.62% $^{w}/_{v}$ whereas at 2.5% $^{w}/_{v}$ a swelling capacity of 7.47%$^{w}/_{v}$ was noted. This could be attributed to the increase in solution viscosity as well as greater availability of amino groups for crosslinkage with genipin.

Thus from the investigation carried out, a conclusion to the most appropriate variable concentrations with regards to the upper and lower limits could be made as depicted in Table 3.1 to produce the most desirable characteristics in terms of film formation and wound treatment. From theses variable obtained a three factor Box-Behnken design template was implemented as portrayed in section B of this chapter.

3.4. Part B: Experimental Synthesis and Statistical Optimization of the Films for Wound Healing

3.4.1. Materials and Methods

3.4.1.1. Materials

Chitosan (CS) (medium Mw poly (D-glucosamine) deacetylated chitin), hypromellose-hydroxymethylcellulose 2910, citric acid (ACS reagent ≥99.5%, M_w=192.12g/mol), genipin (≥98% HPLC grade) powder (M_w=226.23g/mol), and curcumin as well all other reagents of analytical grade used were procured from Sigma-Aldrich Chemie GmbH (Steinheim, Germany).

3.4.1.2. Synthesis of a Semi-Interpenetrating Network Polymer Film

Semi-interpenetrating network (IPN) polymer blends were prepared using the sequential IPN method. Various concentrations of chitosan (CS) ranging from1 to 3%$^{w}/_{v}$ were added to a 5%$^{w}/_{v}$ (5 g/100 mL) solution of citric acid. This was then allowed to stir using a magnetic stirrer until a homogenous solution was formed. Next, the crosslinker genipin was dissolved in deionized water to make an aqueous solution of varying concentrations between 0.1 and 0.4%$^{w}/_{v}$. This was then added to the CS solution to allow crosslinking. Thereafter, various concentrations of hypromellose solution ranging between 0.4 and 1.6%$^{w}/_{v}$ added to a 1%$^{w}/_{v}$ curcumin solution were mixed with the above blend. Lastly, 1 mL of glycerol was added to 40 mL of the s-IPN formulation consisting of all polymers, including the bioactive curcumin and crosslinker genipin and allowed to stir overnight to form a homogenous semi-IPN blend. The

optimum quantity of each blend (10 mL) was poured into a rectangular mold composed of Parafilm (710×260 mm) and cast in film form by solvent evaporation at room temperature with the use of a fume hood under the influence of continuous airflow. After drying, semi-IPN films were removed from the fume hood and placed in a petri dish until further use under Parafilm. A three-factor Box-Behnken experimental design as shown in Table 3.2 (acquired from preformulation studies) was generated to obtain optimal concentration combinations of biopolymers in order to perceive optimal parameters from the design to acquire a semi-IPN film with superlative therapeutic and formulation outcomes. Preformulation experiments led to the search of variables that enabled an upper and lower limit of all factors necessary as discussed in part A of this chapter, to be established in order to run an accurate design. Furthermore, characterization of the design formulations lead to the establishment of an optimized semi-IPN film of optimal concentrations that is adequate as a wound dressing on which further *in vitro* and *ex vivo* studies were conducted.

Table 3.2: Box-Behnken design template for statistically derived semi-IPN film formulations

Formulation No.	Chitosan ($\%^{w}/_{v}$)	Genipin ($\%^{w}/_{v}$)	Hypromellose ($\%^{w}/_{v}$)	Curcumin ($\%^{w}/_{v}$)
1	1	0.25	0.4	1
2	3	0.1	1	1
3	2	0.1	1.6	1
4	1	0.25	1.6	1
5	2	0.25	1	1
6	2	0.4	0.4	1
7	3	0.25	0.4	1
8	2	0.25	1	1
9	3	0.4	1	1
10	1	0.4	1	1
11	1	0.1	1	1
12	2	0.4	1.6	1
13	2	0.1	0.4	1
14	2	0.25	1	1

3.4.1.3. Chemical Structure Analysis by Fourier Transform Infrared Spectroscopy

ATR-FTIR analysis which identifies absorption bands based on vibrational molecular transitions was conducted to characterize complex interactions occurring within bioactive polymer exchanges. A PerkinElmer® Spectrum 100 Series FT-IR Spectrometer fitted with a universal ATR Polarization Accessory (PerkinElmer Ltd., Beaconsfield, UK) was employed

and Spectra over the range 4000-625cm^{-1}, with a resolution of 4cm^{-1} and 32 accumulations was recorded for all semi-IPN film samples.

3.4.1.4. Thermodynamic Property Analysis by Differential Scanning Calorimetry Studies

Differential scanning calorimetry (DSC) measurements were taken for semi-IPN film samples weighing 7–10 mg using an advanced DSC (TMDSC/ADSC) (Mettler Toledo DSC-1 STARe System, Schwerzenback, ZH, Switzerland) at a heating rate of 10°C/min from −10 to 350°C under a nitrogen atmosphere. Weighed samples were placed in a covered aluminum sample holder with a central pin hold. Calibration of the DSC modulus was done in respect to enthalpy and temperature. Thermoanalysis of the samples was carried out with regard to the glass transitions, melting points, chemical reactions, and phase change temperatures of the polymeric system.

3.4.1.5. Surface Morphological Analysis by Scanning Electron Microscopy Imaging

Surface topographical structure of the dry semi-IPN films was analyzed by scanning electron microscopy (SEM; Phenom ™, FEI Company and Hillsboro, OR, USA) for porosity, surface roughness, and particle size of films. Samples were cut from films and mounted into metal stubs whereby samples were gold coated with an in-house SPI-Module Sputter Coater (SPI Supplies, Division of Structure Probe Inc., West Chester, PA, USA) prior to analysis.

3.4.1.6. Determination of the Physicomechanical Properties of the Films by Textural Profile Analysis

Semi-IPN film samples were subjected to texture analysis using a highly sensitive texture analyzer (TA.XT *plus* Texture Analyser, Stable Microsystems, Surrey, UK) fitted with a 50- kg load cell. The physicomechanical properties of the film was measured by fixating film samples between two brackets placed 3 cm apart and a tension force of 0.5mm/s applied to the system to determine the force at breaking point. This approach was employed to generate force-distance profiles to determine the tensile strength and work of extensibility which can be computed from the peak tensile force required and using Equation 3.1. The parameters marked for textural analysis are presented in Table 3.3. Tensile strength was measured using the Young's modulus.

$$E = \frac{Tensile\ \ stress}{Tensile\ \ strain} = \frac{\delta}{\varepsilon} = \frac{FL_o}{A_o \Delta L} \qquad \text{[Equation 3.1]}$$

Where, E= Young's modulus (modulus of elasticity), F= force applied to the object; A_0= original cross-sectional area (πr^2) through which the force is applied, ΔL= quantity by which the length of the object changes and L_0=original length of the object.

Table 3.3: Parameters employed for textural analysis

Parameter	Settings
Test mode	Tension
Pre-Test speed	0.50mm/sec
Test speed	0.50mm/sec
Post test speed	5.0mm/sec
Trigger type	Auto
Trigger force	5kg
Contact time	5sec

3.4.1.7. Durability Testing of the Films by Nano-Tensile Mapping

The tensile properties (at a nano-sensitivity level) of the semi-IPN films were evaluated using a nano-Tensile Analyser (nanoTensile^{TM} 5000, Hysitron Inc., MN, USA). Samples were mounted within nano-tensile brackets that were held rigidly together by a frame thus aiding in sample alignment and positioning. An accurate measurement of the width, thickness and length of all film samples were taken using a digital calliper prior to mounting of samples. To determine the Young's Modulus, brackets were made to move apart at a constant rate of 5μms^{-1} until a breaking force was established.

3.4.1.8. Determination of the Swelling Capacity and Equilibrium Water Content

Pre-weighed samples of the semi-IPN films were dispersed in 15mL of phosphate buffer solution (PBS; pH 7.4) and allowed to equilibrate at room temperature (37,1°C) for 24 hours. Samples were then removed periodically at 1 hour intervals, excess buffer was removed and samples were reweighed. The swelling capacity (%) and equilibrium water content was determined using Equations 3.2 and 3.3 (Bindu et al., 2010).

$$\%\ Swelling\ Capacity = \frac{Final\ \ Weight - Initial\ \ Weight}{Initial\ \ Weight} \times 100 \qquad \text{[Equation 3.2]}$$

$$\%\ Equillibrium\ Water\ Content = \frac{Ws - Wd}{Wd} \times 100 \qquad \text{[Equation 3.3]}$$

Where, W_s = weight of film in the swollen state when dispersed in deionised water and W_d= weight of film in the dry state after been dispersed in deionised water (hourly).

3.4.1.9. Analysis of the Water Vapor Transmission Rate into the Semi-IPN Films

Water vapor transmission rate (WVTR) tests were performed. Film samples were placed on the top of glass polytops having an area of 144mm^2 and containing 10mL of phosphate buffer solution of pH of 7.4. This set up was pre-weighed and then placed in an oven at 35°C for 24 hours. Samples were then re-weighed at regular intervals and a plot of weight loss due to Vapor Transmission vs. Time was deduced. The transmission rate was determined using Equation 3.4.

$$WVTR = \frac{wi - wt}{A} \times 10^6 \, g/m^2 day^{-1} \quad \text{[Equation 3.4]}$$

Where, *WVTR* is expressed in g^2 h, *A*=area of the polytop opening (mm^2), *wi* and *wt* = the weight of the polytop before and after been placed in the oven, respectively (Kim et al., 2007).

3.4.1.10. Measurement of the Rheological Properties of the Semi-IPN Polymer Blends

A Haake Modular Advanced Rheometer System (MARS) (ThermoFisher Scientific, Karlsruhe, Germany) was used to determine the rheological parameters of the polymer solution blends employed for formulating the semi-IPN films. Samples were placed on a sample stage whereby a C35/1° titanium rotor was immersed in the polymer solution at a temperature maintained at 24°C, shear rate at 100s^{-1} and a time period of 360s (Shaik et al., 2012). Stress-Strain rheological parameters were then obtained for all samples quantified.

3.4.1.11. *In Vitro* release of Bioactive

The release of bioactive curcumin from the semi-IPN films was performed in a modified Franz Diffusion Cell (FDC) apparatus study setup. Films were cut in a circular section and placed on the receptor compartment to allow diffusion, which had a surface area of approximately 1.8cm^2. Each receptor compartment was filled with 12mL of isotonic phosphate buffer solution and was further thermo-regulated at 37°C by a water jacket throughout the study. Receptor compartments were constantly stirred using a magnetic stirrer. At time periods 0.5, 1, 2, 3, 4, 6, 8, 10 and 12 hours, 0.1mL of solution was withdrawn from the receptor compartment and replaced by an equal quantity of fresh PBS buffer immediately after each sampling. Samples were then evaluated using a nanophotometer (Implen, GmbH, Munich, Germany) at a wavelength of 425nm.

3.4.1.12. *Ex Vivo* Permeation Studies through the Sprague Dawley Rat Skin Model

Permeation studies were undertaken using full thickness skin excised from Sprague Dawley rats. Rats were euthanized using pentobarbitone intraperitoneally (i.p) and the skin was carefully removed. Rat skin was stored in isotonic phosphate buffer solution (pH 7.4) at -

80°C until further use. Prior to experimental procedures skin was removed and thawed by placing in water at 37°C. The dorsal region was shaved and further subcutaneous and adipose tissue was carefully removed (Amnuaikit et al., 2005). Skin sections were excised to fit receptor compartments having a surface area of approximately 1.8cm^2. To ensure that the integrity of the full thickness skin samples was maintained throughout the study, electrical resistance was measured across the skin membrane before and after permeation studies. This was performed by passing a fixed current across the skin specimen sample using a Mettler Toledo Seven Multi GmbH, Analytical CH-8603 (Schwerzenbach, Switzerland) connected to an electrode that was adjusted to isotonic environments by placing the probe into isotonic PBS solution before insertion with skin sections. Thereafter the resistance and conductance measurements were recorded as shown in Table 3.4 at a temperature of 37°C (Davies et al., 2003).

Table 3.4: Resistance and conductivity of skin preparations to determine skin integrity before and after *ex vivo* permeation studies

Skin preparation	Resistance (Ω/cm)	Conductivity (µs/cm)
Before	0.37×10^3	18
After	0.86×10^3	68

The prepared skin was then placed between the donor and receptor compartment of the Franz Diffusion Cell apparatus. Semi-IPN films having a surface area of approximately 1.8cm^2 was then placed over the skin and covered by the upper compartment of the FDC. Experimental procedures were performed as outlined for the *in vitro* bioactive release studies. The concentration of permeated curcumin was then determined using a nanophotometer (Implen, GmbH, Munich) whereby the extent of bioactive permeation across the membrane was evaluated by computing the drug flux. The flux (mg.cm^{-2}.hr^{-1}) of curcumin across the skin tissue was calculated per unit area by linear regression analysis of permeation data using Equation 3.5.

$$Js = \frac{Qr}{A\times t} \qquad \text{[Equation 3.5]}$$

Where, Js= the flux, Qr (mg) = the quantity of drug within the receptor compartment that has diffused through the skin, A (cm^{-2}) = the effective cross-sectional area that is available for permeation and t (h) = the time of drug exposure to the skin tissue.

3.5. Results and Discussion

The film cast method was used to synthesize films of various polymeric concentrations and degree of crosslinking obtained from the Box-Behnken design template. From experimental

observations it was noted that films of yellow to green color were produced due to the presence of curcumin and crosslinkage by genipin. When lower polymeric concentrations were used and the degree of crosslinking was minimal, films tend to have weaker mechanical properties, are more yellow in color and highly adhesive to skin tissue. Upon an increase in polymeric concentration and crosslinker a greenish colour is more dominant in films and mechanical properties are improved. Further increases in concentration lead to greater rigidity of films and decrease in flexibility. The addition of glycerol also played a significant role in improving the texture and mechanical properties of the films. Formulary optimizations lead to the production of films having transitional Young's modulus values and swelling capacity thus revealing advanced film characteristics as to be discussed. Experimental characterization lead to the acquisition of an optimal formulation containing 3%$^{w}/_{v}$ chitosan, 0.1%$^{w}/_{v}$ genipin and 0.4%$^{w}/_{v}$ hypromellose.

3.5.1. Chemical Structure Stability and Vibration Transitional Analysis

Physical and chemical interactions involved in IPN formation of various polymer blend concentrations were evaluated using FT-IR. This determined the degree of alteration within the native polymers. The crosslinking within the films were characterized by the change in color from yellow (due to bioactive incorporation) to a dark deep green colour when crosslinked with genipin as depicted in part A of this chapter. Furthermore, the disappearance of a peak, at 1223.62cm^{-1} as seen in the uncrosslinked structure, representative of C-O stretching within the aromatic ring, upon crosslinking indicated the formation of a crosslinking bridge at the aromatic site of genipin with chitosan (CS) supporting the formation of a crosslinked network. Furthermore, O-H stretching indicated by the large broad band at 3260.11cm^{-1} was observed shifting to 3278.79cm^{-1} and absorbance from 0.34–0.35A when crosslinked suggesting an increase in conjugation and intensity, impacting improved stability and physicomechanical properties to the film. It was further deduced that a change in polymer concentrations resulted in a slight change within the spectra. A broad strong band representing hydrogen bonding for O-H stretching within the range of 3200 and 4000 cm^{-1} was observed with all semi-IPN films. A shift within the spectrum varied with the degree of crosslinking. Film 9 displayed a wavelength at 3923.54cm^{-1}, whereas a wavelength of 3289.37 and 3268.02cm^{-1} was present in Films 1 and 2, respectively (annotated in Figure 3.8), characteristic to the bioactive curcumin indicating that an increase in crosslinker concentration resulted in a shift to a greater wavelength thus promoting conjugation and bond formation. In addition, the absence of a peak at the wavelength of 1281.98cm^{-1}, representative of the presence of an additional amino group in Film 1, indicated no presence of free amino groups as seen with Films 2, 5, 9, and 10. This was due to low CS concentration and more crosslinker, thus the formation of steric hindrance ensuring no presence of free amino groups. Film 5 showed the presence of

a band at 1980.69cm^{-1} (demarcated in Figure 3.8), which was not characteristic of any polymer entity but representative of the formation of C=C conjugation asymmetrical stretch and occurs when an intermediate amount of polymer entities are used thus the formation of intermolecular bonds. Semi-IPN formation resulted in significant differences in infrared absorption frequencies of the final product in relation to the original compounds. Network formation resulted in a change in the vibrational energy and frequency thus the presence of skeletal vibrations at wavelengths of 2937.54 and 2881.46cm^{-1} which were characteristic of C-H stretching and at 1712.30cm^{-1} characteristic of C=O stretching was noted. C-H bending within the aromatic ring was seen at wavelengths 921.85, 808.96, and 621.69cm^{-1} related to the incorporation of a C-N group in place of the C-O group within the ring due to crosslinking. C-N stretching is also present at the wavelengths of 1318.16 and 1280.60cm^{-1}. These peaks occur at higher vibrational frequencies and are associated to the degree of polymer network formation as well as crosslinking resulting in a change within the structural environment. As the concentration of crosslinker increased so did the intensity of the band formation as is indicated in the FTIR spectra, resulting in stretching and conjugation within the structure and bending between CH bonds in the aromatic ring. Formulations displaying greater band intensities corresponded to a higher degree of crosslinking. Hence, it can be deduced that the degree of semi-IPN film formation was affected largely by the polymers and crosslinker concentration.

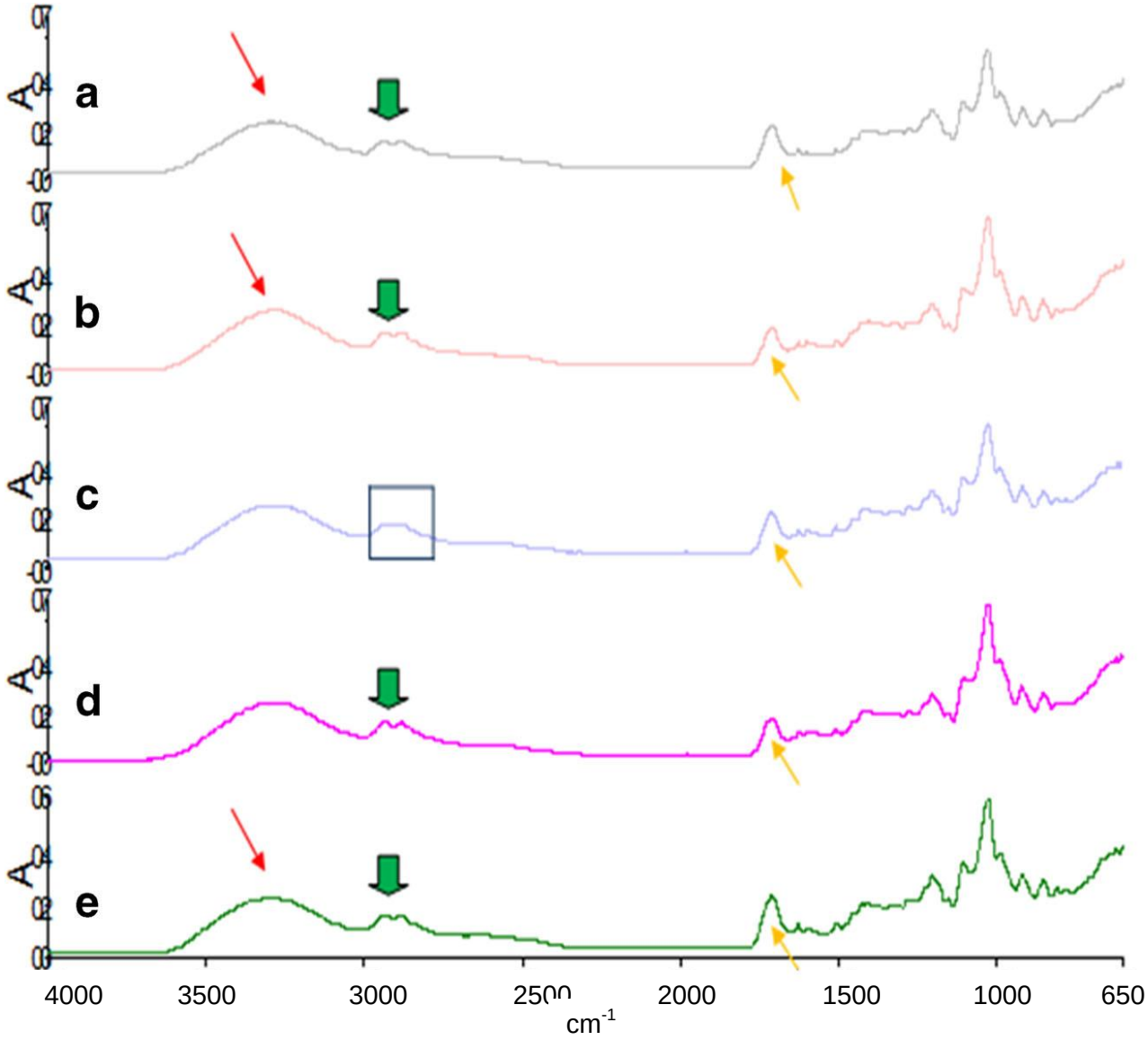

Figure 3.8: Fourier transform infrared spectroscopy of semi-IPN films: a: film 1, b: film 2, c: film 5, d: film 9 and e: film 10

3.5.2. Assessment of the Thermodynamic Behaviour of the Semi-IPN Films

The DSC thermograms of the various films showed a glass transition temperature (T_g) ranging between 28 and 30°C as shown in Figure 3.9. This was related to a change in heat capacity when a transition occurred due to network formation and crosslinker concentration. Film 1 presented with the greatest T_g value due to the presence of amino groups capable of crosslinking at the temperature of curing. Film 1 also exhibits semicrystalline behavior, therefore affecting the mobility of the amorphous region influencing a higher T_g value. In addition, the degree of crosslinking affected the amorphousity of the structure; the highest T_g was thus observed in Film 1 that had amino groups within the structure capable of crosslinking at the temperature of curing. A decrease in the degree of crosslinking due to crosslinker concentrations lower than the optimum was seen in Film 2, which resulted in a lower T_g value, thus was likely to display a quicker onset of degradation. Film 10 which had the highest recorded crystalline temperature (T_c) of 213.96°C (displaying a more ordered

molecular arrangement) resulted in decreased molecular motion, whereas Film 9 (demarcated in Figure 3.9b) has a lower degree of crystillinity with a T_c at 128.19°C. These observations are attributed to lower polymer concentration in Film 10 while higher polymeric concentrations were present in Film 9, thereby varying the degree of crosslinking. This suggested that Film 10 had a greater degree of regular molecular arrangements due to the formation of inter- and intramolecular bonds when lower polymeric concentrations are used, therefore a well-defined structure was obtained. Furthermore, Film 10 also displayed the lowest degree of decomposition at a high-temperature range of 213.96°C which was attributed to its crystalline state. Film 9 on the other hand displayed a lower degree of crystallinity that was related to the random orientation of molecules displaying amorphous behaviour due to free non-crosslinked groups within the structure with a poor polymer backbone. In addition, the amorphous form of Film 9 was linked to the lack of crosslinking (curing) as displayed by the exothermic peak which preceded the endothermic melting transition phase present in all films (Film 6) showing semicrystalline behavior. Furthermore, the data obtained from the differential scanning calorimetry profiles reveal that all formulations degrade between a temperature rate of 230 and 300°C; this is largely due to the known fact that natural polymers are highly biodegradable due to properties such as their hydrophilic nature, they are easily swellable and water wettable as well as greatly sensitive to temperature changes, thus they tend to degrade easily on thermal exposure. Sarasam and Madihally (2005) suggest that chitosan, degrades at a temperature of 270°C prior to melting. Thus, it can be deduced that a temperature of 350°C will greatly impact the stability of natural polymers as the temperature range from 230 to 300°C already causes decomposition of polymeric material.

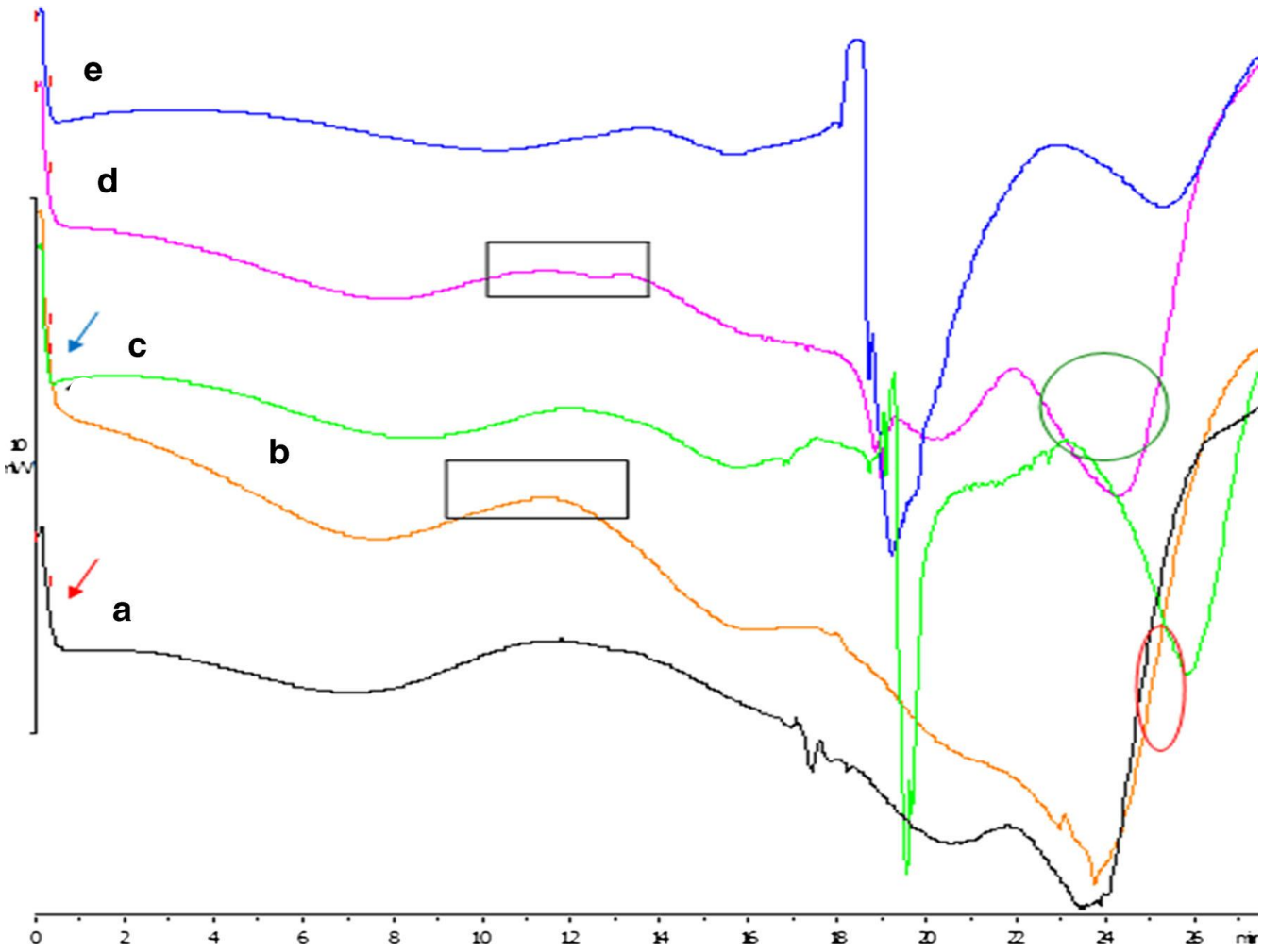

Figure 3.9: Differential scanning calorimetry of semi-IPN films: (a): film 1, (b): film 9, (c): film 2, (d): film 10, and (e): film 6

3.5.3. Structural Morphological Analysis of the Semi-IPN Films

Figure 3.10 a–g demonstrates the SEM images of the semi- IPN films and the difference in surface morphologies of the films prepared using various polymer and crosslinker concentrations. Zhao and co-workers (2009) and Bhuvaneshwari and co-workers (2000) have reported that the surface morphology of pure CS films is relatively smooth, nonporous, flat, and homogenous. However, with the introduction of a polymer IPN, the addition of bioactives and crosslinking modification to the surface revealed a slightly rough surface texture with the existence of pores and cracks in some instances, confirming a porous network microstructure which is one of the essential features required to optimize gaseous exchange at the wound site. Porous structures were clearly observed in all micrographs of films but the pore size and shape differed as shown in Film 6 (Figure 3.10e) which had a slightly more rough surface topology with pores that were elongated and small in shape, whereas Film 10 (Figure. 3.10 g) showed a surface morphology with a more fibrous like structure, pores tend to be long, larger, and rod-like in shape. Film 9 (Figure. 3.10 f) showed pores that are much larger and clearly hollow with a definite border, whereas Film 1 (Figure. 3.10c) and Film 2 (Figure 3.10d) showed a similar surface morphology with randomly

orientated pores that are indefinite in size, shape, and structure with the presence of a few cracks on the film surface. These differential surface features were attributed to the different polymer concentration and degree of crosslinking in the respective films. Film 9 (Figure 3.10f) and Film 10 (Figure 3.10g) have the highest quantity of crosslinker relating to the greatest degree of crosslinking. However, distinguishing features of pores of the various films such as those in Film 9 (Figure 3.10g) and Film 10 (Figure 3.10f) could be accounted to a lower concentration of CS at 3% and higher CS concentrations of 1% being used in Film 9 (Figure 3.10g) and Film 10 (Figure 3.10f), respectively. A lower degree of crosslinking results in cracks within the surface due to poor tensile properties as observed for Film 2 (Figure 3.10d). When both the crosslinker and CS were used in intermediate quantities in films, the pores were notably smaller and the surface topology was rougher relating to the percentage crystallinity as observed in Film 5 (Figure 3.10e).

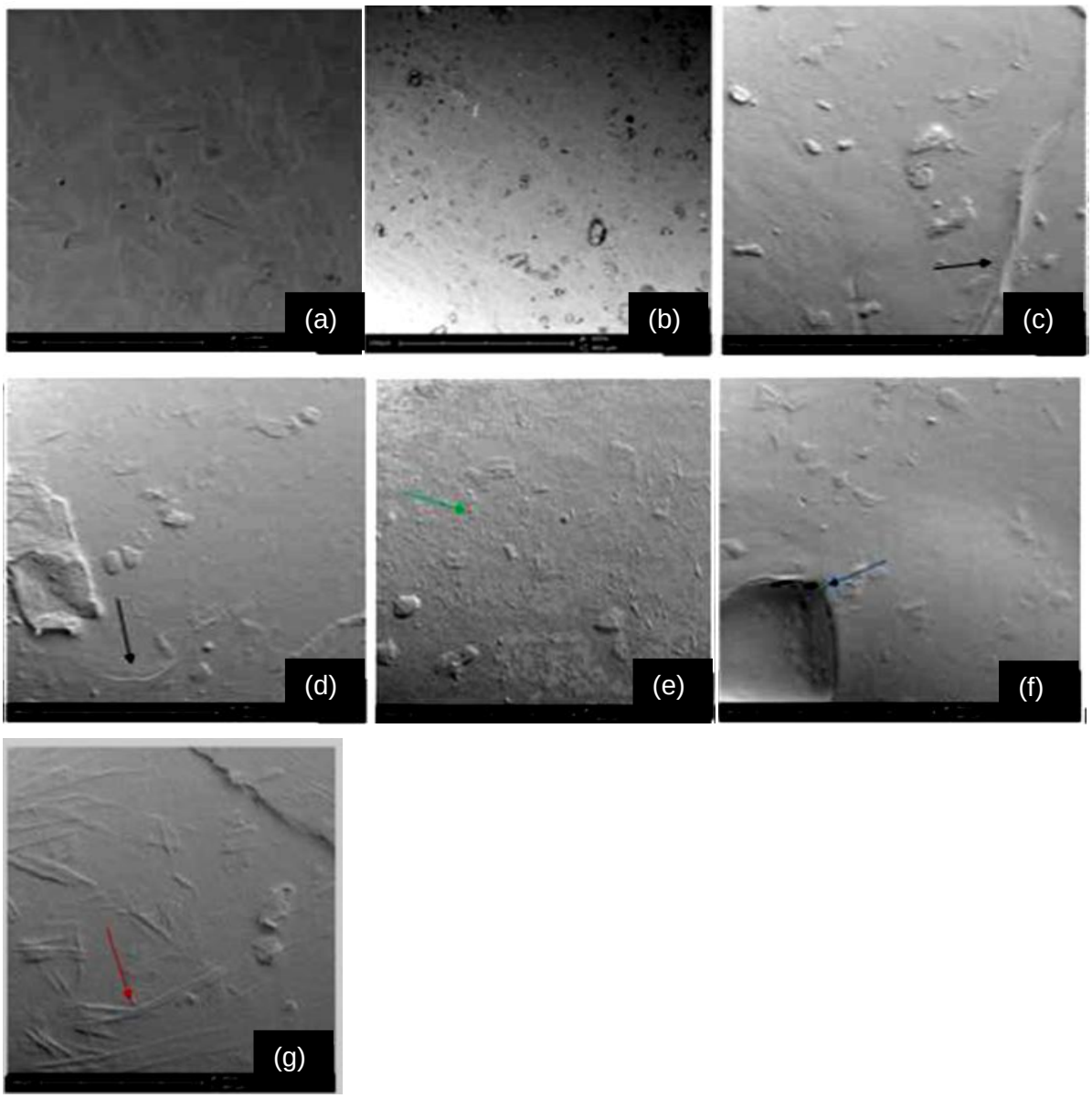

Figure 3.10: Scanning electron micrographs of semi-IPN films: (a), (b): optimized film, (c): film 1, (d): film 2, (e): film 5, (f): film 9, and (g): film 10

3.5.4. Textural Profile Analysis and Young's Modulus Determination of the Semi-IPN Films

The tensile and mechanical properties of all films were investigated by textural and nanotensile analysis. Figures 3.11 and 3.12 revealed that an increase in polymer concentration yielded a greater Young's modulus (YM) and tensile strength values as presented by Film 12. A greater degree of rigidity and stiffness is observed in Film 12 as an increase in crosslinking and polymeric concentration affects the polymer backbone formation and polymer chain flexibility which inevitably have an impact on the stress–strain relationship of the film. Semi- IPN films with a smaller Young's modulus value showed defined flexibility and thus a limited amount of stress was required to produce a relatively high amount of strain. Figure 6 illustrates the linear portion of the slope showing linear elastic deformation at this point thus an optimized, fairly flexible film will have a relatively small Young's modulus value as it is representative of both the rigidity and stiffness of the films. Interestingly, when an intermediate quantity of crosslinker was used (0.25%$^{w}/_{v}$), the ultimate strength (σu) was the greatest among all films as was seen in Films 4, 5, 7, 12, and 14, represented by the highest point on the stress–stain curve (Figure 3.13). However, films with a high σu value were also likely to have a high Young's modulus value as ultimate strength and Young's modulus are directly proportional and thus have poorer flexibility and elastic properties. Thus, the degree of crosslinking and polymer concentration has a distinct effect on elasticity and flexibility of films as ultimately a higher percentage causes a distinct increase in film rigidity and stiffness. Giovino and co-workers (2012) and Boatang and co-workers (2013) reported on the use of glycerol in films as a plasticizer to improve film properties and prevent a fracture, therefore the addition of glycerol also greatly improves the flexibility and elasticity index of films. Improved flexibility properties were impacted by the formation of H-bonding of glycerol with CS and at the same time ensuring the semidestruction of hydrogen network formation by the breakage of both intramolecular and intermolecular bonds.

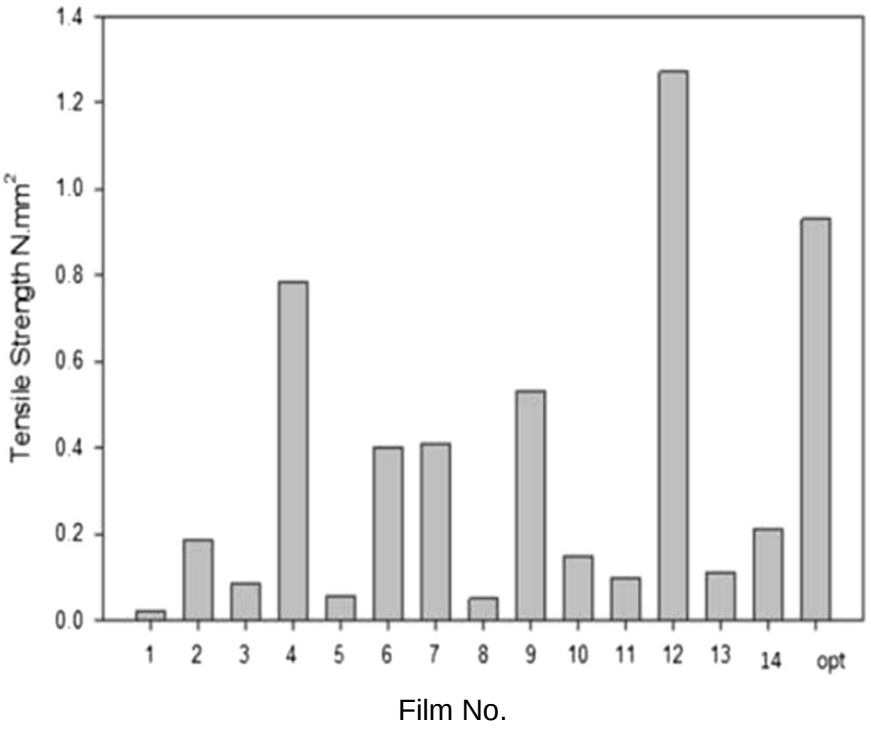

Figure 3.11: Tensile strength (N.mm^2) of the various semi-IPN Films

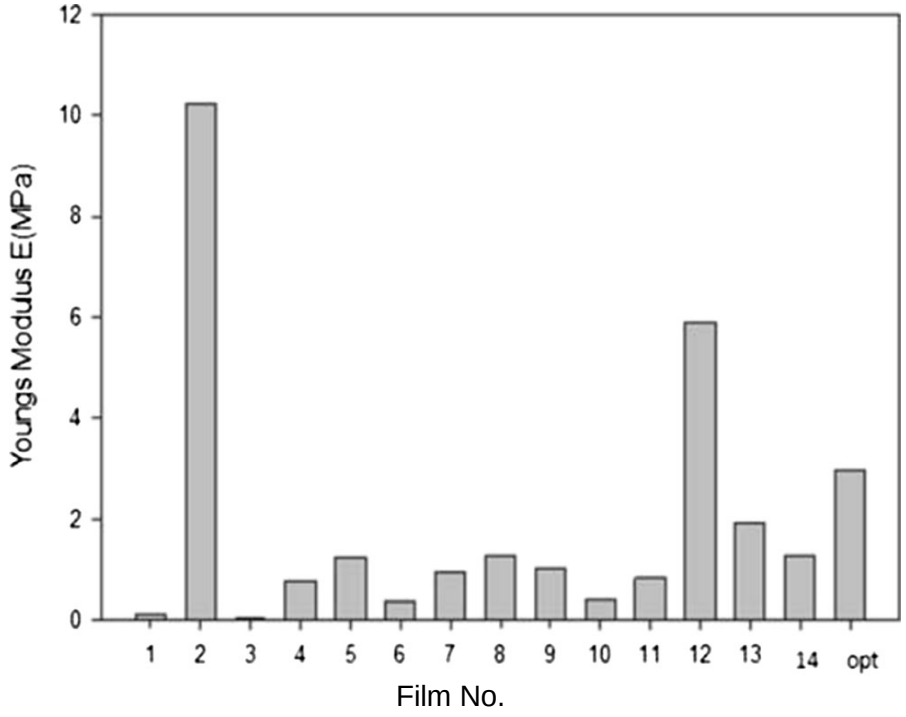

Figure 3.12: Young modulus E (MPa) for various film formulations via nano-tensile analysis

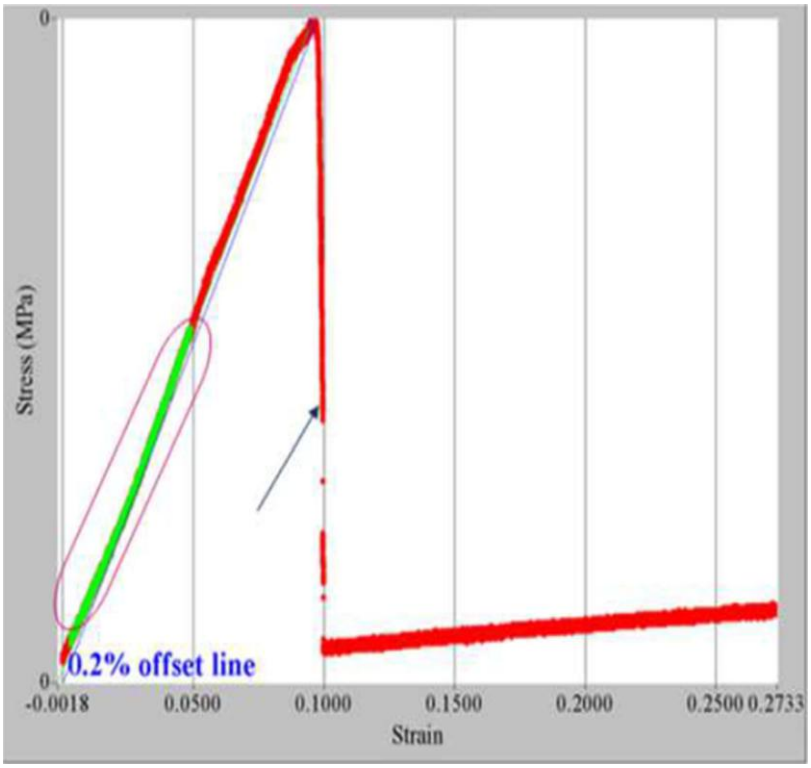

Figure 3.13: Stress–strain nano-Tensile profile and Young's modulus

3.5.5. Swelling Capacity and Equilibrium Water Content Analysis of the Semi-IPN Films

The swelling capacity, water absorption, and equilibrium water content are important factors when considering the rate of absorption of polymeric films when in contact with the skin surface. Thus, the swelling capacity (%) and equilibrium water content (%) was evaluated in phosphate buffer solution (37°C; pH 7.4) (Figures 3.14). Plots clearly revealed that Film 11, Film 13, followed by Film 2 had the greatest swelling capability occurring within the first hour after immersion. This can be directly attributed to the low crosslinker concentration, thus covalent bond formation between polymers and polymer chains occur to a lesser extent providing enhanced hydrodynamic free volume to accommodate more water molecules, therefore exhibiting a greater swelling capacity. Poor crosslinking resulted in an increase in porosity which leads to fast initial rates of liquid uptake and a higher extent of equilibrium swelling. This suggests that a faster onset, degree and rate of bioactive absorption will occur. When the concentration of crosslinker was increased as in Films 2, 6, 8, 9 and 14, the swelling capacity and water content decreased, due to greater covalent bond formation overcoming porous sites, thus allowing penetration and absorption to occur at a reduced rate. This ensured sustained release of the bioactive (curcumin) throughout every stage of the wound healing phase (i.e. inflammation, granulation, proliferation, and remodelling). Thus, it can be deduced that the overall delivery rate was dependent on the rate of swelling as a decrease in the swelling rate promoted prolonged and controlled release of bioactive.

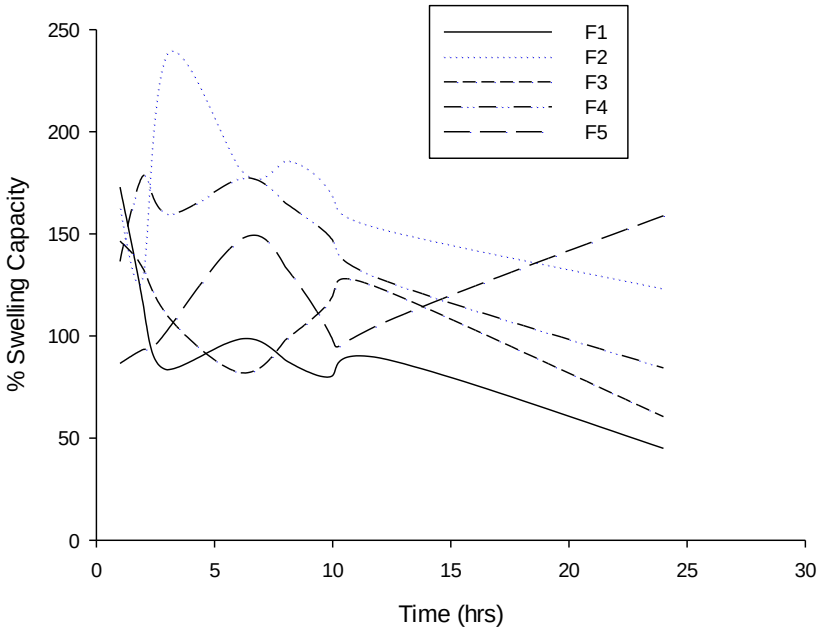
F1
F2
F3
F4
F5
% Swelling Capacity
Time (hrs)
0
50
100
150
200
250
0
5
10
15
20
25
30

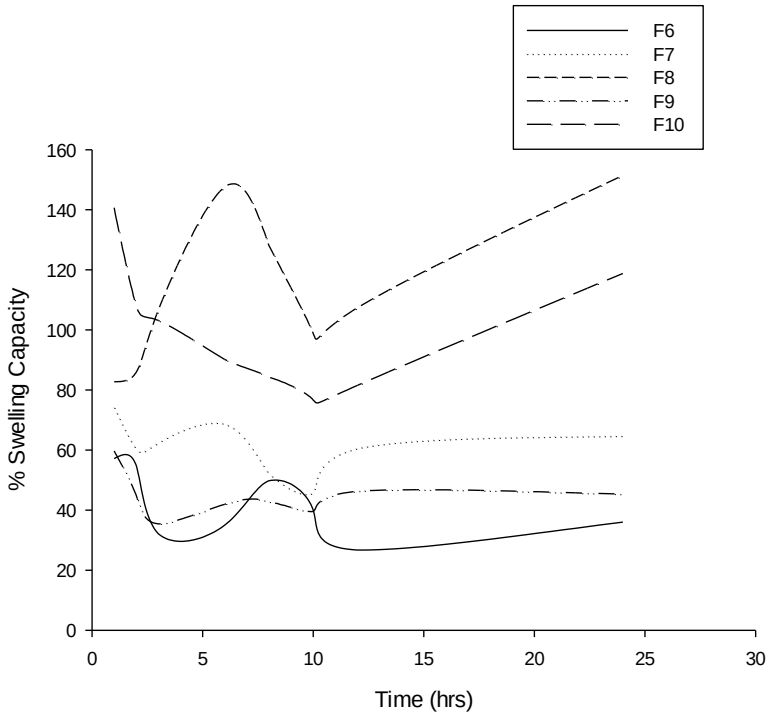
F6
F7
F8
F9
F10
% Swelling Capacity
Time (hrs)
0
20
40
60
80
100
120
140
160
0
5
10
15
20
25
30

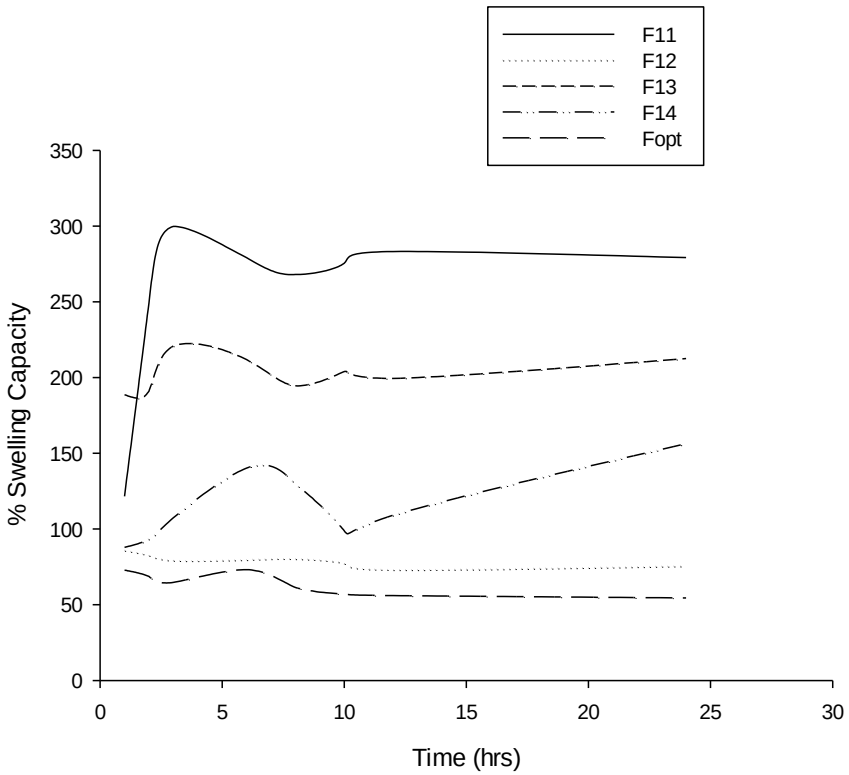

Figure 3.14: Profile of swelling capacity of the semi-IPN films 1–14 and the optimized film

3.5.6. Water Vapour Transmission Rate Analysis

Figure 3.15 represents the effects of various polymer concentrations on the water vapour transmission rate (WVTR). In the case of wounds, particularly burn wounds, the WVTR plays a key role with regard to moisture balance as it needs to be maintained throughout the repairing process. A low WVTR value could lead to numerous clinical challenges due to the build-up of exudates, whereas a very high value can lead to wound dehydration that decelerates the healing process. Furthermore, Sung and co-workers (2010) and Queen (1987) stated that a transmission rate between 2,000 and 2,500 g/m^2 per day would yield the adequate moisture environment required for optimal healing. In this study, it was deduced that the highest WVTR value was seen in Film 12 where a high concentration of polymer and crosslinker was used, thus promoting wound dehydration. Furthermore, it was noted that the WVTR value increased with an increased quantity of CS rather than hypromellose. Thus, it can be deduced that the WVTR value was directly proportional to the CS concentration and therefore for optimal gaseous exchange, an intermediate quantity of polymer and crosslinker was required as observed in Film 5a and b.

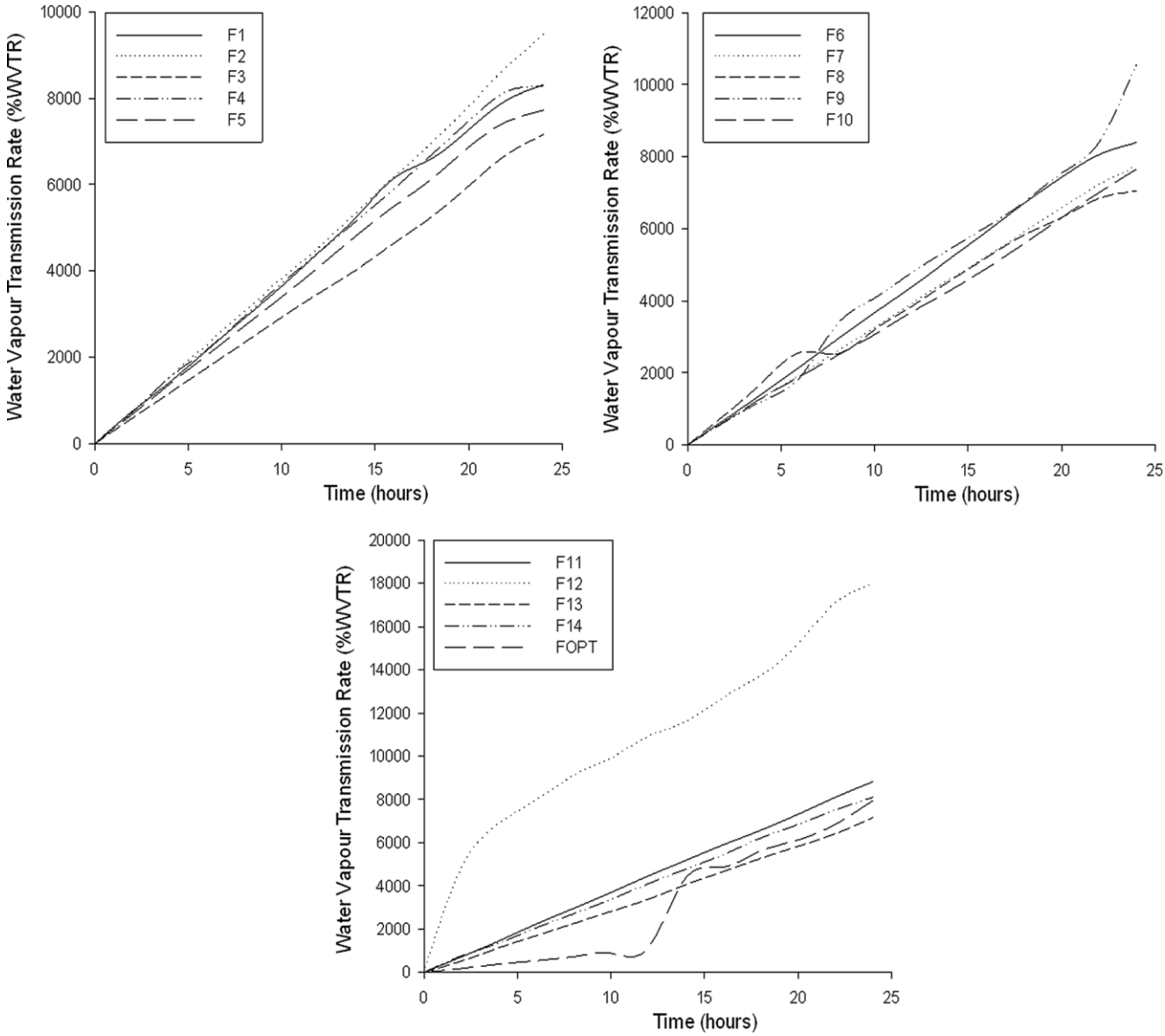

Figure 3.15: Profile of the rate of water vapour transmission within the semi-IPN films 1–14 and the optimized formulation

3.5.7. Rheological Characterization of the Semi-IPN Film Polymer Blends

Table 3.5 represents the rheological characteristics, in particular viscosity and yield stress, of formulation blends. From the results obtained, Films 3, 11, and 13 have the lowest shear viscosity rates and this was attributed to low-percentage crosslinking, suggesting weaker bonds due to lower chemical interactions between the amine groups of CS and genipin. Interestingly, it was noted that the degree of shear rate was directly proportional to the concentration of CS and the quantity of crosslinker used. At higher concentrations of CS (as in Film 2) where $3\%^{w/}_{v}$ CS was used, hydrodynamic volume expansion occurred, which resulted from the protonated NH_3 groups caused by repulsive forces thus increasing the shear rate (Pakravan. 2011). Furthermore, when higher concentrations of crosslinker was used, such as $0.025\%^{w/}_{v}$ (Films 1, 4, 5, 7, 8, and 14), the viscosity shear rate increased. Stronger interactions due to a greater extent of crosslinking resulted in a remarkable

increase in shear viscosity. The yield stress under experimental conditions can be defined as that stress under which no flow can be observed and is related to the polymer viscosity (Barnes and Walter. 1985). From Table 3.5, it is observed that lower viscosity rates such as those in Films 9-11 resulted in a weaker yield. Thus, semi-IPN films are able to exhibit greater strain results when a stress is applied in the presence of a high yield stress. This directly influences the elasticity of the films which is an important property regarding wound dressings for topical use. From the results obtained, it was noted that the best rheological and mechanical properties are observed in Films 2, 4, 12, 14, and the optimized film. Post characterization of semi-IPN films generated through the Box-Behnken experimental design lead to an ultimate optimal formulation of 3%$^{w/}_{v}$ CS, 0.1%$^{w/}_{v}$ genipin, and 0.4%$^{w/}_{v}$ hypromellose. This optimized formulation was further subjected to *in vitro* and *ex vivo* studies.

Table 3.5: Effects of various concentrations of polymer and crosslinker on the formulation viscosity and yield stress

Formulation no:	**Viscosity at a shear rate of 100s^{-1} (MPa)**	**Yield Stress (Pa)**
F1	742.51	20.97
F2	605.36	38.55
F3	32.93	38.46
F4	529.48	38.59
F5	578.53	38.52
F6	219.67	38.63
F7	516.38	38.62
F8	579.62	38.62
F9	115.27	29.65
F10	40.92	32.29
F11	6.51	25.03
F12	46.85	38.51
F13	1.24	9.97
F14	578.32	38.57
F optimized	62.53	38.59

3.5.8. Bioevaluation of the Curcumin-loaded Semi-IPN Film

A transdermal permeation and release study was undertaken on the optimum candidate formulation obtained. Bioactive release and permeation studies of curcumin are depicted in Figure 3.16 a, b. Interestingly; an initial burst release is observed within both systems at 1.1mg (bioactive release) and 2.23µg (bioactive permeation) within the first hour but is more pronounced during the permeation study. The first phase of the healing process is

inflammation and begins within a few minutes of injury and may last up to 24 hours or longer (Pawar et al., 2013), thus an initial burst release as seen initiates the delivery of curcumin at the wound site thus potentiating a therapeutic anti-inflammatory and antibacterial therapeutic effect at the wound site in association to inflammation. Furthermore, throughout this study, it was noted that bioactive release occurs at a fine rate when permeated through the skin. This can be directly attributed to the hydrophobic nature of curcumin, thus enhanced release rates were observed when in contact with skin tissue as preferential interactions occur with lipid-based membranes such as the phospholipid bilayer present in the skin. Therefore, this directly impacts the major barrier associated with curcumin release improving its bioavailability and clinical efficacy (Zhao et al., 2013).

The stratum corneum of the skin only allows moderately lipophilic molecules that are small to partition across it passively, into the deeper layer of the skin (Zhao et al., 2013). The stratum corneum is not an inert structural material and behaves as a reactive medium that may alter in response to changes in the sorption or desorption of penetrant molecules, thus deviation to Fick's law occurs (Scheuplein. 2011). Between 4 and 6h, an intermediate second burst release was seen in Figure 3.16b from 3.39 to 6.19µg, thus further potentiating a deviation from Fick's law. The flux rate of permeated bioactive release reveals substantial deviation, thus revealing that steady-state release profiles are not maintained throughout the study. Therefore, curcumin-loaded IPN films will serve as a dressing with ideal characteristics intended to be applied topically to wounds. Variation to steady-state release profiles potentiating wound healing is further supported by Seetharaman et al. (2011) whom also state that ideal characteristics for wound healing is potentiated by this type of release. When considering factors that affect the permeation rate across skin tissue, evaluation of characterization studies such as the FTIR analysis discussed in text, it can be seen that introduction of crosslinking by genipin resulted in the formation of crosslinking bridges at the aromatic site thus supporting the formation of a crosslinked network. This brought about an increase in intermolecular conjugation. Augmentation of crosslinking resulted in greater mechanical properties such as an elevated Young's modulus which could be seen as the crosslinking increased thus forming stiffer and more rigid films. Therefore, an increase in crosslinking decreases the permeation ability as a denser network structure occurs. Rana and co-workers (2005) also state that stronger crosslinking of chitosan by increasing the crosslinker concentration seems to restrict the permeation of drug.

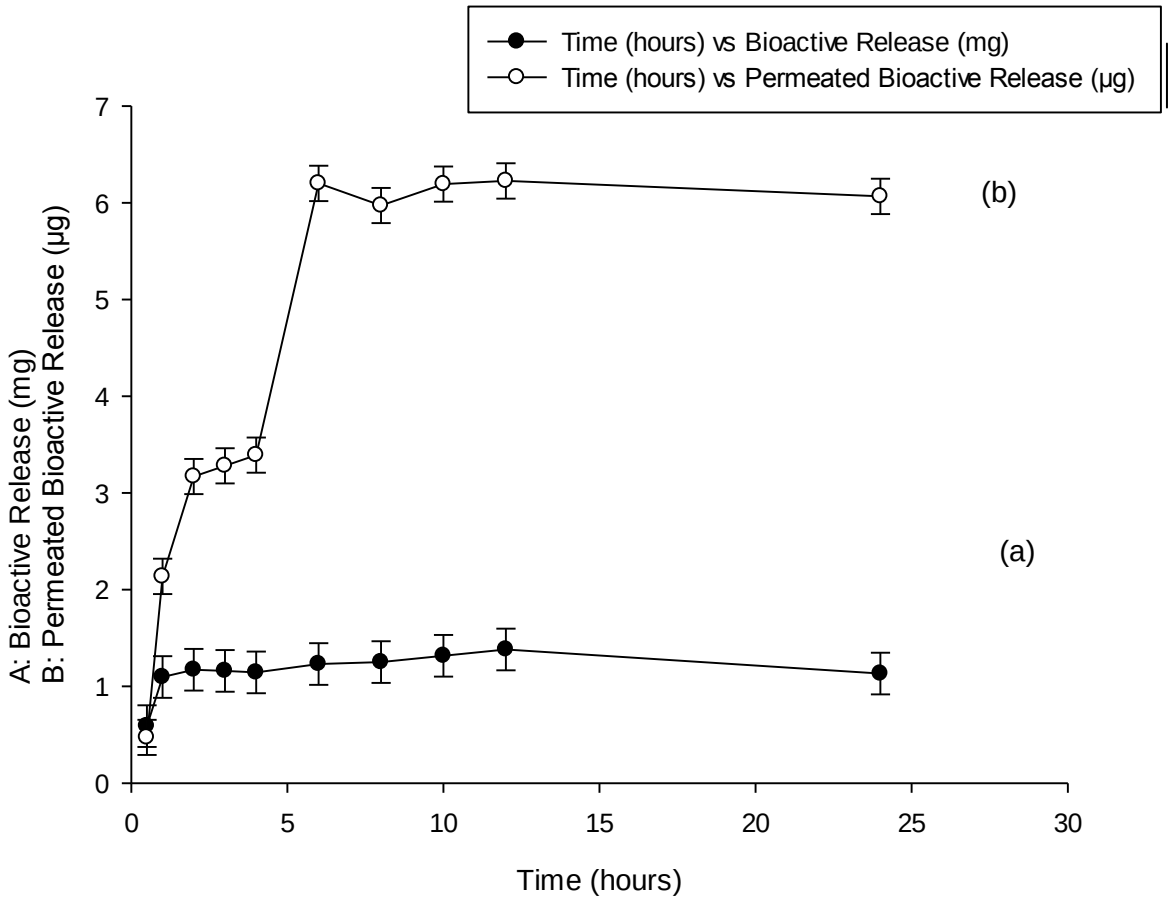

Figure 3.16: (a): Drug release profile of curcumin-loaded semi-IPN films and (b): drug release permeation through the Sprague-Dawley rat skin.

3.6. Concluding Remarks

Preliminary studies led to the rational identification of the formulation variables most suited for film formation. Further studies were then conducted to ensure development and optimization of the novel semi-IPN film composed of CS and its derivatives, crosslinked and incorporated with a bioactive (curcumin). Medium molecular weight CS was dissolved in citric acid and successfully crosslinked with genipin before the incorporation of biopolymers such as hypromellose and curcumin in a stepwise manner to structure an IPN that ensured the bioactive can be gradually diffused through the Sprague-Dawley rat skin model. The films have shown the potential to swell and release the bioactive to stimulate proliferation, differentiation, and remodelling of the targeted skin tissue.Outstanding release and permeation rates were noted when the system was in contact with the skin tissue thus suggesting that topical application of the films at a wound site would augment bioactive release. An important outcome of this chapter was to identify variable polymer concentrations to obtain an optimal formulation bearing the most advantageous characteristics in terms of bioactive release, flexibility, toughness and the ideal rheological properties.

The attainment of a design of experiments (DoE) from the statistically derived Box-Behnken design and mathematical conceptualisation lead to the attainment of optimal concentrations

of biopolymers for synthesis of the ideal film. Inclusion of genipin was thus shown to be beneficial as the mechanical properties of the film were improved greatly. This chapter served to identify the candidate formulation which led to the identification of three variables with their corresponding upper and lower limits for input into the Box-Behnken Design as described. Formation of the films serves as an ideal comparative constituent when compared against the nanofibrous mat as will be discussed in Chapter 4 and 5. Attainment of the optimal candidate formulation also aids the fabrication of nanofibres.

CHAPTER 4
FABRICATION AND CHARACTERISATION OF THE CROSSLINKED NANOFIBROUS MAT AS A WOUND HEALING DELIVERY SYSTEM

4.1. Introduction

Wound healing is a dynamic process (Said et al., 2011) that involves a complex sequential cascade that may occur simultaneously involving mediators such as parenchymal cells, blood cells and the extracellular matrix (ECM) of the skin (Moura et al., 2013). These mediators may be activated to synergistically restore healing integrity thus preventing organism homeostatic deregulation (Jayakumar et al., 2011) throughout the phases of inflammation, proliferation, re-epithelisation and remodelling,(Moura et al., 2013) the main phases that occur during healing. To ensure optimal and accelerated healing of a wound area, coverage of the wound site is a requirement for provision of a protective environment (Gu S-Y et al., 2009). As also mentioned in previous work (Mayet et al.,2014) and stated in Chapter 2 the native skin serves as the perfect wound dressing thus the ideal artificial dressing should be designed in such a way as to replicate its essential properties and functions(Morin et al., 2007; Moura et al., 2013). Some of the ideal properties that should be incorporated in a wound healing dressing include protection from bacterial invasion, moist wound environment, gaseous exchange, debridgement, non toxic, non adherent, non allergenic (Jayakumar et al., 2011) and mimicking the essential functions of the skin tissue (Boatang et al., 2008; Mayet et al., 2014). Thus the goal in producing an optimal dressing would be to ensure these functions are incorporated together as a porous dressing structure, suitable wound barrier that has the capacity to mimic the extracellular matrix (ECM) of the skin.

Structures that are nanofibrous based are of increasing interest in the wound healing field as they can be applied in biomedical applications in the form of dressings, scaffolds etc. Materials based on nanofibres enable architectural, structural and morphological similarities to the extra cellular matrix of the native skin to be obtained (Pinho et al., 2009). Nanobiotechnology provides opportunities that enable these features to be improvised as it is incorporated in the field of research, molecular biotechnology, nanosciences and materials. It is a novel interdisciplinary field that utilises the use of biopolymers and materials, both of organic and inorganic nature to fabricate devices on the nano-metre scale, that possess mesoscopic architectural properties (Niemeyer, 2006). Of interest in this chapter is an advanced innovative novel system synthesized by the process of electrospinning of biomaterials to form nanofibres as a wound healing application, as our published study indicated and explicated in Chapter 3, the use of biomaterials in the form of a wound healing film (Mayet et al., 2014). Electrospinning involves the use of a unique approach to fabricate

nanofibres by the use of electrostatic forces. A high potential is applied to a polymeric solution to produce a jet whereby nanofibrous webs can be collected on the surface of the collecting end of the foil (Taylor, 1969; Reneker and Chun., 1996; Zahedi et al., 2010). Nanofibrous wound dressing applications produced by the process of electrospinning have many more unique qualities as compared to dressings produced by other conventional methods (Zhang et al., 2005; Zahedi et al., 2010) such as: semi-permeability which allows for high gaseous exchange and provision of a moist environment due to the many small pore size between fibres. Further homeostasis is maintained as the nanofibres structure has the ability to mimic the extracellular matrix of the skin (ECM), thus no further homeostatic agent need be even included (Zahedi et al., 2010). A scar free recovery can be obtained as normal tissue growth is encouraged, in particular by the use of biomaterials that are biodegradable and biocompatible encouraging tissue self repair and promoting blood flow and good cell conductivity which facilitate the wound healing process (Martindale. 2000). Nanofibres possess a 3D conformity due to their structure and morphology thus allowing an increase in flexibility and resilience at the wound site, in addition they also provide for greater absorbability in comparison to conventional dressings as their structure allows for a high surface area to volume ratio, thus capable of absorbing increasing amounts of exudates (Dabney et al., 2002; Zahedi et al., 2010).

4.2. The Technique of Electrospinning

Within the tissue engineering community, electrospinning has gained much interest due to its ability to mimick the biological and structural features and functions that ensure a replica of the native extracellular matrix. Furthermore, it has gained much attention as an attractive feature for scaffolding and nanofibre formation due to its inexpensive setup nature and simplicity (Pham et al., 2006). This technique allows the configuration of fibres on the nanoscale meter ranging from few nanometres to hundreds of nanometres. In addition, a porous nanofibrous structure can be generated to ensure incorporation of gene factors, bioactives and drugs (Chong et al., 2007).

The process of electrospinning involves the use of an apparatus that consists of a high voltage source, syringe pump and collecting disc as illustrated in Figure 4.1. Electrospinning expresses the use of a high-voltage electric current which runs through the polymer solution inducing a charge in the polymer which results in a charge repulsion. The solution is held at the needle tip by surface tension which is opposed by the electrostatic forces induced by the electric field charges. Over time, charge repulsion within the polymeric solution overcomes the surface tension due to the applied high-voltage source. This results in the creation of a polymeric solution jet. Solvent evaporates from the jet, as the jet travels to the appropriate collecting disc whereby polymeric nanofibres can be collected (Pham et al., 2006).

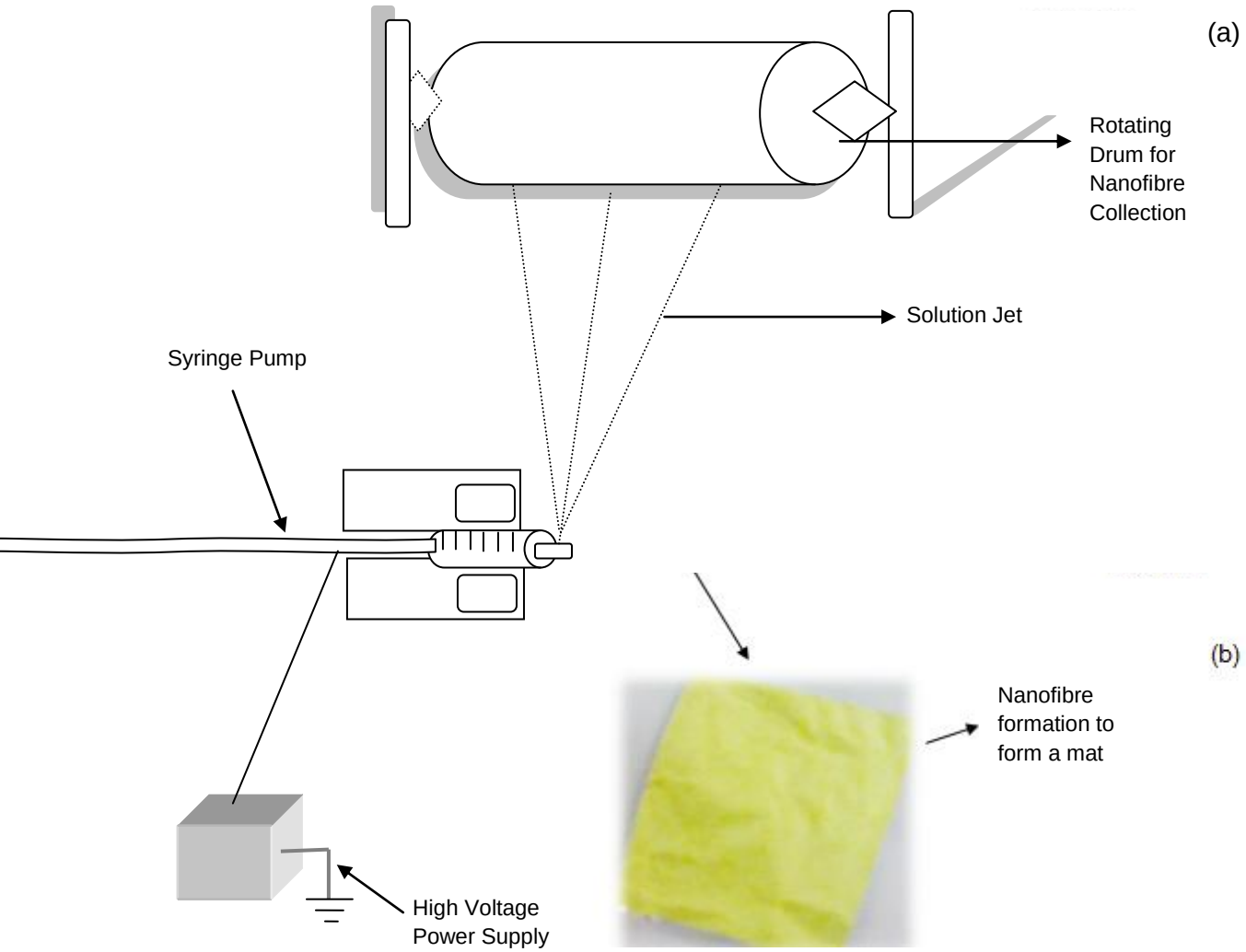

Figure 4.1: (a) The electrospinning apparatus with significant elements to fabricate the (b) nanofibrous mat.

In addition, in order to ensure the fabrication of optimal nanofibres the stability of the polymeric jet is of significant importance. Pham and Sharma (2006) classify polymeric jets into four varying regions as follows:

- **Base Region:** This specifies the formation of a cone known as the 'Taylor Cone' which occurs upon the emergence of the polymeric jet from the needle. Electric field forces applied as well as the surface tension occurrence denote the shape of the base.
- **The Jet:** Jet formation is dependent upon the surface tension and the electric field force. A higher conductivity will prevail in greater jet formation and strong electrostatic forces will allow jet formation from flat surfaces. Jet formation transpires upon the application of electric forces which cause acceleration and stretch of the jet consequently decreasing the diameter and increasing the length. Furthermore when a

solvent of high vapour pressure is utilised, jet velocity as well as fibre diameter is further decreased (Reneker and Chun, 1996).

- **The Splay:** This occurs upon radial charge repulsions which produce nanofibres of approximately equal charge and diameter per unit length (Reneker and Chun.1996). Splaying dominates when a solitary swift whipping jet transpires due to the use of high electric fields and frequency when the jet is travelling a short distance. Instability occurs resulting in bending and stretching of fibres (Shin et al., 2001; Shin et al., 2001).
- **The Collection:** The collection surface plays a significant role in the collection of nanofibres. The nature of composition and material signifies the type of fibres to be collected for example; metal surfaces would obtain smooth fibres whereas water surfaces would result in shrinkage of fibres. The uniformity and alignment of fibres also depend on the geometry of the collecting surface. Parallel plates, frame conductors as well as rings have been used (Huang et al., 2003).

4.3. Limitations Pertaining to the Degree of Successful Nanofibre Formation utilizing the Bioactive Polymeric Solution

In the last few decades, electrospinning has become a popular revenue for polymeric nanofibre formation due to its electrohydrodynamical phenomena launching broader realms of material science and nanotechnology. Nanofibre formation has now been altered to include large scale production and processes, low cost, environmentally and economically friendly as well as involving a high capital intensive (Reneker and Yarin., 2008). However, there are many limitations and challenges faced when considering the electrospinning process as the production of nano-scale dimension materials is no trivial task. Hydrodynamic instabilities and mechanical constraints are the main intrinsic physical limitations pertaining to electrospinning (Kowalewski et al., 2005). The production of nanofibres via the electrospinning technique produced many notable limitation characteristics as follows (Thompson et al., 2007):

- Diameter distribution as well as as-spun nanofibres diameter predictions is unreliable.
- Aligned orientation of fibres is difficult to produce. Production of non-woven mats is much simpler and easier to produce as opposed to orientated nanoropes, crossbars and nanofibres arrays.
- Many models have been generalised for the process of electrospinning and multiple jet formation, however precise process control has not reached the desirable level.
- Relatively low production rates are produced when electrospinning, however Yarin and co-workers (2004) have reported that a 12 fold increase in production is possible.
- Nanofibrous bead formation due to capillary instabilities as well as nanofibre diameter uniformity and morphology is multifarious to control.

- A characteristic of electrospinning such as elongation behaviour with regards to extremely strong uniaxial elongation flows as well as elemental aspects regarding rheological properties and behaviour of concentrated and semi-dilute polymeric solutions is absent.

According to Sarkar and co-workers (2010) electrospinning is known to be the most successful way of nanofibre production for commercial use. Nonetheless due to its many limitations as discussed, many researchers have aimed at modifying the traditional electrospinning method to enhance the electrospinning process to overcome the inherent challenges faced with using a traditional electrospinner and the polymeric solution. Of significant importance when undergoing the electrospinning procedure is the jet stability. Rutledge and co-workers (2000) provided a model to display the instabilities of the jet. Jet instabilities were classified as Rayleigh instability and two 'conducting' modes. Rayleigh instabilities which are axisymmetric involve the use of high electric fields and charge densities whereby the instability is dominated by surface tension. In contrast to this, the conducting modes are independent of surface tension and are dominated by electric forces whereby one mode produces a 'whipping instability' known to be non axisymmetric and one conducting mode that is axisymmetric(Shin et al., 2001).

In order to overcome these limitations and challenges, the various parameters affecting the electrospinning process needs to be taken into account. Table 4.1 depicts the various parameters, their effect on electrospinning as well as resolutions to be undertaken to overcome this (Haghi and Akbari, 2007; Pham et al., 2006).

Table 4.1: Parameters pertaining to limitation occurrence during the electrospinning process

	Consequence on electrospinning	**Parameters**	**Resolution**
Solution Properties			
Viscosity/ Concentration	Fibre diameter size and morphology, nanobead formation	↑viscosity, ↑fibre diameter size,↓ nanofibre formation	↑polymer concentration
Conductivity	Jet formation, nanobead formation, diameter size	↑conductivity, ↑jet and nanofibres formation, ↓bead formation and diameter size, ↑fibre uniformity	Addition of ethanol, NaCl (salt), Electroconductive agents: Polyethylene Oxide (PEO) and Polyvinyl Alcohol (PVA) and charged surfactants
Surface Tension	Nanofibre size and morphology, Electrospinning process, nanobead and droplet formation	↓surface tension,↑ nanofibre formation, ↓bead formation	Addition of PVA and PEO, Choice of solvent
Polymer Molecular Weight	Morphology and nanofibres diameter size, nanobead formation	↑molecular weight;↑ uniformity,↓ nanobead and droplet formation	Polymers with ↑ molecular weight
Controlled Variables			
Flow Rate	Fibre diameter, nanobead formation	↑↑ flow rate: nanobeading due to ↓evaporation time,↓↓rates: fibres with smaller diameters	Alter flow rate accordingly
Electric Field Strength	Fibre diameter size, junction and bead formation, Jet and Taylor cone formation	↑voltage: receding Taylor cone, ↑nanobead formation, jets with ↑diameters.↑↑voltage, no visible Taylor cone. ↓voltage: jets with Taylor cone forming bead free spinning	Alter or ↓voltage accordingly
Distance	Fibre size and morphology	Varies according to polymers used, effect on bead formation and electrospraying.	Alter distance between tip and collector accordingly.
Collector Composition/ Geometry	Fibre texture, packing density and alignment	Conductive collectors influence the packing density of fibres.↓conductivity:↑ porous structures. Metal collectors produce smooth fibres whereas water surface collectors cause fibre	Choice of collector according to desired outcome

		shrinkage.	
Ambient Parameters			
Temperature Humidity	Fibre diameter Porous surface on fibres	↑temperature,↓diameter ↑humidity,↑pore formation	↑temperature accordingly ↓humidity accordingly

4.4. Selection of Optimal Parameters for Advantageous Nanofibre Formation

During the electrospinning process many drawbacks had been noted such as minimal to no jet formation thus poor to no nanofibre formation, electrospraying as well as nanobead formation. Thus, many steps were undertaken to improve the spinning process.

To reduce toxicity and augment the natural nature of the system, the solvent of choice was deionised water. An attempt was made to electrospun nanofibres using the polymeric solution, but failure to obtain fibres was noted. Thus many challenges were identified such as poor conductivity properties, low viscosity and weak charge density which lead to the instability of the polymer jet solution. To overcome this many progressions were implemented to improve the solution properties. This included advancing the conductivity and charge density to overcome surface tension at the jet and Taylor cone by the addition of PEO (Fong et al., 1999). The addition of a PEO solution gave rise to a higher viscosity due to intermolecular and intramolecular interactions thus reducing nanobead formation; furthermore absorption of PEO molecules at the solution surface facilitated a decrease in the surface tension (Duan et al., 2004). To enhance this phenomena ethanol was added to make a PEO solution at a ratio of 2:3 of ethanol: deionised water respectively. Addition of ethanol/alcohol to the solvent augments the conductivity of the polymeric solution resulting in the formation of smoother fibres and amplifying the stability of the jet formation (Pham et al., 2006). Furthermore it was noted that addition of a PEO solution on its own did not successfully enhance nanofibre formation and thus a second electroconductive agent was needed to be introduced. PVA was the conductive polymer of choice, further reducing surface tension by increasing available electrostatic charges. The addition of both PEO and PVA solutions simultaneously allowed for the successful configuration of nanofibres together with the addition of other auxiliary excipients. The addition of other agents such as non ionic surfactants, Polyoxyethylene Sorbitan Monooleate (Tween 80) in small amounts, further augments nanofibre formation by minimising bead formation enhancing the effects of formed nanofibres. Enhancement of fibre fabrication is expanded by the addition of salt (NaCl) in minute amounts which increases the solution conductivity and charge density ensuring optimal nanofibre formation (Pham et al., 2006).

Nanofibre morphology, uniformity and diameter size are also largely dependent upon the processing parameters or variables that can be controlled such as flow rate, distance and

voltage supply. Trial and error using variable parameters regarding the above was undertaken to optimize the process. With regards to distance it was noted that a very short distance lead to electrospraying where nanofibres were not obtained. Increasing the distance allows for evaporation and drying of the solvent therefore maximising fibre formation. Increasing the distance further lead to unwanted bead formation. Applied voltage has an effect on both fibre diameter and bead formation. A lower voltage will produce fibrous mats with minimal bead formation and larger diameters. Higher voltages produce fibres of smaller and greater bead formation (Haghi and Akbari. 2007). Upon investigation using the polymeric solution an optimal voltage rate was attained.

Lastly viscosity plays a significant role in the fibre formation process as well as the eminence of the fibres formed. Low solution viscosities lead to minimal and poor nanofibre fabrication as well as electrospraying and nanobead formation. Thus, improvision of the ideal viscosity is of significant importance as a very high viscosity will lead to no Taylor cone formation at all. Based on this and various other characteristics required a Box-Behnken design template was implemented to optimize fibre synthesis as discussed in the sections to follow.

Design of the Biopolymeric Nanofibrous Mat employing a Design Strategy

4.5. Materials and Methods

4.5.1. Materials

All experiments conducted employed the use of chitosan, medium molecular weight poly (D-glucosamine) deacetylated chitin, hypromellose (hydroxymethylcellulose 2910), citric acid (ACS reagent ≥99.5%, M_w=192.12 g/mol), genipin (≥ 98% (HPLC) powder (M_w= 226.23 g/mol) and curcumin, all obtained from Sigma Aldrich Chemie GmbH, Steinheim, Germany. PVA- mowiol® 4-88 with a M_w=31000 g/mol and PEO-Polyox™, WSR 303 obtained from Sigma Aldrich Chemie GmbH, Steinheim, Germany as well as Tween 80 obtained from uniLAB®(Merck Chemicals (Pty) Ltd, Wadeville, Gauteng, RSA) was utilised

4.5.2. Preparation of Crosslinked Nanofibrous Mats

Solution A: A1+A2+A3+A4 (to 100ml)

Chitosan (CS) (A1) solution is prepared by dissolving in an aqueous acidic solution comprising of a 5%$^{w}/_{v}$ (50 mg/mL) citric acid as a solvent medium. The chitosan used is of medium molecular weight and varies in concentration between 1%$^{w}/_{v}$ (10 mg/mL) to 3%$^{w}/_{v}$ (30 mg/mL). Aqueous solution of Hypromellose (A2) ranging between 0.4%$^{w}/_{v}$ (4 mg/mL) to 1.6%$^{w}/_{v}$ (16 mg/mL) was then added. Crosslinking and the formation of a semi interpenetrating polymer network were obtained by the addition of genipin (A3) at

concentrations ranging from 0.01%$^{w}/_{v}$ (10mg/10mL) to 0.05%$^{w}/_{v}$ (50mg/10mL). Lastly the bioactive curcumin (A4) [1%$^{w}/_{v}$ (10 mg/mL)] was added.

Where A1: Chitosan
A2: Hypromellose
A3: Genipin
.A4: Curcumin

Solution B: Electroconductive agents polyvinyl alcohol (PVA) at a concentration of 10%$^{w}/_{v}$ dissolved in deionised water (10.0g of PVA dissolved in 100ml deionised water)

Solution C: 2%$^{w}/_{v}$ polyethylene oxide (PEO) dissolved in 40% ethanol and 60% deionised water (2.0g dissolved in 100ml 40:60 – ethanol: deionised water)

Final Formulation:
Solutions A+B+C was added at a ratio of 1:1:1 (300ml) together with a surfactant Polyoxyethylene Sorbitan Monooleate (5ml) and a net charge density enhancer NaCl (7.5mg). The solution was left overnight to stir before electrospinning.

Figure 4.1 describes the electrospinning process, parameters and setup which involves the application of a voltage of 20kV supplied by Glassman high voltage inc,(high bridge NJ USA) to the biosolution via a pipe attached at one end to a 10mL syringe that is inserted in the slot provided by the pump (Chemyx Inc syringe infusion pump). The solution was fed into the syringe and allowed to run whereby nanofibres were collected on an aluminium foil attached to the collecting surface whereby a nanofibrous mat was formed.

4.5.3. Strategic employment of the Box-Behnken Experimental Design for Optimization of the Nanofibrous System

For the most favourable development of the wound healing system, statistical formulation optimization has to be undertaken. This is achieved by employing a systemic design of experiments (DoE) that led to the utilisation of a three factor Box-Behnken Design template which consist of 15 formulations indicating the optimal formulatory components indicated in Table 4.2. The Box-Behnken design template was based on three variables which determined formulary characteristics in terms of the release and physicomechanical properties of the system.

Table 4.2: Box-Behnken Design Template for statistically derived s-IPN Nanofibrous Mats

Formulation No.	Chitosan (%w/w)	Genipin (%w/w)	Hypromellose (%w/w)
1	3	0.25	1.6
2	1	0.25	0.4
3	3	0.1	1
4	2	0.1	1.6
5	1	0.25	1.6
6	2	0.25	1
7	2	0.4	0.4
8	3	0.25	0.4
9	2	0.25	1
10	3	0.4	1
11	1	0.4	1
12	1	0.1	1
13	2	0.4	1.6
14	2	0.1	0.4
15	2	0.25	1

4.5.4. Determination of the Molecular Vibrational Transitions of the Nanofibrous Mats by Fourier Transform Infrared Spectroscopy

A PerkinElmer® Spectrum 100 Series FT-IR Spectrometer fitted with a universal ATR Polarization Accessory (PerkinElmer Ltd., Beaconsfield, UK) was employed and Spectra over the range 4000-625cm^{-1}, with a resolution of 4cm^{-1} and 4 accumulations was used in order to determine molecular transitions by the identification of absorption bands that occur at various wavelengths due to bioactive polymer interactions.

4.5.5. Surface Morphology and Nanofibre Density by Scanning Electron Microscopy

A SEM (Phenom™, FEI Company, and Hillsboro, Oregon, USA) was used to conduct analysis of nanofibre samples. The surface morphology of the nanofibrous mats were evaluated for nanofibre size range, diameter and bead formation.

4.5.6. Determination of the Thermal Analysis by Advanced Differential Scanning Calorimetry

Thermoanalysis of samples were carried out using an Advanced DSC (TMDSC/ ADSC) (Mettler Toledo DSC-1 STAR^{e} System, Schwerzenback, ZH, Switzerland) whereby factors such as glass transition and phase change temperature, melting points as well as thermal

degradation could be identified and compared. Samples were weighed and prepared by placing then in aluminium crucibles with a central pin hole in ambient nitrogen conditions at a heating rate of 10°C/min from -10 to 350°C.

4.5.7. Determination of the Tensile Properties of Nanofibrous Mats by the application of Texture Analysis

A texture analyser (*Ta.XT.plus texture analyser*, stable microsystems, surrey, UK) that is fitted with a 50kg load cell and is highly sensitive was used to evaluate the physicomechanical properties of nanofibrous mats by inserting mats within brackets that were calibrated at a distance of 30 mm/sec and a return speed of 5mm/sec. A pre-test speed of 0.5mm/sec was used to apply a tension force in order to obtain the peak force required to establish the breaking point. Work of extensibility and tensile strength of the mats were then obtained by computing the peak tensile force into the following equation (equation 3.1): Settings employed using the texture analysed to depict tensile strength and work of extensibility as well as to generate force-distance profiles are shown in Table 3.3 in Chapter 3.

Tensile strength was measured using the Young's Modulus equation as follows:

$$E = \frac{Tensile\ \ stress}{Tensile\ \ strain} = \frac{\delta}{\varepsilon} = \frac{FL_o}{A_o \Delta L} \qquad \text{[Equation 3.1]}$$

Where: E is the Young's modulus (modulus of elasticity); F is the force applied to the object; A_0 is the original cross-sectional area (πr^2) through which the force is applied; ΔL is the amount by which the length of the object changes; L_0 is the original length of the object.

4.5.8. Determination of Young's Modulus and Tensile Properties by the Application of Nano Tensile Analysis

Various tensile properties as well as Young's Modulus was determined by the application of a nano tensile analyzer (nanoTensile® 5000 Hysitron Inc. Nanomechanical Test Instrument, Minneapolis, MN). Samples cut to size were placed and securely held by a cardboard frame into specially designed mounting brackets as indicated in Figure 4.2. A digital calliper was used to accurately determine the length, thickness and width of samples after they were cured. Samples were gripped between the upper and lower brackets and the system was run at a constant rate of 5μms^{-1} until a stress-strain profile was established.

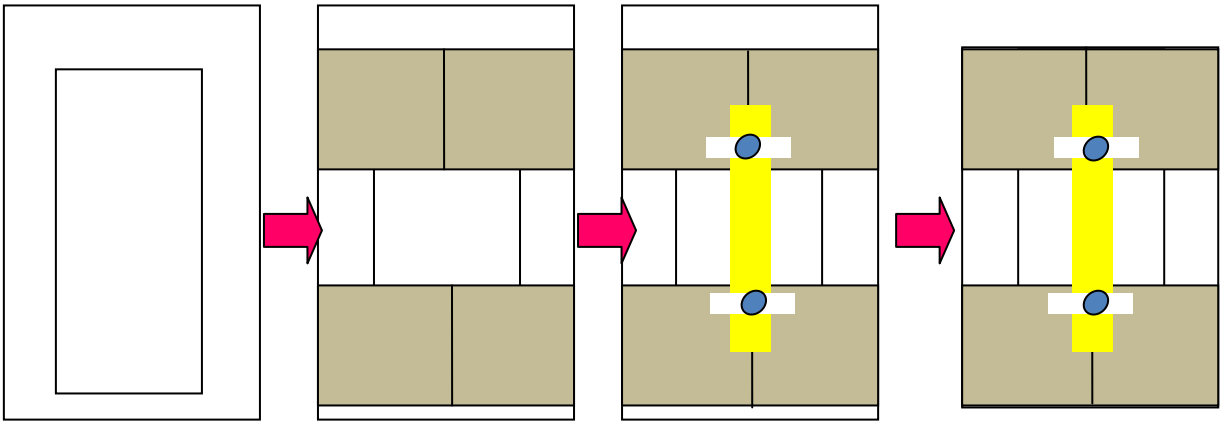

Figure 4.2: Schematic representation of mounted nanofibres secured on template for nanotensile mapping.

4.5.9. Electrospun Polymer Solution Elucidation of Pertinent Rheological Characteristics and Properties

The rheological properties of biopolymer based solutions were determined using a Haake Modular Advanced Rheometer System (ThermoFisher Scientific, Karlsruhe, Germany). The electrospinning process is influenced by properties related to rheological stress and strain parameters. These factors are important when considering electrospinning as optimized characteristics are required in order to obtain electrospun polymer blends. Of particular interest, changes in viscosity, yield stress, stress and frequency sweep were evaluated. Samples were analysed by placing polymeric solution blends onto a sample stage whilst immersing the C35/1° titanium rotor into the solution. Parameters employed are displayed in Table 4.3

Table 4.3: Parameters employed to carry out varies rheological analysis on polymer solutions for electrospinning.

Test Performed	Parameters Employed
Viscosity	Temperature: 24°C
	Shear Rate: $100s^{-1}$
	Time: 360s
Yield Stress	Temperature: 24°C
	T: 200Pa
	Time: 30s
Stress Sweep	Temperature: 24°C
	Frequency: 0.1Hz
	Oscillatory T: 0.1pa
	70pa
Frequency Sweep	Temperature: 24°C
	Frequency: 0.964 Hz
	T= based on result from stress sweep

4.5.10. Bioevaluation of Nanofibrous Mats as a Wound Healing Platform

4.5.10.1. *In vitro* Release of Bioactive

At time periods of 0.5,1,2,3,4,6,8,10 and 12 hours the release of curcumin, a bioactive was investigated using a modified Franz Diffusion Cell. Nanofibrous mat were cut into sections of approximately 1.8cm^2 and placed on the receptor compartment of the Franz Diffusion cell whereby it was kept in contact with Phosphate Buffer solution (PBS) of pH 7.4, at a temperature of 37°C that was thermoregulated by a water jacket. The cell was filled with 12 mL of isotonic buffer, stirred constantly using a magnetic stirrer and periodically during the study as stipulated above 0.1mL was removed for evaluation. Immediately an equal amount of fresh PBS was replaced into the compartment and allowed to stir. Sample PBS removed was then evaluated using an Implen nanophotometer GmbH, Munich, at a wavelength of 425nm.

4.5.10.2. *Ex Vivo* Bioadhesivity Testing of the Nanofibrous Mats

Excision of skin tissue from the Sprague Dawley rat skin model

Sprague Dawley Rats weighing between 200-250g were euthanized using pentobarbitone intraperitoneally (i.p) and the skin was carefully removed. Rat skin was stored in isotonic buffer solution in an airtight jar at -80°C until further use. Prior to experimental procedures skin was taken out and thawed by placing in water at 37°C. The dorsal region was shaved

and further subcutaneous and adipose tissue was carefully removed. Skin sections were then cut to fit the head of the probe.

Textural Profiling Analysis to determine the bioadhesivity of the nanofibrous mats

A TA.XT plus texture analyzer was utilised to evaluate the bioadhesivity of the mats. Excised skin tissue was secured to the probe using bioadhesive tape. The bioadhesivity characteristics was determined at 37°C whereby the attached excised skin tissue was lowered onto the surface of the nanofibrous mats at a constant speed of 0.1mm.s^{-1} and a contact force of 0.5N. The probe was then vertically removed upward at the same constant speed after a contact period of 120s. A plot of force against distance was procured and the area under the curve obtained to determine the work of mucoadhesion per square centimetre (mJ. cm^2)

$$Work\ of\ mucoadhesion\ (mJ.cm^{-2}) = \frac{AUC}{\pi r^2} \qquad \text{[Equation 4.1]}$$

Whereby πr^2: Surface area of the skin tissue which is in contact with the mats

4.6. Results and Discussion

Following generation of the experimental design formulations, the formation of fibres by electrospinning was endeavoured. However many factors pertaining to the process of nanofibre formation as discussed herein this chapter had to be taken into account which lead to the optimization of these parameters as indicated in Table 4.4. Upon observation it was noted that polymeric concentrations at a lower range tend to provide lower tensile strength and are easily degradable when exposed to an aqueous medium whereas at a higher concentration range, they show enhanced physico-mechanical properties that tend to degrade at a much slower rate. Furthermore concentrations of the crosslinking agent at or above 0.04%$^{w}/_{v}$ result in tearing and rapid degradation of the nanofibrous mats or no nanofibres formation at all. In addition solution and electrospinning parameters are of crucial importance. The synthesis of nanofibres involves a polymeric solution of paramount viscosity, electroconductivity, charge density and polarity as well as an optimal voltage supply as discussed. A deviation from this results in subordinate, minimal or no nanofibre formation. Table 4.5 indicates the outcome from the experimental design.

Table 4.4: Parameters pertaining to optimal nanofibres formation

Parameters	Nanofibrous Mat
Solution Parameters and properties	
Electroconductive agent-PVA	10%$^{w}/_{v}$
Electroconductive agent-PEO	2%$^{w}/_{v}$
Solvent for PEO, decrease in bead formation and surface tension	40% ethanol
Surfactant	Polyoxyethylene Sorbitan Monooleate (1ml)
Net charge density enhancer	NaCl (1.5mg)
Electrospinning Parameters	
Supply of Voltage	20 Kv
Distance	31-39.5cm
Flow Rate	1500µl/h

Table 4.5: Representation of nanofibre fabrication from the Box-Behnken experimental design

Formulation No.	Chitosan (%$^{w}/_{v}$)	Genipin (%$^{w}/_{v}$)	Hypromellose (%$^{w}/_{v}$)	Nanofibre Formation
1	3	0.25	1.6	x (High Viscosity)
2	1	0.25	0.4	√(with beads)
3	3	0.1	1	√
4	2	0.1	1.6	√
5	1	0.25	1.6	√(Dense)
6	2	0.25	1	√(Dense)
7	2	0.4	0.4	x(↑[crosslinker])
8	3	0.25	0.4	x
9	2	0.25	1	√(Dense)
10	3	0.4	1	x(↑[crosslinker])
11	1	0.4	1	x(↑[crosslinker])
12	1	0.1	1	x (↓ Viscosity)
13	2	0.4	1.6	x (↑[crosslinker])
14	2	0.1	0.4	x(↓ Viscosity)
15	2	0.25	1	√(Dense)

4.6.1. Chemical Vibrational Analysis of the Nanofibrous Mats

FTIR analysis was conducted to determine structural and chemical modifications occurring upon crosslinking and electrospinning. Of particular interest is the electrospinning process of aqueous based solutions and to what extent the nature of native polymers are modified. Figure 4.4 illustrates the FTIR spectra of various nanofibrous mats. A broad band indicative of O-H stretching is present in all formulations. This also represents the presents of PVA in the structure. This peak occurs at 3294.23cm^{-1} in F2 where weaker band intensity is seen and shifts to 3310.52cm^{-1} and 3329.67cm^{-1} in F4 and F15 (demarcated in Figure 4.3) thus suggesting greater band intensity when the degree of crosslinkage is increased. Crosslinking with genipin occurs by its linkage to free amino groups within the structure, mostly present in chitosan. F2 contains a lower percentage of chitosan (1%$^{w}/_{v}$) thus limiting the amount of amino groups available for crosslinkage weakening network formation and encouraging steric hindrance, in comparison to F4 and F15 where greater rigidity is observed. An increase

in the wavelength results in greater conjugation and intensity, thus showing greater stability and physicomechanical properties in F3 and F7.

Further a second broad band is seen at 2891.95cm^{-1} in F4 and F15 due to C-H vibrational stretching occurring within the structure. A shift in the band intensity occurred from 2891.95cm^{-1} to 2906.55cm^{-1} in F15 and 2909.36cm^{-1} in F6 (demarcated in Figure 4.3). This further suggests that when an increase in crosslinking occurs, band intensity and conjugation strengthens. When crosslinking occurs to a greater degree and the percentage concentration of hypromellose is larger, additional O-H interactions are allowed to occur between molecular chains. PVA in its semi-crystalline state interacts with polymeric chains by hydrogen chemical binding between available hydroxyl groups thus greater linkage occurs (Han et al., 2009) and broader bands between the 1300-1400cm^{-1} spectrum is observed. Furthermore absorbance was observed shifting from 0.09A in F5 to 0.12A and 0.13A in F4 and F6. Thus it can be deduced that a shift in absorbance is directly related to the degree of crosslinkage occurring when electrospinning, as when lower concentrations of chitosan are used such as that in F5, crosslinkage is limited. Thus an increase in conjugation and intensity providing greater stability to the structure will be enhanced in F4 and F6 as crosslinkage occurs to a greater extent.

Another important infrared band observed in the spectrum is that of PEO observed at 1373.74cm^{-1}. The C-H vibrational group is sensitive to intermolecular changes and the environmental changes. When the percentage crosslinker is increased from 0.01%$^{w}/_{v}$ to 0.025%$^{w}/_{v}$ as is seen in F9 and F12, a shift in the spectra is observed from 1359.84cm^{-1} to 1373.74cm^{-1} strengthening the band intensity thus reinforcing conjugation properties. Crosslinking occurring at a higher degree results in greater intermolecular interaction thus symmetric deformation of C-H band vibrations signifying the presence of PEO in its amorphous state (Su et al., 2002). A weak peak of 1061.12cm^{-1} is found in F2 only (demarcated in Figure 4.3) and a peak at 960.06cm^{-1} in all formulations, signifies the presence of C-H bending in the structure most likely due to the presence of supplementary amorphous PEO.

In addition the presence of a peak at 1341.82cm^{-1} and 1241.83cm^{-1} indicated the presence of free amino groups in all formulations thus no crosslinking occurring by genipin at these structural sites, most likely due to the domination of hydroxyl intermolecular interactions occurring due to PVA and PEO and a lower concentration of crosslinker used. Nanofibre and semi-IPN formation resulted in significant differences in the infrared spectrum absorption frequencies of the final product in relation to the original compounds. The presence of polymeric compounds in amorphous or crystalline state further impacted the structural

crosslinking ability as well as the peak intensities of wavelengths. Minimal crosslinkage resulted in smaller band intensity formation resulting in bending of the C-H groups within the aromatic ring and stretching and conjugation within the structure which is further impacted by intermolecular interactions occurring between hydroxyl groups. Formulations displaying greater band intensities correspond to a higher degree of crosslinking hence it can be deduced that molecular transitions occurring within the structure leading to semi-IPN and nanofibres formulation is greatly affected by intermolecular interactions, the degree of crosslinking and the amorphous state of the polymers involved.

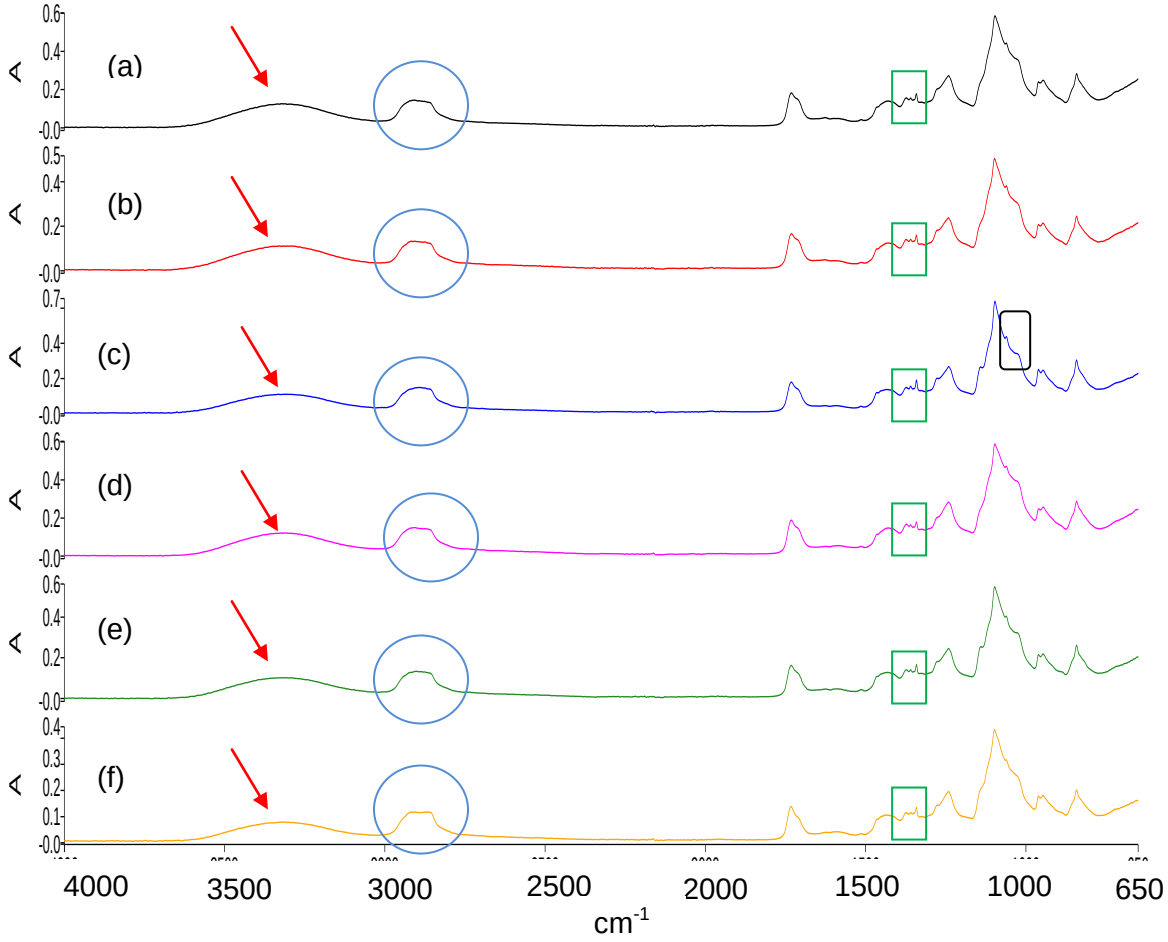

Figure 4.3: Fourier Transform Infrared Spectroscopy of Nanofibrous mat (a) F6, (b) F15, (c) F2, (d) F4, (e) F9, (f) F5

4.6.2. Determination of Surface Morphology and Network Density of Polymeric Nanofibrous Mats

Profiles obtained by scanning electron microscopic evaluation revealed the presence of fibres that were randomly orientated, cylindrical, solid and varying in diameter. Furthermore fibres presented with a porous surface structure and characteristics were dependent on both polymer and crosslinker concentrations. A porous surface morphology is required for the process of wound healing and will be necessary for skin reconstitution. This is favourable for the process of homeostasis, adequate nutrient and gaseous exchange as well as aiding the

process of proliferation and cellular infiltration. The generation of porous sites are made possible for cellular in growth by the formation of nanofibres orientated in a random loose manner as can be clearly seen in the images displayed in Figure 4.4. The presence of nanofibres loosely located over one another in a arbitrary manner provides an overall network architecture that best mimics the native extra cellular matrix (ECM) of the skin thus potentiating cellular regenerative effects (Chong et al., 2007).

The formation of nanofibres by electrospinning has gained much attention, however several challenges are faced as various systematic parameters need to be considered. Uniformity, size and diameter of nanofibre morphology are greatly affected and dependent on parameters such as the solution viscosity. A solution with a higher viscosity results in nanofibres with a larger diameter, prevents the formation of beads and beaded fibres as well as the presence of junctions and bundles which indicate wet fibres on reaching the collector (Pham et al., 2006; Haghi and Akbari., 2007). Figure 4.4b reveals the presence of nanobeads (demarcated in the figure) that are large and spherical in shape and are due to low polymeric chitosan and hypromellose concentrations used, crosslinked to a lesser degree thus depicting Rayleigh instability with regards to solution viscosity. As polymeric concentrations are increased (i.e.: chitosan from 1-3%$^{w}/_{v}$ and hypromellose from 0.4-1.6%$^{w}/_{v}$) so does the instability decrease thus resulting in fibres that demonstrate uniformity, larger diameters as well as the absence of nanobeads as can be seen in Figure 4.4a, Figure 4.4c and Figure 4.4g. Increasing polymeric solution viscosity also results in a larger diameter size. F3 reveals a diameter size of 28.32 as opposed to 37.93 and 62.61nm seen in F4.

The effect of increasing polymeric concentration is clearly illustrated in Figure 4.4a, c and d. Furthermore it can be seen that the polymeric solution viscosity as well as the diameter size is greatly influenced by the concentration of chitosan from 1-3%$^{w}/_{v}$. As the concentration of chitosan was increased, so too did the viscosity and diameter size increase. The addition of a crosslinker contributed to an adjustment within the nanofibrous morphology thus substantiating the physicomechanical properties of the system. Crosslinking within nanofibrous mats resulted in a dense, narrowly packed structure seen in Figure 4.4d, Figure 4.4e and Figure 4.4f due to the contraction of nanofibres by genipin. In addition to improving physicomechanical properties of the system, crosslinking also prolongs the release of bioactives due to the change brought about to the structure morphology decreasing surface area and the fusion occurring between individual fibres (Shaikh et al., 2012) as a result of crosslinking as is clearly depicted in Figure 4.4e.

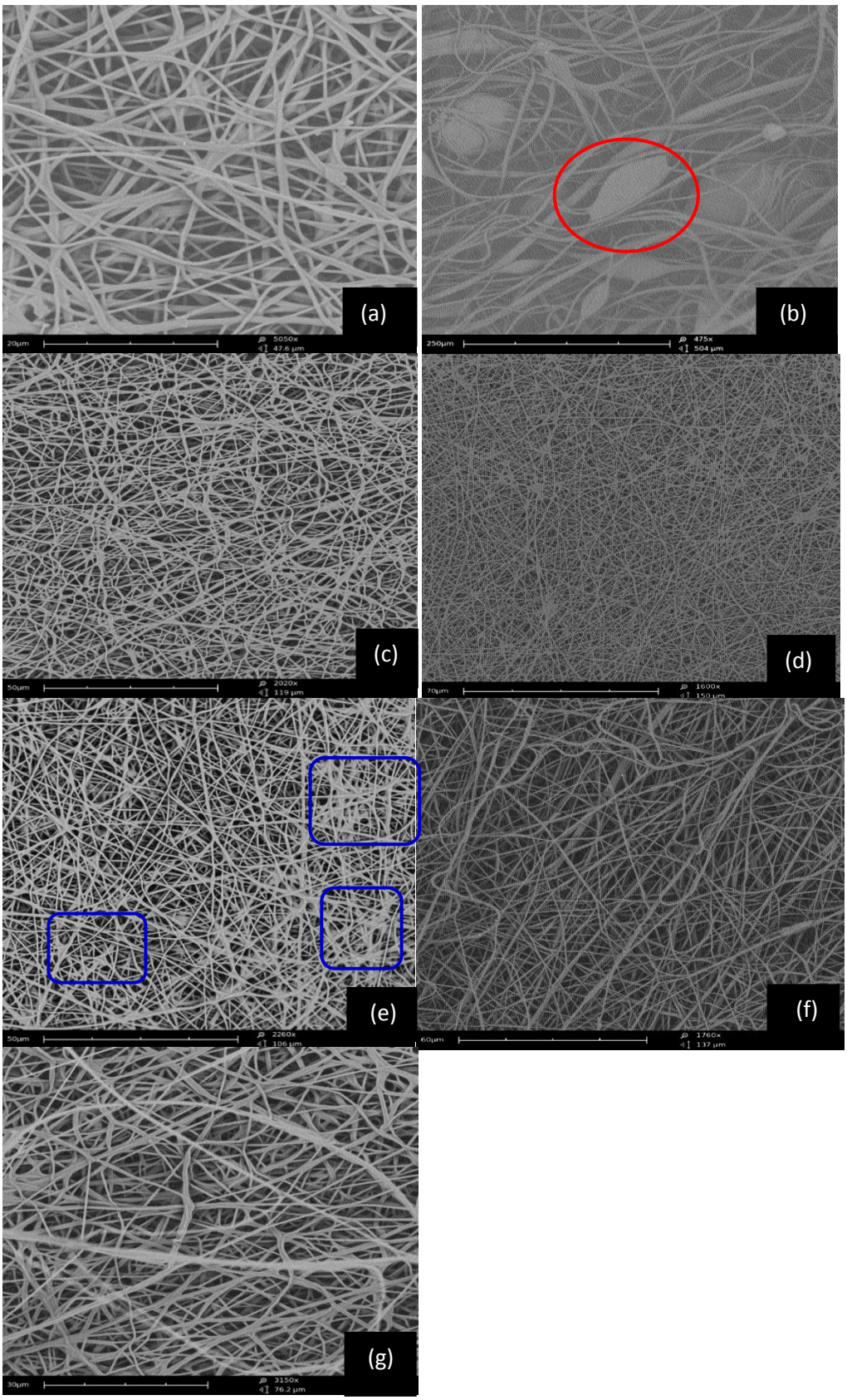

Figure 4.4: Scanning electron microscopic profiles of (a) F3, (b) F2, (c) F4, (d) F5, (e) F9, (f) F6 and (g) F15.

4.6.3. Thermodynamic Evaluation of the Nanofibrous Mat

Differential Scanning Calorimetry (DSC) is associated with the transitions that occur in materials influenced by temperature and heat flow as a function of time in a controlled environment whereby physical and chemical changes associated to changes in the heat capacity can be measured. Figure 4.5 depicts the DSC profiles of the various nanofibrous mats. A glass transition occurred in all samples and varies between the range of 20°C and 45°C. In addition a change in inclination between the Tg of the various mats occurred resulting in a second phase transition where an increase in heat capacity occurs, whereby Figure 4.5b and Figure 4.5d show the broadest inclination (Demarcated by the red arrows in the figure) indicating the greatest bond formation in the structure. The small change in inclination between peaks representing the Tg of various mats can be directly attributed to chitosan which is a semi-crystalline polymer and due to the small specific volume of the rigid chains by network formation caused by crosslinking, that are formed (Dong et al., 2004). Glass Transition Temperature is directly related to network formation and the concentration of crosslinker used. These factors influence transitions to occur which affects the amorphosity of the structure thus altering the heat capacity resulting in a glass transition to occur. Crosslinking by genipin occurs when free amino groups are present such as those present in chitosan allowing crosslinkage to occur at the temperature of curing. When an increased amount of crosslinker is used such as 0.025% as in Figure 4.5b and Figure 4.5d, then broader Tg inclinations are seen whereas lower Tg transitions are seen when the concentration of crosslinker used is decreased (0.01%), thus is more likely to undergo a quick onset of degradation. A narrower and sharper inclination is observed such as that in Figure 4.5a (demarcated by the blue arrow in the figure).

All nanofibrous mats exhibited an endothermic peak following the glass transition. This can be attributed to a melting phase occurring upon heating whereby fusion occurs and the structure converts to the polymer liquid phase. This indicates the presence of non-perfect crystals or impurities that cause the melting point to drop and polymorphism occurs. The endothermic peak occurs at 65.90°C in Figure 4.5e, 69.94°C in Figure 4.5a and 294.22°C in Figure 4.5d. This strongly indicates that the rate of endothermic transition upon heating is related to the degree of crosslinking and the concentration used. Figure 4.5a and 4.5e have a 0.01%$^{w}/_{v}$ concentration of genipin whereas in Figure 4.5d, 0.025%$^{w}/_{v}$ crosslinker is used. Crosslinking results in stronger network formation thus enhanced regularly arranged molecules in a well defined structure that are able to withstand transitions at greater temperatures. The presence of co-polymers and semi-crystalline polymers are strongly indicated by the presence of an exothermic peak subsequent to a fusion endothermic peak as discussed above. Furthermore literature has revealed that chitosan is a partially crystalline polymer (Dong et al., 2004) and PEO occurs in the amorphous state (Su et al.,

2002). This strongly suggests that the exothermic peak present is a result of cold crystallisation. Cold crystallisation occurs in semi-crystalline polymers that have been quenched into a highly amorphous state. Figure 4.5d shows the greatest crystallisation at 140.82°C, whereas Figure 4.5a has a cold crystallisation at 137.63°C (annotated by the black block). Thus it can be deduced that greater crosslinkage results in a higher temperature requirement to cause a transition of both endothermic and exothermic peaks to occur. A transition occurred displaying an endothermic melting transition proceeding the cold crystalline state at a higher temperature due to its kinetic nature. This represents semi-crystalline behaviour of the structures.

Curing (crosslinking) was observed to occur at higher temperatures when the endothermic peak preceding it transpire at lower temperatures as in Figures 4.5a and 4.5b at a temperature of 145.10°C and 140.89°C. Thus it can be deduced that Figures 4.5a and 4.5b display a lower degree of crystillinaty that is related to random orientation of molecules due to free non-crosslinked groups available in the structure having a poor polymer backbone. Figure 4.5d displays a higher temperature requirement to produce an endothermic peak thus representing a greater crystalline state and more ordered arrangement of molecules.

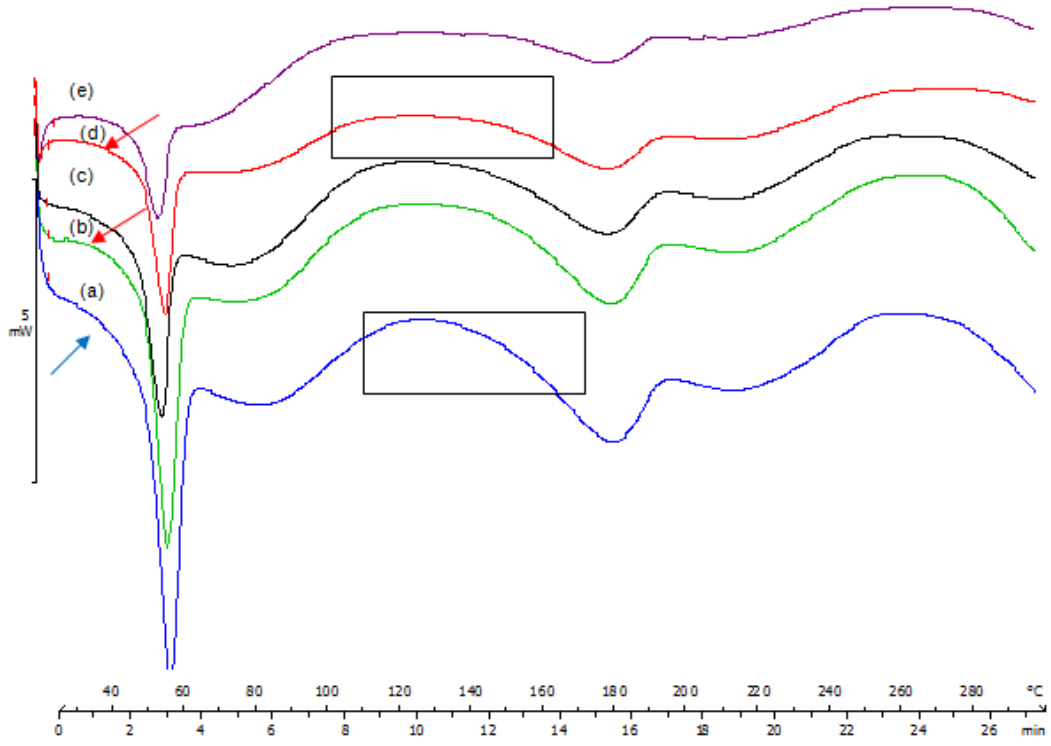

Figure 4.5: Differential Scanning Calorimetry profiles of nanofibrous mats (a): F4, (b): F5, (c): F15, (d): F9, (e): F6

4.6.4. Young's Modulus Analysis of Nanofibrous Mats to determine Mechanical Characteristics

The tensile strength and mechanical properties of nanofibrous mats were investigated and evaluated by Young's Modulus. Young's Modulus is a measure of the ratio of stress to strain when a force is applied to the cross-sectional area of a specimen or sample in a tension test (Govindjee and Sackman, 1999). A sturdy but flexible delivery system is required to be applied topically as a wound healing platform thus the stress-strain relationship of a sample plays a major role when characterising topical systems. The strength of the materials used and the flexibility of polymeric chains determine the stress-strain relationship of the materials used. A material will be considered flexible when a relatively small Young's modulus, which is the slope of the linear portion of a stress-strain curve as illustrated in Figure 4.6 is observed such as that depicted by F3 in Figure 4.8b.

Figure 4.7 depicts the profile of a nanofibrous sample whereby area under the curve A resembles the resilience of the sample to break and A+B shows the toughness of the nanofibre sample, thus the ultimate strength which is the maximal quantity of stress that can be applied to cause total deformation at rupture (maximum amount of strain endured) can be derived from this curve. Therefore the area under the curve gives a indication of the tensile strength of the sample tested whereby the energy or work required to break through the sample can be measured, which constitutes the measure of toughness of brittleness of the samples. Resilience (A) is the property of a material to endure a load that does not exceed the elastic limit when a tension is induced and toughness (A+B) indicates the energy that is absorbed when an average force and maximum tension is applied in order to cause a fracture or break in the sample (Lee and Moon, 2003). Thus it can be deduced that samples with higher tensile strengths such as F4, F5 and F6 as shown in Figure 4.8a have a larger area under the curve and require a greater amount of energy for deformation to occur. This can be directly attributed to the degree of crosslinkage and the density and alignment of nanofibres networks. As depicted in the scanning electron micrographs of nanofibres in Section 3, crosslinking resulted in more densely and narrowly arranged nanofibres thus substantiating the physicomechanical properties of the nanofibrous mats as the strength of samples is dependent on the architectural arrangement, size and number of nanofibres.

F2, F9 and F15 show considerable strength as they have the maximum ultimate strength as depicted in Figure 4.8d. Figure 4.8b to Figure 4.8f illustrates the Young's Modulus (E), yield stress (σy) (the magnitude of stress on the stress–strain curve at which appreciable deformation takes place without any appreciable increase in the stress), ultimate strength (σu) (the maximum stress a material can withstand), ultimate strain (εu) and toughness ($J.cm^3$). Thus it can be deduced that an increase in the % crosslinker resulted in a greater

Young's Modulus and thus a decrease in the elasticity of the sample such as that in F4, F5 and F6, therefore tend to be more brittle. When an intermediate amount of crosslinker is used such as that in F2, a smaller Young's Modulus of 4.25MPa is seen and a greater ultimate strength occurs as is illustrated in Figure 4.8d. Furthermore F2 also shows the greatest toughness of 0.20J/cm^3 in contrast to all other nanofibres samples as depicted in Figure 4.8f. Variations in the degree of crosslinking led to deviation in the elastic modulus of samples and thus the ultimate strengths. Samples crosslinked to a lesser degree such as F3 and F15 where a Young's modulus of 0.63 and 1.97 MPa shows greater elastic properties in contrast to those with greater Young's modulus of 10.32 and 14.74MPa as in F4 and F5 resemble a lesser degree of elasticity. Differing fibre diameters contribute to the variation in elasticity. When a greater degree of intermolecular crosslinked bonds are formed between nanofibres, a greater degree of rigidity and stiffness is noted between the nanofibres within the nanofibrous mat. However, when a lower degree of intermolecular crosslinked bonds are formed, fibres tend to align along the tensile pull axis and slip pass one another thus substantiating the elastic modulus (Shaikh et al., 2012).

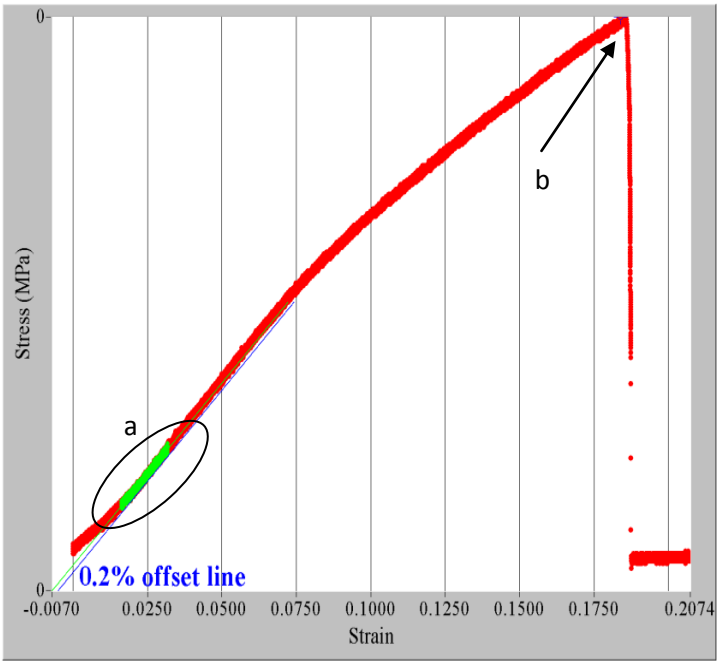

Figure 4.6: Stress-Strain relationship profile of nanofibrous mats where (a) is the linear portion of the slope from which Young's Modulus can be derived and (b) represents the fracture point of the sample

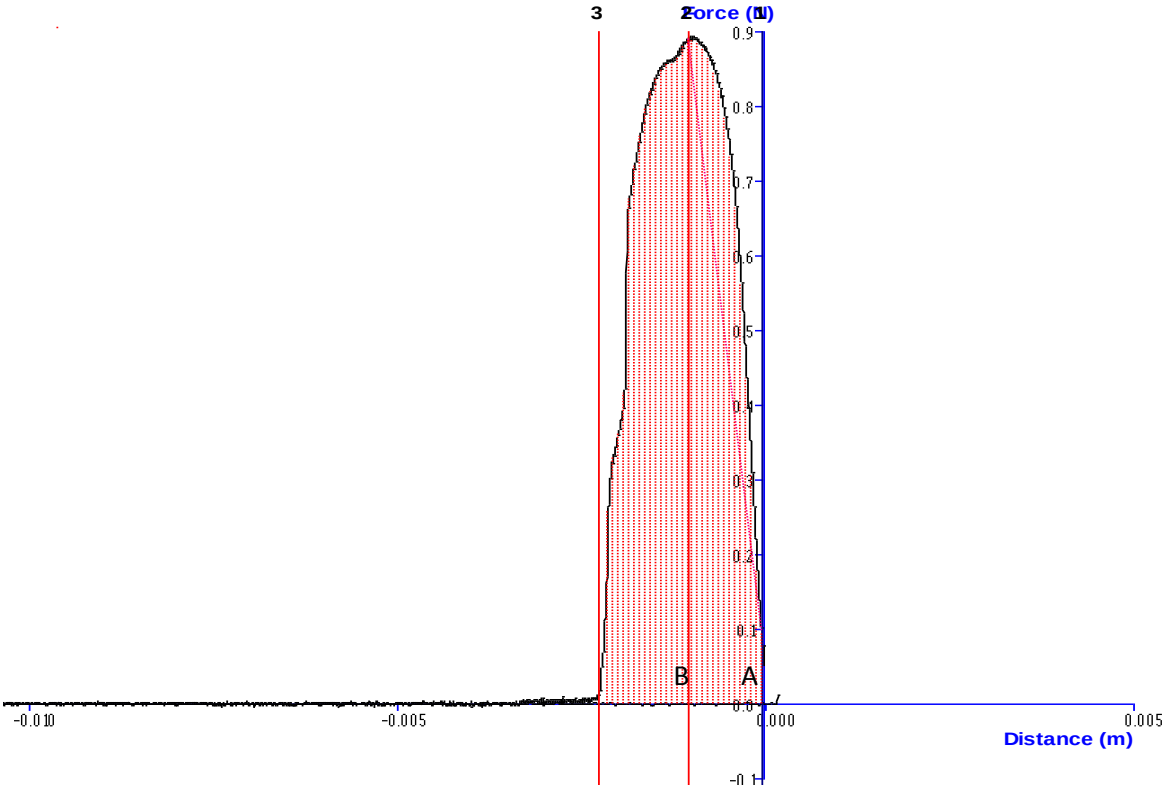

Figure 4.7: Force versus distance curve whereby the tensile strength can be derived. Area A resembles the resilience and Area A+B the toughness of measured samples.

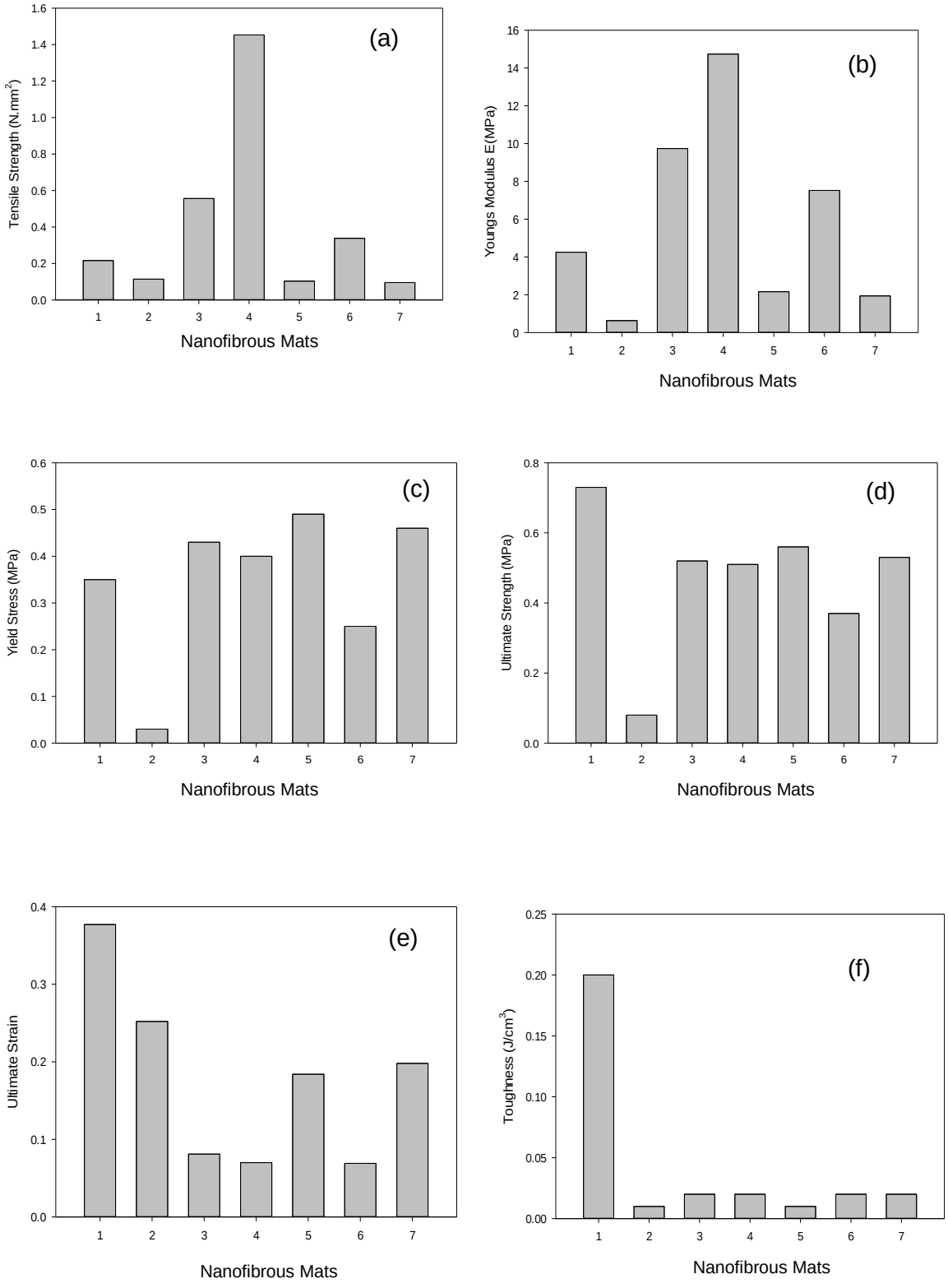

Figure 4.8: Vertical Bar outlining the variations between nanofibrous mats of (a) Tensile Strength (N.mm^2), (*b*) Young's modulus (*E*; MPa), (*c*) yield stress (*σy*; MPa), (*d*) ultimate strength (*σu*; MPa), (*e*) ultimate strain (*εu*) and (*f*) toughness (*uf*; J cm−3) of nanofibrous mats 1–7 (where 1: F2, 2:F3, 3:F4, 4:F5, 5:F9,6:F6,7:F15).

4.6.5. Rheological Characterisation of the Nanofibrous Mats

The ability of a polymeric hydrogel solution to electrospin, its physical integrity and retentive behaviour are significant measures when synthesising nanofibres with bioactive incorporates as topical delivery systems, thus its mechanical strength and viscoelastic properties should be measured (Anumolu et al., 2010). Viscosity plays a significant role in transforming a polymer solution into nanofibres. Changing of polymeric solution concentrations directly impacts the viscosity of the solution and is found to be one of the greatest factors influencing morphology and fibre diameter size when electrospinning polymeric solutions. Fibre diameter is one of the most important quantities related to the process of electrospinning and is primarily dependent on the polymer contents within a jet to be electrospun as well as the size of the jet. When a solution of higher viscosity is obtained, larger fibre diameter is observed, thus the solution concentration is directly proportional to nanofibres diameter size (Huang et al., 2003).

Table 4.6 depicts the solution viscosity of the various nanofibrous solutions. F6 reveals a viscosity of 216.66MPa when crosslinked thus forming cylindrical, more uniform nanofibres of slightly larger diameters as seen in Figure 4.4f and g. It can thus be deduced that an increase in polymer concentrations used results in greater diameter size and thus can be described as a power law relationship as deduced by Deitzel and co-workers. When lower polymer concentrations are used, lower viscosities are obtained as is pragmatic to F2 where a viscosity of 71.23MPa is seen and defects in the system are observed in the form of beads and droplets such as those distinguished in Figure 4.4b. This is directly attributed to electrospraying rather than electrospinning. Furthermore the presence of bundles and junctions within a nanofibrous mat is also observed and this can be directly attributed to wet fibres hitting the collection disk (Pham et al., 2006), thus suggesting inadequate evaporation of solvent due to lower concentrations of polymer used. Therefore when polymer concentrations increased thus increasing the viscosity, uniform fibres with minimal junctions and beads are yielded. Thus it can be observed that morphological changes occurring upon electrospinning are directly related and dependent on the variation of viscosity of the polymeric solution been electrospun. Additionally when solutions of very high viscosities are used, electrospinning did not occur such as that in F1 and F8 where viscosities of 252.38MPa and 231.13MPa occur upon crosslinking forming huge droplets at the jet site that tend to dry out not allowing optimal jets for electrospinning to be maintained.

In addition, crosslinking plays a significant role in the determination of solution viscosity as is depicted in Table 4.6. Addition of crosslinker such as genipin led to greater intermolecular forces occurring between the molecules thus increasing the viscosity. Polymeric solutions crosslinked to a greater extent resulted in nanofibres with a more uniform alignment that

were densely packed and narrower nanofibres that are interlaced decreasing the surface area thus promoting prolonged release such as those resembled in Figure 4.4 c,d and e.

The yield stress is a measure of the stress required to initiate measurable flow. Yield stress measurements are significant to determine the pharmaceutical shelf life of a product. When low stresses are applied, formulations tend to be very viscous. However, as the shear stress applied increases breakdown of the structural network of hydrogels occurs as macroscopic flow begins to occur and is known as the dynamic yield stress. Macroscopic flow begins to occur when the viscosity drops by several orders of magnitude over a very narrow stress range. Table 4.6 outlines the yield stress measurements of formulations, whereby it can be seen that all formulations depict a comparable yield stress range. Thus it can be deduced that the "apparent" yield stress is designated as a single point and the critical stress range is very small (Saak et al., 2001).

Topologically a gel can be defined as a three dimensional network system that mechanically is soft in nature having both liquid and solid like characteristics. On application of a force gels tend to deform to an extent and take an infinite time to reach equilibrium, thus they tend to be viscoelastic in nature. Dynamic moduli can be applied to distinguish gels from sols. This can ideally be evaluated by the application of oscillating small strains, namely the *storage modulus G'* which is a measure of the elasticity of a material and the *loss modulus G"* which represents the viscous components, when an oscillatory frequency ω is given. Ideally a solid-like mechanical spectrum should be exhibited by gels whereby G'>G" (Ikeda and Nishinari, 2001). Figure 4.9 represents the oscillatory stress ramping obtained from stress and frequency sweep data obtained for the various formulations. From the profiles obtained it can be seen that in Figure 4.9b and e, the storage modulus G' dominated thus suggesting that these hydrogels are more elastic then viscous within the investigated frequency range thus more structural systems will be obtained. These systems will have a greater ability to resist structural changes when a stress or strain is applied (Diez-Sales et al., 2007). This can be attributed to higher polymeric concentrations used as well as the influence of crosslinking.

Diez-Sales and co-workers (2007) state that when increased concentration of chitosan was used, dynamic moduli was also increased. Figure 4.9a, d and c demonstrate a low G' modulus that exhibits an elastic region only below a frequency of 60pa. This suggest that these hydrogels show greater viscous properties then elasticity as G">G' and correspond to the characteristic behaviour of solutions whereby a non structured system is prevailing. This can be attributed to lower concentrations of polymer been used. Furthermore it can be perceived that the effect of crosslinking has a immense impact on the dynamic moduli of the solutions as all uncrosslinked solutions represented by figure 4.9f to j depict a greater G"

modulus suggesting a less structured system whereby nanofibres with insufficiencies such as nanobeads and electrospraying will occur. Thus crosslinking plays a pivotal role in providing a polymeric solution that can be electrospun to form uniform, cylindrical fibres with no to minimal defects such as nanobeads ensuring an optimal nanofibrous mat. The rheological data show that hydrogels with a greater G' value are more elastic in nature, having enhanced viscoelastic properties, thus serving as appropriate mediators that may prolong transdermal bioactive residence time thus providing a longer pharmacological effect (Anumolu et al., 2010).

Table 4.6: Viscosity and Yield Stress of the various hydrogel formulations for nanofibre synthesis

Nanofibre Mat Formulation #	**Viscosity (MPa) [crosslinked]**	**Yield Stress (Pa) [crosslinked]**	**Viscosity (MPa) [uncrosslinked]**	**Yield Stress (Pa) [uncrosslinked]**
1	252.38	40.23	246.35	39.74
2	71.23	38.54	68.92	38.51
5	140.57	38.57	136.58	37.69
8	231.13	39.12	224.52	38.89
6	216.66	38.60	208.87	38.58

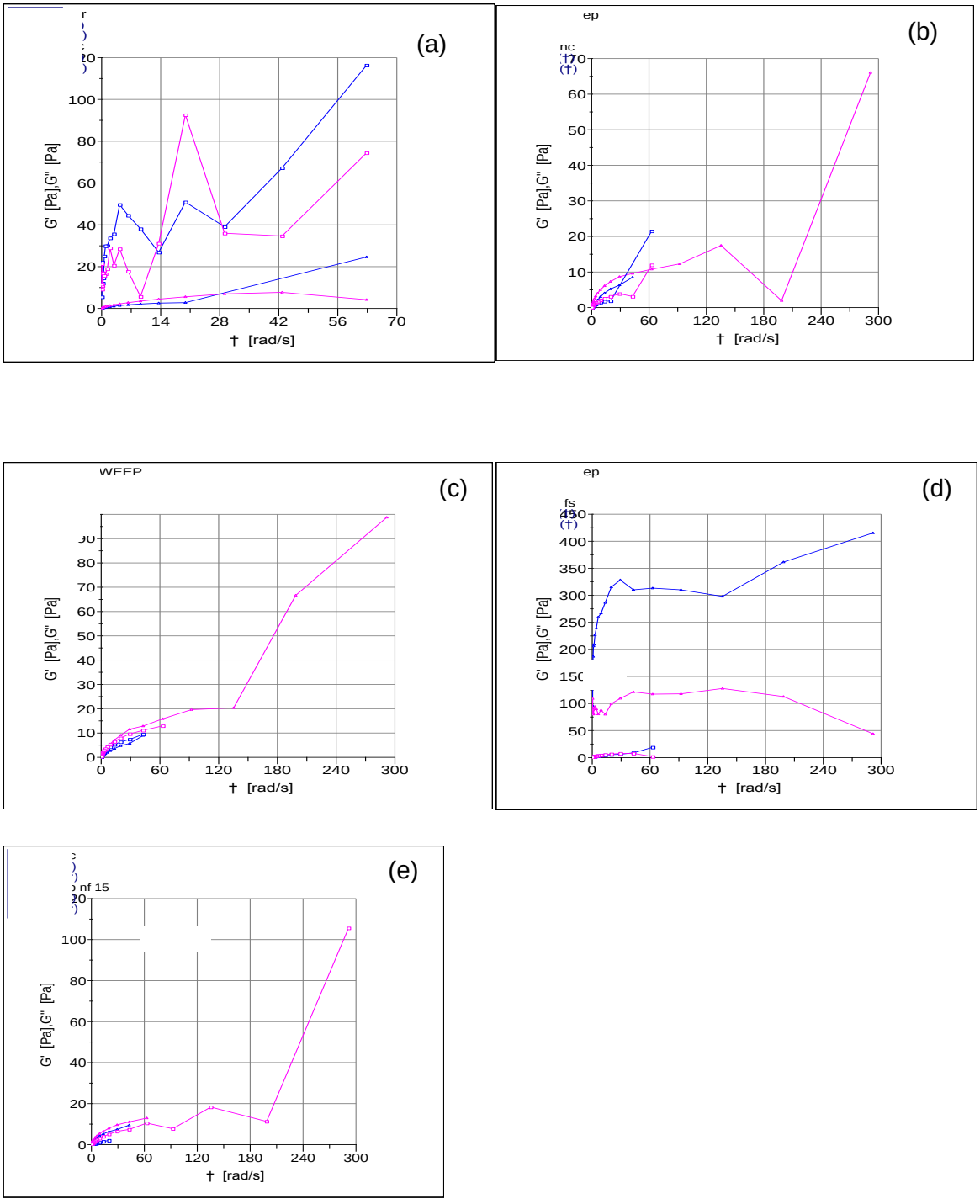

Figure 4.9: Dynamic Modulus G' and G" of [crosslinked] (a) F1, (b)F2, (c) F5, (d) F6, (e) F8; [uncrosslinked] (a) F1, (b) F2, (c) F5, (d) F6, (e) F8

Crosslinked nanofibrous solutions: △
Uncrosslinked nanofibrous solutions: □
G': 
G": 

4.6.6. *In Vitro* Release Kinetics of Curcumin

Figure 4.10 shows the curcumin release profiles from chitosan/hypromellose nanofibrous mats fabricated at different concentrations. It was observed that curcumin release is increased within the first six to ten hours of the study in all formulations. This can be attributed to diffusion of the bioactive curcumin as well as the mechanism of polymer erosion (Charernsriwilaiwat et al., 2012) when in contact with phosphate buffer solution (PBS). Furthermore it was observed that crosslinked nanofibrous mats with genipin to a lower degree had a greater initial release rate of bioactive as compared to those nanofibrous mats crosslinked to a greater degree. However crosslinking supported sustained release of bioactive over a longer period of time thus improving its therapeutic activity. Nanofibrous mats crosslinked with genipin at higher concentrations such as 0.025% exhibited minimal swelling and release rates over the 24 hour period. This is ascribed to the intermolecular and intramolecular bonds occurring between molecules of the structure due to crosslinking. In addition, when decreased concentrations of genipin are used resulting in subordinate linkage formation, weak intermolecular and intramolecular bonds are formed thus encouraging faster bioactive release (Rana et al., 2005). This phenomenon is exhibited by F3 and F4, whereby the greatest release of drug is seen reaching a peak of 0.243 mg/mL at 12 hours and 0.229 mg/mL at 10 hours respectively, when the percentage crosslinker used is 0.01%$^{w}/_{v}$. Furthermore F2, F5 and F15 exhibited poorer release at 0.150 mg/mL, 0.151 mg/mL and 0.208 mg/mL, respectively at 8 hours and can be accredited to the greater network formation occurring due to crosslinking thus impeding the bioactive release. Thus it can be deduced that the *in vitro* drug release across the nanofibrous mats were significantly influenced by the concentration and degree of crosslinking occurring within the structure.

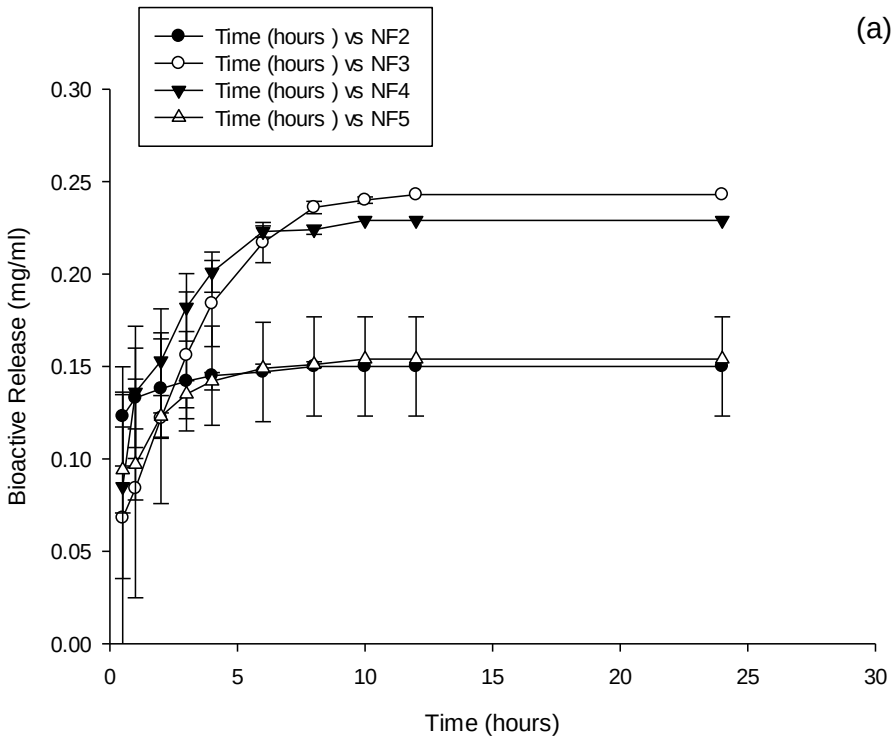

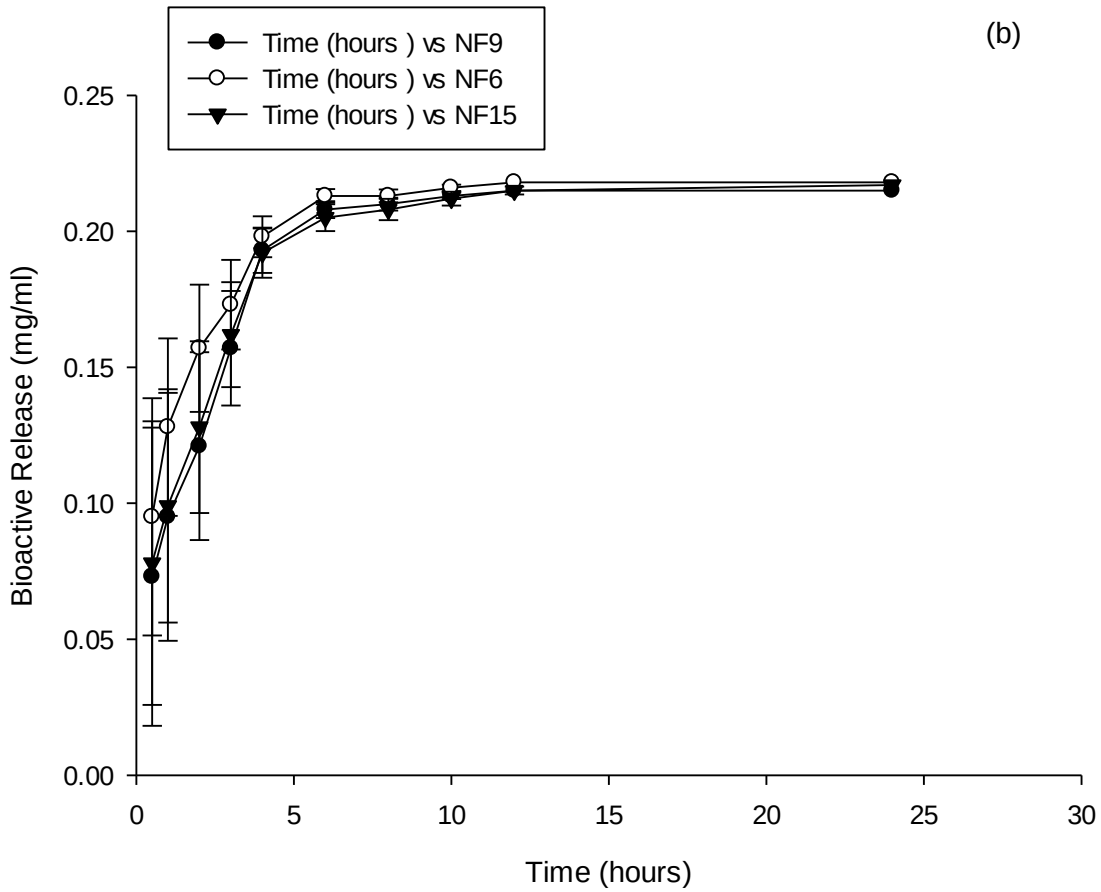

Figure 4.10: Release profile of curcumin of the various nanofibrous mats, **(**a): F2-5, (b): F6, 9, 15

4.7. Mucoadhesive Characteristics of the Nanofibrous Mats

The ability of biopolymers both synthetic and natural to attach to biological tissue can be termed as mucoadhesion. Wound dressings that possess a mucoadhesive attribute upon topical application have the capability of sustaining bioactive release and thus increasing the bioavailability of the active compound therefore ensuring controlled release to the wound site. Mucoadhesion occurs upon direct interaction between biopolymers and the tissue causing a chemical reaction to occur that results in the swelling of polymers allowing interpenetration to occur (Cevher et al., 2008). Figure 4.11 depicts a force-distance profile whereby the pertinent adhesion force was obtained, thus from the results obtained it was noted that the adhesive properties of the mats increased as the concentration of the biopolymer chitosan increased from 1% to 3%. Furthermore an increase in crosslinkage resulted in declined mucoadhesive ability. F6 disclose a work of adhesion of 0.182 mJ cm^{-2} when a chitosan concentration of 3% is used. Employment of 1% chitosan as that used in F2 and F5 revealed a work of mucoadhesion of 0.0631mJ cm^{-2} and 0.0748mJ cm^{-2} respectively. The mucoadhesive ability of chitosan can be directly attributed to its ability to adhere to biological tissue, hence making its use an optimal candidate for site specific delivery. Work of adhesion is based on a mechanism of action that involves ionic interactions, hydrogen bonding and swelling upon direct contact with the tissue. Positively charged amino groups present within the chitosan chemical structure interact with the negatively charged particles within biological tissue at a molecular level allowing an attraction to occur via electrostatic forces (George and Abraham., 2006). Thus increasing the molecular weight of chitosan improves and results in stronger mucoadhesion that is clearly detected in the study carried out.

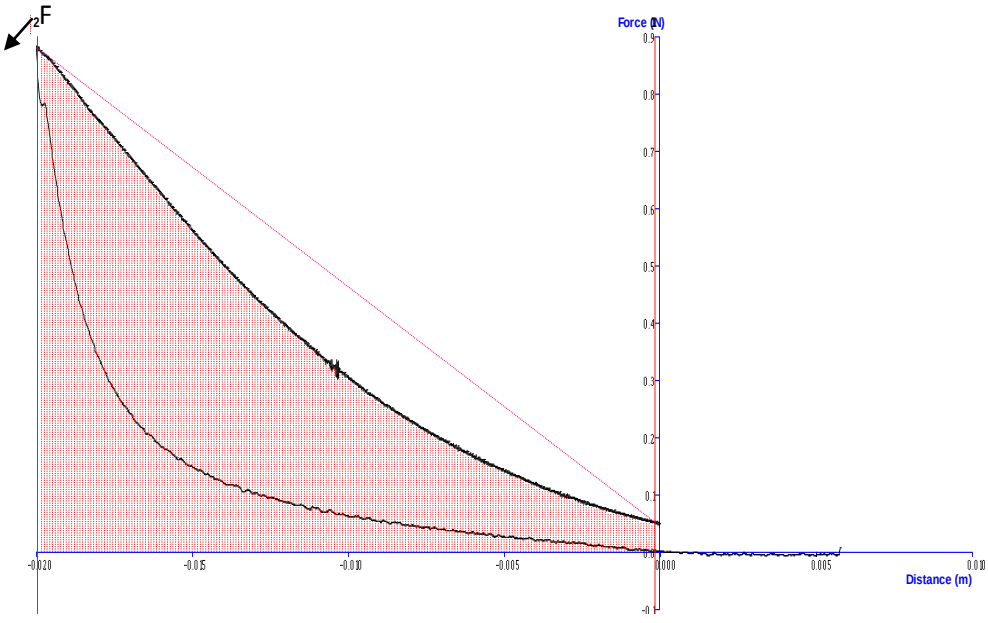

Figure 4.11: Force-distance textural profile employed to compute work of adhesion and the peak adhesion force

4.7. Concluding Remarks

The development of nanofibrous mats using natural polymers and deionised water as a solvent was successfully attained by exploration and investigation exercising the various parameters as discussed. Furthermore it was noted that a modification to these parameters could significantly influence the fibre morphology such as diameter, porosity, strength, bioactive release and fibre functionality. Generation of a Box-Behnken template signified a design of experiments whereby 15 formulations were generated and characterised in terms of the physico chemical, mechanical and biological release properties. Various polymer concentrations were investigated in order to develop optimal nanofibrous mats whereby it was noted that an increase in polymeric concentration lead to higher viscosities which greatly impacted the nanofibre morphology. Higher solution viscosities lead to the fabrication of nanofibres with a greater diameter, more cylindrical in shape with uniform alignment. Reducing the viscosity lead to poorer mechanical properties, greater droplet and nanobead formation as well as substandard fibre alignment. However at very high viscosities jet formation was unattainable and mechanical properties in terms of flexibility and elasticity declined substantially. The rates of crosslinked bridge formation between polymers as well as the extent of inter and intramolecular forces also greatly impact the fibre characteristics as well as bioactive release. Increasing crosslinkage and genipin concentration resulted in sustained and greater control release of bioactive. Thus it could be deduced that a successful optimal polymeric formulation can be obtained from the detailed characteristic analysis carried out as is discussed herein within the chapter to follow. Chapter 5 provides a detailed portrayal of an optimized formulation for nanofibre formation mathematically attained for a response methodology as is described in greater detail in the chapter to follow.

CHAPTER 5

STATISTICAL OPTIMIZATION OF THE CROSSLINKED NANOFIBROUS MAT AND THE INFLUENCE OF CROSSLINKING ON DYNAMIC CHARACTERISTICS OF THE SYSTEM AS A CONSTITUENT OF A MULTI-COMPONENT STIMULI RESPONSIVE PROTOTYPE DEVICE

5.1. Introduction

The successful development of wound delivery systems require approaches that lead to statistical formulary optimization. This can be achieved by the employment of a design strategy enclosing an outline of the most proficient experiments. The use of this strategy allows for efficiency in terms of cost, time and accuracy. The step wise methodology employed a design of experiments (DoE) employing the Box-Behnken design strategy and response surface methodology. The DoE encompassed 15 formulations on a varying scale of low, medium and high and is in accordance with the various variable parameters identified for the most favourable characteristics.

Criterion followed for assertion of statistical optimization of the nanofibrous delivery system followed a series of events that included:

- Formulary component identification of the natural biopolymers and crosslinker for employment in the experimental factorial design
- Recognition of significant characteristics through the employment of various variables leading to the assibilation of the design strategy
- Modulation of the three factor Box-Behnken design
- Characterisation and analysis of the design formulations utilising identified reactions
- Design implementation using the Response Surface Methodology (RSM) aiding statistical optimization
- Coefficient evaluation using regression analysis
- Validation and prediction of responses for optimization
- Statistical optimization of the nanofibrous system in accordance to a required protocol

Nanoscale fibres composed of natural biopolymers serve as successful candidates for various applications which include drug delivery, mimicking the extracellular matrix, tissue engineering, and wound dressings as is described in more detail in Chapter 4. Nanofibres produced by electrospinning of natural origin have many advantageous properties that include biodegradability, non-toxicity, biocompatibility and are economically friendly. However, there are many drawbacks related to this which include its high degradability

limiting its long-term biomedical application, furthermore the shelf life is also shortened amongst others. Thus, in order to improve these properties, the electrospun mats were crosslinked improving its thermomechanical performance as well as advancing the water-resistant ability of the fibres (Zhang et al., 2006). The investigation to follow in this chapter will provide a pointer on the fibre characteristics of the nanofibrous mats upon crosslinking.

A Box-Behnken (B-B) statistical design template was employed to generate desirable formulary components, in order to devise an optimal, economical and efficient formulation appropriate for fabricating a biopolymeric nanofibrous mat of natural origin that would ultimately serve as an optimized healing device. The design template generated 15 multifactorial experimental formulations to establish the measured responses which ultimately lead to the innovation of a distinct optimal formulary composition preserving desirable results which is the main focus of this chapter. The optimization process involves the attainment of optimal stability, biological responses and physicomechanical validation as is described above.

5.2. Materials and Methods

5.2.1. Materials

Fabrication of nanofibres employed the use of chitosan, medium molecular weight poly(D-glucosamine) deacetylated chitin, hypromellose(hydroxymethylcellulose 2910), citric acid (ACS reagent ≥99.5%, M_w=192.12 g/mol), genipin (≥ 98% (HPLC) powder with an M_w= 226.23 g/mol) and curcumin, all obtained from Sigma Aldrich Chemie GmbH, Steinheim, Germany. PVA- mowiol® 4-88 with an M_w=31000g/mol and PEO-Polyox™, WSR 303 were used as electroconductive agents and was obtained from Sigma Aldrich Chemie GmbH, Steinheim, Germany. Tween 80 was obtained from uniLAB® (Merck Chemicals (Pty) Ltd, Wadeville, Gauteng, RSA).

5.2.2. Fabrication of the Optimized Nanofibrous Mat

An optimized polymeric solution was prepared under ambient room conditions from statistically derived superlative concentrations as indicated in Table 5.1 for solution A and shown in Figure 5.1.The optimised formulation was prepared by:

Solution A: A1+A2+A3+A4 (to 100ml)

Chitosan (CS) (A1) solution is prepared by dissolving in an aqueous acidic solution comprising of a 5%$^{w}/_{v}$ (50 mg/mL) citric acid as a solvent medium. The chitosan used is of medium molecular weight with an optimised concentration of 3%$^{w}/_{v}$ (30 mg/mL). Aqueous solution of Hypromellose (A2) with a concentration of 0.4%$^{w}/_{v}$ (4 mg/mL) was then added.

Crosslinking and the formation of a semi interpenetrating polymer network were obtained by the addition of genipin (A3) at a concentration of 0.01%$^{w}/_{v}$ (10mg/10mL). Lastly the bioactive curcumin (A4) [1%$^{w}/_{v}$ (10 mg/mL)] was added.

Where A1: Chitosan

A2: Hypromellose

A3: Genipin

.A4: Curcumin

Solution B: Electroconductive agents polyvinyl alcohol (PVA) at a concentration of 10%$^{w}/_{v}$ dissolved in deionised water (10.0g of PVA dissolved in 100ml deionised water)

Solution C: 2%$^{w}/_{v}$ polyethylene oxide (PEO) dissolved in 40% ethanol and 60% deionised water (2.0g dissolved in 100ml 40:60 – ethanol: deionised water)

Final Formulation:

Solutions A+B+C was added at a ratio of 1:1:1 (300ml) together with a surfactant Polyoxyethylene Sorbitan Monooleate (5ml) and a net charge density enhancer NaCl (7.5mg). The solution was left overnight to stir before electrospinning.

Thus, the final polymer ratios per 100ml in the final optimised formulation were chitosan: 1%, genipin 0.03%, Hypromellose 0.13%, curcumin 0.33%, citric acid 1.67%, PEO 0.67% and PVA 3.33%. The polymeric solution was then processed through a pump (Chemyx Inc syringe infusion pump) attached to the electrospinner (Glassman high voltage Inc, (high bridge NJ USA)) and a voltage of 20kV was applied. Nanofibres were collected on a collecting surface employing the parameters indicated in Table 5.2.

Table 5.1: Statistically derived superlative concentrations for crosslinked and uncrosslinked nanofibres

	Chitosan (%$^{w}/_{v}$)	**Genipin (%$^{w}/_{v}$)**	**Hypromellose (%$^{w}/_{v}$)**
Optimized Formulation	3	0.1	0.4
Optimized Formulation (uncrosslinked)	3	-	0.4

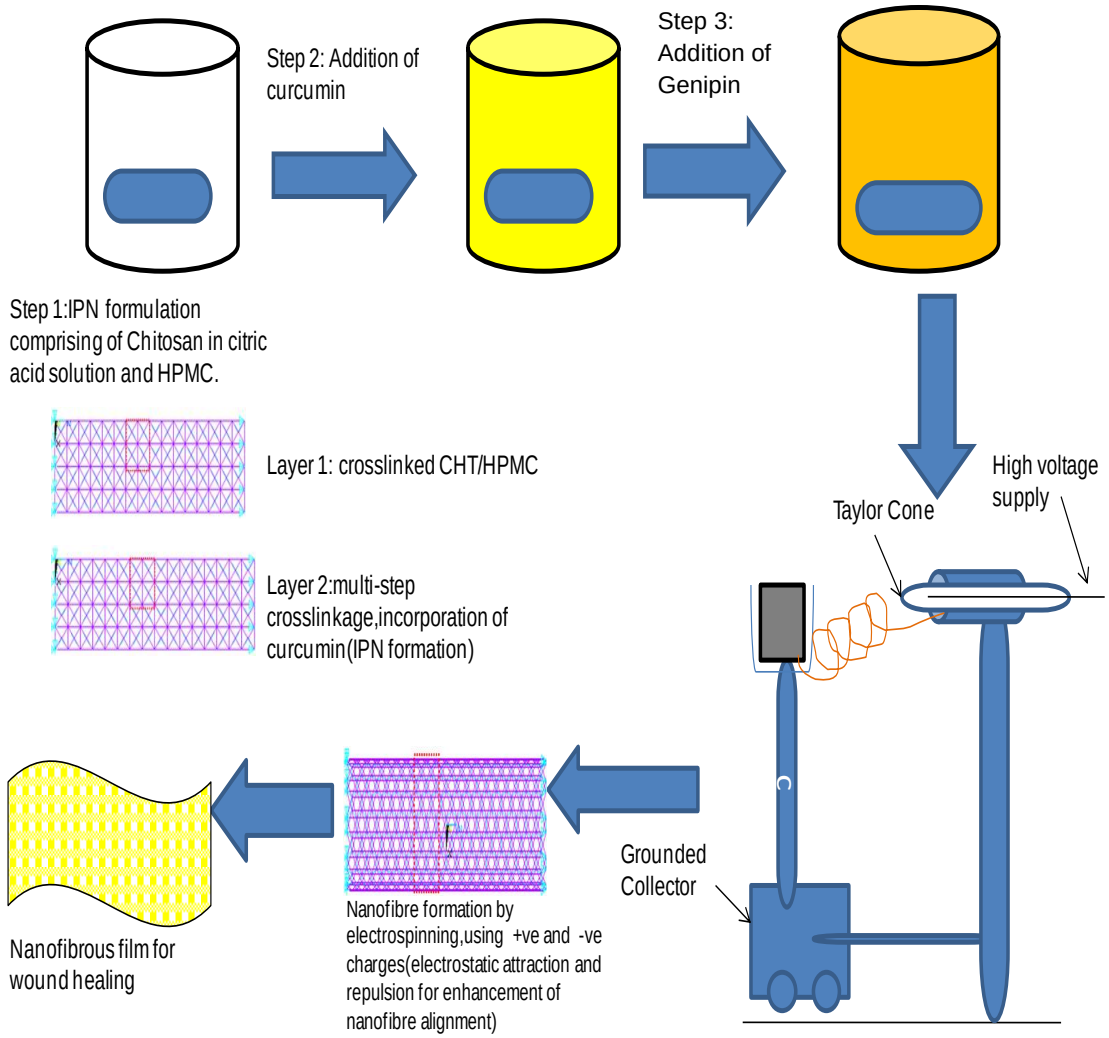

Figure 5.1: Schematic conceptualization of nanofibre production comprising of s-IPN formation and electrospinning

Table 5.2: Depicting parameters and properties related to nanofibre solution and electrospinning

Parameters	**Nanofibrous Mat**
Solution Parameters and properties	
Electroconductive agent-PVA	10%$^{w}/_{v}$
Electroconductive agent-PEO	2% $^{w}/_{v}$
Solvent for PEO, decrease in bead formation and surface tension	40% ethanol
Surfactant	Polyoxyethylene Sorbitan Monooleate (1mL)
Net charge density enhancer	NaCl (1.5mg)
Electrospinning Parameters	
Supply of Voltage	20 Kv
Distance	31-39.5cm
Flow Rate	1500µl/h

5.2.3. Characteristics of the Optimized Nanofibrous Mat

5.2.3.1. Evaluation of the Polymeric Vibrational Frequency and Structural Properties

Changes in vibrational frequencies and absorbance occur upon chemical interactions between polymers, bioactives and crosslinking agents. This was investigated upon bioactive crosslinked and uncrosslinked bioactive free samples using a PerkinElmer® Spectrum 100 Series FT-IR Spectrometer fitted with a universal ATR Polarization Accessory (PerkinElmer Ltd., Beaconsfield, UK). FTIR Spectra was recorded over a range of 4000-625cm^{-1}, with a resolution of 4cm^{-1} and 32 accumulations

5.2.3.2. Evaluation of Surface Morphology and Topography

Phenom™Microscope (FEI Company, Hillsboro, Oregon, USA) was used to analyse the surface morphology of the nanofibrous mat. Samples were sputter coated after been mounted on aluminium stubs. Coating employed the use of argon gas at a pressure of 0.1 torr using a SPI-Module™Sputter Coater and SPI-Module™Control (SPI Supplies, Division of Structure Probe Inc., West Chester, PA, USA) for a time period of 90 seconds. The prepared sample was then analysed in terms of surface morphology, nanofibre density, size and range under the Phenom™scanning electron microscope.

5.2.3.3. Evaluation of Thermodynamic Transitions occurring over a Specified Heating Range

Weighed samples prepared in aluminium crucibles were evaluated to determine thermodynamic behaviour in terms of crystalline, semi-crystalline, melting points, chemical reactions, glass transition and degradation analysis. An Advanced DSC (TMDSC/ADSC) (Mettler Toledo DSC-1 STAR^e System, Schwerzenback, ZH, Switzerland) at a heating rate of 10°C/min from -10°C to 350°C under a nitrogen atmosphere was employed.

5.2.3.4. Determination of the Young's Modulus and Tensile Properties of the Crosslinked and Uncrosslinked Fibres

Tensile strength, Young's Modulus and other pertinent physicomechanical properties were evaluated employing both a nanoTensile®5000 (Hysitron Inc. Nanomechanical Test Instrument, Minneapolis, MN) and a Texture Analyzer (TA.XT*plus* Texture Analyzer*,* Stable Microsystems, Surrey, UK) fitted with a 50kg load-cell. Both apparatus, the nano tensile and texture analyser was calibrated prior to sample testing to ensure accuracy. Thereafter samples cut to approximately 20×5mm strips were mounted as indicated in Figure 5.2 and allowed to run until a fracture point was established. Texture analysis was employed using the parameters as indicated in Table 3.3. The tensile strength was analyzed using equation 3.1.

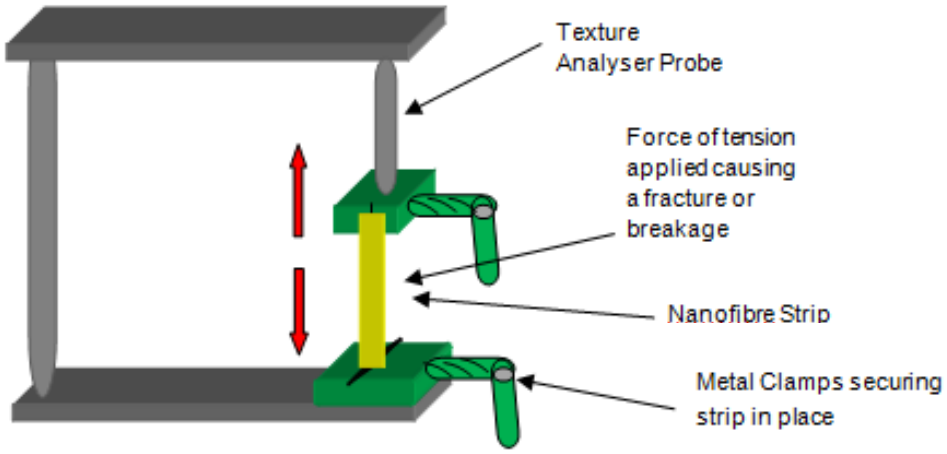

Figure 5.2: Schematic illustrating the textural analysis procedure employed to cause a break or fracture in the nanofibrous strip so that a force against distance plot could be generated to determine the tensile strength

5.2.3.5. Analysis of the Pertinent Rheological Properties of the Polymeric Formulations

A Modular Advanced Rheometer System (ThermoHaake MARS Rheometer, Thermo Fischer Scientific, Karlsuhe, Germany) was used to determine the rheological properties of the polymeric formulation. Stress-strain rheological parameters play a vital role upon electrospinning as these factors greatly influence the electrospinning process. Of particular importance is the viscosity and yield stress of the polymeric solution to form nanofibres. Samples were mounted on a C35/1° titanium rotor and maintained at a temperature of 37°C. Samples were then analyzed for their pertinent rheological characteristics. Table 4.4 as depicted in Chapter 4 reveals the parameters employed to conduct rheological analysis.

5.2.3.6. Determination of the Degree of Crystallinity by X-Ray Diffraction

An X-Ray Diffractometer (Rigaku Miniflex 600, Rigaku Corporation, Matsubara-cho, Akishima-shi, Tokyo, Japan) was utilised at room temperature to determine the degree of crystallinity and amorphosity chemical composition present in the biopolymeric system within the atomic plane. Samples were prepared by loading the prepared nanofibres on a glass sample holder and quantitative X-ray diffraction patterns were obtained.

5.2.3.7. Determination of *In vitro* Bioactive Release and the Effect of Crosslinking on Release Kinetics

An *in vitro* drug release study was conducted using a modified Franz Diffusion Cell type apparatus to determine the release of the bioactive curcumin. The nanofibrous mat was cut into sections of approximately 1.8cm^2. Samples were then placed into the receptor

compartment exposed to phosphate buffer of pH 7.41 and kept at a constant temperature of 37°C thermoregulated by a water jacket. Cells containing the buffer were constantly stirred using a magnetic stirrer and loaded with 12mL of the isotonic buffer. At periodic time intervals 0.1mL was removed for analysis followed by direct insertion of the same amount of buffer into the cell. Samples removed for analysis were evaluated using an Implen nanophotometer GmbH, Munich, conducted at a wavelength of 425nm.

5.2.3.8. Release Kinetics by *Ex Vivo* Studies using a Franz Diffusion Cell Type Apparatus

Excised skin of full-thickness obtained from Sprague Dawley Rats was used to conduct the permeation study. The excised skin was carefully removed and stored in isotonic buffer at -80°C following euthanasia of the Sprague Dawley Rats using pentobarbitone intraperitoneally (i.p.). Preceding the experimental procedure skin samples were cut to a desired area of approximately 1.8cm$^{2.}$ This was prepared subsequent to thawing at room temperature utilizing water and shaving of excess hair and elimination of adipose and subcutaneous tissue on the dorsal region of the skin. Prepared skin was then placed on the receptor compartment of the Franz Diffusion Cell type apparatus followed by application of the nanofibrous mat and held in place by aluminium clamps. The sample was kept in contact with isotonic phosphate buffer in the cellular compartment filled to 12mL and stirred continuously using a magnetic stirrer. At specified periodic interval 0.1 mL was removed and immediately replaced with isotonic buffer. A removed sample was then evaluated for bioactive release employing an Implen nanophotometer GmbH, Munich, conducted at a wavelength of 425nm.

Skin integrity maintenance throughout the study was ensured by measurement of the electrical resistance across the skin sections before and after *ex vivo* evaluation. This was performed by passing a fixed current across the skin preparation using a Mettler Toledo Seven Multi GmbH, Analytical CH-8603 Schwerzenbach, Switzerland connected to an electrode that was adjusted to isotonic environments by placing the probe into isotonic PBS solution before insertion with skin sections. Table 5.3 reveals the conductance and resistance measurements.

Table 5.3: Resistance and conductivity of skin preparations to determine skin integrity before and after *ex vivo* permeation studies

Skin preparation	Resistance (Ω/cm)	Conductivity (µs/cm)
Before	0.37×10^3	18
After	0.86×10^3	16

5.3. Results and Discussion

5.3.1. Characteristic Analysis of the Optimized Nanofibrous Mat

5.3.1.1. Attainment of an Optimized Nanofibrous Wound Healing System by Residual Analysis and Surface Plot Evaluation

Derivation of an effective optimal formulation was obtain and originated from results generated from the B-B design of statistically diverse formulations that varied in concentrations of biopolymer, i.e.: chitosan (1-3%$^{w}/_{v}$), hypromellose (0.4-1.6%$^{w}/_{v}$) and a crosslinker genipin (0.010-0.040%$^{w}/_{v}$) as indicated in Chapter 4. Results attained in terms of the investigated responses (i.e.: Young's modulus, ultimate strength, swelling capacity and water vapour transmission rate) consigned to phenomenal potential in terms of elastic behaviour and potency, stability as well as distension and conduction capability when generated within specific polymeric concentration arrays. Thus this outcome deduced the polymeric composites of the optimized candidate for formulation.

In order to determine the relationship between the predictor variables and the response variables a full ANOVA analysis was conducted as depicted in this section of the measured formulation responses. Data used for the optimization of the experimental design entailed nanotensile analysis to determine the strength and flexibility of the nanofibres, as well as percentage swelling capacity to determine the capacity of exudate absorption and biopolymeric release. Analysis of the model was employed by the attainment of residual plots as seen in Figure 5.3. Analysis of the normal probability plots reveal normal to regular distribution as all points are in close propinquity to the straight line as indicated in the figure (Figure 5.3A-D) with no evidence of underlying variation. Residual analysis of the response surface design (Figure 5.3) disclose significant response data that generally showed random scatter on either side of the zero line indicating the absence of trends thus assumptions relating to the multiple regression analysis were not grossly violated. Amid the consecutive point displayed in the residual vs. the order of data, a random distribution alternating between positive and negative points is distinguished (Figure 5.3 M-P) further validating the assumptions. This is further convoluted by the histogram of residuals (Figure 5.3 I-L) where constant variation with normal distribution is observed. Table 5.4 depicts a full ANOVA that was carried out.

To establish the level to which the model fitted the data, the coefficient of regression R^2 was determined for all responses whereby it was noted to be above the 50% mark for all. Young's Modulus displayed a value of 84.7%, Water Vapour Transmission Rate (WVTR) 76.8%, % Swelling Capacity 77.9% and Ultimate Strength 61.8% indicating a superior fit.

Regression equations regenerated for the responses are specified in Equation 5.1 a-d:

$$Youngs\ Modulus = 53.44 + (-51.84)[HPML] + (-25.79)[CS] + (-50.64)[GEN] + (11.93)[HPML * HPML] + (3.13)[CS * CS] + (-9088.89)[GEN * GEN] + (11.40)[HPML * CS] + 9233.33)[HPML * GEN] + (90.83)[CS * GEN]$$ [Equation 5.1a]

$$Water\ Vapour\ Transmission\ Rate = 13.441 + (5170)[HPML] + (-6345)[CS] + (-356661)[GEN] + (-2902)[HPML * HPML] + (577)[CS * CS] + (1993285)[GEN * GEN] + (422)[HPMC * CS] + (-10570)[HPML * GEN] + (105543)[CS * GEN]$$[Equation 5.1b]

$$\%\ Swelling\ Capacity = 426 + (-307)[HPML] + (-125)[CS] + (-9023)[GEN] + (104)[HPML * HPML] + (38)[CS * CS+254540GEN*GEN+19HPML*CS+3240HPML*GEN+-2738[CS*GEN]$$[Equation 5.1c]

$$Ultimate\ Strength = 1.0290 + (-0.8944)[HPML] + (-0.2412)[CS] + (-18.5278)[GEN] + (0.4097)[HPML * HPML] + (0.0150)[CS * CS] + (88.8889)[GEN * GEN] + (0.0375)[HPML * CS+0.8333HPML*GEN+5.000[CS*GEN]$$[Equation 5.1d]

Table 5.4: ANOVA analysis of the measured responses

	P Value			
Response Variable				
	YM	WVTR	Swelling	US
Hypromellose	0.011	0.342	0.137	0.11
Chitosan	0.03	0.109	0.324	0.464
Genipin	0.927	0.131	0.249	0.362
Hypromellose*Hypromellose	0.069	0.196	0.188	0.074
Chitosan*Chitosan	0.152	0.447	0.18	0.828
Genipin*Genipin	0.321	0.55	0.067	0.773
Hypromellose*Chitosan	0.012	0.722	0.644	0.736
Hypromellose*Genipin	0.292	0.893	0.272	0.91
Chitosan*Genipin	0.479	0.065	0.142	0.287

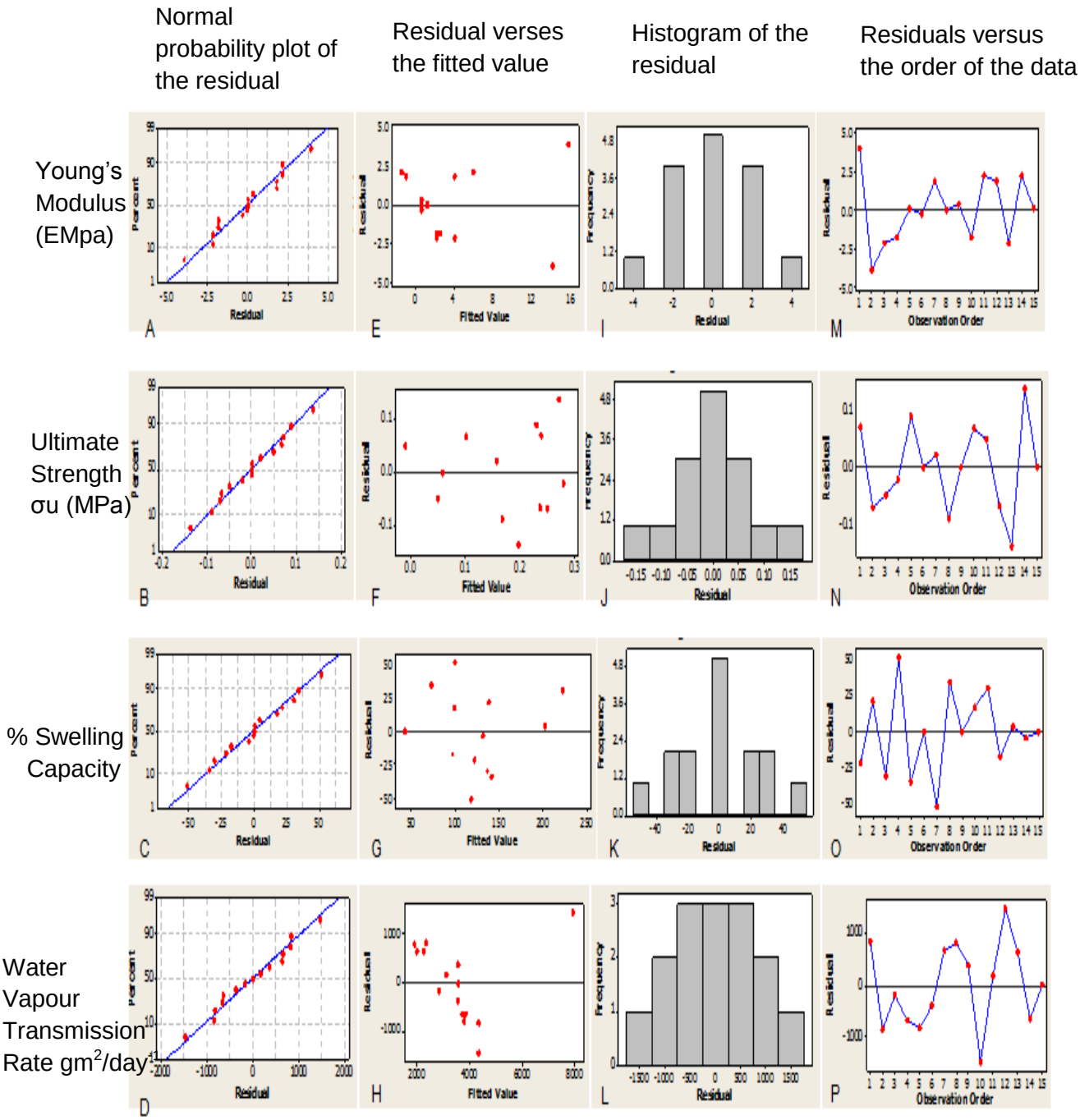

Figure 5.3: Summary of Residual plots for Young's Modulus, Ultimate Strength, Swelling Capacity and Water Vapour Transmission Rate

Further analysis was conducted and explicated by the use of surface plots to optimize the product design and processing whereby significant components and interactions within the nanofibrous system were highlighted. Interactions between the polymers and crosslinker were analysed and addition of a crosslinker at low concentrations of 0.01%$^{w}/_{v}$ was found to significantly influence the characteristics and design properties of the system formulation. Addition of the crosslinker to chitosan considerably enhanced the mechanical properties of the nanofibrous mat by decreasing the Young's modulus and increasing its ultimate strength as discussed in this study and can be microscopically visualised in Figure 5.10. When a larger amount of crosslinker was used by increasing crosslinker concentration, flexibility and elasticity of the system decreased until brittleness was noted. Furthermore increasing the polymer volume resulted in an increase in the

fibrous bulk volume augmenting the mechanical attributes to a certain degree thereafter influencing its elasticity and flexibility for topical application. Figure 5.4 and Figure 5.5 represents the surface plots and contour plots obtained that provides valuable data regarding the responses obtained from the 3 factor Box-Behnken design for optimization.

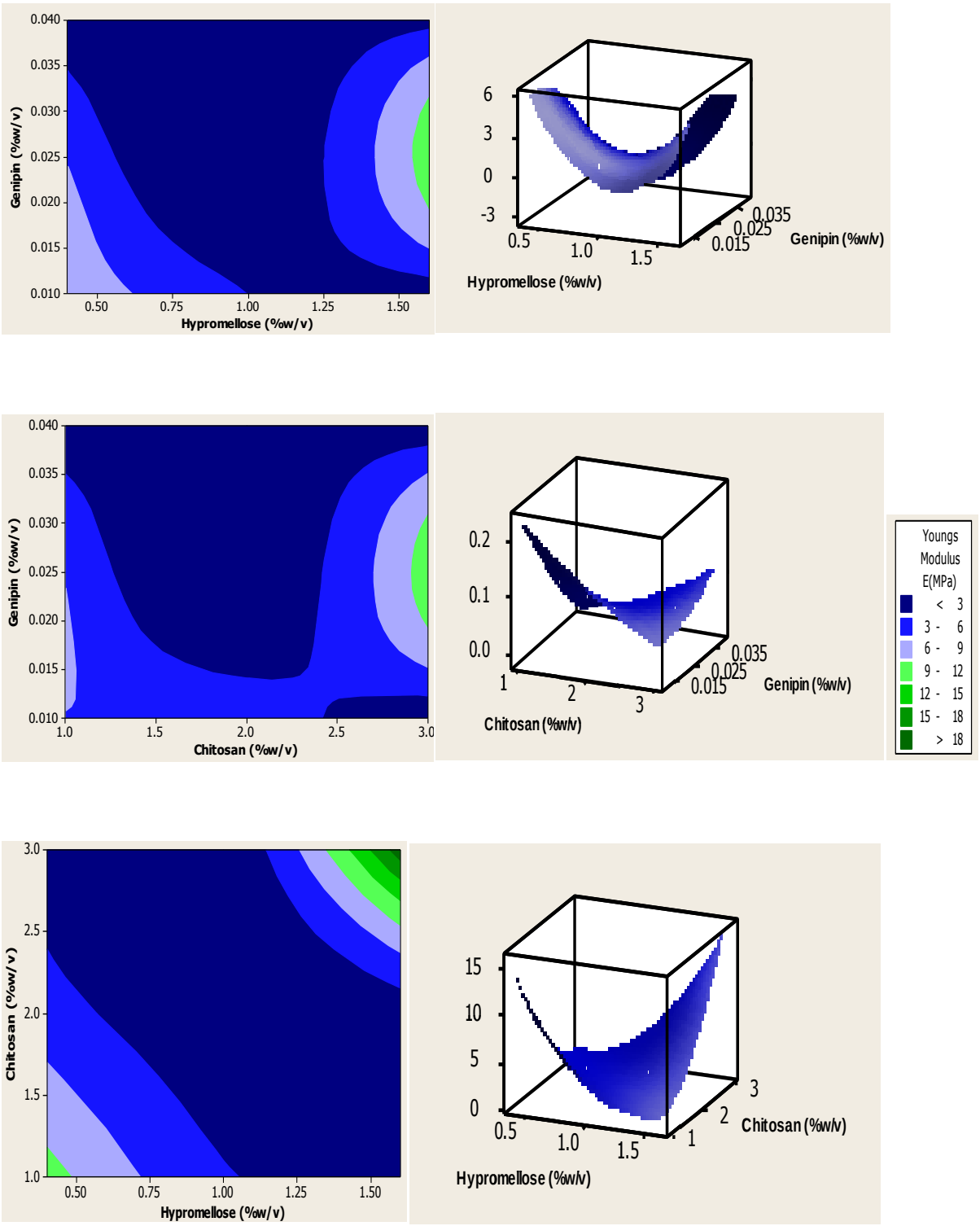

Figure 5.4: Contour and Response Surface Plots depicting the interactions between polymers and crosslinker on mechanical characteristics resembled by Young's Modulus

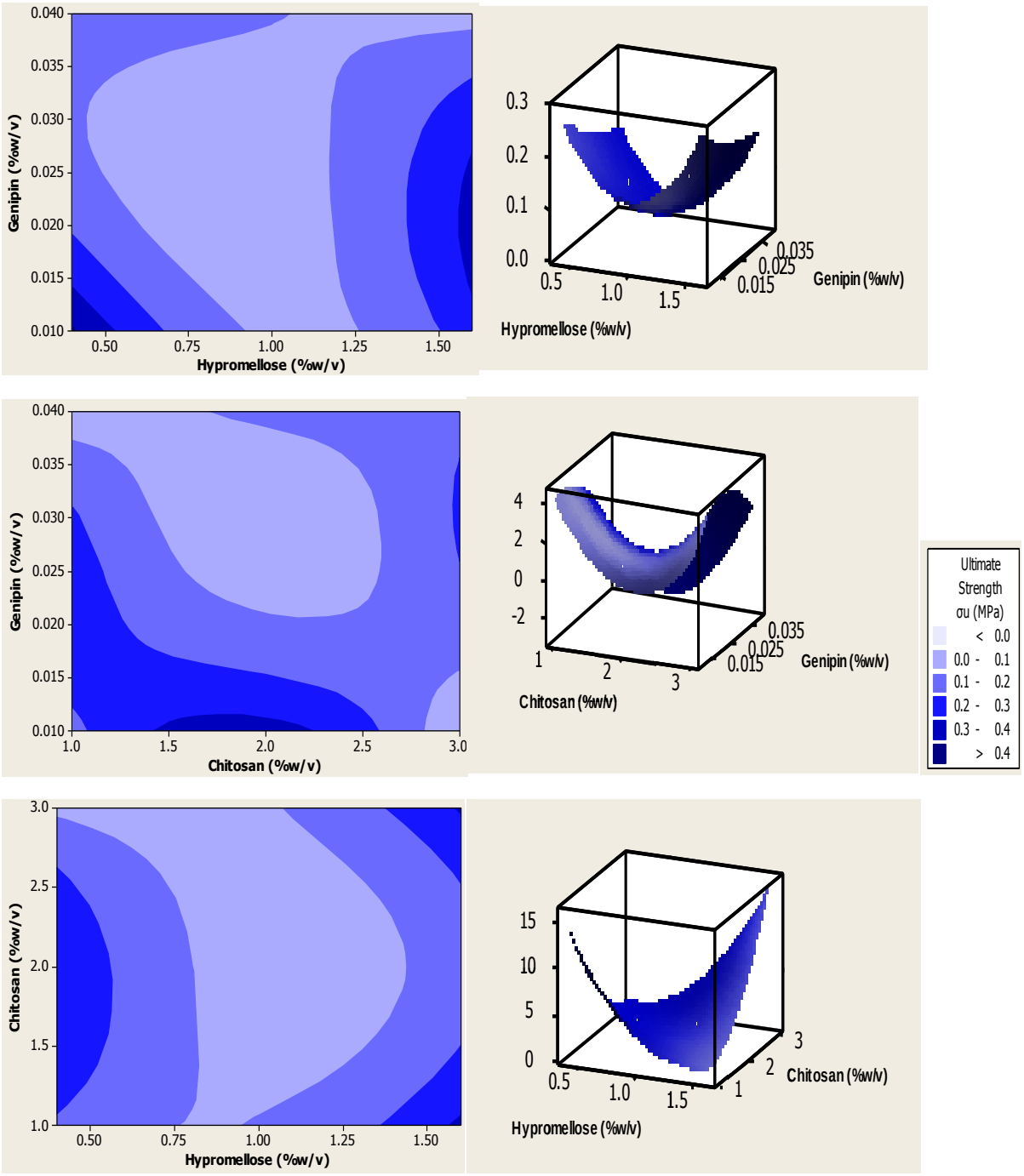

Figure 5.5: Contour and Response Surface Plots depicting the interactions between polymers and crosslinker on mechanical characteristics resembled by Ultimate Strength

Figure 5.6 and Figure 5.7 depict the contour and surface response to swelling and water vapour transmission upon the influence of varying polymer concentration. Minimal swelling is indicated upon utilisation of low volume of polymer from 1-1.6%$^{w}/_{v}$ hypromellose and 2-3%$^{w}/_{v}$ chitosan as depicted in the figures thus sustaining and prolonging the bioactive release. The degree of crosslinking also greatly influenced the swelling and transmission rate as greater intermolecular forces and bonds provides superior control over the rate of swelling and erosion when applied to skin tissue. Furthermore Figure 5.7 depicts the greatest transmission rate when a high degree of

chitosan polymer is used up to 9000g/m^2. The use of lower concentrations provides a lower more suitable transmission rate as is predicted in Figure 5.7.

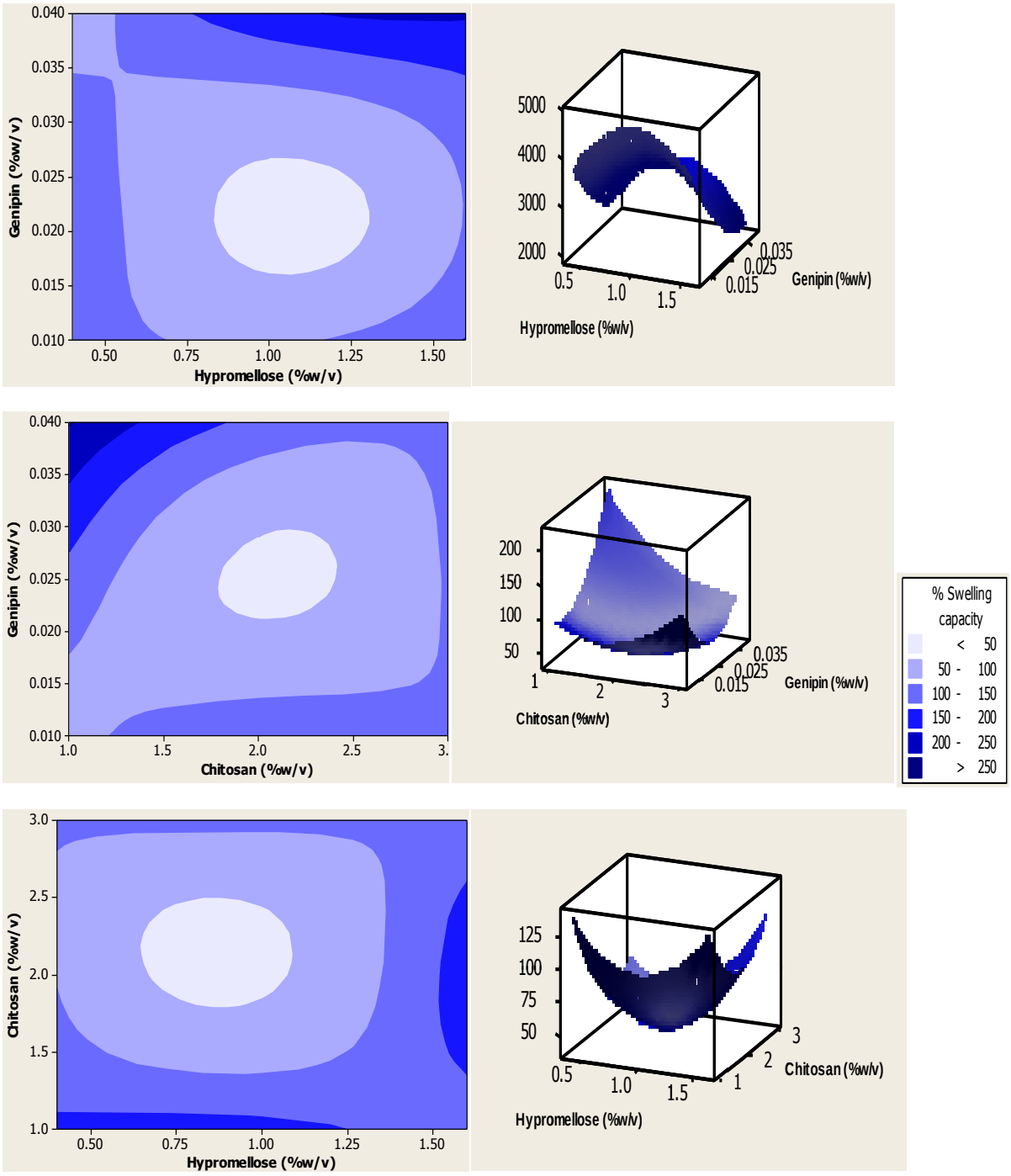

Figure 5.6: Response surface and contour plots depicting the effects of chitosan, hypromellose and genipin on swelling.

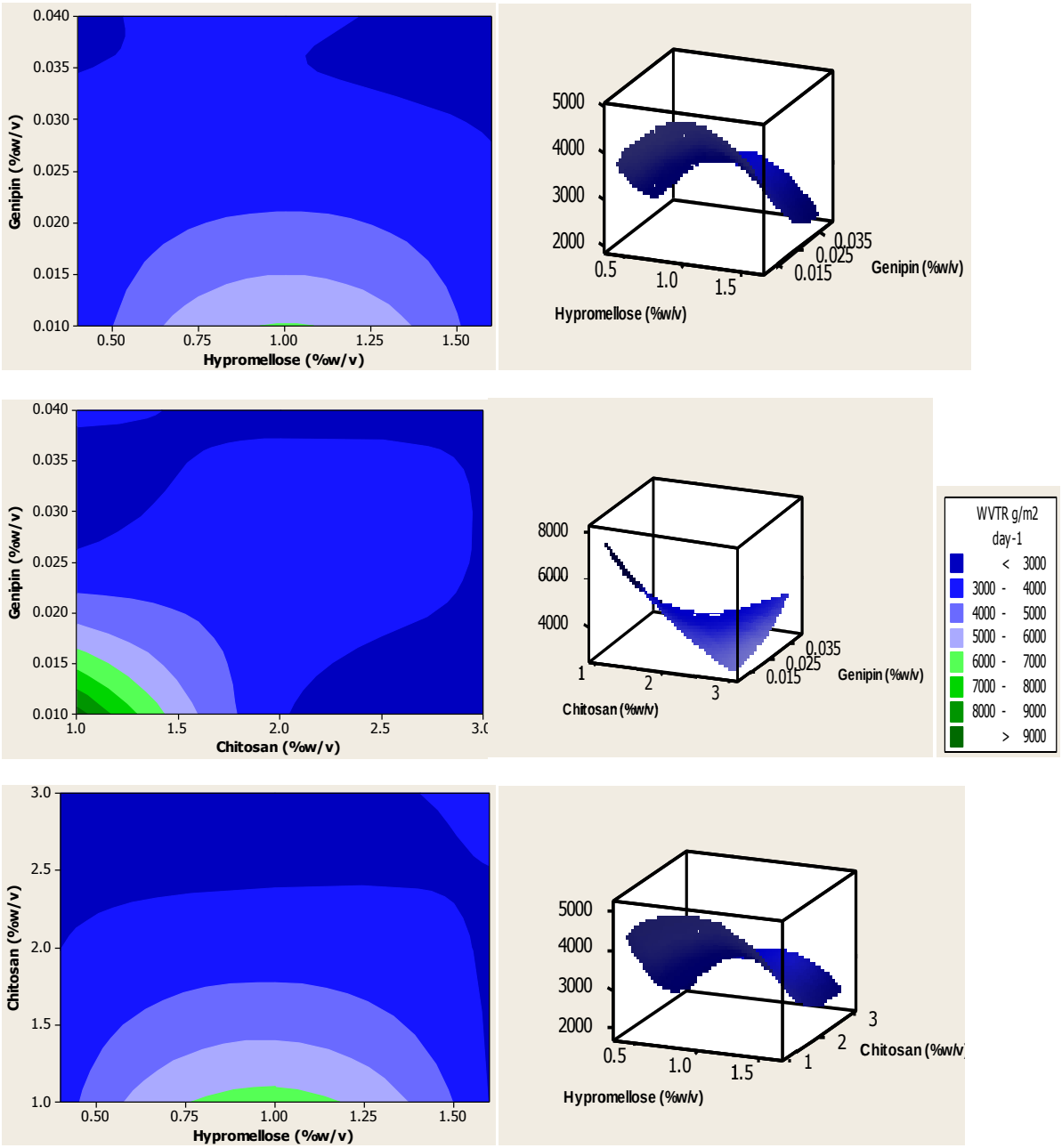

Figure 5.7: Surface and contour plot analysis depicting the influence of swelling and water vapour transmission.

5.3.1.2. Response Optimization

Nanofibre optimization was obtained using the measured responses for the reverent factors as discussed i.e.: Young's Modulus, Ultimate Strength, Water Vapour Transmission Analysis and Swelling Capacity. The procedure was performed (MINITAB®, V15, Minitab, USA) to attain the adjusted levels of polymer and crosslinker incorporated into the nanofibres to prepare an ideal formulation to give flexible yet robust fibres suitable for topical administration from the experimentally derived value as indicated in Figure 5.8 and analysed as discussed in Chapter 4.

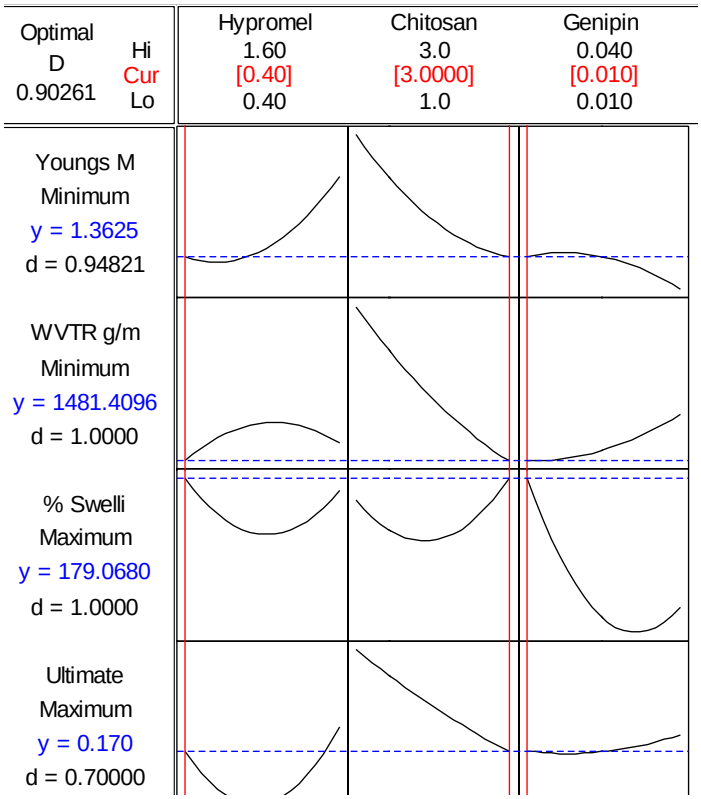

Figure 5.8: Optimization plot for the definition of the optimum nanofibrous system

5.3.2. Stability Analysis in Terms of Chemical Structural Transitions by Fourier Transform Infrared Spectroscopy

Chitosan, a natural polymer and thus highly biodegradable needs to be crosslinked in order to conserve bioactive delivery and controlled release. Crosslinking involves chemical interactions occurring to form a bond between polymer chains that will enhance the general properties by improving both the physicochemical and physicomechanical properties to modulate and control sustained bioactive release. Genipin a natural crosslinker with a low cytotoxicity profile and encompassing wound healing activity is the crosslinker of choice (Muzarelli et al., 2009) as stated before. Figure 5.9 demonstrates the FTIR profile revealing the effects of crosslinking. A wavelength of 1341.74cm^{-1} was eminent in Figure 5.9a(a) which embodied the presence of aromatic C-N stretching representing an amine group due to the presence of genipin. Furthermore a shift in the various wavelengths was seen from 2892.99 in uncrosslinked nanofibres to 2907.16cm^{-1} in crosslinked nanofibres (1), 1416.06 to 1429.29cm^{-1} (2) and 1341.77 to 1373.12cm^{-1} (3) in crosslinked nanofibres representing alkanes C-H bending. This shift in wavelength to the left indicated an increase in conjugation and bond intensity thus establishing an increase in stability and physicomechanical properties to the nanofibrous system. This enhancement assists in sustaining controlled and long lasting bioactive release. In addition, due to improved physicomechanical properties, topical application will be made convenient and durable.

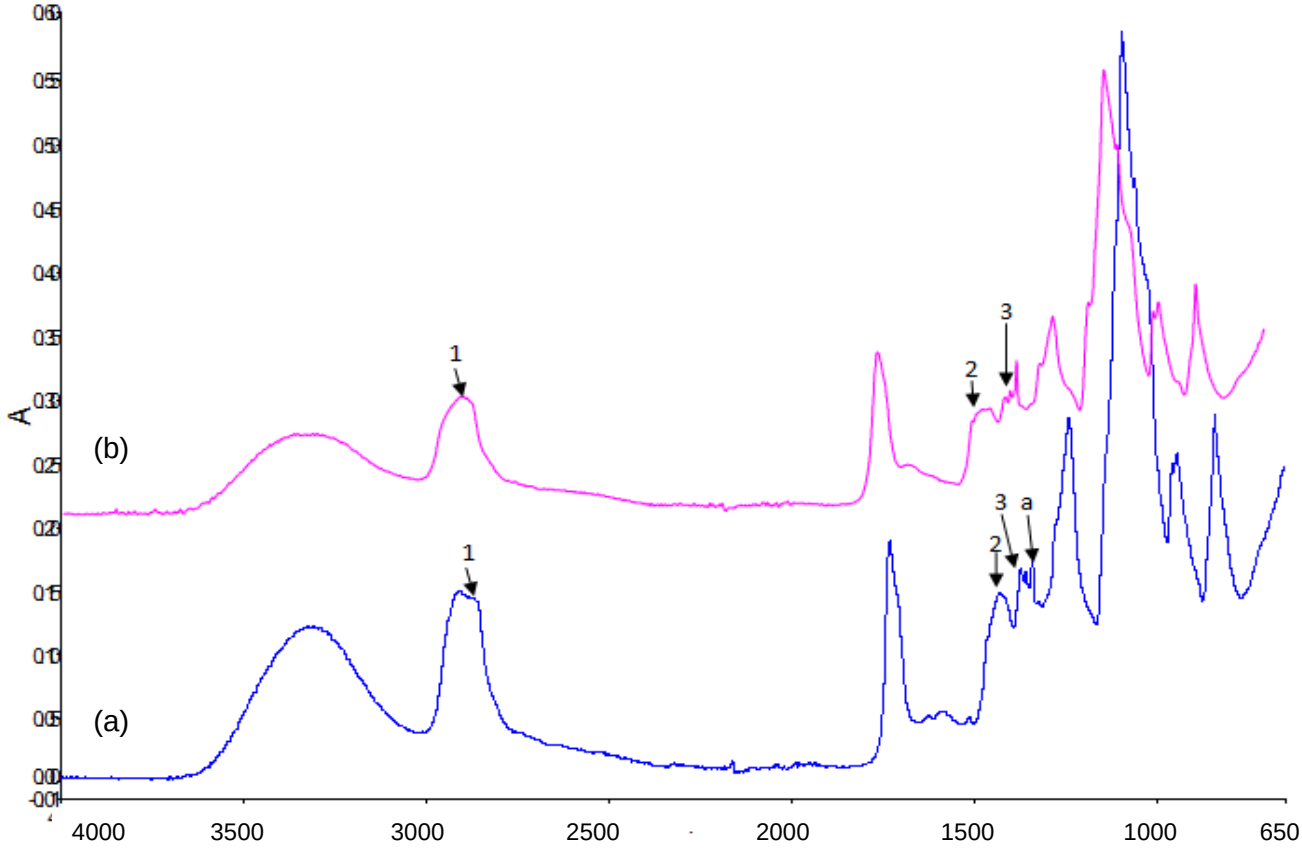

Figure 5.9: FTIR spectra of (a): Crosslinked nanofibrous mat and (b): Uncrosslinked nanofibrous mat

5.3.3. Surface Topographical and Morphological Evaluation by Scanning Electron Microscopy

Morphological analysis of the SEM profiles revealed the influence of crosslinking on nanofibre eminence. Figure 5.10 disclosed the presence of nanofibre structures that were solid, cylindrical, uniform in some instances and of random orientation. The absence of crosslinker resulted in the formation of a nanofibrous mat with nanofibres that vary in diameter as can be seen in Figure 5.10b and 5.10c. Nanofibre diameter was seen ranging between a scale of 22.68nm and 75.43nm. Furthermore it was noted that nanofibres were deposited upon the aluminium collecting surface in a disorganized manner whereby they accumulated in a coiled and tangled fashion, diameter was of varying size and the presence of nanobeads and kinks was clearly distinguished in Figure 5.10c. The incorporation of crosslinker resulted in the formation of a nanofibrous mat with more evenly orientated nanofibres in a structured fashion. Furthermore, crosslinking caused contraction of nanofibres thus endorsing a denser structure with narrowly packed nanofibres (Figure 5.10d, e, f). Crosslinked nanofibrous mats displaying this orientation prolong the release of bioactives thus promoting sustained release due to a decrease in surface area when nanofibre compaction occurs. In addition, the nanofibrous surface demonstrates the absence

of pores which can be attributed to the use of water as a solvent. Water encompasses a relatively low volatility thus preventing surface pore formation (Sheikh et al., 2012). Porous sites were seen occurring between individual nanofibres within the mat which encourages the regenerative process during wound healing due to its close architecture to the native extracellular matrix (ECM) of the skin. Moreover, the addition of a crosslinker improved the physicomechanical properties of the nanofibrous system preventing ruptures and breakage from occurring as seen in Figure 5.10a. Crosslinking provided a nano structure with relevant vapour transmission and swelling thus controlling bioactive release promoting prolonged healing at a much more efficient rate.

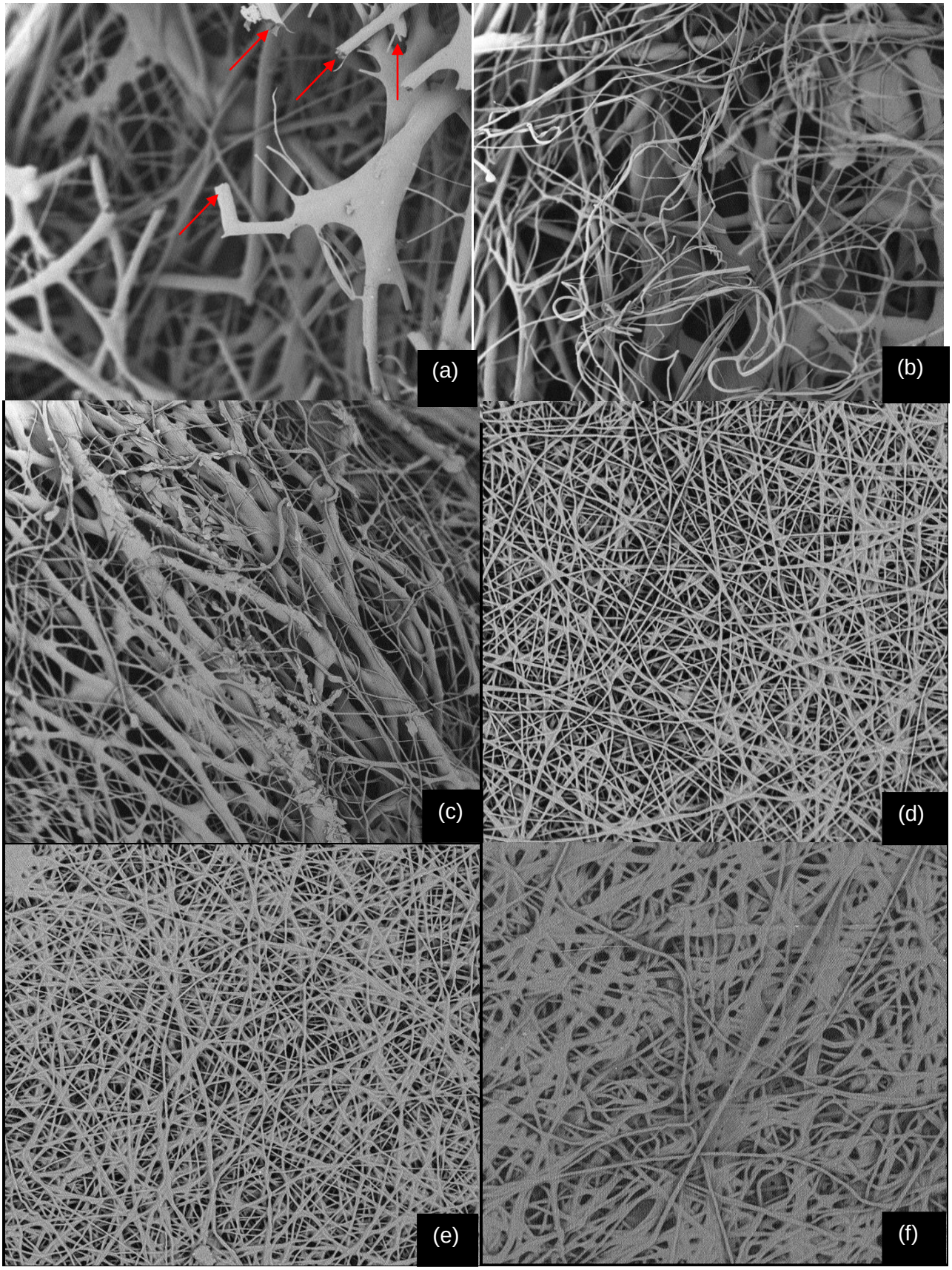

Figure 5.10: Morphological representation of(a), (b), (c): Uncrosslinked nanofibres; (d), (e), (f): Crosslinked Nanofibres

5.3.4. Thermodynamic Behaviour of the Nanofibrous Mats in terms of Differential Scanning Calorimetry

Figure 5.11 displays the DSC transitions occurring upon exposure to heat variation. A glass transition (T_g) was seen in both curves but was more prevalent in the crosslinked nanofibrous mat at 75.13°C whereas when uncrosslinked a glass transition occurred at 30.54°C and was superimposed by an endothermic peak at 101.72°C. This suggests that the provision of a polymer backbone upon crosslinking increased the glass transition therefore allowing decomposition to occur at a decreased and slower rate. A low glass transition of 30.54°C superimposed by the broad endothermic peak revealed melting and the presence of eutectic impurities, thus the uncrosslinked nanofibrous mat subsist in a more defined polymorphic state. An exothermic peak was observed at 148.64°C in Figure 5.11a and 144.63°C in Figure 5.11b indicating crystallization. An elevated crystalline temperature of 148.64°C seen in the crosslinked nanofibrous mat demonstrated a further ordered molecular arrangement thus a decreased molecular motion between molecules due to the intramolecular and intermolecular bonding occurring upon crosslinking. An endothermic melting transition phase was seen in both DSC profiles. However, Figure 5.11b revealed the presence of an exothermic peak arising upon melting as indicated in the figure. This suggested the occurrence of melting with decomposition which could be attributed to the uncrosslinked nanofibrous structure been in an amorphic state with randomly orientated molecules more prone to degradation. Lastly an exothermic peak occurring at 283.96°C in the crosslinked nanofibrous structure and 264.45°C in the uncrosslinked nanofibrous structure disclosed a decomposition event. From the temperatures obtained it was seen that crosslinking improved the stability of the structure, thus slowing down the process of degradation.

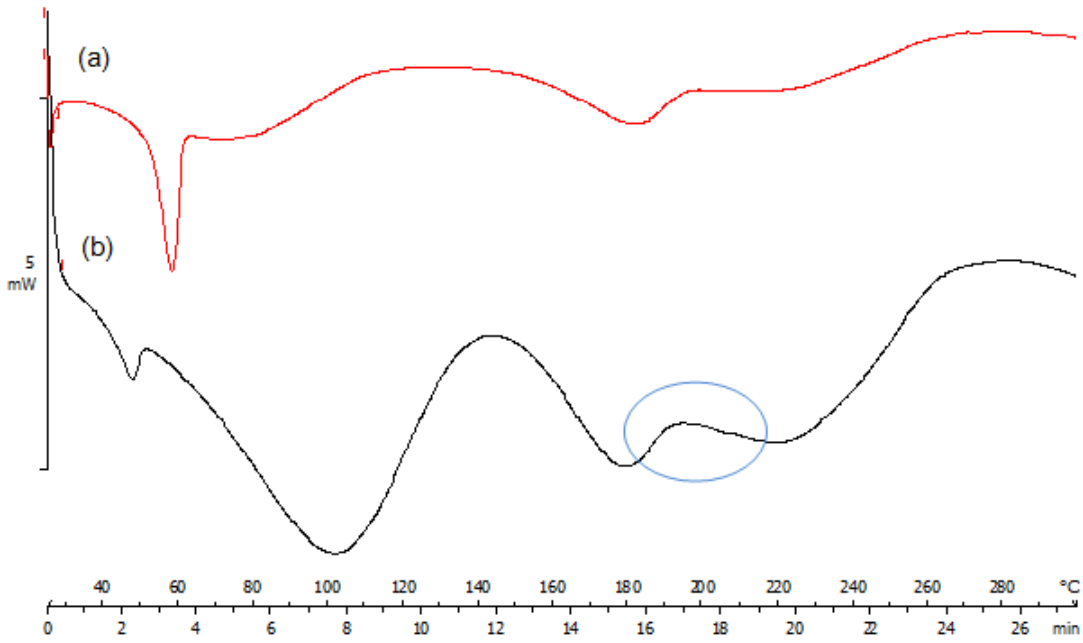

Figure 5.11: Differential Scanning Calorimetry Thermograms of (a): Crosslinked nanofibrous mat, (b): Uncrosslinked nanofibrous mat

5.3.5. Determination of the Young's Modulus and Tensile Properties of the Crosslinked and Uncrosslinked fibres

To investigate the mechanical properties as well as the influence of crosslinking on nanofibre formation, tensile properties were evaluated to determine the tensile strength and Young's Modulus. Figure 5.12 and Table 5.5 reveals the results obtained from nano tensile mapping. Young's Modulus provides a means by which the ratio of stress to strain can be depicted to determine the nanofibrous elasticity. From the stress-strain graphs obtained in Figure 5.12 it was seen that Figure 5.12a displays an irregular pattern of deformation as demarcated in the figure, to finally produce a breaking point. This suggest that a deviation from linear-elastic behaviour occurs thus causing permanent deformation to take place and the uncrosslinked nanofibrous mat exhibits poor elastic properties. The introduction of genipin as a crosslinker to produce an optimum formulation resulted in the formation of a polymer backbone enhancing polymer chain flexibility. From the results obtained in Table 5.5 it was noted that the crosslinked nanofibrous mat displays a greater tensile strength of 0.195N.mm^2 in comparison to the uncrosslinked mat displaying a value of 0.035N.mm^2. It was further seen that the crosslinked nanofibrous mat displays a lower Young's Modulus thus portraying defined flexibility, whereas uncrosslinked nanofibrous mats with elevated Young's Modulus portray a greater degree of rigidity and stiffness promoting the configuration of a brittle structure that is inconvenient for topical application. Furthermore from the table it was seen that crosslinked nanofibrous mats depict a greater ultimate strength, ultimate stress and yield

stress.

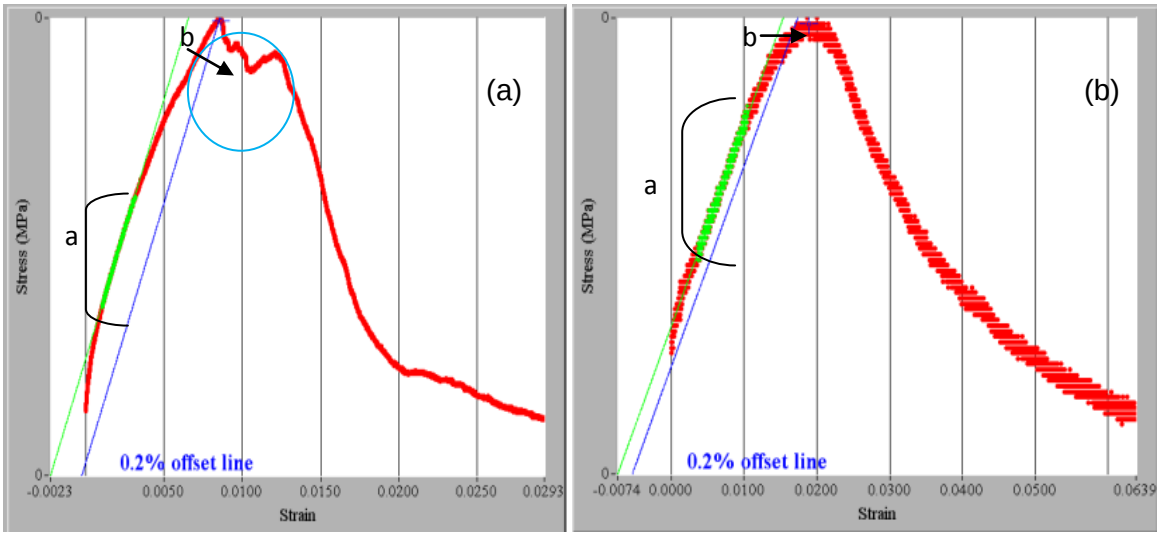

Figure 5.12: Nanotensile mapping depicting comparisons in mechanical strength of (a): Uncrosslinked nanofibrous mat, (b): Crosslinked nanofibrous mat [a: Linear portion depicting Young's Modulus, b: Fracture point]

Table 5.5: Experimental values obtained from the nanotensile mapping of crosslinked and uncrosslinked nanofibrous mats

	Tensile Strength ($N.mm^2$)	**Young's Modulus E (MPa)**	**Yield Stress (σy)**	**Ultimate Strength (σu)**	**Ultimate Strain (εu)**
Uncrosslinked Nanofibrous Mat	0.035	5.96	0	0.07	0.009
Crosslinked Nanofibrous Mat	0.195	7.56	0.13	0.14	0.019

5.3.6. Analysis of the Pertinent Rheological Properties of the Polymeric Formulations

For the process of optimal electrospinning, polymeric hydrogel integrity and retentive behaviour assessment is required by evaluation of their viscoelastic properties and mechanical strength. This was conducted by the application of stress sweep and frequency sweep experimentation. Figure 5.13 displays the outcome obtained from both crosslinked and uncrosslinked formulations by means of the frequency sweep. When a hydrogel displays exceptional physicomechanical properties, its integrity is maintained thus preventing physical drug loss, preserving and prolonging drug delivery *in vivo.* Furthermore hydrogels demonstrating excellent physicomechanical characteristics, endorse the process of electrospinning allowing the formation of uniform, cylindrical and orientated nanofibres which can be observed in Figure 5.10. Evaluation by stress sweep analysis, revealed the linear viscoelasticity range providing a strain value which is employed to conduct a frequency sweep evaluation. G' (elastic or storage modulus) and G'' are pertinent rheological

parameters obtained upon the conductance of a frequency sweep test under non- destructive conditions. G' computes how well structured a hydrogel will be and signifies the elastic storage of energy. G" displays the viscous energy of a hydrogel and adjusts in accordance to the viscosity of the hydrogel. From the results obtained it was seen that G' dominates in the crosslinked formulations therefore suggesting the hydrogel is more elastic then viscous within the investigated frequency range (Anumolu et al., 2010).

Illustrations of the frequency sweep of the uncrosslinked hydrogel solution, whereby G" dominates displayed that the hydrogel exist in a greater viscous state. The results can be further supported by the yield stress obtained whereby the crosslinked hydrogel revealed a yield stress of 36.57Pa and the uncrosslinked hydrogel showed a yield stress of 38.60Pa disclosing that the uncrosslinked hydrogel will cease to behave elastically prior to the crosslinked hydrogel. This was attributed to the introduction of a crosslinker supplying a polymer backbone with the formation of a stronger crosslinking network. The crosslinked hydrogel where G' is dominant displays a greater mechanical strength suggesting its ability to resist any structural changes when an increased strain is applied. Furthermore the crosslinked hydrogel produced nanofibres that were more uniform in diameter producing an organised nanofibrous mat. Nanofibres fabricated from the uncrosslinked hydrogel confirmed the presence of nanobeads and nanofibres of varying diameters as depicted in Figure 5.10.

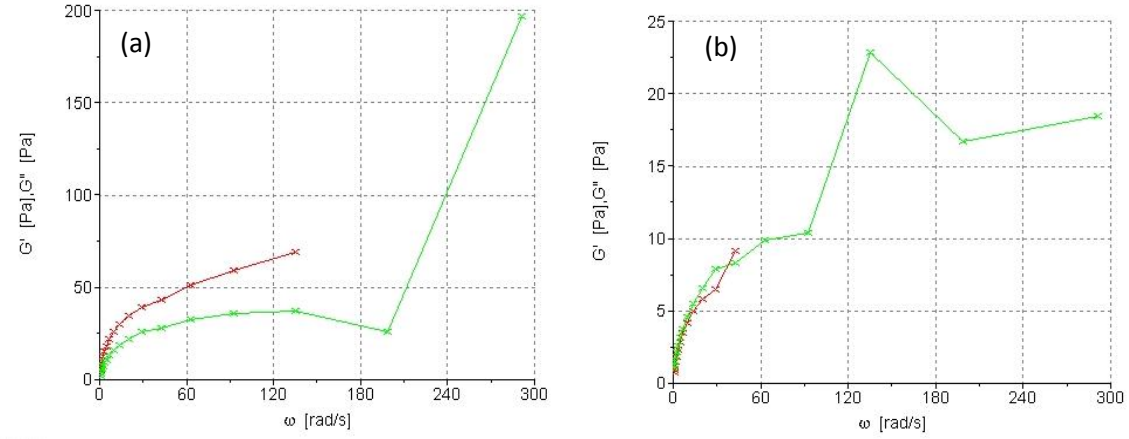

Figure 5.13: Depiction of pertinent rheological parameters affecting nanofibres formation **(**a): Crosslinked hydrogel, (b): uncrosslinked hydrogel

5.3.7. Determination of the Degree of Crystallinity by X-Ray Diffraction

For the establishment of the crystallographic interactions occurring in the nanofibrous mats upon crosslinking, XRD patterns have been determined. Figure 5.14 portrays the x-ray diffraction patterns both, upon crosslinking and uncrosslinked over a 2θ range of 0-80°.From the profiles obtained it was noted that crosslinked nanofibrous systems reveal symmetrical and narrow peaks that are dominated at 38°, 43°, 78° and 81°. A broader peak preceeds

composed of narrow symmetrical peaks, arising prior to 20° 2θ advocating that the nanofibrous character shifts from a polycrystalline state to a more crystalline state. Absence of crosslinking bridges produce a diffraction pattern dominated by broader peaks throughout the diffractogram. Broad asymmetrical peaks were intensified between 60° and 80° 2θ. Irregular stereoregularity detected by the broad peaks in uncrosslinked nanofibrous systems demonstrate a structure that is dominantly amorphous in nature thus containing a randomly orientated entanglement of polymer chains, therefore easily degradible with poor tensile properties. Introduction of crosslinking provides greater stereoregularity to the structure in a crystalline configuration thereby promoting sustained and controlled release of bioactives as well as enhanced mechanical properties.

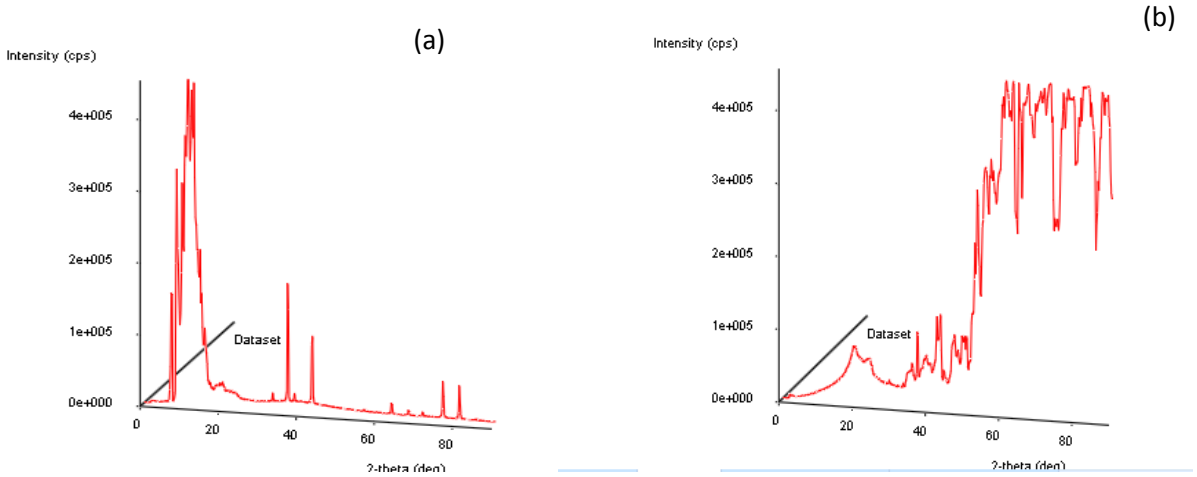

Figure 5.14: XRD profiles of **(**a): Crosslinked nanofibrous mat, (b): uncrosslinked nanofibrous mat

5.3.8. Evaluation of *In Vitro and Ex Vivo* Bioactive Release Kinetics

To determine the release kinetics of the optimum nanofibrous delivery system across permeated skin and in contact with a dissolution buffer medium of pH 7.4, a Franz Diffusion Cell Type Apparatus was used. Samples were removed at 0.5,1,2,3,4,6,8,10,12 and 24 hours during experimentation to determine the cumulative release rate. Figure 5.15a reveals the bioactive and permeated release rate over time. From the outcome obtained it was noted that there was a burst release obtained within the initial two hours of the study in both instances. At 2 hours a release rate of 0.9457mg and 2.1016µg was observed for bioactive release and permeated release rates respectively. The release rate of curcumin was observed to steadily increase for the initial 8 hours and was pronounced in the permeated release profile at 3.1641µg and 1.3193mg in the bioactive release profile. Subsequent to 8 hours, the release rate in both instances seemed to take on a greater equilibrium state thereby commencing a more defined steady state release profile. Curcumin is a yellow to orange crystalline powder with the chemical formula $C_{21}H_{20}O_6$ and is insoluble in water thus

highly hydrophobic (Bharat et al., 2008). Due to its hydrophobic nature, release rates were potentiated across the skin tissue when in contact with the lipophillic phospholipid bilayer, a lipid based membrane present within the skin. Thus accelerated release rates were seen in the permeated bioactive release of curcumin throughout the study advancing the clinical efficacy as shown in Figure 5.15. These results comply with earlier studies carried out in curcumin films (Mayet et al., 2014).

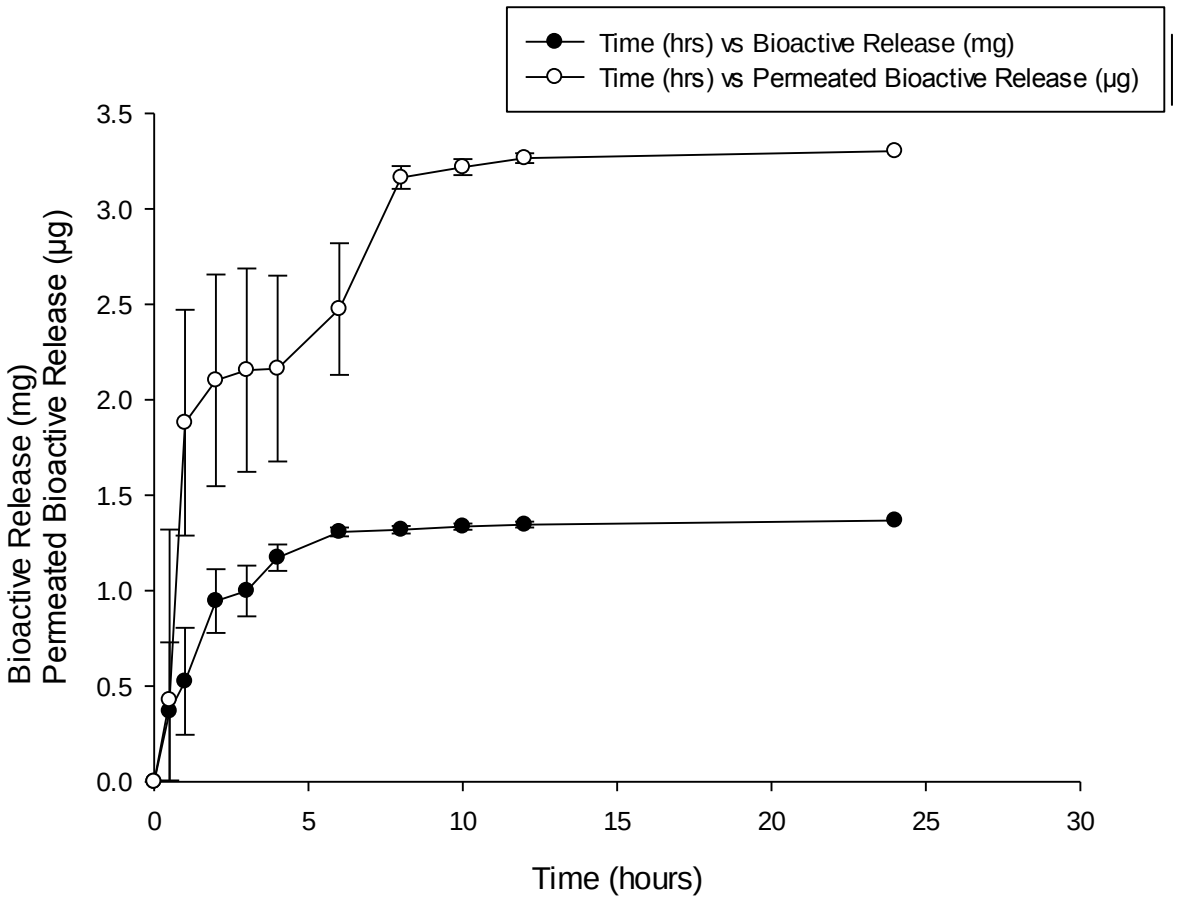

Figure 5.15: *in vitro* bioactive release and *ex vivo* permeated release profile of the optimum nanofibrous mat

5.4. Concluding Remarks

The nanofibrous mats composed of natural biomaterials was successfully developed, optimized and characterised for topical wound administration. Employment of the response surface methodology lead to the development of an optimized formulation by mathematical derivation. Furthermore regression and correlation analysis was used to analyze the dataset thus confirming the statistical adequacy of the models proposed. Optimization of the formulation leads to the expansion of an optimized nanofibrous mat with fine biological and mechanical characteristics. Furthermore the chapter also demonstrated the direct effects of crosslinking on the formation of the nanofibrous mat. To further enhance the system and provide a complete prototype device a novel component was introduced to the system known as the BTDS. Chapter 6 to follow will provide a greater insight to this advancement.

CHAPTER 6
DESIGN OF THE LYOPHILIZED INFLAMMATORY DEPENDENT MATRIX OF THE MULTICOMPONENT STIMULI RESPONSIVE PROTOTYPE DEVICE

6.1.1. Introduction of Advancements to the Bioactive Delivery System

This chapter aims at illustrating the incorporation, design and development of the lyophilized inflammatory dependent matrix to serve as a component of the Bioresponsive transdermal delivery system (BTDS). It explores the mechanism of the device that demonstrates two way communications between the delivery system and biological tissue. Of particular interest is the invention of a biopolymeric network, that when designed may provide an unique opportunity to interact chemically or physically with specific biological mediators for recognising biological processes that pertain to a specific disease state such as wound injury and healing, consequently releasing bioactives upon exposure.

The field of stimuli responsive delivery systems has undeniably gained much insight in the last decade at multi-scaled lengths involving biological systems that govern many living functions. “Stimuli Responsive Systems” can be classified as a polymers response or reaction upon exposure to a specific stimulus and can be categorized in various ways. Responsive polymers, as components in the system may react to a chemical or physical interaction leading to the beginning of diverse events such as acid-base reactions, destruction or configuration of forces both intermolecular and intramolecular involving hydrogen bonds, electrostatic interactions as well as the degradation of various delivery systems such as hydrogels, implants, wafers amongst others upon the application of a particular stimulus. This consequently causes alterations in the polymeric structure which include irreversible or reversible bond breakage of crosslinked groups, polyelectrolyte complexes or the polymer backbone ultimately resulting in the release of the desired active. Application of these smart delivery systems hold great promise in the electronics, biomedical, sensing and drug delivery fields (Roy et al., 2010).

Stimuli responsiveness can be acquired through an array of techniques, both physical and chemical by the employment of heterogeneous polymer networks using smart healing materials. These stimuli techniques include (Liu and Urban, 2010):

- Temperature
- Mechanical
- Light
- Electric
- Magnetic

Physical

- pH
- Biological
- Electromechanical
- Ionic Strength

Chemical

Of significant interest to this research as an advancement and way forward approach is by overcoming challenges faced, by the design of a combinatory bioactive wound healing delivery system. This is done via using a chemical biological stimulus, in particular inflammation as a response. The development of a safe, non toxic and effective matrix that can passively target inflammatory cells at the desired site ensuring controlled and prolonged release and at the same time enhance the anti-inflammatory components of the delivery system was under investigation.

6.1.2. Inflammation as a Stimulus Employed for Controlled Topical Bioactive Delivery

A potentially inflammatory sensitive polymeric device was introduced as an augmentation to the nanofibrous wound healing bioactive system designed as conferred in Chapter 4 and 5. The aim of this ensuing investigation was to build on to the existing nanofibrous system by introducing an inflammatory responsive component thus employing a combinatory delivery system that encompasses the potential to regulate bioactive release from the nanofibrous system and enhance the wound healing impediment of the device.

Wound healing is a dynamic interactive process involving many stages, the first been inflammation. Inflammation presents immediately upon tissue injury whereby extravasation of blood constituents collectively with blood vessel disruption occurs (Singer and Clark, 1999). Inflammation involves the transpiration of manifold events upon exposure to a particular ‘stimulus’ and is not an entity of a solitary event (du Toit, 2013). Of great significance to the process of inflammation is the re-establishment of homeostasis upon injury which materializes as a blood clot or fibrin matrix at the site as a provision of an extracellular matrix. Recruitment of many infiltrates transpire such as macrophages, neutrophils, natural killer cells (NK), monocytes, interleukins (IL), growth factors and platelet plugs as seen in Figure 6.1 (Gurtner et al., 2008). Amongst these there are also chemical mediator’s oxygen metabolites, arachidonic acid metabolites and proteolytic enzymes which are the main perpetrators in establishing tissue damage (Du Toit, 2013). Of pertinent significance to this

investigation was the focus on the above mentioned mediators that lead to the fabrication of the lyophilized matrix.

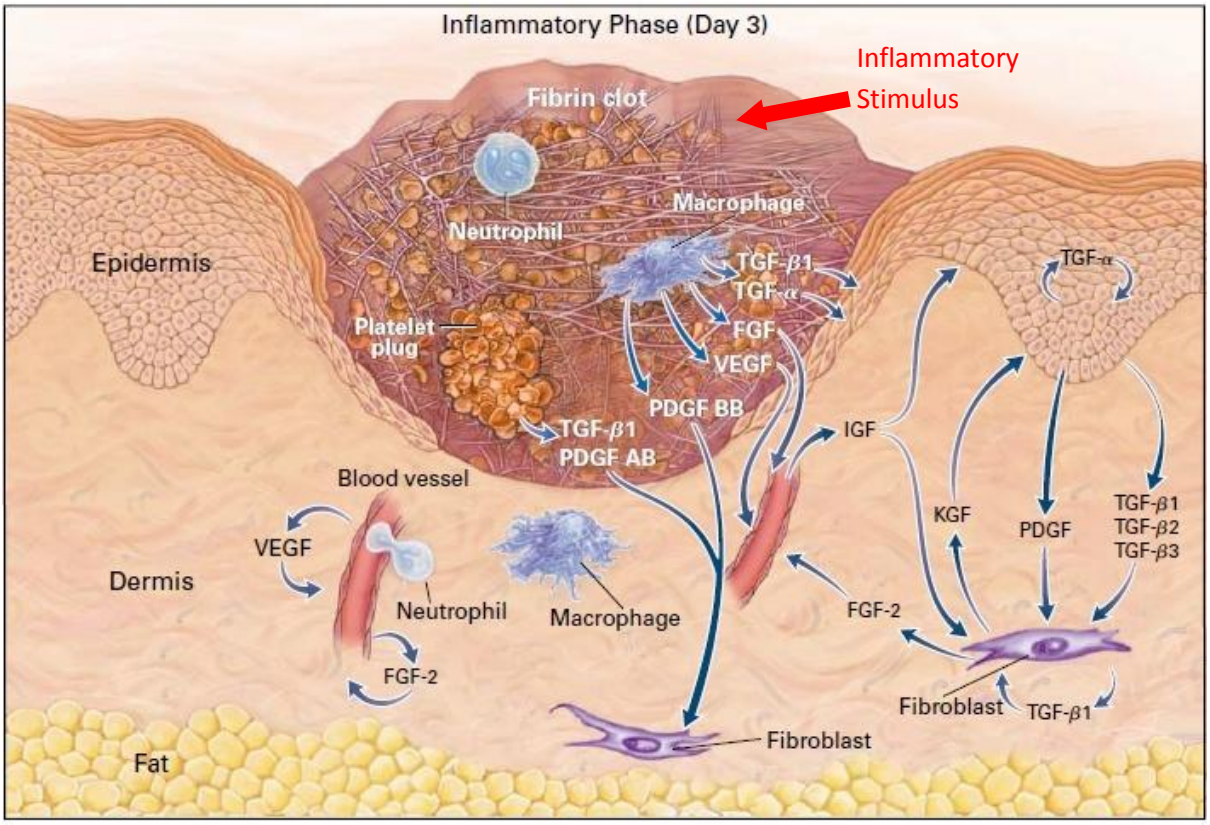

Figure 6.1: Illustration revealing influx of infiltrate mediators to the wound site that will serve as an inflammatory stimulus for the delivery system (Obtained from Singer and Clark, 1999)

6.1.3. Polymeric Components of the Lyophilized Matrix

Hyaluronic acid (HA), a natural constituent that serves as the only non-sulphated glycosaminoglycan (GAG) component within the native extracellular matrix (ECM) of the skin is structured as a linear polysaccharide and comprises of β-1,4-linked D-glucoronic acid (β-1,3) *N*-acetyl-D- glucosamine disaccharide units (Luo et al., 2000). Hyaluronic acid has been found practical for therapeutic use in many delivery systems, in particular tissue engineering as it is biodegradable and biocompatible. Furthermore, it boasts many advantageous properties clinically for wound healing in a variety of tissues as it provides the required structural organisation of the extracellular matrix (ECM) regulating the morphological structure and promoting cell differentiation and regeneration (Kim and Park, 2002). *In vitro* and *in vivo* application of HA derived biomaterials in delivery systems have shown improved *in vivo* residence time and at the same time retaining natural biodegradability and biocompatibility upon chemical modification. In addition to its superior therapeutic attributes, HA exhibits profound pharmaceutical merits whereby chemical modifications allows tailoring of the polymer bonds to suit desired specifications. Functional modifications, drug-polymer conjugates and crosslinking can be applied to progress tissue engineering and controlled, targeted drug release (Luo et al., 2000). The significance of incorporation of HA for the

course of wound healing disclose improved tissue regeneration in the connective tissue ECM by mimicking the native HA found in tissue. Furthermore, HA provides indications that direct responses to improve the superiority of regeneration such as reduced scar tissue formation. Cell adhesion, migration and proliferation are promoted by HA via signalling, both biochemical and biophysical mechanisms (Kreger and Voytik-Harben, 2009).

Sodium alginate was used as a component of the lyophilized matrix. It is a natural algal polysaccharide that is effective as a wound management aid. Attained from the cell walls of the brown algae species seaweeds (*Ascophyllum sp* and *Laminaria sp*) (Lloyd et al., 1998). Alginate is an anionic linear polysaccharide composed of 1, 4 linked β-D-mannuronates and 1, 4 linked α-L-guluronates in varying proportions (Kim et al., 2008). Fan and co-workers have reported the extensive use of alginate in wound management devices and applications due to its many advantageous properties such as non-toxicity, biocompatibility and bioactivity. Above all it possesses haemostatic function, thus is able to absorb exudates from the wound site endowing an elevated absorption capacity and promotion of a moist wound environment. Attainment of a physiologically moist microenvironment promotes the formation of granulation tissue as well as healing (Kim et al., 2008). In addition, alginate dressings serve as one of the most versatile dressings available currently as they demonstrate an eminence to activate macrophages at the wound bed generating pro-inflammatory signals to initiate resolving inflammatory characteristics of wound healing (Fan et al., 2006).

Amongst mammalian species, the structural moieties of hyaluronic acid (HA) have shown great conservation as it is also a naturally occurring biopolymer (Price et al., 2007). Tissue engineering and drug delivery systems can be exceedingly endorsed by the use of HA due to its immunoneutrality properties providing excellent building blocks for synthesis (Prestwich et al., 1998). However, due to its innate nature it is highly biodegradable thus lacking optimal physicomechanical properties. Thus the focus on HA as a major element in drug delivery devices, has brought to attention the addition of partner molecules also possessing advantageous properties to the healing process such as those in alginate to improve on these concerning areas. The use of versatile chemical methodology will allow careful combination of these materials ultimately altering the pharmacokinetic properties diverging its biophysical nature. The use of hydrazides such as adipic acid dihydrazide (ADH) as a crosslinker allows attachment and combination of therapeutic bioactives by covalent attachment of glucuronic acid moieties of HA to the carboxylic acid functions found in hydrazides as shown in Figure 6.2. This allows the availability of amino group arrays along the backbone of HA originating from the attached hydrazides thus improving its biostability and physicomechanical properties, allowing affixment to alginate and encouraging prolonged and controlled release of bioactives (Prestwich et al., 1998).

Stimuli responsive polymer erosion as a drug delivery system has become a superlative route for drug delivery. To a large extent, attention has been focused on this form of drug delivery based on its immense potential when applied *in vivo*. Smart drug delivery systems are able to carry, protect, deliver and then release the active by matching the desired kinetic release by a sequence of complex responses. Employment of a stimuli responsive system to inflammation serves as an ideal contrivance to enhance the efficacy of the bioactive system only when in contact with inflammation allowing activation by degradation of the desired polymeric components (Stuart et al., 2010). As discussed previously in Chapter 1 and in this chapter hyaluronic acid (HA) plays a pivotal role in several physiological functions which include angiogenesis and differentiation, controlled permeation as well as the scavenging of hydroxyl radicals released during the inflammatory process. When used as a therapeutic and responsive agent, HA reacts in the body by two applications:

- Enzymatic degradation by hyaluronidase
- Degradation by hydroxyl radicals as a source of active oxygen

For the purposes of this investigation in terms of a stimuli responsive system, degradation by hydroxyl radicals was further investigated. Affliction of a wound at the tissue site causes the activation of inflammation which results in enhanced capillary permeation. Activation of immune complexes to inflammation causes the release of phagocytic cells, polymorphonuclear leukocytes and macrophages amongst others causing a release of hydroxyl radicals, which in excess may result in tissue damage. The application of an inflammatory responsive system can be understood by the degradation of HA on exposure to these hydroxyl radicals occurring when an acute inflammatory event ensues allowing the development of a stimuli sensitive drug delivery system for wound healing that exhibits inflammation regulated degradation (Yui et al., 1992).

Bearing these considerations in mind, the use of crosslinked hyaluronic acid jointly with alginate in the preparation of an inflammatory dependent lyophilized matrix wherein the bioactive nanofibrous mat is suspended serves as a means to persuade controlled, targeted and prolonged release at the wound site.

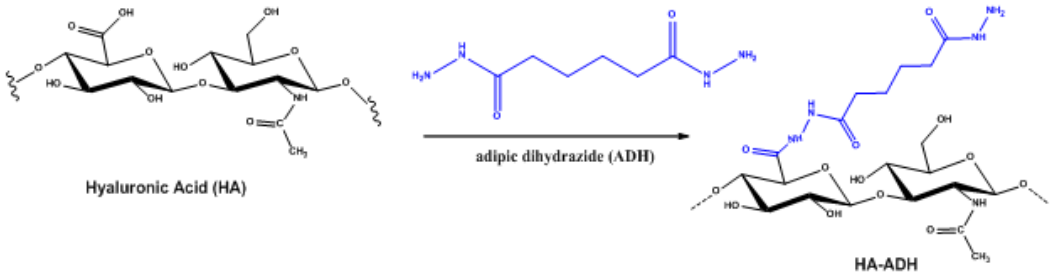

Figure 6.2: Functionalisation of HA with amino groups by the use of ADH

6.2. Materials and Methods

6.2.1. Materials

Glycerol and Tween 80 obtained from Associated Chemical Enterprises Pty Ltd. (South Africa), Alginate (TICA-algin® 400 Powder, medium viscosity) was purchased from Texture Innovation Center® (White Marsh, MD, USA), polyacrylic acid, hyaluronic acid (sodium salt from streptococcus equi (M_W= 8000-15000 g/mol), adipic acid dihydrazide (ADH) M_w= 174.20 ≥ 98% tritration were purchased from Sigma Aldrich Chemie GmbH, Steinheim, Germany. All other materials used were of analytical grade and used as received.

6.2.2. Preparation of Bioresponsive Lyophilized Matrix Component of the BTDS

A three-factor Box-Behnken Design (B-B) was generated by Minitab®, V15 (Minitab® Inc, Pennsylvania, USA) depicted in Table 6.1 in order to derive an efficient, effective and economically favourable end-product. The design comprised of 15 formulations acquired by the input of independent factors based on upper and lower limits as seen in Table 6.2 of the various polymeric concentrations and their responsive impacts. Formulatory component characteristics were based on the acquisition of dependent variables: Bioactive release on exposure to a stimulus represented by a plot of release against time, mechanical and formulary components such as viscosity (mPas) over a period of time at increasing speed and Young's Modulus E(MPa) whereby the attainment of a stress-strain relation curve was established.

Table 6.1: Box-Behnken Design Template of the 15 statistically derived formulations for the design of an inflammatory responsive lyophilized matrix of the BTDS

Experimental Formulation No.	Alginate ($\%^{w}/_{v}$)	Hyaluronic Acid ($\%^{w}/_{v}$)	Adipic Acid Dihydrazide($\%^{w}/_{v}$)
1	2.75	0.5	0.13
2	2.75	0.7	0.16
3	4.5	0.5	0.16
4	4.5	0.3	0.13
5	2.75	0.5	0.13
6	2.75	0.3	0.16
7	1	0.3	0.13
8	2.75	0.5	0.13
9	2.75	0.7	0.1
10	1	0.5	0.1
11	1	0.7	0.13
12	4.5	0.5	0.1
13	2.75	0.3	0.1
14	4.5	0.7	0.13
15	1	0.5	0.16

Table 6.2: Depiction of upper and lower limits of independent variables: polymer and crosslinker concentration

Independent Factors	Lower Level	Upper Level
Polymer concentration (X1) **Alginate**	1%	4.5%
Polymer concentration (X2) **Hyaluronic acid**	0.3%	0.7%
*Crosslinker Concentration (X*3) **Adipic acid dihydrazide**	0.16% (1:3 of hyaluronic acid at 0.5%)	0.1% (1:5 of hyaluronic acid at 0.5%)

6.2.3. Formation of a Stimuli Responsive Topical Delivery System (BTDS) incorporating the Nanofibrous Mat

Formulations were prepared in concentrations according to those specified by the Box-Behnken Design template discussed. A hyaluronic acid hydrogel was made by solution polymerisation using deionised water as the solvent. The hyaluronic acid solution was crosslinked by preparation of a hyaluronic acid-adipic dihydrazide complex to form a hydrazide-functionalised HA hydrogel under continuous stirring using a magnetic stirrer (Luo et al., 2000). Sodium alginate dispersed within deionised water was then added to the HA-ADH functionalised hydrogel to form a multifaceted hydrogel. Wound healing nanofibrous mats were then suspended in the hydrogel allowing polyionic complexes to occur to structure a polyelectrolyte complex. Suspended nanofibrous formulations were immediately subjected to freezing at -80°C (Ultra-low freezer, Sanyo VIP™ Series, Sanyo North America

Corporation, Wood Dale, IL, USA) for a period of 48 hours to maintain stability and prepare formulary samples for the lyophilization process. The prepared samples were then subjected to lyophilization over a period of 24 hours to eliminate entrapped solvent. The system prepared formed a stimuli responsive matrix reservoir that was capable of been adjoined to the backing layer as described in Chapter 7 to form a BTDS system.

6.2.4. Chemical Transitional Analysis through Fourier Transform Infrared Spectroscopy

Evaluation of the chemical compositions and molecular vibrational transitions of the BTDS lyophilized matrix were carried out to determine the degree of crosslinking. FTIR was employed to obtain absorption band spectra using a PerkinElmer® Spectrum 100 Series FT-IR Spectrometer fitted with a universal ATR Polarization Accessory (PerkinElmer Ltd., Beaconsfield, UK). Spectra over the range 4000-625cm^{-1}, with a resolution of 4cm^{-1} and 4 accumulations was utilised as FTIR parameters to determine the degree of crosslinkage occurring between hyaluronic acid and adipic acid dihydrazide by evaluation of the molecular vibrational transitions.

6.2.5. Thermodynamic Analysis through Differential Scanning Calorimetry

An advanced DSC (TMDSC/ADSC) (Mettler Toledo DSC-1 STAR^{e} System, Schwerzenback, ZH, Switzerland) was employed for thermal analysis. This was undertaken on the BTDS lyophilized matrix to determine thermal analysis with regards to chemical reaction transitions, glass transition temperatures (T_g), phase change and melting points of the BTDS samples as well as maximal thermal strain until degradation occurs. DSC measurements were taken at a heating rate of 10°C/min from -10-300°C under nitrogenatmosphere. Weighed samples were placed in a covered aluminium sample holder with a central pin hold.

6.2.6. Analysis of Physicomechanical Properties by Textural Profiling

To determine the tensile strength and force required to cause a defect or break in the system, textural analysis was employed to the BTDS lyophilized matrix. This was done by the use of a texture analyser (*TA.XT. plus Texture Analyzer*, Stable Microsystems®, Surrey, UK) fitted with a 50kg load-cell to determine physicomechanical properties of the system and in particular tensile strength from the generated force-distance profiles computed from the peak tensile force required and using Equation 6.1 given below. The parameters marked for textural analysis are presented in Table 6.3. Tensile strength was measured using the Young's Modulus equation as follows:

$$E = \frac{Tensile\ \ stress}{Tensile\ \ strain} = \frac{\delta}{\varepsilon} = \frac{FL_o}{A_o \Delta L} \qquad \text{[Equation 6.1]}$$

Where: E is the Young's modulus (modulus of elasticity); F is the force applied to the object; A_0 is the original cross-sectional area (πr^2) through which the force is applied; ΔL is the amount by which the length of the object changes; L_0 is the original length of the object.

Table 6.3: Parameters employed for Texture Analysis

Parameters	Settings
Test mode	Tension
Pre-Test speed	0.50mm/sec
Test speed	0.50mm/sec
Post test speed	5.0mm/sec
Trigger type	Auto
Trigger force	5kg
Contact time	5sec

6.2.7. Determination of Young's Modulus by Nano Tensile Analysis

A Nano Tensile Analyser (nanoTensile®5000 Hysitron Inc. Nanomechanical Test Instrument, Minneapolis, MN) was employed to determine Tensile Strength and Young's Modulus. This was employed on nanofibrous mats to determine the nanomechanical properties of the nanofibres to ensure optimal mechanical properties of the nanofibrous mats. In advancement it was then utilised to measure the durability of the BTDS system on a whole at a nano sensitive level. Samples were measured using a digital calliper, pretesting and mounted until a breaking force was established at a velocity of 5μms^{-1}. Stress-Strain curves were then procured to further determine the ultimate strength, strain and toughness of the BTDS system.

6.2.8. Determination of Water Content and Erosion by Analysis using a Kaarl Fisher Volumetric Tritrator

Hydrogel samples of the lyophilized system was analysed using Kaarl Fisher (Mettler Toledo V30 Volumetric KF Tritrator, Mettler Toledo Instruments Inc., Greifensee, Switzerland) whereby water content and swelling ability were evaluated. This was undertaken to evaluate the degree of hydration of crosslinked hydrogel BTDS samples for further correlation to be made with regards to *in vitro and in vivo* biocompatibility studies. The study allows for analysis of the wettability of the system.

The Equilibrium swelling ratio was then calculated employing the following equation:

$$ESR = \frac{(W1 - W0)}{W0} \qquad \text{[Equation 6.2]}$$

Where W_1 is the weight of samples after immersion and W_0 is the weight of samples in the dried state.

6.2.9. Identification of Surface Topographical Structure and Morphology Employing Scanning Electron Microscopy

The surface topographical structure and morphology of design samples were evaluated using a scanning electron microscopy (SEM) (Phenom™, FEI Company, and Hillsboro, Oregon, USA) whereby bulk characteristics such as pore size, texture, roughness and brittleness amongst others were identified in order to evaluate the structural morphology of the system and to analyse the most suitable configuration for suspension of the nanofibres mats within the lyophilized matrix.

6.2.10. Measurement of the Transient Rheological Characteristics of the Bioresponsive transdermal delivery system

A Haake Modular advanced Rheometer system (MARS) (ThermoFisher Scientiofic, Karlsruhe, Germany) was used to evaluate rheological properties of polymer hydrogels used to fabricate the lyophilized matrix in order to ensure an optimal end product with the most advantageous flexibily toughness and strength. Samples were placed on a sample stage whereby a c35/1° titanium rotor was immersed in the polymer solution blends at a constant temperature of 24°C, shear rate of $100s^{-1}$ and a time interval of 360s. Stress-Strain rheological parameters were then obtained for quantified samples and an evaluation was made with regards to viscosity and yield stress. These parameters play a vital role in shaping a lyophilized matrix that is able to suspend nanofibrous material.

6.2.11. Evaluation of the Stimuli Responsiveness of the Bioresponsive transdermal delivery system to an Inflammatory Stimulus through *In Vitro* Release Studies

To ascertain inflammatory dependent behaviour of the BTDS, an inflammatory favourable environment was created. This was undertaken by formulating Fenton's reagent that has the ability to mimick the constituents of a natural inflammatory response. *In vitro* degradation of the crosslinked BTDS was analysed by employing the Fenton's reaction. Fenton's reagent was used as a stimulus resulting in the release of hydroxyl radicals as stipulated below in equation 6.3. Degradation of the BTDS matrix leading to the release of nanofibrous mats was then evaluated on exposure to the liberated radicals (Yui et al., 1992).

$$Fe^{2+} + H_2O_2 \rightarrow Fe^{3+} + OH\cdot + OH^- \qquad \text{[Equation 6.3]}$$

The BTDS was immersed in phosphate-buffered saline (PBS) set at physiological pH (7.4), and in an appropriate *in vitro* stimulus (Fenton's reagent) at a pH of 5.5 to correlate with the pH of inflammation. Samples were placed in dialysis tubing with a molecular weight of 12 000 in a closed vial and placed in an oscillating laboratory incubator (Labcon® FSIE-SPO 8-35,

California, USA), set to 25 rpm (du Toit et al., 2008). At predetermined periods samples were removed and subjected to analysis for bioactive release using a nanophotometer (Implen nanophotometer GmbH, Munich,) at a wavelength of 425nm to determine maximum absorption

6.3. Results and Discussion

Within the field of controlled drug delivery or bioactive delivery, a significant field of interest is stimuli-responsive polymeric drug delivery systems. They function by allowing a controlled amount of drug/bioactive to be released as according to the physiological need of the significant disease state. They have the capacity to undergo swift modifications in their microstructure as well as in their macrostructure on activation of changes in the environment making the system more adaptable to the therapeutic requirements of the disease state in question (Bawa et al., 2009). The selection and employment of hyaluronic acid (HA) a natural biopolymer plays a significant role in inflammatory responsive systems as it plays a significant role in *in vivo* physiological functions that include angiogenesis, differentiation, controlled permeation and significantly scavenging of hydroxyl radicals which plays an important role in its responsiveness to inflammation (Yui et al., 1992). The present investigation provides an insight to the prototype BTDS device and its function to inflammatory responses.

6.3.1. Determination of the Chemical Stability and Transitions of the Lyophilized Component

HA has been portrayed to possess many advantageous properties for the utilization in tissue engineering applications which include soft tissue augmentation and adhesion formation (Kwang et al., 2007). In order to investigate the chemical composites of the structure as well as the reactions involving crosslinked bond formation and back bone structure FTIR spectra were obtained as indicated in Figure 6.3. Figure 6.3a reveals the spectra of uncrosslinked HA which demonstrates four main peaks at a specified wavelength. A broad peak was seen at 3257.06cm^{-1} (as demarcated) indicating C-H stretching due to the presence of an aromatic compound with possible weak to moderate bonds. The peak also indicated hydrogen bonding and an O-H stretch. The formation of a hydrogel with HA crosslinked to ADH and alginate showed a broad more defined peak with a shift in the spectra to a greater wavelength. This can be directly attributed to the introduction of a crosslinking agent which resulted in a break in the aromatic structure of hyaluronic acid as indicated in Figure 6.2, whereby hydrogen bonding and the hydroxyl groups of the aromatic ring is replaced with aliphatic molecular fragments. F8 revealed a peak of 3292.76cm^{-1} whereas F2 and F14 revealed a peak at 3254.55cm^{-1} and 3246.58cm^{-1} respectively. This analysis revealed that as the degree of crosslinking was increased, the wavelength was shifted to the left. A shift in the

wavelength suggests an increase in conjugation and bond intensity. An intermediate quantity of crosslinker and polymer was used in F8 thus the rate of crosslinked bond formation was shown to be the highest. As polymeric concentrations were further increased whilst maintaining the ADH concentration, bond intensity and conjugation decreased as shown by the wavelength in the FTIR spectra of Figure 6.3f. The addition of a bi-functional crosslinker ADH revealed the appearance of a peak to the spectra at 2049.76cm^{-1} which is attributed to the introduction of amine groups from ADH that interacts with the aldehyde groups of HA. The double bonded nitrogen groups, such as the amino groups tend to exhibit absorption bands close to the carbonyl (C=O) and alkene (C=C) double bond stretching region as can be seen in Figure 6.2. Furthermore, a breakage in the aromatic ring and crosslinkage by ADH resulted in the formation of conjugated ketones at 1634.54cm^{-1} in the formulations depicted in the figure which is not a characteristic peak of HA. The peak was also seen at 1634.26cm^{-1} in F5 and 1635.04cm^{-1} in F10. Distinct peak formations at 1605.68cm^{-1} and 1021.08cm^{-1} in HA (illustrated in the figure) was seen to disappear due to aromatic ring breakage and ADH backbone formation in the crosslinked formations. In addition disappearance of the peak at 1021.08cm^{-1} is attributed to the consumption of the aldehyde groups found in HA to form an imine bond between HA and ADH. Incorporation of alginate to the modified HA lead to the formation of intra- and intermolecular chains by ionic bonding with divalent cations. Alginate could be linked to ADH and HA by covalent linkages between carboxylic acid groups in alginate chains and the amine groups of ADH (Liu et al., 2013).

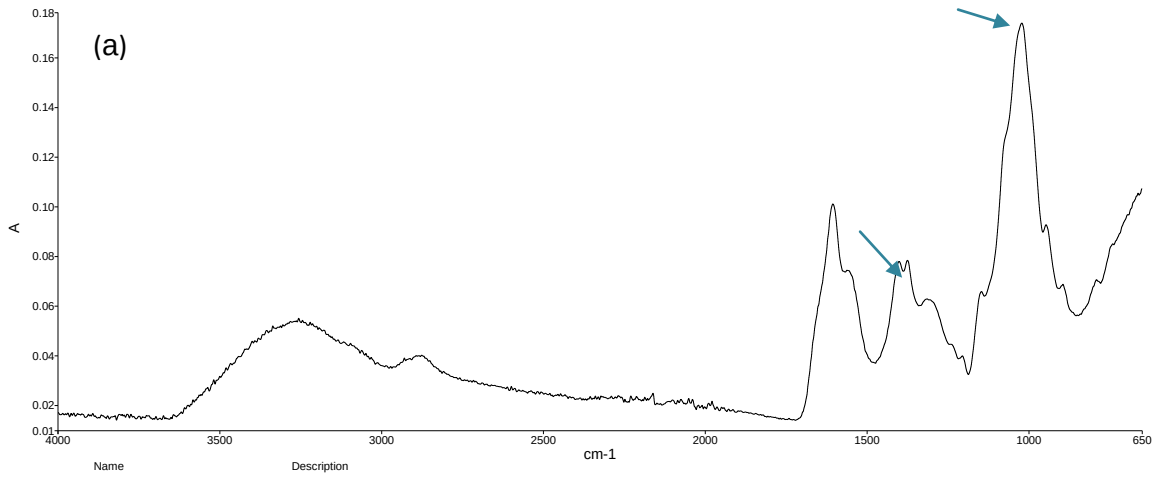

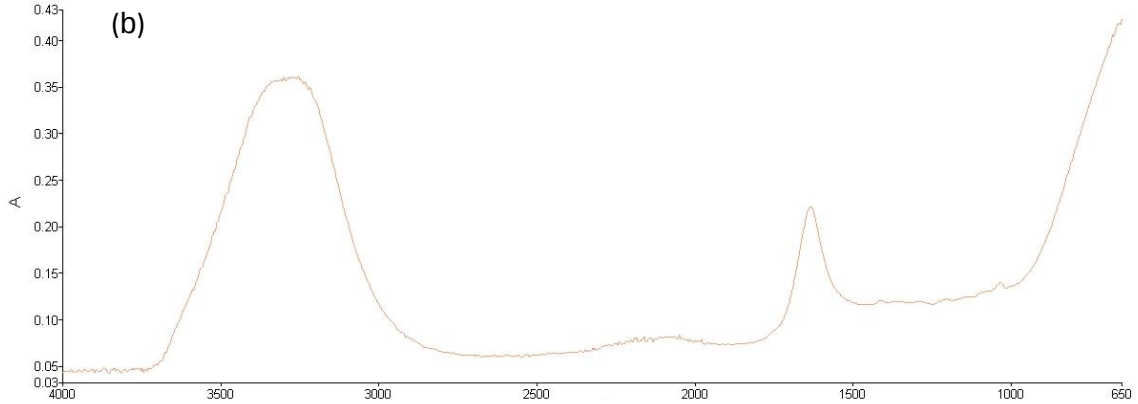
(b)
A
0.43
0.40
0.35
0.30
0.25
0.20
0.15
0.10
0.05
0.03
4000
3500
3000
2500
2000
1500
1000
650

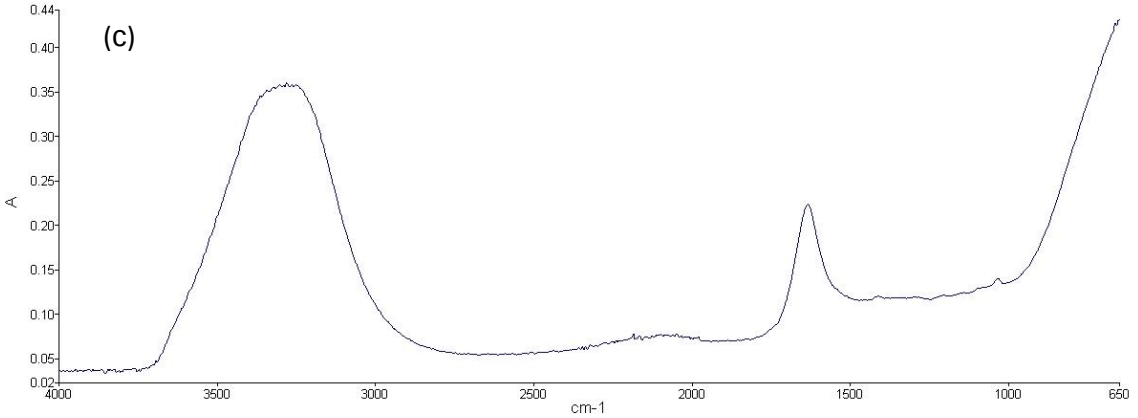
(c)
A
0.44
0.40
0.35
0.30
0.25
0.20
0.15
0.10
0.05
0.02
4000
3500
3000
2500
2000
1500
1000
650
cm-1

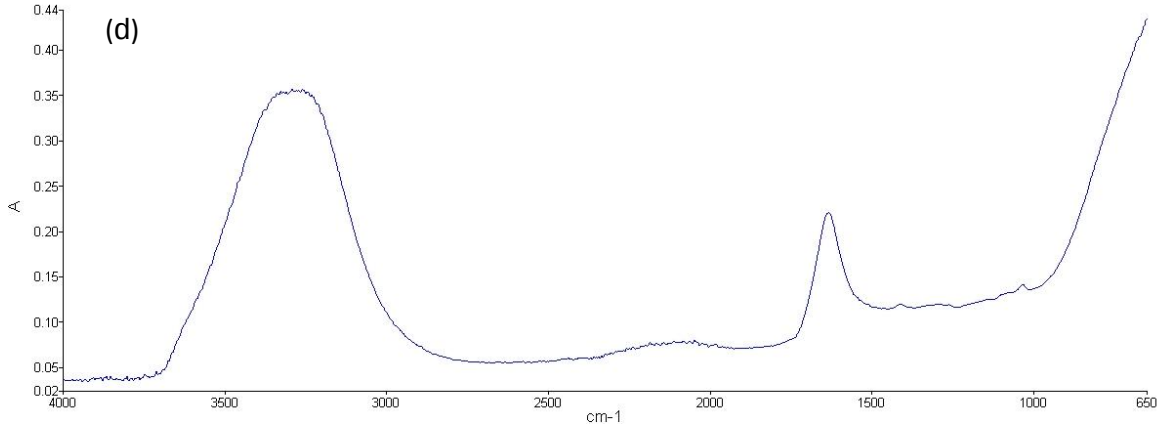
(d)
A
0.44
0.40
0.35
0.30
0.25
0.20
0.15
0.10
0.05
0.02
4000
3500
3000
2500
2000
1500
1000
650
cm-1

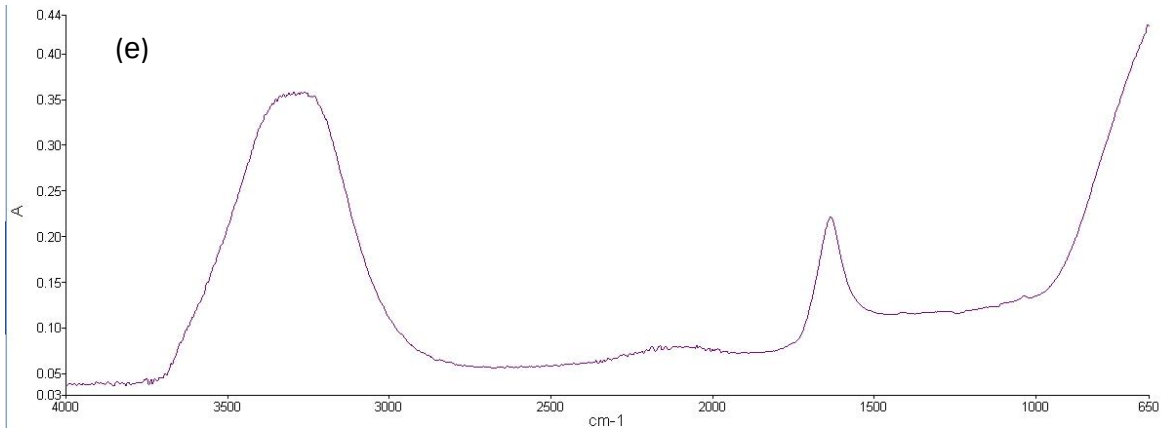
(e)
A
0.44
0.40
0.35
0.30
0.25
0.20
0.15
0.10
0.05
0.03
4000
3500
3000
2500
2000
1500
1000
650
cm-1

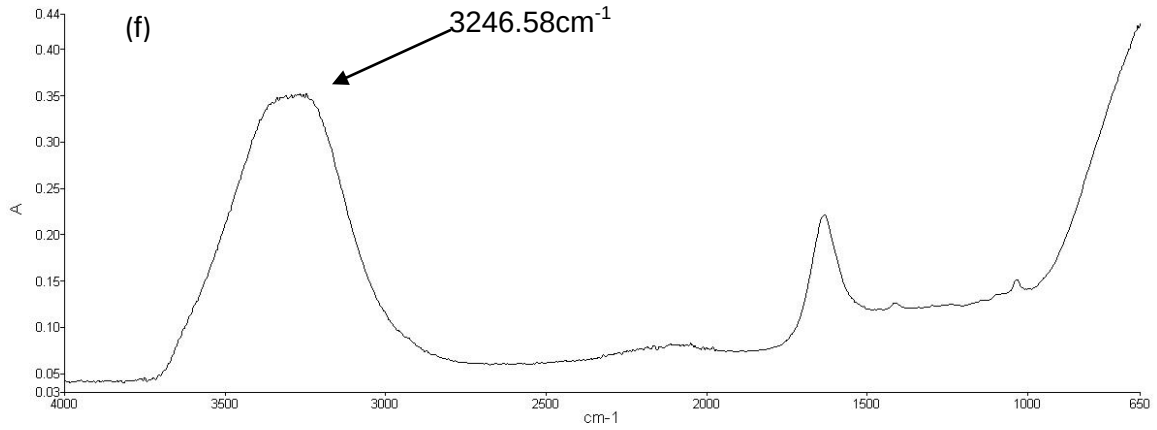

Figure 6.3: Chemical vibrational transitions of (a): Hyaluronic Acid, (b): F2, (c): F5, (d): F8, (e): F10, (f): F14

6.3.2. Identification of the Thermodynamic Properties of the Bioresponsive Transdermal Delivery System

The thermal behaviour of the various lyophilized formulations was investigated to determine the degree of thermal degradation by differential scanning calorimetry (DSC). The DSC thermograms of the various formulation composites are shown in Figure 6.4. Upon analysis it was noted that all formulations exhibited an endothermic and exothermic peak. Endothermic peaks were surveyed at temperatures ranging from 77°C to 120°C. The presence of an endothermic peak reveals a phase transition to melting and the presence of polymorphism. Furthermore it was noted that the endothermic peak present was superimposed upon the glass transition (as demarcated in the figure) due to gradual enthalpy changes. F2 depicts a broad endothermic peak at a temperature range of 113°C representing the temperature of melting T_m whereas F5 depicts an endothermic peak at a T_m of 102.70°C. A very low melting temperature is seen in F7 at a T_m of 77.94°C. This observation deduces that the energy of heat required for phase transition and decomposition is directly attributed to the degree of crosslinking. Su and co-workers (2010) reported that crosslinking density is greatly influenced by the concentration of adipic-acid dihydrazide (ADH/crosslinker) which further affects the degradation of the system. Hydralyzation and degradation tends to be slower when higher concentrations of ADH is used in comparison to lower concentrations as further depicted in Section 6.3.1. From the T_m temperatures obtained it was depicted that when low ADH concentrations are used such as in F7, a $\%^w/_v$ concentration of 0.13% is used, energy for transition required is minimal in comparison to a greater concentration such as $0.16\%^w/_v$ ADH in F2, energy required for enthalpy transitions is greater. Thermodynamic kinetics was seen at elevated temperatures whereby the thermal profiles exhibit the presence of a sharp exothermic peak. Exothermic peaks were seen ranging between temperatures (T_C) of 210°C and 255°C. The sharp exothermic peaks represent a phase transition whereby an altered polymer microstructure occurs associated to the configuration of a polymeric crystalline structure. F15 exhibited the highest T_C of 250.23°C in comparison to F13 depicting a T_C of

214.82°C. The crystalline temperature (T_C) is a measure of the exothermic transition that occurs upon cooling from liquid to a crystalline state and is a measure of both time and temperature. Analysis of the T_C revealed that increasing ADH concentration had a direct effect on the rate of phase transition and cleavage of bonds to render a crystalline state. A greater degree of molecular bonding and the formation of a crosslinked backbone requires greater enthalpy energy to exhibit the transition to a crystalline state as F15 encloses an ADH concentration of 0.16%$^{w}/_{v}$ in comparison to F13 depicting a concentration of 0.1%$^{w}/_{v}$. Intermediate amounts disclose a T_C of 225.55°C and 244.38°C in F5 and F7 respectively. This was attributed to the intermediate crosslinker volume of 0.13%$^{w}/_{v}$ and an intermediate polymeric concentration of 0.5%$^{w}/_{v}$. Furthermore Luo and co-workers (2000) report that uncrosslinked hydrogels of hyaluronic acid exhibits a sharp exothermic peak with a relatively small T_C indicating that the gel exist primarily in an amorphous rather than a crystalline state. This observation indicates that bondage and the formation of an HA-ADH structure provides greater stability (Liu et al., 2007) and bondage of the two polymers clearly produces a novel material with properties that are distinguished from both the original components utilised (Luo et al., 2000).

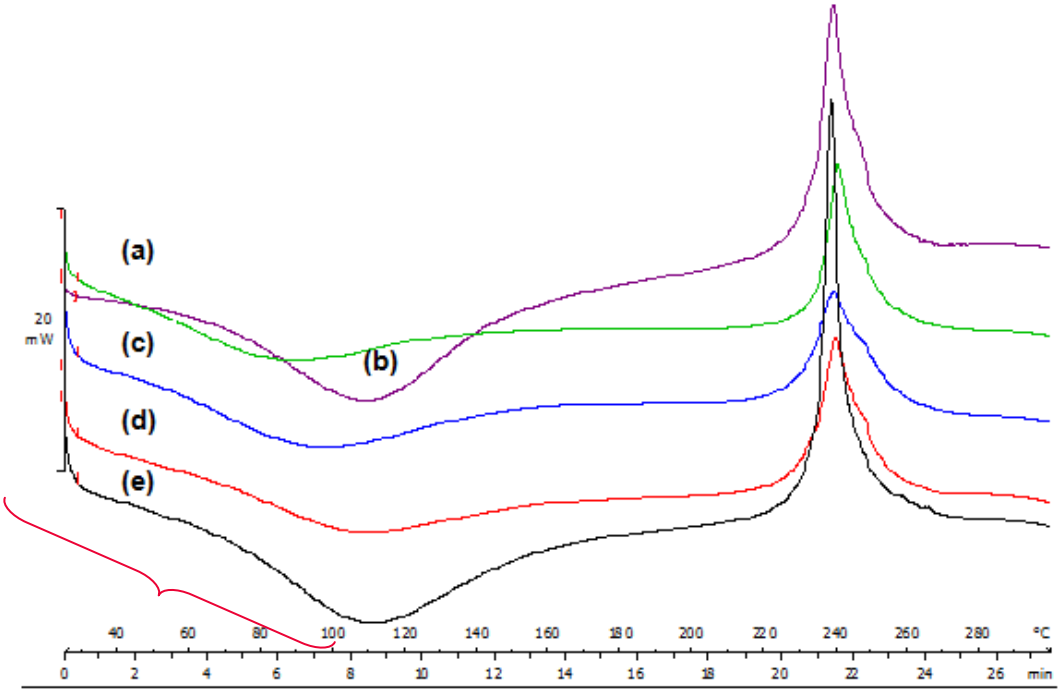

Figure 6.4: DSC analysis illustrating the thermal behaviours of the various formulations: (a): F7, (b): F5, (c): F15, (d): F13, (e): F2

6.3.3. Determination of Tensile Strength and Young's Modulus by Textural Profiles

Dynamic mechanical analysis of wound dressings and devices are of utmost importance for biomedical applications. Young's Modulus can be described as a 1 dimensional tensile test in which the Young's modulus is the ratio of the normal stress (θ) to the normal strain (ε)

(Govindjee and Sackman, 1999). Figure 6.5 depicts the stress-strain curve of the lyophilized matrix whereby the fracture point and Young's modulus can be detected. From the data obtained it was seen that a very high yield stress and Young's modulus was presented by F13 and this can be attributed to the greater crosslinkage degree between HA and ADH. Interactions between HA and ADH resulted in the formation of a network structure that provided a polymeric backbone to the configuration as seen in the topographical images and described by the FTIR spectra, thus increasing its rigidity. However, as seen in Figure 6.5c the ultimate strength of F13 was considerably lower at 0.01θ μ (MPa). For topical applications such as wound dressings, a significant requirement is a device that entails physical characteristics such as toughness yet flexibility as described in greater detail in Chapter 4. F13 enclosed a Young's modulus of 2.14 E (MPa) thus disclosing a high Young's modulus which is not ideally suitable for wound dressings. A very high Young's modulus would provide a dressing structure that is tough, rigid and prone to brittleness. Thus, the ideal dressing should be of a lower Young's modulus providing greater elasticity and flexibility to the system. A greater ultimate strength was seen when a lower Young's modulus is produced such as that of F9 and F14 whereby an ultimate strength of 0.03 θμ (MPa) is depicted when a Young's modulus of 0.38 and 0.53 E (MPa) is noted. It was deduced that the mechanical properties of the structure is attributed to the concentration of HA. When the concentration of HA was increased to $0.07\%^{w}/_{v}$ such as in F9 and F14, so too did the ultimate strength of the system. Furthermore it was also noted that the viscosity of the hydrogel solutions increased with an increase in the HA concentrations as will be discussed in more detail in the section to follow herein the chapter. F3 and F7 depicts a very low tensile strength and Young's modulus at 0.07E (MPa) and 0.05E (MPa) respectively thus no ultimate strength was noted and very low ultimate strains are deduced. It was noted that in these formulations obtained from the Box-Behnken design, lower concentrations of HA is used at $0.05\%^{w}/_{v}$ and $0.03\%^{w}/_{v}$ respectively. Mechanical properties such as the tensile strength, elastic modulus and viscosity are important attributes when considering the bioactive release rates on response to a stimulus, as the rate of degradation and erosion are dependent upon the breakdown of the system.

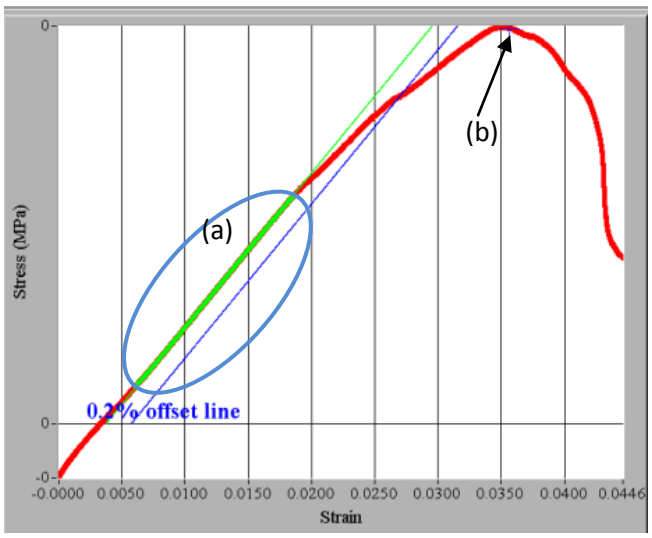

Figure 6.5: Stress-Strain relationship profile of the lyophilized matrix where (a) is the linear portion of the slope from which Young's Modulus can be derived and b resembles the fracture point of the sample

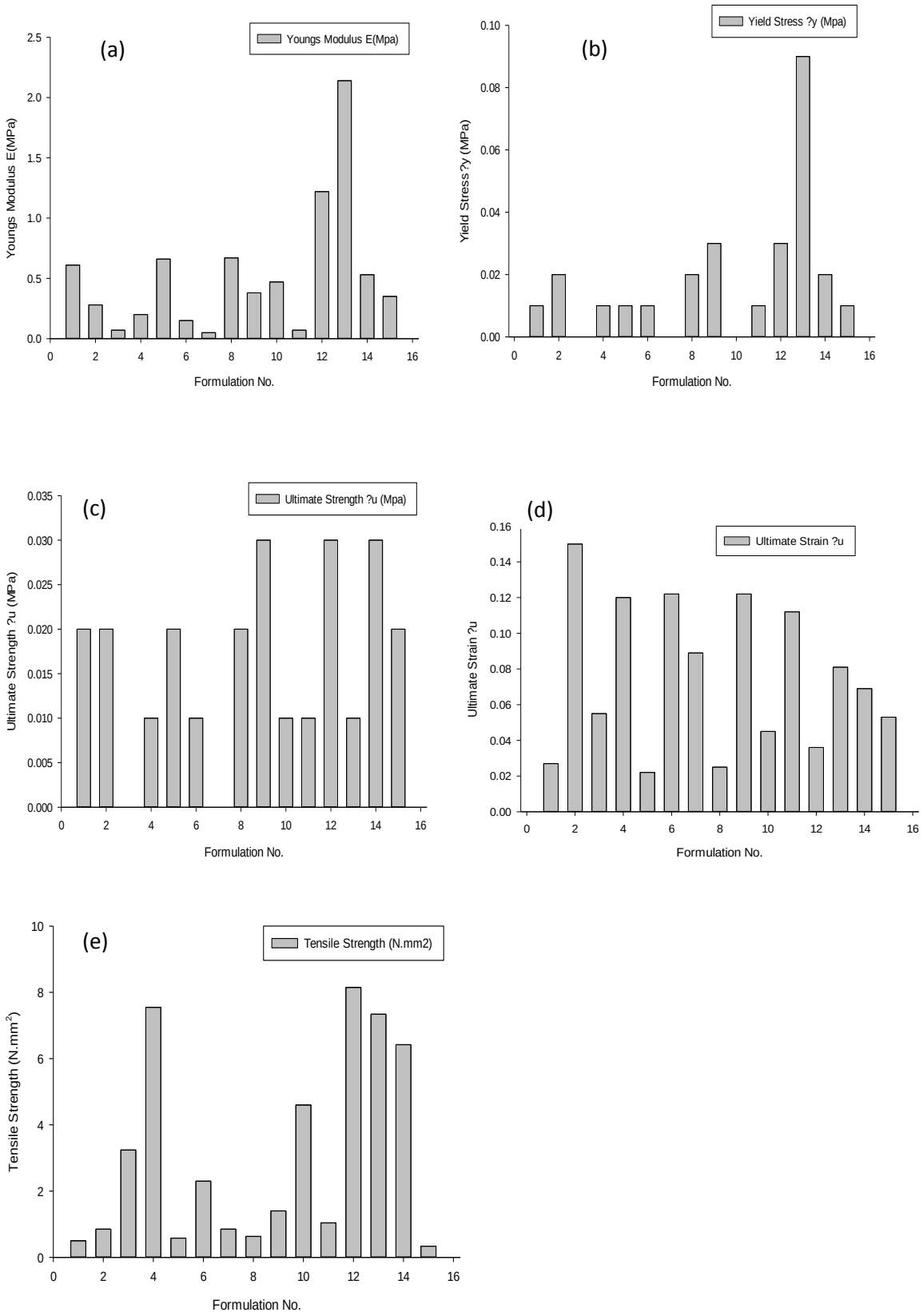

Figure 6.6: Vertical bar charts outlining the variations in mechanical properties amongst the various formulations where (a): Young's modulus (*E*; MPa); (b): yield stress (*σy*; MPa); (c): ultimate strength (*σu*; MPa); (d): ultimate strain (*εu*) and (e): Tensile Strength (N.mm^2)

6.3.4. Water Content Determination of the Bioresponsive Transdermal Delivery System

The swelling behaviour, kinetics, water content and erosion is linked to the polymeric hydrophilicity and nature, crosslinkage forces, as well as the diffusion process. From the results obtained as is depicted it was seen that F13 had the lowest water content and thus can be directly attributed to the low crosslinker and polymeric concentration. As the concentration of adipic acid dihydrazide (ADH) was increased to 0.13% in F4 and 0.16% such as those in F2, F3 and F6 the water content percentage decreased making the lyophilized matrix less viable to swelling and erosion. These phenomena can be attributed to the degree of crosslinking which results in the formation of stiffer and dense three dimensional structures as elaborated in the FTIR spectra which prohibit or minimise the diffusion and transport of water molecules. Furthermore it was noted that slightly lower water content was generated when the polymeric concentrations were decreased thus making the device more susceptible to the diffusion of water molecules due to minimal intermolecular bonding and greater free space availability due to the less dense structure of the molecules. Increasing the polymeric concentration influenced the total monomer concentration of the device which directly impacted on the swelling capacity and gel content of the system. Pourjavadi and co-workers (2007) state that sodium alginate is widely used in commercial products due to its biodegradable, renewable and natural nature; furthermore it has a high gelatinization capacity. Thus increasing the monomer concentration of alginate led to an increase in gel content and water absorbency. In addition, increasing the polymeric concentrations provides a gel formation of greater viscosity and a denser matrix which results in a more augmented chance of chain transfer to monomer molecules as well as the hindering of free radical movement and monomer molecules (Pourjavadi et al., 2007). The low water content values obtained were attributed to the lyophilization process undertaken, thus leaving more free space for exudates uptake upon application to a wound site. The degree of crosslinking also greatly impacts upon the swelling capacity of the system. As discussed at elevated crosslinker concentrations, the system would be less viable to water uptake thus the ideal system would have an intermediate amount of crosslinker thereby augmenting the system mechanical characteristics and ensuring absorption of exudates.

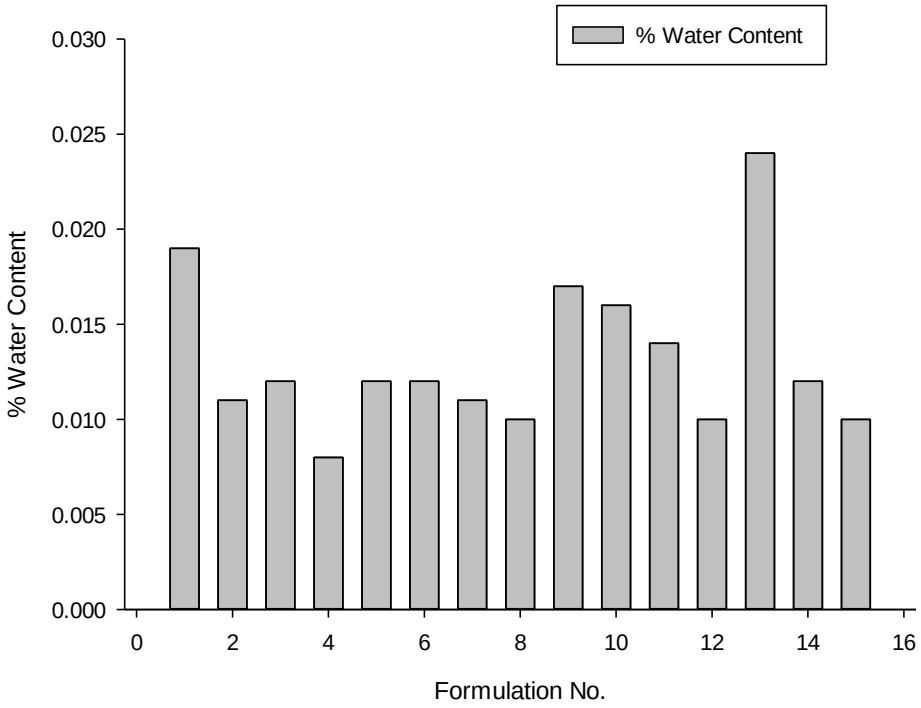

Figure 6.7: Percentage water content analysis of formulation 1-15

6.3.5. Identification of Surface Topographical Structure and Morphology employing Scanning Electron Microscopy

Scanning electron microscopic images were obtained in order to determine the morphologies and microstructure of the lyophilized matrix at different sample angles. Figure 6.8 reveals the various topographic morphologies of the various formulations. Samples were prepared by freeze drying to remove access water particles after been frozen at -80°C. According to Zhang and co-workers (2011), the process of freeze drying also greatly influences the morphology of the microscopic images obtained due to the formation of ice nuclei, thus in order to preserve better morphology, hydrogel samples were first frozen at -80°C. From the morphologies obtained, Figure 6.8 revealed the topographical structures on different scales. Crosslinking of HA to ADH resulted in the formation of porous sites where interconnecting pores can conspicuously be observed as illustrated in Figure 6.8 a, b and e. In addition, Figure 6.8c and f demonstrated a greater domain of fibrillogenesis with the presence of a slight fibril structure as demarcated. This was attributed to interactions occurring between water molecules and hydrophobic groups in the structure. From the figures illustrated it was noted that the pore size decreased significantly with an increase in ADH. Introduction of ADH causes the addition of an amino group as discussed in detail in Section 6.3.1 which leads to the formation of a polymeric backbone in the structure improving the mechanical properties by the introduction of molecular bonding. Figure 6.8c clearly demarcates the impact of crosslinking on the surface structure. The various reactions and interactions results in a surface morphology of a more coarse character which was attributed to the formation of

clusters of molecular entanglements and ionically associated domains, a characteristic trait by the presence of alginate. Figure 6.8e revealed a highly porous structure with pores ranging in the domain of approximately 2.5μm with absence of a backbone structure. The figure represents F9 whereby a very low ADH concentration is used with a high HA polymeric concentration. Significantly low crosslinker concentration leads to minimal intermolecular bondage formation thus a greater porous site in contrast to F15 or F2 represented by Figure 6.8a and c respectively. A higher concentration of ADH was employed (0.16%$^{w}/_{v}$) thus the structure is more rigid with a perceived backbone structure as can be seen. The surface topography also portrayed minimal pores with a pore size ranging at 0.5μm to 1.5μm. At very low concentrations of ADH and a higher concentration of alginate, the surface matrix also appeared to be more brittle with irregular pore sites as seen in Figure 6.8g representing F12 illustrated in the figure whereby 0.1%$^{w}/_{v}$ of ADH is used and 4.5%$^{w}/_{v}$ alginate is employed. Lyophilization and freeze drying lead to the formation of layers in the matrix as clearly demarcated in Figure 6.8d, and with the presence of interconnecting pores, making it suitable and beneficial for cell survival in a 3D environment, advantageous for waste and nutrient transport (Su et al., 2010). The surface topography of the various lyophilized samples provided a representation of the degradation of the HA-ADH models and the approximate behaviour in terms of degradation and bio erodible behaviour *in-vivo* and on exposure to an inflammatory stimulus.

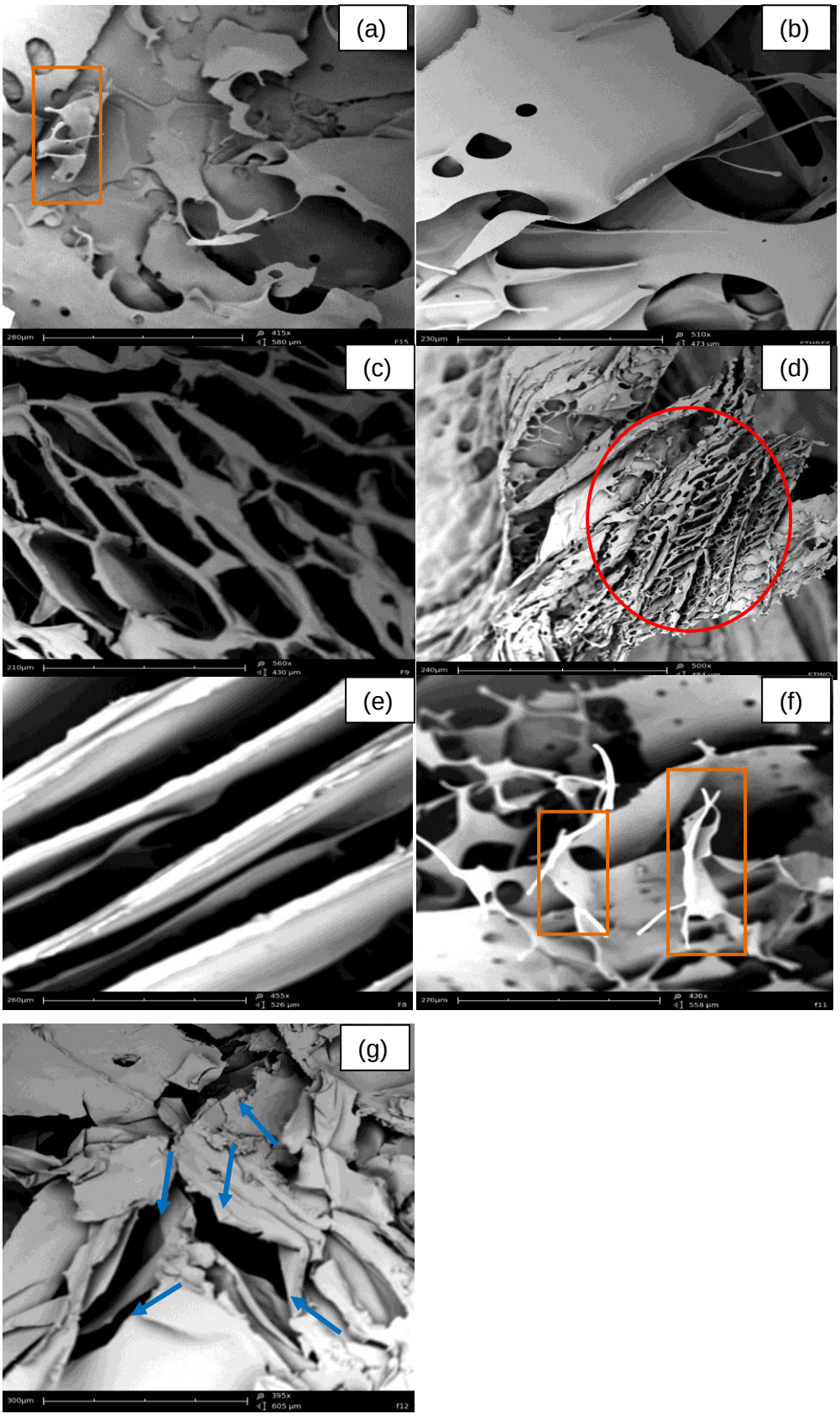

Figure 6.8: Topographical imagery by scanning electron microscopy of (a): F15, (b): F3, (c): F2, (d): F8, (e): F9, (f): F11, (g): F12

6.3.6. Measurement of Transient Rheological Characteristics of the Bioresponsive transdermal delivery system

To determine the flow behaviour and mechanical characteristics of the various crosslinked hydrogel formulations, rheological analysis was carried out in accordance with the procedure as described above in this chapter. Furthermore, this analysis was carried out as a complementary technique in order to assess the crosslinking characteristics of the crosslinked HA hydrogel. Table 6.4 provides the viscosity measurements obtained from the various formulations attained by means of the Box-Behnken design. Viscosity provides a measurement of the flow characteristics of the hydrogel when an applied stress is applied. The formation of molecular entanglements and ionically associated domains as seen in the topographical imagery greatly influences the visco behaviour of the hydrogel upon a shear stress. Figure 6.9 provides an illustration of the characteristics pertaining to viscosity, flow and deformation properties of the hydrogel matter. From the figure it was seen that dilatant flow is exhibited initially due to the high concentrations of small deflocculated particles. Under zero shear conditions, the hydrogel behaves in a manner whereby particles are closely packed and interparticulate voids are minimum. Consequently as the shear rate is increased over a longer period of time, the slope of the curve gradually decreases as depicted in Figure 6.9 and the HA hydrogel begins to exhibit Newtonian behaviour whereby thixotrophy is observed. Increase in shear rate resulted in a decrease in the apparent viscosity due to energy exhibited disrupting the bonds (Schnaare et al., 2005) thus dilatant flow is observed at low to moderate shear rates and pseudoplastic flow at higher shear rates (Schnaare et al., 2005). Furthermore, Table 6.4 illustrates the impact of varying polymeric concentration and crosslinker on the rate of viscosity. From the table it was seen that the viscosity is directly attributed to the polymeric concentrations and crosslinker, thus the degree of crosslinking. It was further seen that at low HA concentrations the viscosity was minimal. F13 revealed a viscosity of 212.319MPa when HA revealed a low concentration of 0.3%$^{w}/_{v}$ and a low ADH concentration of 0.1%$^{w}/_{v}$. As the concentration of HA increased to 0.7%$^{w}/_{v}$ such as that in F9, a viscosity of 1888.028MPa is seen. In addition, this pattern was observed with all the formulations, as the degree of crosslinking was increased due to higher concentrations the viscosity values depicted were greater. Lower values were seen at lower concentrations. The yield stress can be defined as the resistance of a material to flow, i.e.: the minimal amount of shear stress required to initiate a flow. From the results obtained in Table 6.4 it was seen that the yield stress was directly proportional and dependent upon the viscosity. As the viscosity increased so too did the yield stress. Furthermore, it was detected that the “apparent” yield stress is designated as a single point and the critical stress range is very small. The yield stress of the hydrogels could also be directly related to the Newtonian flow properties of the gels. As the shear stress applied increased so too did the yield stress as the 3D structure

incorporating inter and intramolecular forces break down as a consequence of the energy induced.

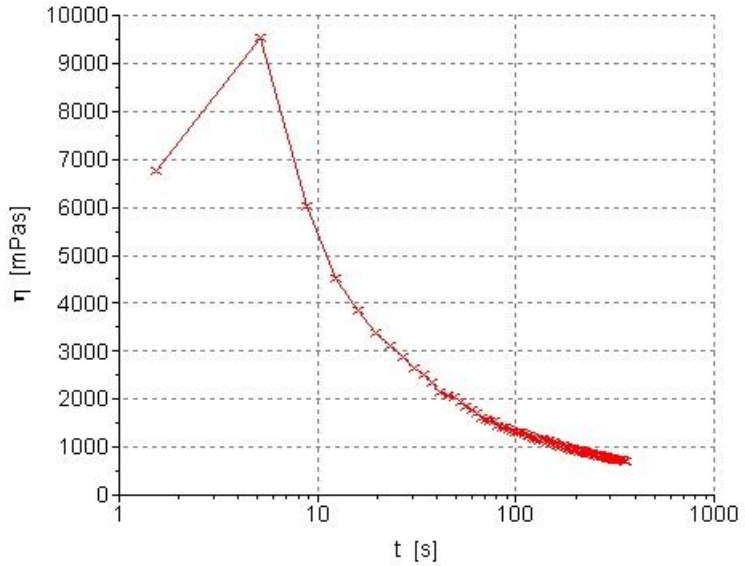

Figure 6.9: Depiction of flow behaviour of a crosslinked HA hydrogel upon an applied shear stress over time

Table 6.4: Viscosity and Yield Stress values of the various formulations

Formulation	Viscosity (MPa)	Yield Stress (Pa)
1	1308.091	38.57
2	1819.196	38.54
3	1294.021	38.61
4	864.686	38.58
5	1270.786	38.57
6	963.528	38.43
7	850.622	22.73
8	1265.171	38.57
9	1888.028	38.6
10	1105.243	29.58
11	1532.955	32.21
12	1192.109	38.56
13	212.319	32.21
14	953.712	38.59
15	1151.313	29.61

6.3.7. Evaluation of the Stimuli Responsiveness of the Bioresponsive Topical Delivery System to an Inflammatory Stimulus through *In Vitro* Release Studies

On exposure to pathological conditions (i.e.: hydroxyl radicals created by Fenton's Reagent), bioactive release profiles were generated for the experimentally derived formulations whereby the bioresponsive potential was evaluated. Figure 6.10 reveals the bioactive release profiles of the various experimentally derived formulations on exposure to the inflammatory stimulus. A general pattern was seen whereby the degree of release was dependent upon the concentration of HA and thus the degree of crosslinking. This analysis correlates to the

results obtained by the mechanical strength evaluation as well as the rheological examination whereby similar traits are seen. Both viscosity and physicomechanical characteristics increased with HA concentration. As can be seen by the drug release profiles, a greater release is seen at lower concentrations, thus increasing polymeric HA concentrations lead to prolonged bioactive release. The bioactive release mechanism under the influence of a stimulus operates by the degradation of HA under the influence of hydroxyl radicals. Stimuli dependent degradation occurs upon the rapid autooxidation of Fe^{2+} to Fe^{3+}. A release of hydroxyl radicals caused a reaction to occur with HA whereby glycosidic cleavage occurs. This involves the abstraction of hydrogen on the carbon adjoining the carboxyl group in the *D*-glucoronic acid unit. Thus, the degree of degradation of HA depends upon the generation of hydroxyl radicals in the presence of oxidising agent's therefore promoting pulse or responsive release of the bioactive by degradation and erosion (Yui et al., 1993). From the profiles obtained, further analysis as depicted in Figure 6.10a revealed that a greater release profile is seen with F3 then F1 and F2 with the greatest cumulative release rate been at 4 hours at 0.15mg in F3 and 0.062mg and 0.0295mg in F1 and F2 respectively. This was attributed to the lower concentration of HA present in F3 leading to a lower crosslinking degree, thus interactions leading to degradation by hydroxyl radicals are of a greater extent. Furthermore, it can be deduced that the release profile of F3 been greater then F1 is greatly influenced by the presence and polymeric concentration of alginate. As discussed in Section 6.3.4 alginate has a high gelatinization capacity thus a great tendency to absorb fluid and cause swelling and erosion of the polymer matrix thus leading to a greater bioactive release profile as in F3 where a polymeric concentration of 4.5%$^{w}/_{v}$ is utilised in contrast to the 2.75%$^{w}/_{v}$ concentration used in F1. Additionally a greater release profile is also seen in F12 whereby a release rate at 24 hours is seen at 1.95mg in contrast to F10 and F11 depicting release rates at 0.098 and 0.086mg respectively where a greater concentration of alginate (4.5%$^{w}/_{v}$) is used in F12 then F10 (0.1%$^{w}/_{v}$) and F11 (0.13%$^{w}/_{v}$). A similar prototype is distinguished with F14 when a higher concentration of alginate is used.

Table 6.5 lists the various MDT release rates of the experimentally derived formulations. F14 revealed a higher MDT release profile at 42.39 whereas a lower rate is surveyed in F12 and F13 at 33.21 and 35.76 respectively. The use of a lyophilized HA matrix serves as an auto-feedback drug delivery system in response to inflammation. Lui and co-workers (1992) state that rapid *in vitro* degradation of an HA matrix occurs upon the incorporation of $FeSO_4$ to the system, thus causing rapid as conferred above. Hydroxyl radicals produced have a short lifespan thus disappear rapidly therefore the matrix can be tailored to the biological needs based on the unique characteristics of the HA structure. Experimentation and analysis of the various derived formulation revealed that the use of a crosslinker ADH at intermediate amounts (0.13%$^{w}/_{v}$) modified the HA structure in an approach to delay the release of

bioactive and the degradation of the HA matrix on exposure to the hydroxyl radicals. F14 showed a high concentration of HA crosslinked by ADH thus protracting degradation by hydroxyl radicals. As depicted by the FTIR spectra a shift in the wavelength is also seen in F14 to the left thus displaying greater bond intensity and conjugation lowering the rate of degradation. MDT results obtained from Table 6.5 depicted lower values for F12 and F13, thus greater hydroxyl degradation of the matrix resulting in a more rapid bioactive release rate. This can be attributed to a very low ADH concentration of 0.1%$^{w}/_{v}$ been used forming weaker and less covalent bonding thus making the system more prone to degradation. Furthermore low polymeric concentrations of HA were also used at 0.5%$^{w}/_{v}$ for F12 and 0.3%$^{w}/_{v}$ for F13 respectively. The value obtained further illustrates the effect of HA on bioactive release as a greater release is seen in F13 then F12 as well. Thus, it can be deduced that release rates is dependent upon the concentrations of all polymers and crosslinker as well as the rate of degradation by hydroxyl radicals upon exposure.

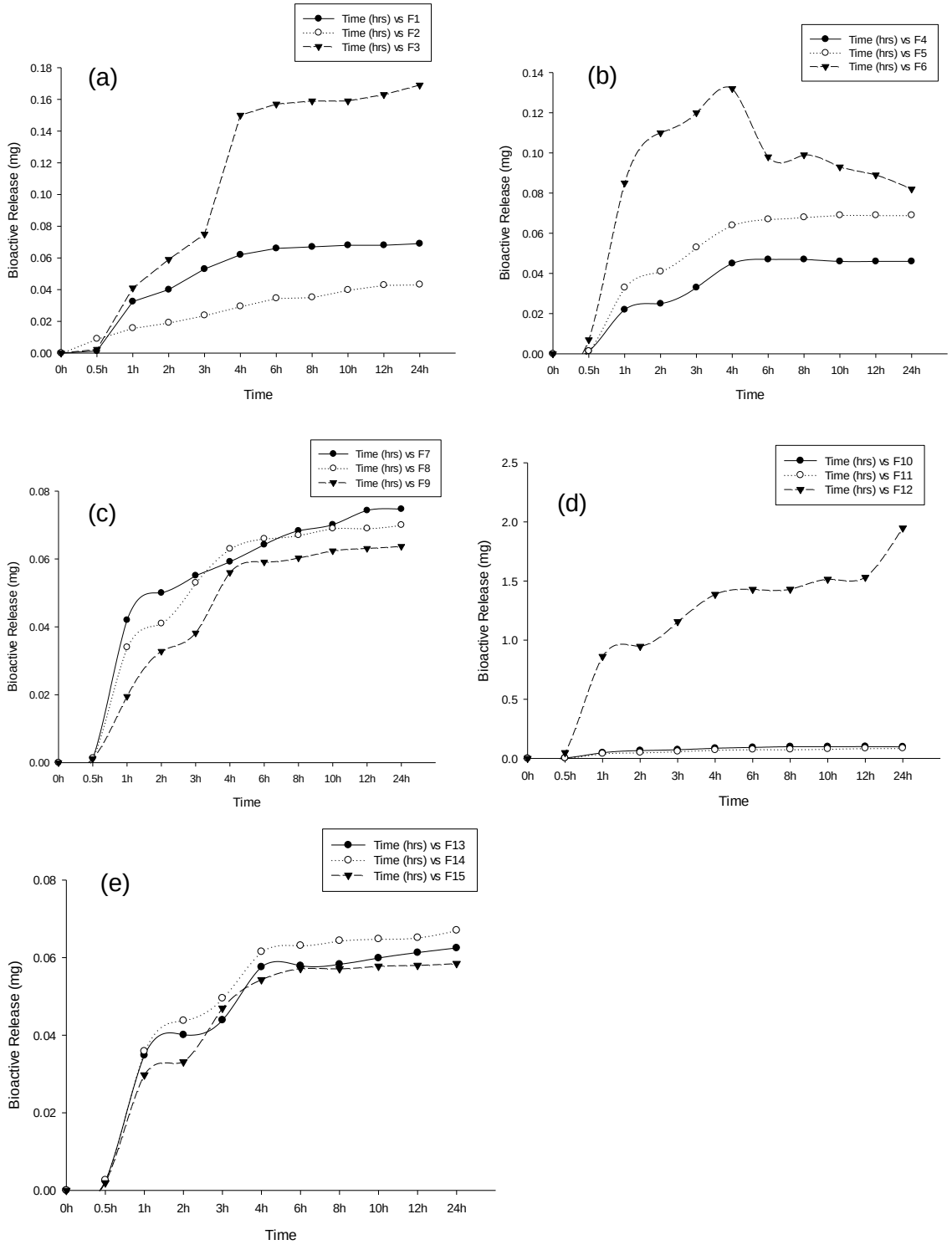

Figure 6.10: Bioactive release profiles based on an inflammatory stimulus of (a): F1-3, (b): F4-6, (c): F7-9, (d): F10-12, (e): F13-15

Table 6.5: MDT bioactive release profiles of formulation 1-15

Formulation	Stimuli Responsive Bioactive Release (MDT)
F1	36.54
F2	34.01
F3	35.91
F4	52.09
F5	36.98
F6	34.43
F7	35.72
F8	36.83
F9	41.67
F10	37.95
F11	37.02
F12	33.21
F13	35.76
F14	42.39
F15	41.42

6.4. Concluding Remarks

This chapter described the formation of the bioresponsive matrix by utilisation of hyaluronic acid and alginate lyophilized polymer blends. The results demonstrated using three variables, namely the concentration of HA, alginate and ADH in order to derive a Box-Behnken design template containing superior combinations whereby 15 formulations were obtained. Various characteristic analysis was conducted in terms of the chemical, mechanical and bioactive release properties whereby it was clearly noted that the relative ratios as well as polymeric concentrations significantly affect these properties, with the greatest been the HA concentration.

The chapter to follow will describe the derivation of a single optimal formulation based on the results obtained in order to formulate a device with enhanced characteristics. Further characterisation in terms of the physicochemical and physicomechanical properties will be evaluated and described in the chapter to follow as a step to determine the efficacy of the design and development of the BTDS for eventual *in vivo* studies.

CHAPTER 7
CONCEPTUALIZATION AND STATISTICAL OPTIMIZATION OF THE SMART INFLAMMATORY RESPONSIVE MATRIX AS A COMPONENT OF THE PROTOTYPE DEVICE

7.1.1. Introduction

The main outcome of this study was to develop and design a novel prototype as an inflammation bioresponsive device for superior wound healing incorporating a nanofibrous mat. This Chapter will provide insight to the smart device as a complete prototype providing prospection and facilitating advanced marketing potential. Further, elaboration is provided in terms of interactions of the BTDS with the wound environment providing pertinent statistics to the bioresponsive capabilities of the device. The chapter aims at providing a detailed insight into the stimuli responsive function and optimization of the BTDS by demonstration of the pertinent rheological characteristics considerably influencing the matrix formation, determination of the overall BTDS architecture by carrying out the various test in terms of nano mapping, tensile strength, FTIR spectra, topographical imaging by SEM, alterations in system properties by thermal influences as well as modification impacts by nanofibre incorporation. In addition, this chapter aims at justifying the bioresponsive nature of the lyophilized component of the BTDS by conducting in detail *in vitro* studies and pharmacokinetic analysis of the optimized BTDS. The versatility and latency will also be evaluated for conduction of *in vivo* studies.

As discussed in greater detail within Chapter 2 of this thesis, wound healing is a complex biochemical process entailing many stages that need to be adequately managed for effective healing, thus many factors need to be taken into account when designing a wound healing device. To date, very few to no single system has been implemented that provides all the necessary requirements for optimal healing processes. Thus, this research development aims at introducing a single prototype device consisting of momentous components introducing foremost characteristics to the wound healing process. The featured design focuses on innovative layered technology whereby the unique multi layered design provides elevated breathability and absorbency thus reducing the risk of bacterial invasion and maceration. Figure 7.1 depicts an illustrated schematic revealing the mechanism of the prototype. The BTDS prototype device will comprise of:

- **A Backing Layer**: The incorporation of a backing layer secures the device in place, furthermore the mucoadhesive and adherent properties presents self adherence to the wound site thus facilitating patient care and convenience with enhanced management of everyday daily challenges of dressing change. Due to its

mucoadherent properties, the device will remain in place and can be easily removed thus making it friendly for use on fragile skin. A significant feature of its adherent properties is its ability to be lifted and repositioned without the loss of its adherent quality, furthermore disruption of healing tissue will be minimised as it will not adhere to the wound bed. Incorporation of a backing layer averts strikethrough and prevents invasion and provides protection against external bacteria and viruses.

- **Inflammatory responsive lyophilized matrix**: Chapter 6 of this thesis provided a greater insight to the bioresponsive function of the lyophilized matrix as a component of the prototype device. To provide a brief rationalization, the lyophilized matrix will serve as a two way communication between the device and the biological tissue. Initiation of the wound healing process will occur in a stimuli responsive nature whereby a biological interaction will occur upon exposure to inflammation releasing the various bioactives.

- **Nanofibrous mat**: Chapters 4 and 5 of this thesis provided a detailed insight to the many advantages of fabrication of a nanofibrous system. Incorporation of the nanofibrous mat as a component of the prototype device will supply the BTDS with a 'pseudoskin' feature whereby the extracellular matrix of the native skin is mimicked providing enhanced wound healing potential. Many of the ideal wound healing characteristics is also incorporated into this component such as adequate gaseous exchange, debridgement of wound site, moist wound environment, absorption of excess exudates, and minimal frequency of dressing change, infection protection and bacterial invasion protection.

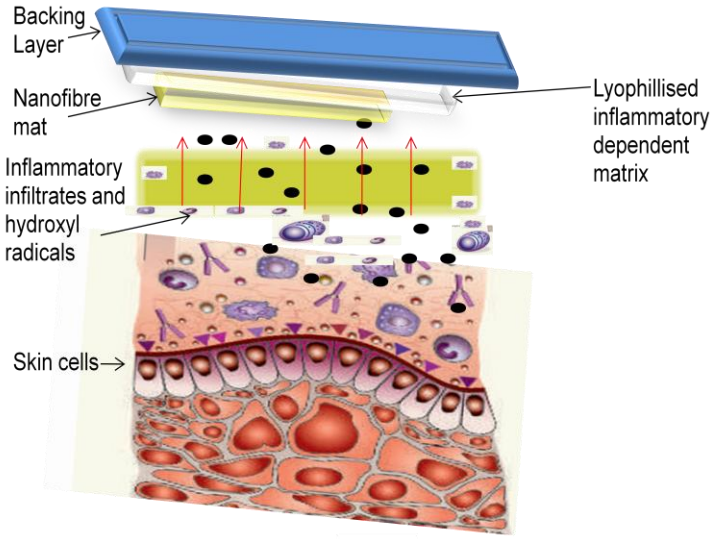

Figure 7.1: Mechanism of action of the prototype device

7.1.2. Formation of the Polyelectrolyte Complex

A polyelectrolyte complex (PEC) can be defined as an electrostatic interaction between oppositely charged polyions (Nam and Lee, 1997). A PEC is formed within a solution when oppositely charged electrolytes are mixed and the resultant interaction leads to the formation of strong yet reversible electrostatic links altering the original assembly of links in the structure. These interactions lead to non-permanent structures via the formation of a polyelectrolyte complex network without the need to form covalent bonds. Formation of PECs results in structures that are more sensitive to changes in environmental conditions, show greater biocompatibility and are more well tolerated (Hamman. 2010). Anionic natural polymers such as both alginate and hyaluronic acid can form polyelectrolyte complexes with chitosan. PECs between chitosan and alginate occur at the guluronic and manuronic acid groups containing negatively charged carboxylic acids, thus interacting electrostatically with the positively charged amino groups of chitosan. PECs formed between these natural polymers still possess biodegradability and biocompatibility but are notably stronger mechanically (Hein et al., 2008). Composition of the complete prototype device can also lead to the formation of a polyelectrolyte complex between chitosan and hyaluronic acid. Hyaluronic acid is a natural constituent of the native extracellular matrix of the skin and the only nonsulphated glycosaminoglycan found in the ECM. It is a linear anionic polysaccharide that forms electrolyte complexes with chitosan making it less prone to enzymatic hydrolysis

thus improving its stability and mechanical characteristics (Denuziere et al., 1998; Hamman. 2010).

7.1.3. The Employment of Mucoadhesion to Promote Effective, Targeted and Convenient Topical Bioactive Delivery

Within the field of pharmaceutical sciences, a larger interest has been focused on the region of mucoadhesion and mucoadhesive materials as well as polymers. Distinctiveness of bioadhesion can be explained as a linkage between two materials with at least one been biological in nature for an extended period of time by an interfacial force. When one of these materials conforming to the adhesive attachment is a mucus membrane or mucus, it can be termed as mucoadhesion (Gu et al., 1988). A mucus membrane consists of biological tissue in which the surface is made moist by the presence of a mucus layer. Specialised cells known as goblet cells amongst others are present within the tissue that secretes mucus onto the epithelial surface as a gel layer adherent. Glycoproteins present within the mucin are the major components forming the characteristic adhesive, cohesive and gel-like properties (Smart et al., 2005). To investigate the process of mucoadhesion there are six general adhesive theories that have been adapted. These include (Smart et al., 2005):

- *The mechanical theory*: Interlocking of a liquid adhesive on a rough surface thereby allowing adhesion.
- *The electronic theory*: Formation of an adhesive bond due to attractive forces present forming an electrical double bond when electronic transfer occurs at a surface interface due to divergence in the electronic structure.
- *The diffusion theory*: Interdiffusion of polymer chains across an adhesive interface that is driven by a concentration gradient.
- *The wetting theory*: Involves interfacial and surface energies when applied to liquid systems. As a prerequisite for adhesion, the liquid is required to spread spontaneously onto a surface.
- *The fracture theory*: Adhesion in this instance is related to the detachment after adhesion of the two involved surfaces whereby failure to adhere usually occurs at the weakest point which is considered to be a cohesive failure within one of the adhering surfaces.

For incorporation of mucoadhesive abilities within a pharmaceutical dosage form, smart mucoadhesive polymers can be utilised. Mucoadhesion via the use of polymers are said to occur upon the formation of bonds such as van der waals forces, hydrogen bonds, ionic interactions as well as physical interpenetration effects of mucus and polymer chains. Polymer chain flexibility provides a greater understanding of the mucoadhesive properties of

a polymer. A stronger adhesive bond will be accomplished by more flexible chains thus enhancing the interpenetrating effect of polymer chains and mucus to a satisfactory depth. Thus, in addition the use of crosslinkers and the formation of covalent strong bonds will decrease the flexibility of the polymer chain thus rendering the material less adhesive. Therefore for improved mucoadhesive characteristics, the use of low molecular weight, uncrosslinked polymers provide ideal properties for mucoadhesion (Leitner et al., 2003). Polymers comprising of a greater charge density serve as superior mucoadhesive agents. Furthermore, polyanion polymers serve as greater bioadhesives then non-ionic and polycationic polymers. Alginate serves as a prospective mucoadhesive agent owing to its anionic polymeric state at the carboxyl end groups. George and Abraham. (2006) have reported that studies have shown that alginate serves as a greater mediator for mucoadhesion then other natural polymers which include chitosan, poly (lactic acid), polystyrene and carboxymethyl cellulose. The use of alginate improves effectiveness as an adhesive agent and bioavailability. Incorporation of poly acrylamide (PAA) further enhances mucoadhesive properties due to its high charge density and polyanionic nature (Park and Robinson. 1987).

7.1.4. Optimization of the Lyophilized Matrix in terms of its Inflammatory Responsive Nature of the BTDS

The main aim of this chapter is the development of an optimum lyophilized matrix for incorporation within the BTDS, therefore the requisite goals of a pharmaceutical scientist is the expansion and design of an immaculate drug delivery system covering the indispensable requirements, thus casing many objectives. In order to obtain the optimum formulary design, many steps and objectives were put in place which include the attainment of a Box-Behnken design template whereby the most suitable formulations, a design of experiments (DoE) was statistically derived where upon in detail characterisation is undertaken as elementary discussed in Chapter 6 of this thesis. Subsequent to this for achievement of optimization, a response surface methodology (RPM) is needed to be implicated as will be discussed in this chapter in order to generate mathematical models that will adequately predict and describe the bioresponsive release behaviour, mechanical properties and rheological characteristics of the derived formulations leading to an optimal formulation.

This chapter will focus on the optimization of the inflammatory responsive component of the BTDS following the generation of the RPM, under conditions simulating both inflammation at an inflicted wound site and normality. Consequently overall bioactive release kinetics will be undertaken and the assurance of the rationality and applicability of the system will be carried out by application of the various characteristic analysis.

7.2. Materials and Methods

7.2.1. Materials

Hyaluronic acid (Sodium salt from streptococcus equi, M_w=8000-15000 g/mol), adipic acid dihydrazide (ADH) M_w=174.20 g/mol ≥98% tritration purchased from Sigma Aldrich Chemie GmbH, Steinheim, Germany. Alginate (TICA-algin® 400 Powder, medium viscosity) was purchased from Texture Innovation Center® (White Marsh, MD, USA) and Poly (acrylic acid) (Carbopol 974P®) (Noveon Inc., Cleveland, USA). Glycerol and Tween 80 obtained from Associated Chemical Enterprises Pty Ltd. (South Africa), Silicon (BDH, VWR International Ltd, London, UK), and Paraffin Liquid (Saarchem Wadeville, Gauteng, South Africa). All other reagents used were of analytical grade.

7.2.2. Synthesis and Formation of a Backing Layer to serve as a Component of the Prototype Device

The film casting method was employed whereby a ratio of 3:1 was used for film formation. 0.17g of alginate was dissolved in solvent, deionised water with 0.5g polyacrylic acid. A hydrogel was subsequently formulated by sequential blending of the polymer solutions, followed by the addition of the plasticizer glycerol at a concentration of 2:1 (polymer: plasticizer). Thereafter 1 drop of antifoaming agent silicon was added to the solution. Solution blends were then allowed to stir on a magnetic stirrer until a homogenous solution was formed. 10mL of each blend was poured into a mould composed of parafilm, rectangular in shape (710mm x 260mm) lubricated with liquid paraffin and cast in film form by solvent evaporation at room temperature with the use of a fumehood under the influence of continuous airflow. After being dried, membrane films were removed from the fumehood and parafilmed, this was utilised as a backing layer for the BTDS

7.2.3. Formulation of the Crosslinked Bioresponsive Lyophilized Matrix incorporating the Entrapped Nanofibres

An optimized formulation was prepared from the statistically derived superlative concentrations as indicated in Table 7.1. A hyaluronic acid hydrogel was formulated by solution polymerization using deionised water as the solvent. Crosslinking was then undertaken by preparing a hyaluronic acid-adipic dihydrazide complex as a hydrogel. The HA-ADH solution was then allowed to stir continuously under ambient room temperature conditions using a magnetic stirrer. Sodium alginate in concentrations indicated in Table 7.1 dispersed within deionised water was then added to the HA-ADH solution to form a complex hydrogel whereby wound healing nanofibrous mats were then suspended in the gel and immediately frozen. The above system was then lyophilized to form a stimuli responsive

matrix reservoir that can be adjoined to the backing layer as described in Section 7.2.2 in order to formulate the BTDS.

Table 7.1: Statistically derived superlative concentrations of the bioresponsive and non-bioresponsive component

	Alginate $\%^{w}/_{v}$	**Hyaluronic Acid $\%^{w}/_{v}$**	**Adipic Acid Dihydrazide $\%^{w}/_{v}$**
Bioresponsive lyophilized matrix	2.75	0.5	0.13
Nonbioresponsive lyophilized matrix	2.75	-	-

7.2.4. Optimization of the Formulary Components

A statistically derived optimized formulation was derived by mathematical modelling and simulations using the response surface methodology (RSM) from the statistically derived design of experiments (DoE) of the Box-Behnken Design as stipulated in Chapter 6. The response optimization procedure (MINITAB®, V15, Minitab, USA) was used to obtain the adjusted levels of biopolymer and bioactive to be incorporated within the lyophilized component of the BTDS. Cumulative bioactive release, Young's Modulus in terms of the tensile and mechanical characteristics as well as the rheological characteristics for simultaneous constrained optimization were identified as the most pertinent responses for successful operation of the bioresponsive topical wound healing delivery device. Undertaking simulations relating to these responses ensures the successful establishment of a nano incorporated system with constant stimulated bioactive release, stability and mechanical flexibility for topical application. An optimized level of the independent variables, predicted response (y), goal of the response, factor settings and desirable scores was established for optimization. The optimized responsive lyophilized component of the BTDS was then tested for various characteristics in comparison to a normality whereby the major responsive polymeric component (hyaluronic acid) was omitted as illustrated in Table 7.1.

7.2.5. Evaluation of the *In Vitro* Bioresponsive Bioactive Release Behaviour by employing the Fenton's Reaction

In Vitro degradation of the lyophilized crosslinked matrix was analysed by selecting inflammation as a stimulus whereby chemical inflammatory mediators (production of hydroxyl radicals) by the generation of the Fenton's reaction was produced:

$$Fe^{2+} + H_2O_2 \rightarrow Fe^{3+} + OH\cdot + OH^- \qquad \text{[Equation 6.3]}$$

Samples prepared were immersed in saline phosphate buffer at a pH of 7.4 and in the appropriate *in vitro* stimulus at a pH of 5.5 to correlate with the pH of inflammation. Samples

were placed in dialysis tubing with a molecular weight of 12 000 in a closed vial and placed in an oscillating laboratory incubator (Labcon® FSIE-SPO 8-35, California, USA), set to 25 rpm (du Toit et al., 2008). At predetermined periods samples were removed and subjected to analysis for bioactive release using a nanophotometer (Implen nanophotometer GmbH, Munich,) at a wavelength of 425nm to determine maximum absorption. A comparison to this was undertaken whereby samples were prepared omitting the inflammatory responsive component as well as the crosslinker. Samples were then placed under the equivalent environmental conditions and the bioactive release profiles were then taken.

7.2.6. Characterisation in terms of the Hydration Dynamics Behaviour

In order to determine the swelling capacity of the samples, a Karl Fischer Titrator (Mettler Toledo V30 Volumetric KF Titrator, Mettler Toledo Instruments Inc., Greifensee, Switzerland) was used for analysis whereby water is quantified using electrical conductivity and as a standard a methanol-water solution is utilised. The unreacted Karl Fisher reagent left determines the endpoint analysis whereby the conductivity difference is indicated. Samples were immersed and allowed to run until the endpoint was reached and validated. Samples were weighed prior and after immersion and the % swelling capacity was then calculated using equation 6.2 as follows:

$$ESR = \frac{(W1 - W0)}{W0} \quad \text{[Equation 6.2]}$$

Where W_1 is the weight of samples after immersion and W_0 is the weight of samples in the dried state.

7.2.7. *Ex Vivo* determination of Mucoadhesive Properties through Textural Profiling

A TA-XT plus texture analyzer was utilised to conduct mucoadhesive studies. Full thickness excised skin tissue from Sprague Dawley rat models were sectioned at 2mm thickness and attached to the lower end of a probe. The mucoadhesion studies was carried out at 37°C whereby the attached excised skin tissue was lowered onto the surface of the BTDS at a constant speed of 0.1mm.s^{-1} and a contact force of 0.5N. The probe was then vertically removed upward at the same constant speed after a contact period of 120s. A plot of force against distance was procured whereby the area under the curve was calculated to determine the work of mucoadhesion per square centimetre (mJ.cm^2) (Cevher et al., 2008)

$$Work\ of\ mucoadhesion\ (mJ.cm^{-2}) = \frac{AUC}{\pi r^2} \quad \text{[Equation 7.1]}$$

Whereby πr^2: Surface area of the skin tissue which is in contact with the gel formulations.

7.2.8. Characterisation in terms of Chemical and Vibrational Transitions

A PerkinElmer® Spectrum 100 Series FT-IR Spectrometer fitted with a universal ATR Polarization Accessory (PerkinElmer Ltd., Beaconsfield, UK) was utilised in order to determine the molecular vibrational transitions and chemical compositions of the various formulations as well as the effect of crosslinker incorporation on the optimized lyophilized matrix component of the BTDS. Spectra over the range 4000-625cm^{-1}, with a resolution of 4cm^{-1} and 4 accumulations was utilised as FTIR parameters.

7.2.9. Evaluation of the Thermodynamic Behaviour of the Matrix

To assess the thermal behaviour of the constituents, an advanced DSC (TMDSC/ ADSC) (Mettler Toledo DSC-1 STAR^e System, Schwerzenback, ZH, Switzerland) was utilised. This was carried out to ascertain temperature phase change in terms of chemical reaction temperatures, glass transition (T_g) and melting points of the lyophilized matrix of the BTDS.

Analysis was conducted in terms of the total heat flow (ΔH) across the samples, whereby variation in magnitude of the peaks were analysed in terms of the magnitude of the crystallisation temperature (T_c), melting temperature (T_m) and glass transition (T_g). The procedure was carried out whereby samples (±10mg) were accurately weighed into standard 40µL aluminium open pans and hermetically sealed in perforated 40µL aluminium pans. Measurements were employed at a heating rate of 10°C/min from -10°C to 300°C under nitrogen atmosphere.

7.2.10. Surface Structure and Morphological Analysis

To determine the effect of crosslinking and incorporation of the responsive polymer (HA), surface comparisons were made by attainment of the topographical imagery using scanning electron microscopy (SEM) (Phenom™, FEI Company, and Hillsboro, Oregon, USA). In order to maintain matrix integrity the lyophilized samples were first blot-dried and submerged in liquid nitrogen. Samples were evaluated for bulk characteristics such as pores and pore size, texture and roughness.

7.2.11. Determination of Young's Modulus by Nanotensile Mapping

A Nano Tensile Analyser (nanoTensile®5000 Hysitron Inc. Nanomechanical Test Instrument, Minneapolis, MN) was employed to determine the Tensile Strength and Young's Modulus of the lyophilized matrix. The mechanical characteristics were employed to measure the durability of the BTDS system at a nano sensitive level. Samples were first measured using a digital calliper, pretested and mounted until a breaking force is established at a velocity of 5µms^{-1}. Stress-Strain curves were procured to further determine the ultimate strength, strain and toughness of the BTDS system.

7.2.12. Physicomechanical Characterisation by Textural Profiling

To determine the tensile strength and force required to cause a defect or break in the system, textural analysis was employed on the BTDS system. This was done by using a texture analyser (*TA.XT.plus texture analyser*, Stable Microsystems®, Surrey, UK) fitted with a 50kg load cell that was utilised to determine physicomechanical properties of the system and in particular tensile strength from the generated force-distance profiles computed from the peak tensile force required and using Equation 6.1 given below. The parameters marked for textural analysis are presented in Table 7.2. Tensile strength was measured using the Young's Modulus equation as follows:

$$E = \frac{Tensile\ stress}{Tensile\ \ strain} = \frac{\delta}{\varepsilon} = \frac{FL_o}{A_o \Delta L} \qquad \text{[Equation 6.1]}$$

Where: E is the Young's Modulus (Modulus of elasticity); F is the force applied to the object; A_0 is the original cross-sectional area (πr^2) through which the force is applied; ΔL is the amount by which the length of the object changes; L_0 is the original length of the object.

Table 7.2: Parameters employed for Texture Analysis

Parameters	Settings
Test mode	Tension
Pre-Test speed	0.50mm/sec
Test speed	0.50mm/sec
Post test speed	5.0mm/sec
Trigger type	Auto
Trigger force	5kg
Contact time	5sec

7.2.13. Evaluation of the Transient Rheological Properties

The rheological analysis studies of the BTDS were carried out using a Thermo Scientific HAAKE MARS Rheometer (Thermo Fischer Scientific, Karlsuhe, Germany). The viscosity of the gel solutions were measured at a constant temperature of 37°C. Samples were placed on a sample stage whereby a c35/1° titanium rotor will be immersed in the polymer solution blends at a shear rate of $100s^{-1}$ and a time interval of 360s. Stress-Strain rheological parameters were obtained for quantified samples and an evaluation was made with regards to viscosity, yield stress, stress and frequency sweep. These parameters play a vital role in shaping a lyophilized matrix that is able to suspend nanofibrous material.

7.3. Results and Discussion

7.3.1. Optimization of the Lyophilized Component of the BTDS

The pragmatic design of the bioresponsive topical delivery system incurs superlative optimization in order to ensure safe, reproductive and effective drug delivery systems exhibiting therapeutic requirements and responses both *in vitro* and *in vivo.* In order to ensure this (i.e.: attainment of an optimized formulary component) a response optimization procedure (MINITAB®, V15, Minitab, USA) was used to attain the adjusted levels of biopolymer and crosslinker to be incorporated within the lyophilized component. Data used for the optimization of the experimental design formulations related to Young's Modulus and tensile analysis to determine the strength and flexibility of the system, bioactive release rate on exposure to a stimulus at a pH of 5.5 and the rheological viscosity in the hydrogel form of the various formulations.

The residual plots for MDT indicating stimuli responsive bioactive release of curcumin, Young's Modulus and viscosity were employed for analysis of the model. This was undertaken in order to determine the relationship between the response variables and the predictor variables to measure the suitability of the multiple regression models through residual analysis. Figure 7.2 depicts the residual plots of the MDT, Young's Modulus and viscosity whereby it was noted, upon analysis of the normal plots of the residual reveals normal distribution as all plots are in close proximity to the straight line. Furthermore, viscosity normal residual plots depict point distribution in clusters along the straight line indicating strong linear relationships. The residual scatter plot where the residual was plotted against the fitted values or model predictions emit points around the 0 residual and generally show random scatter. Thus these demarcations point out that no trends are indicated thus underlying assumptions relating to the multiple regression analysis were not grossly violated. Furthermore variance within the residuals was noted indicating non constancy due to the presence of some fanning and outliners (du Toit. 2013). Normal distribution of data is represented by a bell shaped histogram (Hazel. 2011). The residual histograms for stimuli responsive bioactive release and viscosity reveal slight irregularities which could be due to a random area on the data set. The histogram residual of Young's Modulus revealed symmetry thus depicting a relatively uniform distribution. Plots depicting the residual versus observation data indicate the performance of the model. A non random error is indicated by points that remain at constant magnitude whereas fluctuation on either side of the centre line displays non correlated errors with one another (Hazel. 2011).A full ANOVA was carried out as depicted in Table 7.3.

Table 7.3: ANOVA analysis of the measured responses

Response Variable/ Term	*P-Value*		
	Stimuli Responsive Bioactive Release (MDT)	Young's Modulus	Viscosity
Constant	0.952	0.048	0.952
Alginate	0.772	0.175	0.772
Hyaluronic Acid	0.757	0.119	0.757
Adipic Acid Dihydrazide	0.955	0.067	0.955
Alginate*Alginate	0.784	0.320	0.784
Hyaluronic Acid*Hyaluronic Acid	0.494	0.981	0.494
Adipic Acid Dihydrazide* Adipic Acid Dihydrazide	0.893	0.147	0.893
Alginate*Hyaluronic Acid	0.790	0.683	0.790
Alginate* Adipic Acid Dihydrazide	0.407	0.210	0.407
Hyaluronic Acid* Adipic Acid Dihydrazide	0.435	0.046	0.435

Complete Regression equations indicated for stimuli responsive bioactive release rate (MDT), Young's Modulus and viscosity are in depicted below in equations 7.2-7.4.

$$Stimuli\ Responsive\ Bioactive\ Release\ (MDT): 113.17 - 9.15(ALG) - 129.67(HA) - 640.40(ADH) + 2.61(ALG * ALG) + 183.75(HA * HA) + 2963.89(ADH * ADH) - 7.86(ALG * HA - 3.67ALG*ADH - 263.75(HA*ADH)$$ [Equation 7.2]

$$Youngs\ Modulus: 11.613 + 0.973(ALG) - 11.761(HA) - 132.211(ADH) - 0.067(ALG * ALG) + 0.115(HA * HA) + 355.093(ADH * ADH) + 0.221(ALG * HA) - 4.905(ALG * ADH) + 78.750(HA * ADH)$$ [Equation 7.3]

$$Viscosity: 353.7 - 235.8(ALG) + 2557.1(HA) - 4251.8(ADH) - 22.0(ALG * ALG) + 4286.3(HA * HA) + 36675.6(ADH * ADH) - 179.8(ALG * HA) + 3851.4(ALG * ADH) - 31605.7(HA * ADH)$$ [Equation 7.4]

(a)

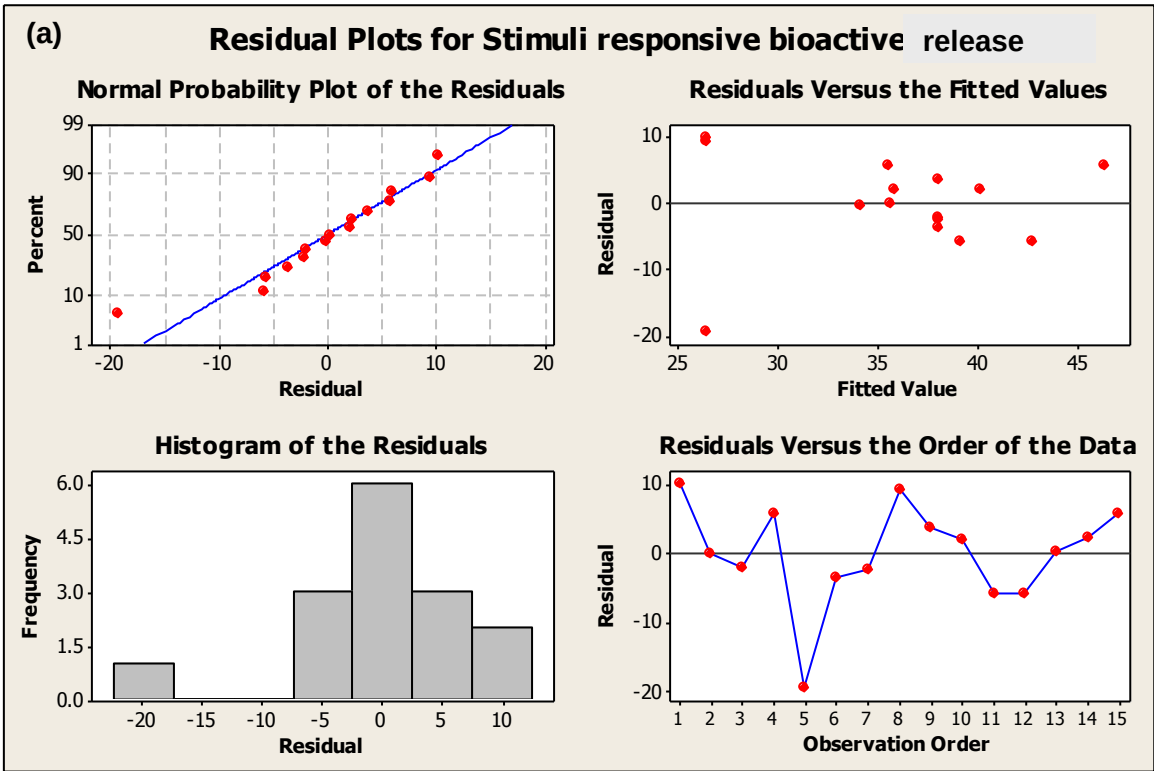
Residual Plots for Stimuli responsive bioactive release
Normal Probability Plot of the Residuals
Percent
Residual
Residuals Versus the Fitted Values
Residual
Fitted Value
Histogram of the Residuals
Frequency
Residual
Residuals Versus the Order of the Data
Residual
Observation Order

(b)

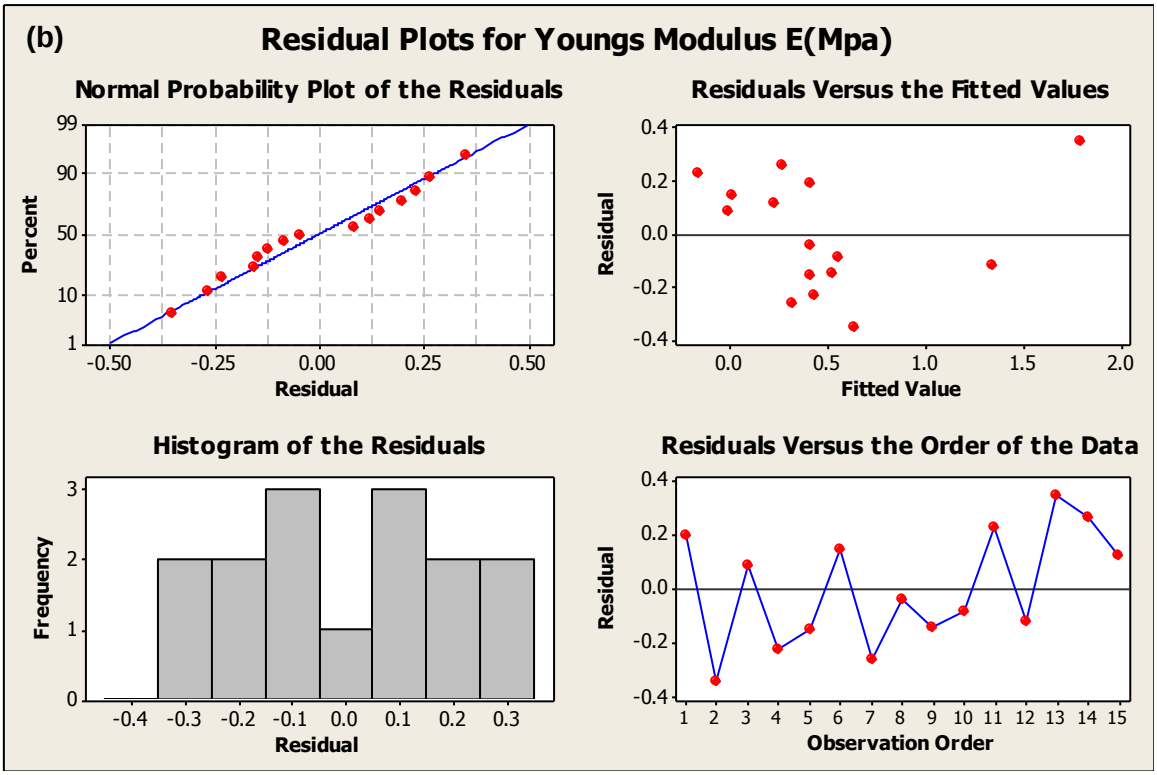
Residual Plots for Youngs Modulus E(Mpa)
Normal Probability Plot of the Residuals
Percent
Residual
Residuals Versus the Fitted Values
Residual
Fitted Value
Histogram of the Residuals
Frequency
Residual
Residuals Versus the Order of the Data
Residual
Observation Order

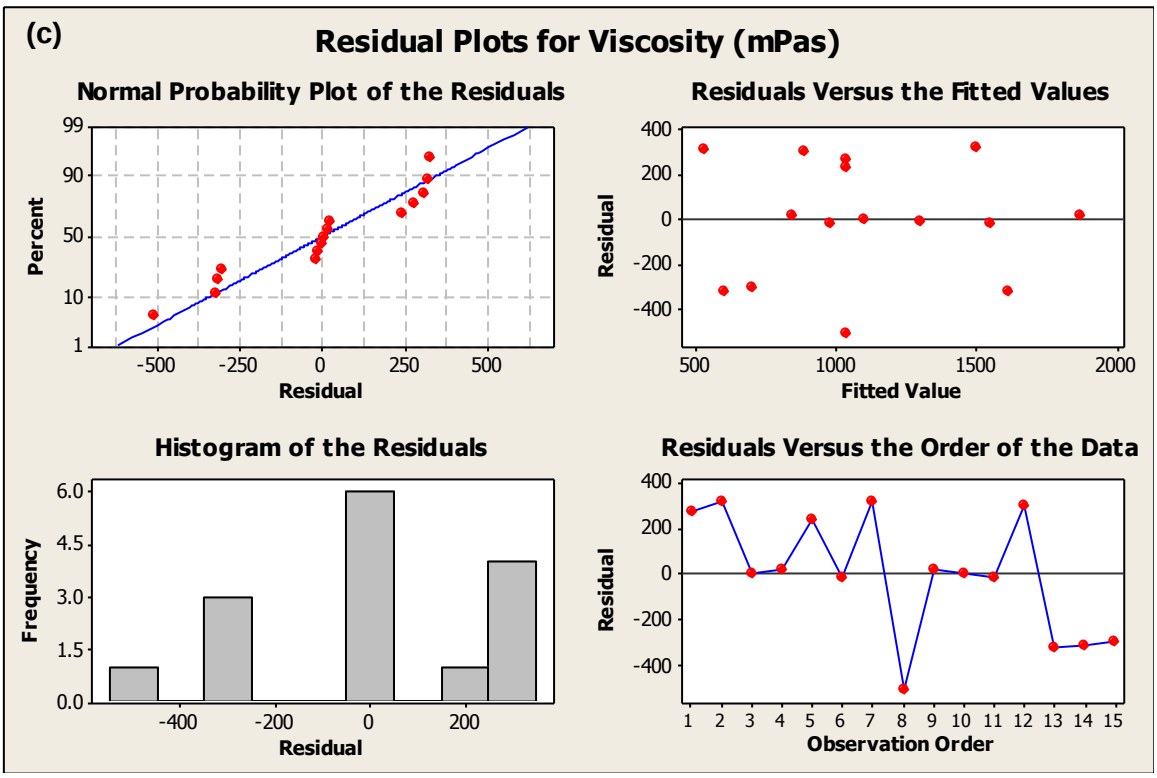

Figure 7.2: Residual plots of (a) stimuli responsive bioactive release; (b) Young's Modulus (c) Viscosity

7.3.1.1. Response Surface Plot Analysis for Formulary Optimization

For design product optimization and processing, optimization techniques such as the response surface methodology need to be put in place. Attainment of the response surface methods provides a relation between the various biopolymers and crosslinker salt concentration. As mentioned prior the responses tested against is the bioactive release MDT for curcumin, the strain the system can withstand before fracturing in terms of its tensile strength as well as the Young's Modulus and the viscosity when in the hydrogel form. Surface plots illustrated in Figure 7.3, 7.4 and 7.5 provide valuable data pertaining to the responses and the factors.

The response surface plot analysis of the stimuli responsive bioactive release (MDT) provides information regarding the effects of interactions between the various variables on the release rates of the bioactive. Many factors impact on the bioactive release from polymeric matrices, which include polymer swelling and erosion. Swelling and erosion characteristics from a polymeric system can be directly attributed to the various properties of the system. Incorporation of alginate plays a major role in terms of swelling and erosion due to its gelanisation characteristics and pH dependency making it more prone to erosion resulting in bioactive release. To determine the functional relationship between the responses achieved and the experimental variables, plots were employed. Responses obtained from the polymers employed which include blends of alginate and hyaluronic acid is

depicted in Figure 7.3. Furthermore the induction of crosslinking by the incorporation of a crosslinker adipic acid dihydrazide (ADH) greatly influenced the bioactive release rates. To visualise the relationships between the variables a contour plot was included as illustrated in Figure 7.3. A prolonged, greater controlled release rate was seen by the addition of crosslinker. Furthermore it was noted that the bioactive release rate was prolonged to a greater extent when interactions between hyaluronic acid and the crosslinker were analysed. This observation provides a greater insight to the stimuli responsiveness of the system as the active polymeric system for stimuli (inflammation) responsiveness is the integration of hyaluronic acid. The formation of crosslinked bonds prolongs and minimises the degradation by hydroxyl radicals on exposure to an inflammatory site. Therefore the formation of covalent bonds by crosslinking and the concentration of crosslinker play a vital role in the release rates of bioactive. The interactions between polymers i.e.: hyaluronic acid and alginate revealed a more rapid release rate then release rates by the incorporation of a crosslinker.

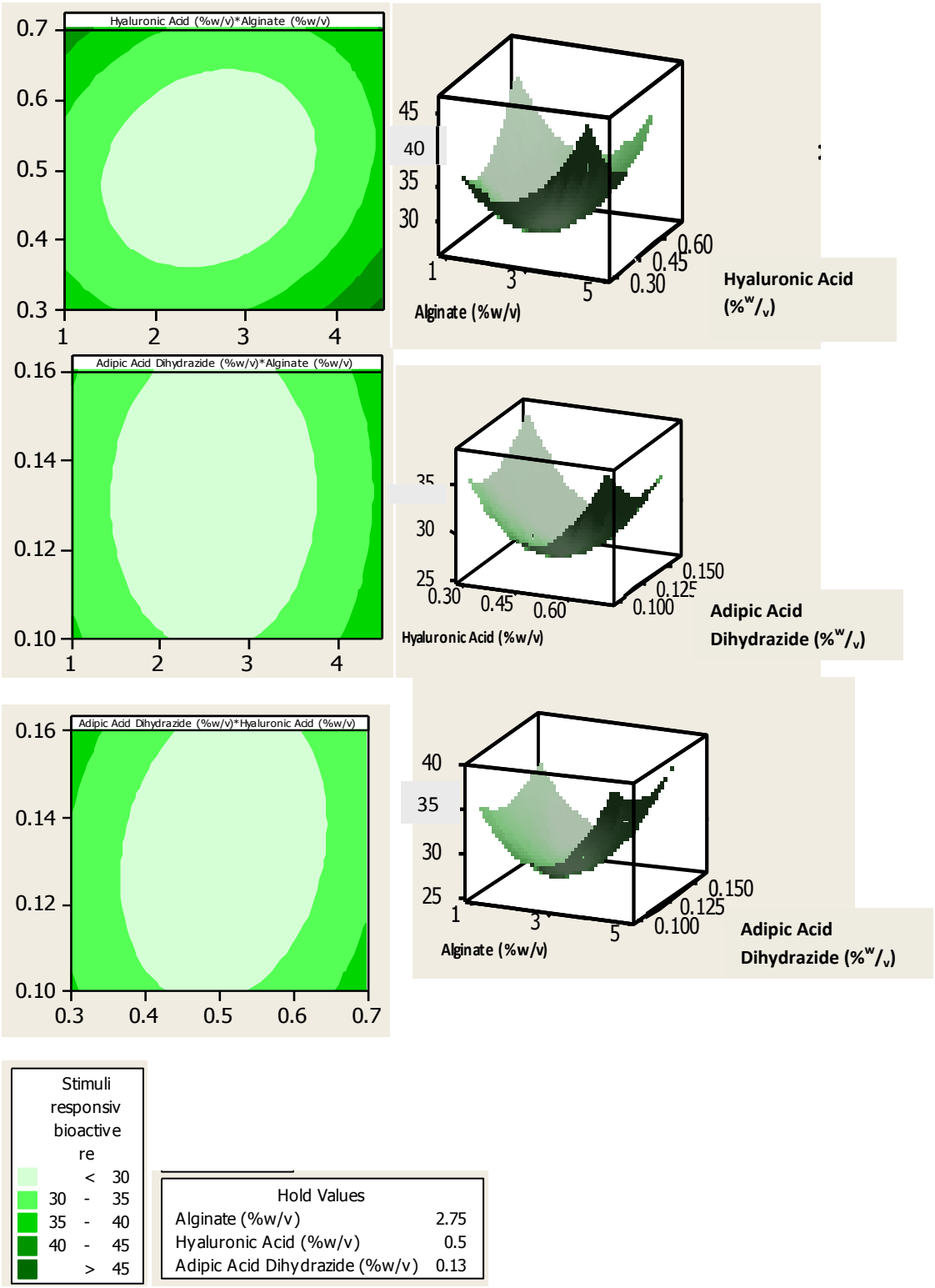

Figure 7.3: Contour and Surface Plots of the stimuli responsive bioactive release (MDT) in relation to amendment in concentration of polymer and crosslinker

The surface and contour plots in Figure 7.4 depict the effects of the interactions between variables on the Young's Modulus and tensile strength of the system. Crosslinking the lyophilized component of the BTDS provided a significantly greater Young's Modulus, thus the system exhibited greater rigidity and stiffness. Furthermore it was noted that by

increasing the degree of crosslinking further the stiffness and rigidity of the system was augmented which can lead to brittleness. Decreasing the degree of crosslinking in the system lowered the Young's Modulus thus improving the elasticity and flexibility of the BTDS. Interactions between polymers alginate and hyaluronic acid portrays a lower Young's Modulus as can be seen in the surface plot of Figure 7.4 thus weaker in comparison to the addition of a crosslinker, making the system more prone to effortless tearing and fracturing.

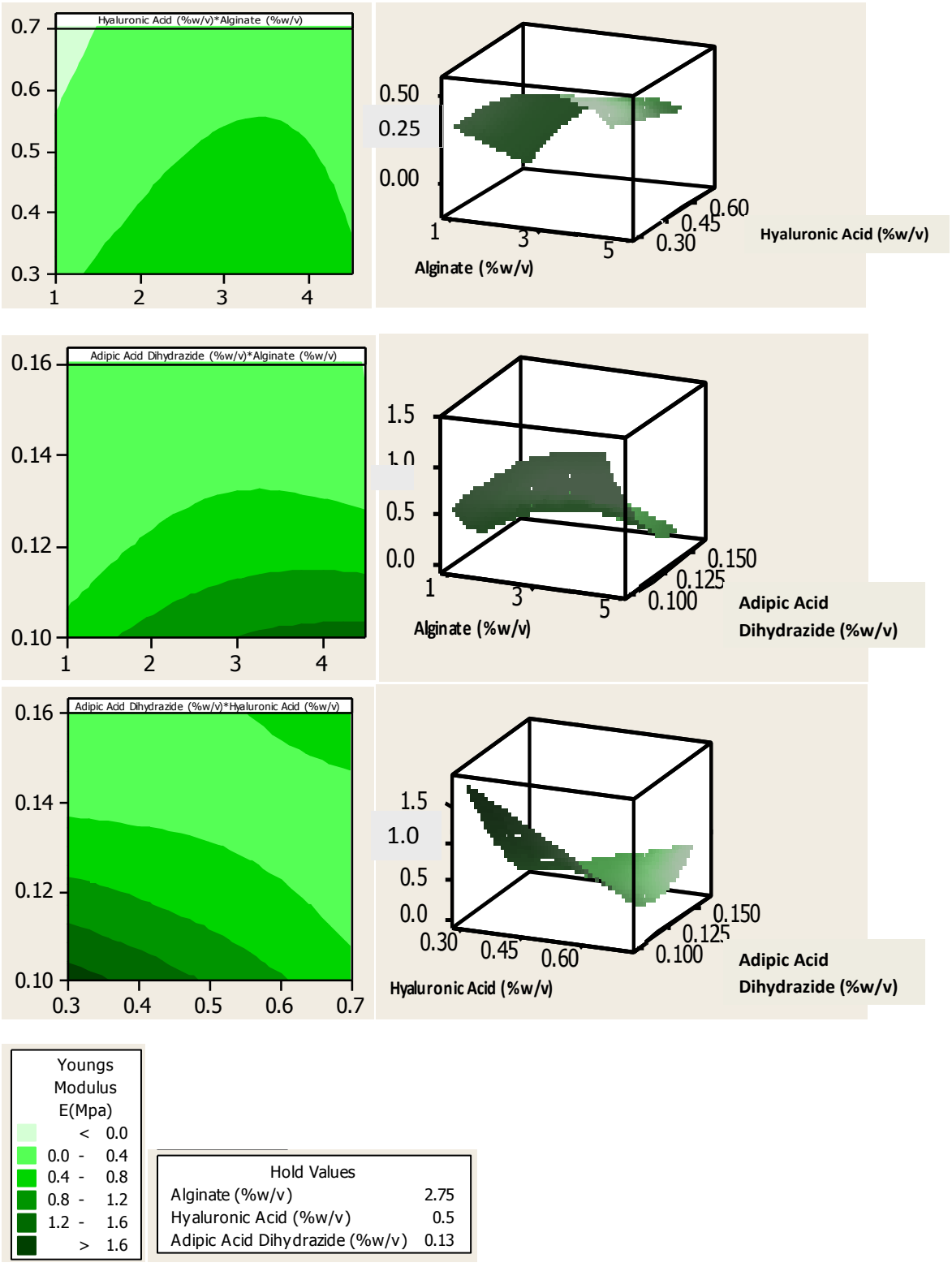

Figure 7.4: Surface and Contour Plots depicting the effect of varying polymeric and crosslinker concentration on the Young's Modulus and tensile strength

The analysis of viscosity of the system in a hydrogel form provides pertinent information regarding the system properties. Viscosity characteristics provide a measure in which the systems resistance to gradual deformation can be analysed when a shear stress or tensile stress is applied. In addition characteristics relating to erosion and degradation for bioactive release can be investigated. Varying concentrations of the polymers and crosslinker had a

direct attribution to the viscosity of the system. Increasing polymeric concentration lead to greater viscosity thus the system displayed a greater resistance to the applied forces consequently opposing degradation. Thus it could be deduced that increasing the viscosity augmented its tensile strength properties and delayed degradation thus prolonging bioactive release.

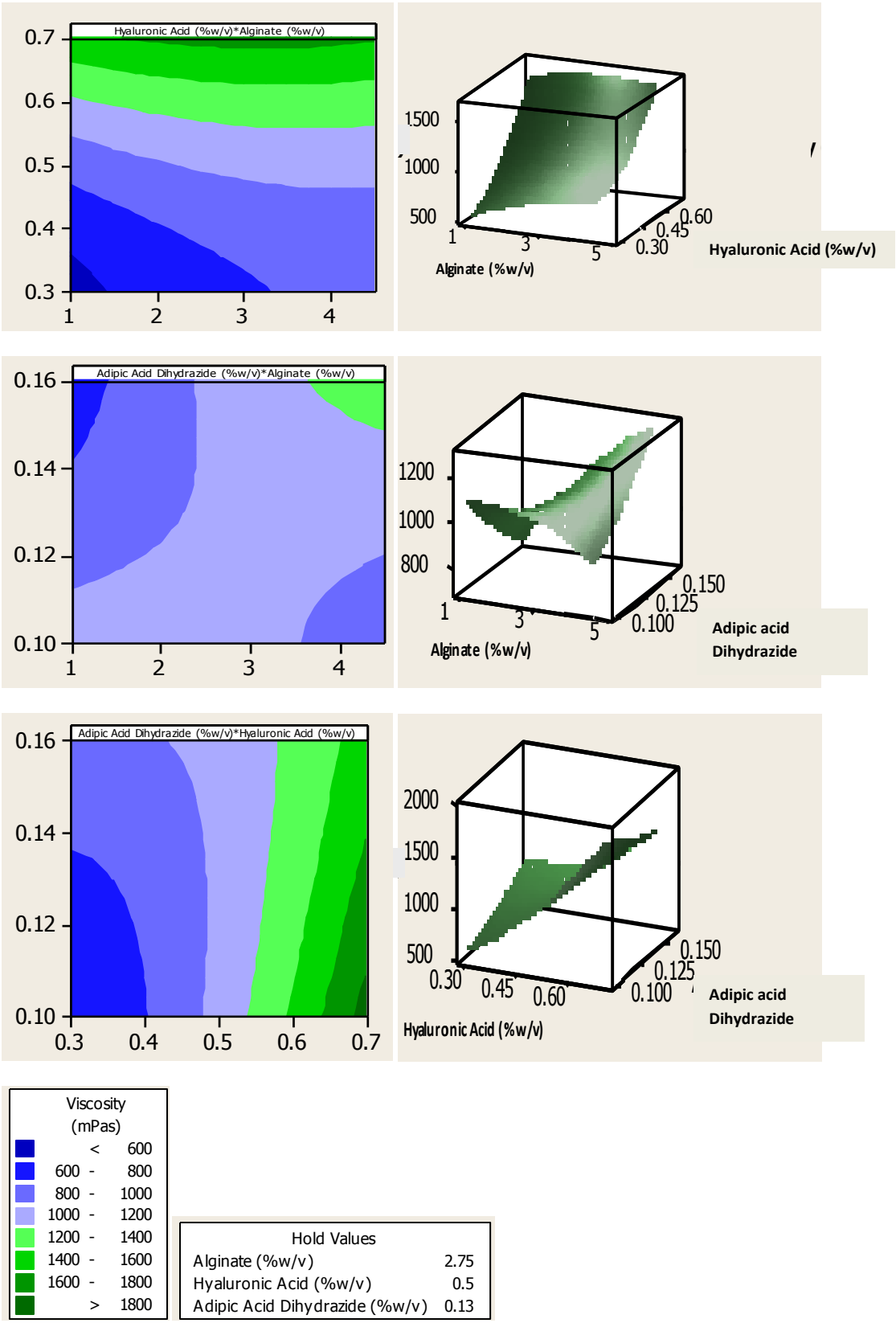

Figure 7.5: Response surface and contour plots depicting the effect of varying concentrations on the viscosity of the formulation

7.3.1.2. Response Optimization of the Bioresponsive transdermal delivery system

Response optimization procedure (MINITAB®, V15, Minitab, USA) was utilised in order to establish the favoured level of biopolymer and crosslinker formulary components.

Simultaneous constraint optimization of the selected responses, inflammatory responsive bioactive release, viscosity of the formulations and Young's Modulus were carried out in order to acquire an optimal formulation. Maximisation of these characteristics was attained to ensure response optimization by establishing the optimized levels of the independent variables and their predicted responses. Figure 7.6 depicts optimized levels of the independent variables, the goal for the response, the predicted response, *y*, at the current factor settings, as well as the individual and composite desirability scores. Based on the statistical desirability function, it was found that the composite desirability's for the formulation was 1.0.

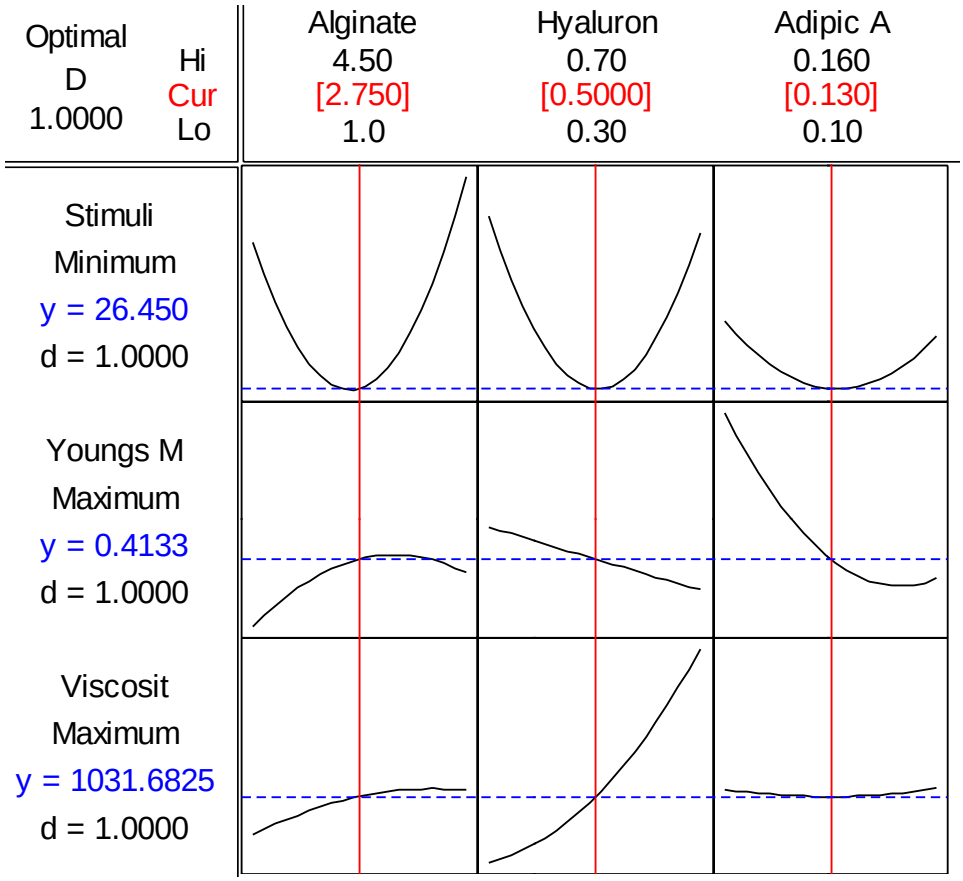

Figure 7.6: Desirability plots representing the levels of Alginate, Hyaluronic Acid and Adipic Acid Dihydrazide required to synthesise the optimized formulation.

7.3.2. Inflammatory Responsive Bioactive Release Behaviour

Intrinsic to evaluation of the optimized stimuli responsive formulation was its *in vitro* performance on exposure to a stimulus (Fenton's reagent) and under normal conditions (saline phosphate buffer). As described an optimized formulation was fabricated enclosing an active component (HA) to a stimulus and compared to a non stimuli responsive (control) system whereby the active component (HA) was omitted. Bioactive release profiles were then taken and revealed that the release rates under normal conditions portrayed a slower release rate of the crosslinked optimized stimuli responsive system. When exposed to the inflammatory conditions the release rate was enhanced. Furthermore it was noted that the

release rate from the non stimuli responsive system that was not crosslinked and contained no crosslinker portrayed a much more rapid rate of bioactive release. Enhancement of bioactive release under inflammatory conditions can be attributed to the prospective disruption of the hydrolysable linkages representing the stimulus responsive mechanism of the system (du Toit et al., 2013). Disruption of these linkages results in the release of the embedded nanofibrous component. Furthermore release rates may be prolonged due to the formation of a polyelectrolyte complex between components of the nanofibrous system embedded and components of the lyophilized matrix of the inflammatory responsive system.

Figure 7.7 depicts the bioactive release rate of curcumin from the system under the various environmental conditions. The optimized stimuli responsive formulations depicted a release rate at 5 hours of 0.064mg when exposed to inflammatory pathological conditions created by Fenton's Reagent and a release rate of 0.045mg at 5 hours when exposed to normal conditions created by the employment of phosphate saline buffer. Enhanced release rates when exposed to pathological conditions is observed and is attributed to the mechanism entailing degradation by hydroxyl radicals as described above in this chapter. Stimuli responsive polymer erosion occurs when the HA matrix comes into contact with inflammatory stimulus releasing hydroxyl radicals which cause the degradation of HA within the lyophilized component of the BTDS which ultimately results in bioactive release in response to the stimulus signal. Addition of the crosslinker modifies the polymeric structure thus prolonging the release of bioactive. Within the optimized formulary component, the lyophilized matrix encompasses a greater backbone structure due to crosslinking with ADH whereby the introduction of the amine group consequently forms covalent linkages with prominent groups of the HA structure as depicted by the SEM images illustrated in Chapter 6 and further depicted in Figure 7.11 of this chapter. Furthermore incorporation of the nanofibrous mat lead to the configuration of a polyelectrolyte complex which further tailored the structure providing greater mechanical strength and modifying release rates. Furthermore, a greater sensitivity to changes in environmental conditions was displayed on formation of a PEC (Hamman. 2010). A PEC was formed between both alginate and hyaluronic acid due to their anionic nature with positively charged amino groups of chitosan, a polymeric component structuring the nanofibrous system embedded. This structural modification further alters the structure providing greater stability and mechanical probability modifying the release rate further. As depicted in Figure 7.7, the optimized stimuli responsive formulation placed under normal saline conditions exhibit the lowest release rates attributed to the covalent crosslinkages, formation of the PEC and non exposure to stimuli responsive conditions. The control exposed to inflammatory pathological conditions reveals the greatest release rates at 0.067mg at 5 hours increasing up to 0.095mg at 24 hours due to the influence of active degradation by hydroxyl radicals and the exclusion of a PEC complex and crosslinkages by

ADH. No influence by hydroxyl radicals imposed a lower release rate of 0.057mg at 5 hours leading to 0.084mg at 24 hours. Thus it was deduced that the crosslinkage and PEC formation generate a positive modification on the structure by prolonging the release rates thus avoiding a burst bioactive providing a more constant release as is illustrated by the optimized (F) (stimuli responsive) release in Figure 7.7. Due to the described phenomena, it was seen that the release rates is primarily due to the exposure to the Fenton's reagent generating hydroxyl radicals causing degradation of HA leading to release of the bioactive curcumin from the modified structure thus exhibiting stimuli responsive behaviour to inflammation.

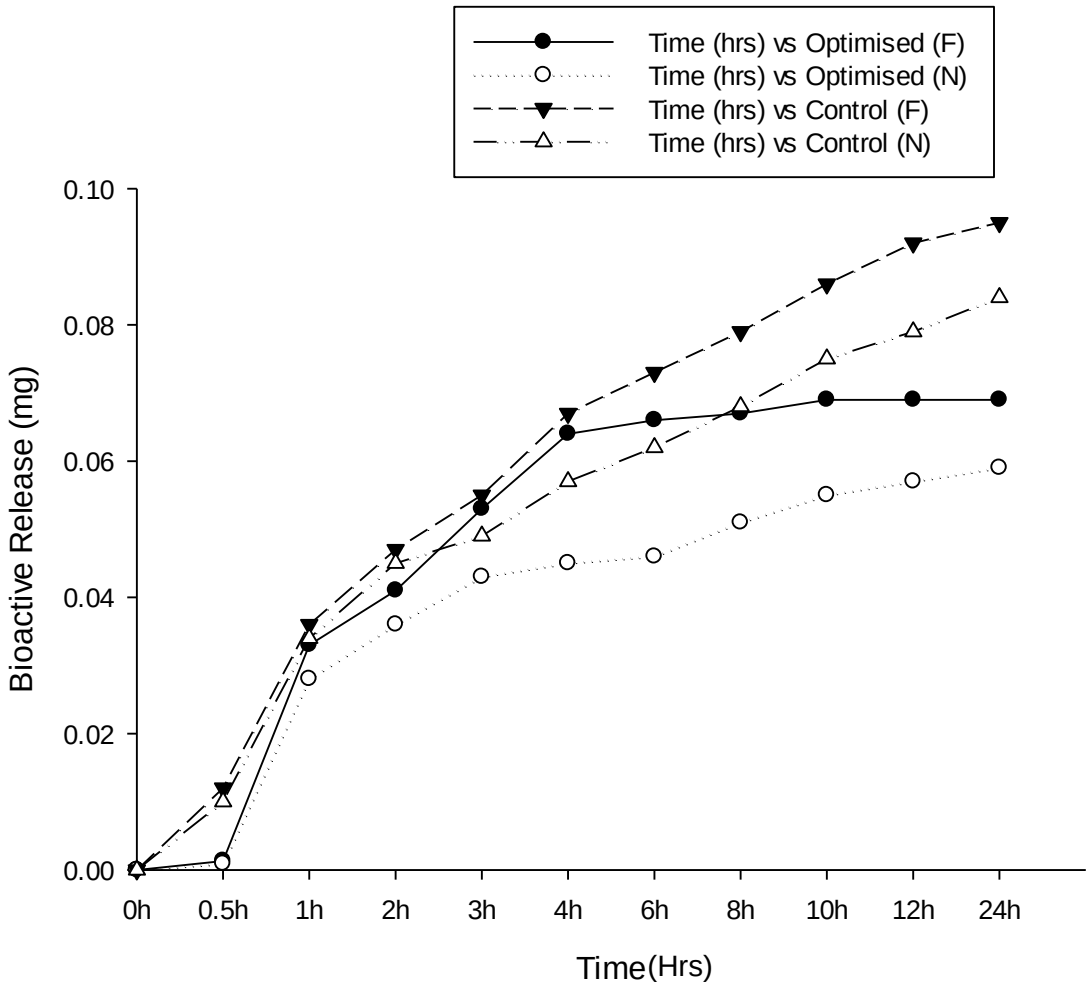

Figure 7.7: Comparative bioactive release profiles for the stimuli responsive (optimized) formulation and non stimuli responsive (Control) under inflammatory (F) and normal conditions (N).

7.3.3. Water Content Analysis of the Bioresponsive Transdermal Delivery System

The swelling ability of the formulations in the hydrogel form was titrated using a Karl Fisher Titrator. Swelling and water penetration is highly dependent upon the degree of crosslinking thus the intermolecular and intramolecular bonding forces occurring between molecules. The results obtained disclose a percentage water content of 16.419% in the stimuli responsive system and 16.826% in the non stimuli responsive system. Thus it was observed that a

slightly higher swelling ratio is obtained in the control system. The higher swelling ability is characteristic of the lack of bond formation due to the absence of crosslinking presenting a low crosslink density thus a greater swelling ability. Uncrosslinked control systems present with a structure whereby polymer chains are flexible and modifications in environmental conditions such as exposure to fluidic molecules may cause a breakage in secondary interactions resulting in more space for liquid uptake within the matrix (Rohindra et al., 2004); therefore the rate of swelling is less in the stimuli responsive formulation due to crosslinked bond formation. Furthermore, the swelling capacity of the hydrogel is largely dependent upon the monomer and monomer concentration used the hydrophillicity as well as the ionic density of the structure. As the hydrophillicity was increased so too did the swelling ability (Pourjavadi and Mahdavinia. 2006). Viscosity also plays a significant role in the swelling and erosional behaviour of the matrix. As the viscosity of the polymeric solution was increased, a greater resistance to swelling was attained and the swelling ratio plummeted. The addition of hyaluronic acid and adipic acid dihydrazide modifies the viscosity properties of the solution in contrast to the control containing only alginate thus rendering the formulation less swellable. Furthermore as mentioned the ionic nature and density directly impacts on the swelling ability of the matrix by the addition of ionisable functional groups such as carboxylic and amino groups. An understanding of the degree of hydration and swelling allows for the conception of transport of small molecules and bioactives through the matrix. Hyaluronic acid been a polyionic compound ionically reacts with various compounds within the structure which include chitosan and alginate. Positively anionic charges present interacts with the negatively charged ions present in alginate thus forming a polyelectrolyte complex, increasing the charge density (Cai and Gupta, 2002). This resulted in a more rigid structure with lower chain flexibility thus providing greater mechanical strength to the system diminishing the swelling ability. A decrease in swelling ability attributes to lower erosion rates thus prolonging the bioactive release rates over time. Effects of this phenomena is observed in the bioactive release profiles illustrated in Figure 7.7 whereby greater release rates over time is noted in the control than the optimized system.

7.3.4. Evaluation of the Degree of Mucoadhesion of the Prototype Device

Mucoadhesion can be defined as a polymers or materials ability to adhere or bind to the desired tissue. This is of crucial importance when developing a system for wound healing as topical preparations require favourable application properties to ensure patient compliance and optimal delivery. Furthermore mucoadhesive delivery systems are capable of increasing the bioavailability of the active compounds thus controlling release of the bioactive at the desired site whilst also extending the retentive time (Cevher et al., 2008). A TA-XT*plus* analyzer equipped with a 5kg load was employed to evaluate the mucoadhesive properties of the prototype device via attachment to excised Sprague Dawley rat skin. The mucoadhesive

tests were carried out to determine the adhesive properties of the formulations for device fabrication. From the work of mucoadhesion obtained from the area under the curve as illustrated in Figure 7.8a and Figure 7.8b, the backing layer formulation displayed a value of 0.079 $mJcm^{-2}$ and 0.031 $mJcm^{-2}$ for the lyophilized matrix formulation (incorporated with nanofibrous mat). Thus the results obtained depicted greater adhesive strength of the gel formulation of the backing layer which serves as an ideal prototype for wound healing. This can be directly attributed to the use of a mucoadhesive polymer such as polyacrylic acid. Literature findings suggest that the presence of more than 90% of acidic groups in non ionised polyacrylic acids avert electrostatic charges and thus demonstrate lower swelling abilities thus enhancing its binding properties directly to proteins and polysaccharides found in skin tissue (El-Kamel et al., 2002). The higher mucoadhesive characteristics displayed by the backing layer reveals superior bioadhesive qualities due to the high molecular weight of incorporating alginate and polyacrylic acid, strong hydrogen bonding, greater surface tension properties and its hydrophillicity. Elevated hydrophilic properties of the backing layer enable strong bioadhesive bonding to the mucosal surface of the skin tissue which ultimately resulted in strong bioadhesive forces. Hydrogen bonding is favoured by the presence of OH^- and $COOH^-$ groups present in polyacrylic acid. In addition, high surface tension characteristics favour the spread of the BTDS prototype over the epithelial layer of the skin (Ndesendo et al., 2010).

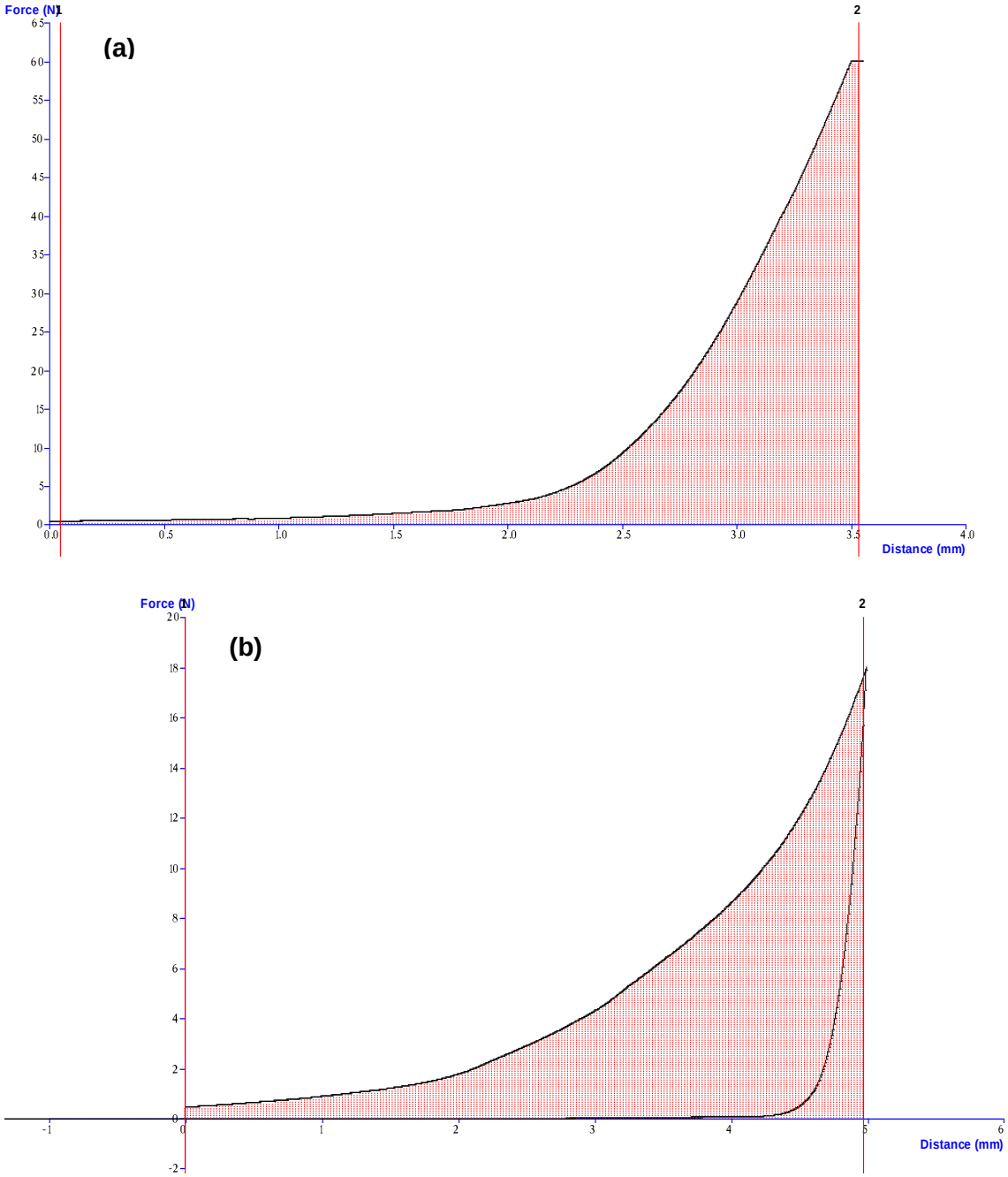

Figure 7.8: Area under the curve for the work of mucoadhesion of the prototype device where (a): Backing Layer, (b): Lyophilized matrix with incorporated nanofibrous mat

7.3.5. Vibrational Transitional Analysis to determine the Molecular Transitions of the crosslinked structures

Infrared spectroscopy serves as a versatile and diverse analytical technique for the determination of molecular vibrational transitions and fundamental absorption frequencies which provides an imperative key to unlocking structure-spectral relationships between associated molecular structures (Coates, 2000). Figure 7.9 reveals the infrared spectra of the stimuli responsive and non stimuli responsive systems, from the spectra attained it is noted that three distinct peaks are presented in both spectra whereby a broad band is observed representing O-H stretching due to hydrogen bonding as well as C-H stretching characteristic

of the presence of an aromatic compound. Figure 7.9a distinguishes the stimuli responsive broad band at 3258.55cm^{-1} and the control at 3255.77cm^{-1} in Figure 7.9b depicted in the figure. This signifies that the introduction of the stimuli responsive component (HA) as well as the crosslinker (ADH) provided greater stability and intensified the intermolecular and intramolecular bonds between the molecules. Furthermore both structures revealed a peak at 2165.56cm^{-1} and 2162.35cm^{-1} respectively in Figure 7.9a and 7.9b. The peak is attributed largely to the presence of a disubstituted medial alkyne group frequency representing C≡C stretching. A more intensified bond is noted in Figure 7.9a which can be attributed to the presence of the polymeric compounds HA as well as ADH providing greater conjugation to the presented bond due to the introduction of amine groups interacting with aldehyde groups exhibiting C=C and C=O stretching. Further peaks are seen at 1635.10cm^{-1} and 1632.54cm$^{-1.}$ This is attributed to skeletal vibrations representing a C=C stretch by the presence of an acetylenic compound whereby the band is more intensified in Figure 7.9a. Intensification of this bond in Figure 7.9a was largely attributed to formation of conjugated ketones due to crosslinking. Furthermore it was noted that a peak at 1034.83cm^{-1} was present in Figure 7.9a due to the presence of amino bonds (demarcated in the figure) by the addition of HA to the structure which is absent in the structure of Figure 7.9b. Thus from the observations made it was deduced that the process of crosslinking and addition of polymeric compounds provided greater intensity and conjugation to the molecular structure.

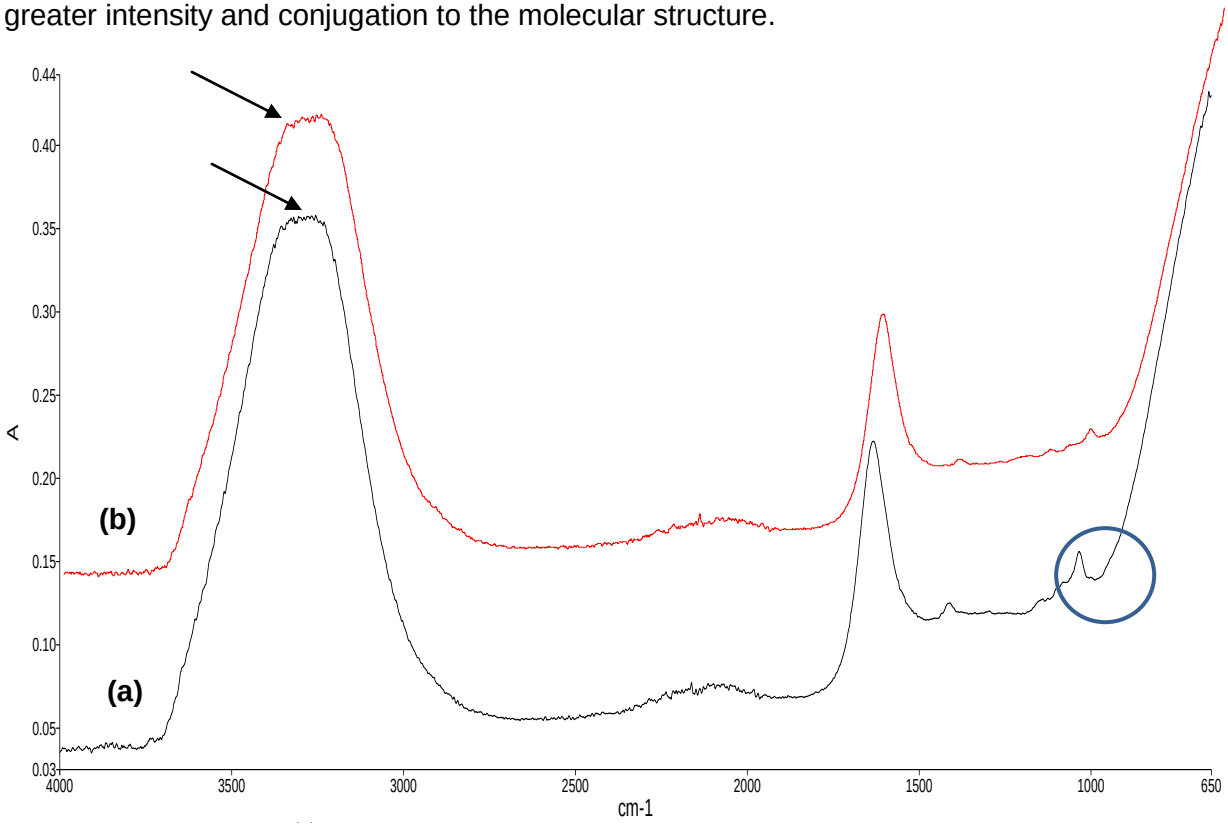

Figure 7.9: Molecular vibrational transitions of a: the stimuli responsive system and b: the non stimuli responsive system

7.3.6. Thermodynamic Evaluation of the Optimized BTDS Device

The DSC profiles for both the stimuli responsive and non stimuli responsive systems was obtained and is depicted in Figure 7.10. A distinct endothermic peak was observed for both formulations at 74.03°C and 102.67°C for the non stimuli responsive and stimuli responsive systems respectively. The presence of the peak relay to melting processes occurring at this point. A broad asymmetric melting peak characterised by Figure 7.10b as demarcated displayed a much quicker onset of melting at the temperature range indicated then the melting transitions occurring in Figure 7.10a of the stimuli responsive system. Furthermore it was noted that the endothermic melting peak observed was superimposed upon the glass transition temperature due to gradual enthalpy changes. From the temperature ranges indicated it was seen that the heat capacity required to cause a melting peak is greater for the stimuli responsive then the non stimuli responsive system. This was ascribed to the incorporation of a crosslinker to the system endorsing crosslinked bonds by intermolecular and intramolecular forces and linkages thus the heat energy required to cause a phase change such as melting is greater. Occurrence of this peak is attributed to polymorphism whereby melting occurs as a result of metastable modifications. Following this, an exothermic peak was then distinguished at 418.96°C and 258.65°C in the non stimuli responsive system contrasting to 236.52°C and 289.53°C in the stimuli responsive system. These temperatures obtained resembling an exothermic peak depicting cold crystallisation demonstrate a lower specific heat capacity for the stimuli responsive formulation thus the structure portrays a greater crystalline state in comparison to the control. A greater crystalline state of the structure designates that the system subsist to a greater molecular order and thus less molecular motion occurs between the particles thus the specific heat capacity required for amorphic phase change is less as depicted by the heat capacity temperatures obtained. Therefore it was deduced that the introduction of a crosslinker provides greater stability and molecular linking between molecules providing greater molecular order thus higher temperatures were required for thermal degradation. Furthermore ionic interactions between molecules further influence the enthalpy for thermal degradation of the system whereby a greater specific heat capacity was required for degradation of the stimuli responsive system.

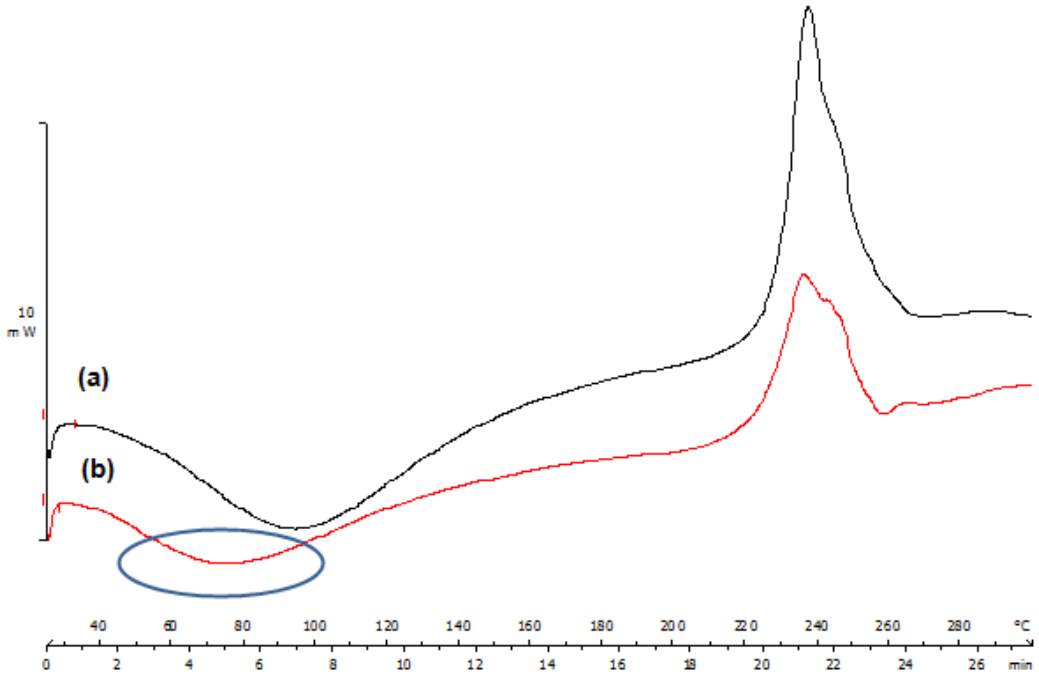

Figure 7.10: Thermographic profiles of a: the stimuli responsive system, b: the non stimuli responsive system

7.3.7. Topographical and Morphological determination of the Bioresponsive transdermal delivery system

For optimal design of the wound healing device, tailoring the microstructure for improved structural performance is of utmost importance. This was performed by the introduction of crystallinity and crosslinking of molecular structures thus advancing the chemical and mechanical properties. Figure 7.11 depicts the surface morphological imagery of the non stimuli responsive system and stimuli responsive system whereby the effects of polymeric addition and crosslinker was observed. From the imagery obtained it was seen that Figure 7.11b displays a greater fibril structure with a greater presence of fibrillogenesis in comparison to the control. Furthermore, interconnected porous sites were conspicuously seen which are attributed to the presence of a polymeric backbone presented by the addition of the crosslinker ADH and HA. It was clearly observed in Figure 7.11b that a more course molecular structure is attained due to the presence of ADH which lead to ionically associated domains and molecular cluster entanglements thus presenting with a greater polymeric backbone structure in comparison to the control thus improvising greater mechanical characteristics to the system with a more perceived and rigid structure. Figure 7.11a reveals the topographical surface imagery of the control whereby a clear split (tearing/cracking) was seen collectively with large porous sites as demarcated thus suggesting poor mechanical

attributes and a relatively weak structure in comparison to the optimized formulation due to the absence of a backbone structure.

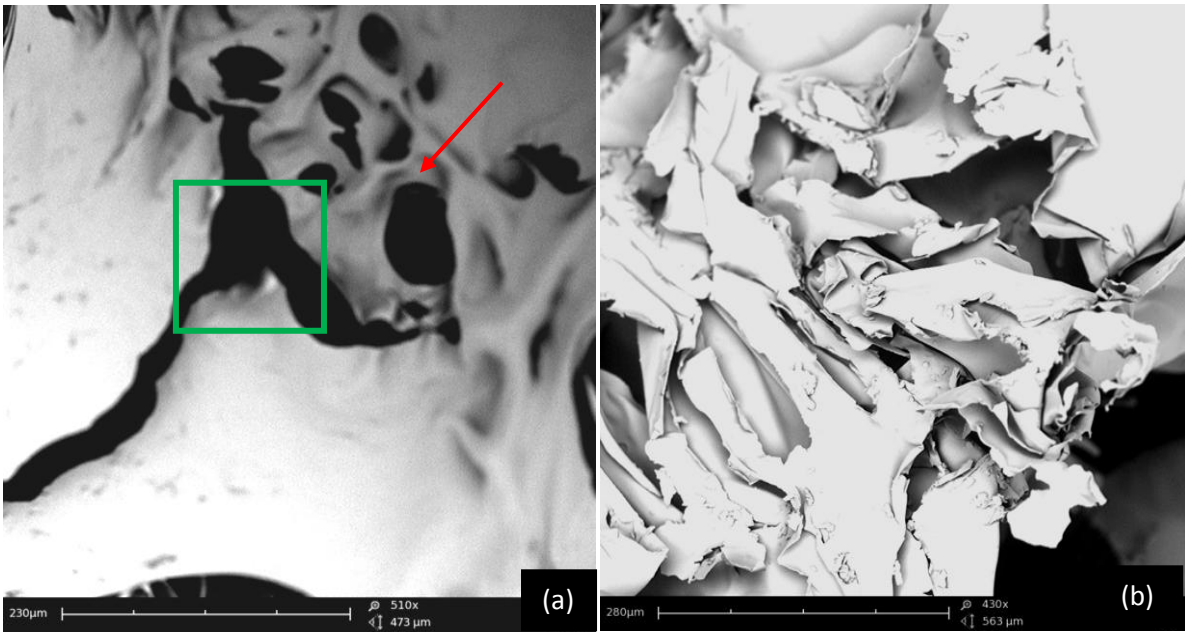

Figure 7.11: Surface topographical imagery of (a): Non stimuli responsive system and (b): Stimuli responsive system

7.3.8. Evaluation of the Tensile Strength and Young's Modulus of the Optimized System

Young's Modulus can be described as the stress ratio coefficient of a substance when a stress is applied causing an alteration in the shape and length of the body of the specific object due to the force applied. The Young's Modulus and elasticity of the system provides an intricate indicator of the material stiffness. The elastic modulus provides an understanding of the materials ability to regain its original geometry when the imposed stress is removed. A highly elevated Young's Modulus value indicates a lower compliance material or stiffer material thus presenting with a lower elastic modulus (Dupps and Wilson, 2006). Figure 7.12 and Table 7.4 represent the various physicomechanical characteristics of the systems. From the data obtained it was noted that the backing layer has the greatest Young's Modulus indicated by the linear portion of Figure 7.12C and thus the greatest strength and rigidity. This is essential and significant as the backing layer serves as the primary source of exposure to the outside foreign environment thus mechanical potency and strength is of utmost importance. A Young's Modulus of 3.92 E(MPa) was detected with a significantly greater tensile strength of 0.37N.mm^2. The backing layer been the primary outer layer of the device is subjected to the greatest tensile stress, therefore requires the greatest magnitude of strength. Table 7.4 reveals a Young's Modulus of 1.22 and 0.86E(MPa) in the stimuli responsive and non stimuli responsive systems respectively thus presenting with lower tensile characteristics in contrast to the backing layer. Furthermore, the ultimate strength of the various components of the BTDS revealed the greatest strength in the backing layer at

0.15θμ(MPa) in contrast to 0.03 and 0.02 θμ (MPa) in the stimuli responsive and non stimuli responsive systems respectively. In addition, the stiffness, strength and rigidity of the system play a vital role in the healing process. Evan and co-workers (2013) have stated that several studies have established the occurrence of wound healing with scar formation when mechanical tension is applied, thus tension reduction systems are more adequate to promote healing endorsing differentiation, proliferation and fibrillogenesis. Therefore based on this ideology, a more rigid backing layer structure provides more advantageous properties to the wound healing process. The introduction of a polymeric component (HA) and crosslinker (ADH) providing crosslinking moieties to the structure provides a polymeric backbone to the structure and intermolecular linkages between the molecules thus endorsing the mechanical stability of the device as indicated in Table 7.4. The positive influence of molecular crosslinking is further substantiated by the topographical surface morphology as shown in Section 7.3.7 of this chapter and the enhanced conjugation and intensity between molecular bonds as indicated by the infrared spectra of Section 7.3.5. From the nanomapping profiles obtained in Figure 7.12a and 7.12b it was noted that a more defined linear portion is surveyed in Figure 7.12a thus suggesting a greater Young's Modulus. Furthermore Figure 7.13 portrays the tensile strength profile revealing the mechanical characteristics of the system whereby it was noted that the stimuli responsive system shows a greater tensile strength of 0.265N.mm^2 in disparity to the non stimuli responsive system displaying a tensile strength of 0.11N.mm^2. Thus it was deduced that at the Young's Modulus and tensile strength obtained the stimuli responsive system portrays greater tensile characteristics then the non stimuli responsive system portraying enhanced stringency and at the same time displaying elastic properties making a suitable application for topical delivery whereas the non stimuli responsive system displays more feeble characteristics in terms of mechanics. A Young's Modulus of 1.22E (MPa) resembles an intermediate to moderate value thus avoiding the high rigidity and brittleness associated with a very high Young's Modulus value.

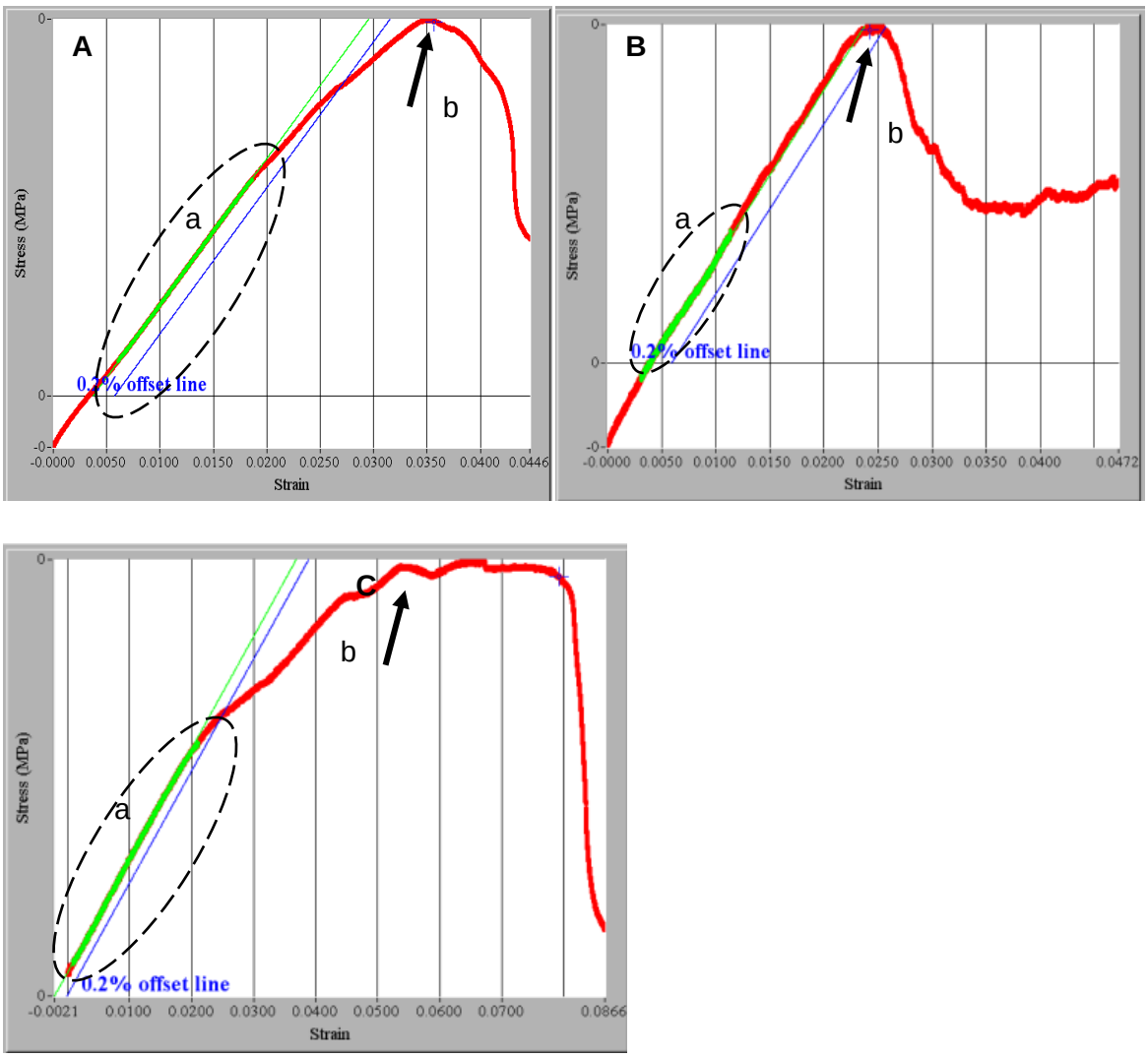

Figure 7.12: Nanomapping profiles revealing Young's Modulus (a) and fracture points (b) of A: Stimuli responsive system, B: Non stimuli responsive system, C: Backing Layer

Table 7.4: Physicomechanical analysis revealing the various values for evaluation in terms of mechanical characteristics

	Stimuli responsive system	**Non stimuli responsive system**	**Backing Layer**
Young's Modulus E(Map)	1.22	0.86	3.92
Yield Stress θγ(MPa)	0.03	0	0.10
Ultimate Strength θμ(MPa)	0.03	0.02	0.15
Ultimate Strain εμ	0.036	0.024	0.079
Tensile Strength (Nmm^2)	0.265	0.11	0.37

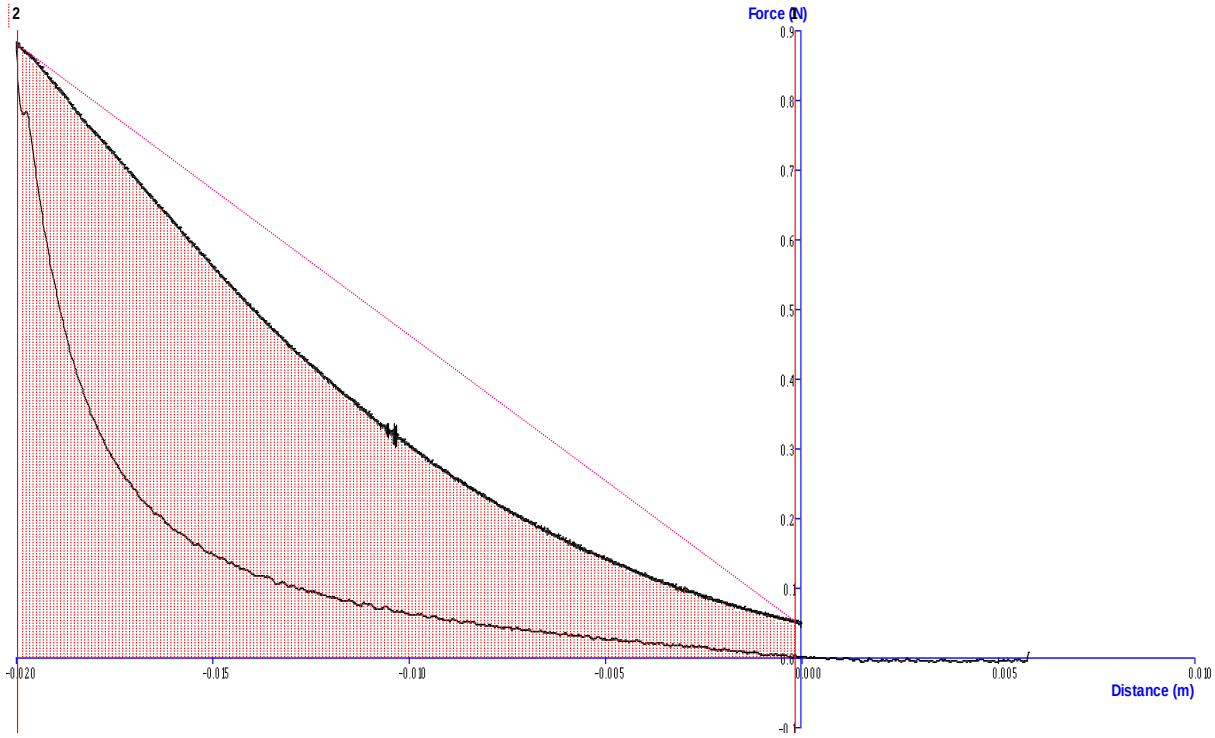

Figure 7.13: Characteristic tensile strength profile

7.3.9. Rheological Elucidation of the Stimuli Responsive and Non Stimuli Responsive Systems

When a tensile strength or shear stress is applied to a substance, its ability to resist gradual deformation can be termed the viscosity of the substance. Intermolecular and intramolecular interactions occurring between molecules giving rise to collisions between neighbouring particles in a fluid at altering viscosities can be termed as a property of viscosity. The maximum amount of stress or strain applied to the polymeric system upon which degradation occurs can be expressed as its yield stress. The polymeric systems composed of hyaluronic acid components whereby entangled coil formation occurs resemble a viscous solution with shear thinning behaviour. An increase in the shear rate revealed a decrease in the shear viscosity. The rheological behaviour in terms of its steady shear viscosity is dependent and controlled by the molecular weight as well as network entanglement (Ambrosio et al., 1999). At increased shear rates, interruption of the molecular entanglements is more prominent leading to shear thinning behaviour but is more dominant in the uncrosslinked non stimuli responsive system.

Oscillatory frequency studies revealed characteristics of the system in terms of its viscoelasticity whereby G'(ω) the shear storage modulus and G"(ω) the shear loss modulus was obtained. Energy stored within the system as well as the elasticity is characterised by G' whereas the G" parameter provides information regarding the heat energy dissipated as well as the viscous character of the system (Barbucci et al., 2000). Figure 7.14 reveal the stress-

strain frequency sweep profiles of the crosslinked stimuli responsive and non stimuli responsive systems. The viscous and elastic responses of these systems were detected through quantitative rheological evaluation whereby it was noted that the responses coincide and are related to the chemical structure and degree of crosslinking. Moreover the mechanical characteristics are also directly related and proportionate. From the profiles obtained it was noted that the elastic modulus is always higher than the viscous modulus in the non stimuli responsive (control) system as portrayed in Figure 7.14b, consequently depicting that the system possesses the features of 'gel-like' structures. As the stress-strain shear rate frequencies increased, the storage modulus revealing shear thinning behaviour also increased, detecting that the system reflects strain independent behaviour only for small deformation regions. Within the non stimuli responsive uncrosslinked system no to minimum entanglement occurs amongst polymer chains as the macromolecules in the structure may be deemed individual flow units. The rheological behaviour of the crosslinked stimuli responsive system portrays a different profile to that of the unresponsive system. The elastic modulus furthermore transpires at a higher frequency range as noted in Figure 7.14a then that of the non stimuli responsive system. The system portrays viscoelastic properties whereby at lower frequencies they exhibit shear independent behaviour. The process of crosslinking and molecular entanglement lead to the formation of a stable network also characterised by the process of hydrogen bonding and ionic interactions with a subsequent decrease in the intrinsic mobility (Barbussi et al., 2000). The crosslinked stimuli responsive system revealed a greater initial viscous modulus followed by an elevated elastic modulus, increasing over time and frequency thus displaying greater viscoelastic properties then the non stimuli responsive system consequently exhibiting enhanced mechanical properties and chemical interactions.

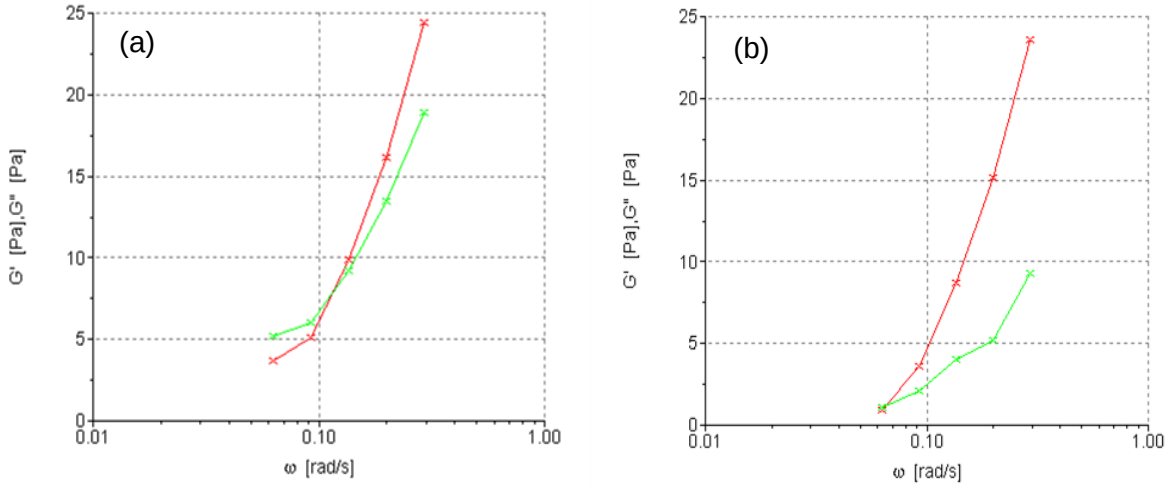

Figure 7.14: Pertinent rheological properties in terms of the G' and G" Modulus of a: Stimuli responsive system, b: non stimuli responsive system

7.4. Concluding Remarks

The optimized device showed a rapid response for bioactive release. A bioactive release rate is a significant requirement as it indicates the stimuli responsive bioactive behaviour to inflammation. The optimized device system has been proven to have responsive behaviour and furthermore increase the residence time of release. The mechanical properties were also enhanced by the formation of the crosslinked linkages as well as a polyelectrolyte complex. As observed in the topographical surface imagery a more course molecular structure is configured leading to a molecular backbone infrastructure which directly attributed to the mechanical characteristics and chemical interactions of the system as perceived by the infrared spectra, Young's Modulus and viscoelastic characteristics by means of the elastic Modulus.

Under the influence of Fenton's reagent, the system portrayed bioactive release in a more rapid manner whereas under normal saline conditions, bioactive release presented at a more dormant rate. Addition of ADH at 0.13%$^{w}/_{v}$ improved the residence time of release thus maintaining the bioactive concentrates throughout the process of the wound healing cascade and preventing burst release rates. Furthermore the anionic and cationic nature of the various polymeric components of the system further influenced the release rates due to the formation of a polyelectrolyte complex enhancing system performance.

CHAPTER 8
IN VIVO ANALYSIS OF THE MULTI-COMPONENT INFLAMMATORY RESPONSIVE BIOACTIVE DELIVERY DEVICE

The animals used in this study were approved by the Central Animal Services (CAS), Animal Ethics Screening Committee (AESC), University of Witwatersrand, Parktown, Johannesburg, South Africa. All experimental procedures were carried out in accordance with the AESC guidelines for the use and care of animals as pertained to the terms of Section 23 (1) (c) of the Veterinary and Para-Veterinary Professions Act (19 of 1982). (See Appendix 11.3)

8.1. Introduction

In vivo experimentation provides precise and supplementary information regarding the processes of what is occurring within the actual cell tissue or organism which may sometimes vary with *in vitro* experimentation as the physico-chemical properties *in vivo* are usually different from that of dilute aqueous solutions utilised to carry out the various *in vitro* tests (McConell. 1995).

The activity of the wound healing device will be subjected to the presence of exudates, inflammation and the wound site itself, thus the results obtained of *in vitro* data will merely mimick the *in vivo* environment and hence is not sufficient to provide accurate results and data. An *in vivo* model will provide optimal histopathological, pharmacokinetic and pharmacodynamic results. In addition observational data and more realistic clinical extrapolation can be successfully correlated.

In vivo experimentation provides insight to possible risks or side effects with the use of the device, since biomaterials are biodegradable and biocompatible and should not be associated with any ill effects. It is unethical to conduct such a study directly on human subjects therefore the Sprague-Dawley Rat was the animal of choice that serves as a suitable model due to its availability, low cost, small size and it is widely used in the study of skin wound healing and the efficacy of different treatment modalities. Charerensriwilaiwat and co-workers, 2012 investigated a lysosome loaded chitosan based nanofibre mat by subjecting an incision of 0.8 cm^2 at the back of the neck of all rats. In another study Ramli and Wong, 2011 evaluated the healing efficiency on the burn wound model in the rat by the use of heated deionised water on the dorsal area of the rats. This research focuses on conduction of a burn wound model and the subsequent healing process.

The purpose of this research was to design and develop a “smart” inflammatory responsive wound healing device intended to deliver the various bioactives to the targeted site at the determined time intervals significant to the wound healing cascade. Therefore, the device

structured of several components assembled in a manner best suited to the healing requirements as summarised in Figure 8.1. The device described was then employed for *in vivo* application to determine the healing success rates.

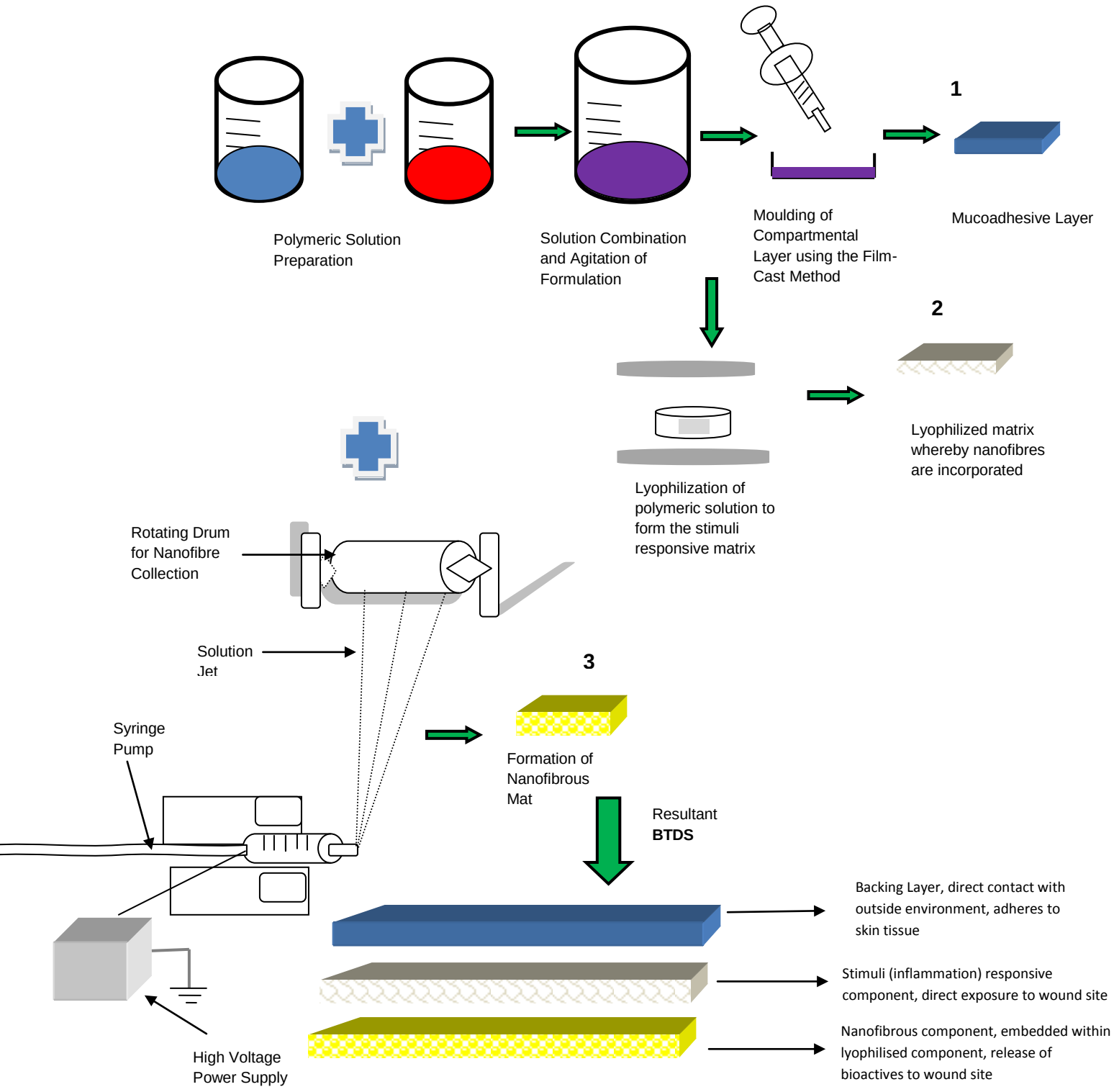

Figure 8.1: Schematic overview of the componential architecture and formulation of the BTDS

8.2. Materials and Methods

8.2.1. Materials

Sprague Dawley Rats were utilised in this research and obtained from the Central Animal Services (CAS) as per the protocol in accordance with University of Witwatersrand animal services guidelines. All elementary gear used was of ultrapure grade and obtained from the Central Animal Services unit of the University of Witwatersrand. Dental syringe obtained from the dental department of the University of Witwatersrand and H-Dent dental needles (27GX1-$^{3/8"}$) obtained from Hakusui Trading Co LTD. Osaka, Japan.

8.2.2. Animal Husbandry

The non-fasted rats were housed in groups of 5 initially and then in single cages for procedure purposes. The rats were provided with water and food in accordance with a standard rat diet *ad libitum* and maintained on a 12 hour light/12 hour dark cycle at a controlled temperature (+/-25°C). They were weighed weekly so as to indicate their general state of well being. Cage activity by means of observation for 1 hour periods daily was also carried out to assess their state of well being. Prior to *in vivo* experimentation, rats were acclimatised to laboratory conditions and held in vivarium for 7-14 Days. The South African Standard for care and use of animals for scientific purposes was followed to execute favourable housing conditions according to the relevant SOPs.

8.2.3. *In Vivo* Experimental Design

Thirty Sprague Dawley Rats within the weight range of 250-300mg were utilised within the *in vivo* animal study (Ethics clearance was obtained from the Animal Ethics Committee of the University of the Witwatersrand for this study, Ethics Clearance No 2013/24/05, see Appendix A). The rats were randomly assigned within six groups of five rats each (N=5 per group) whereby the experimental study consist of three experimental groups, a comparative group, control group and a placebo group. The various delivery systems were applied in accordance with the following criteria (Figure 8.2):

Group A: Experimental Group: Nanofibrous Mats
Group B: Experimental Group: Curcumin loaded films
Group C: Comparative Group: Conventional System
Group D: Control Group: Non Medicated Plain Gauze
Group E: Experimental Group: Inflammatory responsive device
Group F: Placebo Group: Non inflammatory responsive device

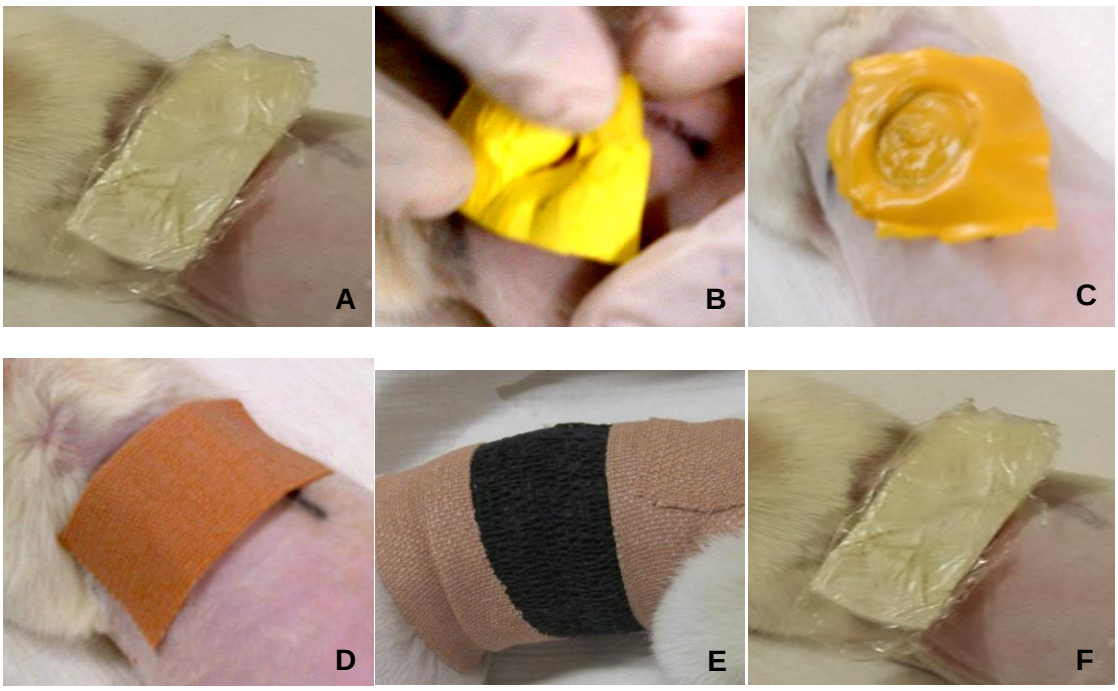

Figure 8.2: Photographic images pertaining to the administration of the various delivery systems whereby A is the inflammatory responsive device, B: nanofibrous mat, C: films loaded with curcumin, D: application of the conventional system, E: topical administration of non-medicated gauze and simple bandage and F: non inflammatory responsive device

8.2.4. Preparation of the Wound Area

Rats were made to lie dorsally whereby the hair of the upper back, dorsal region was removed by shaving using a sharp razor blade and disinfected using an alcohol swab. The rats were given jelly cubes medicated with Tramadol®, dosed at 4mg/kg 12 hours before the procedure and then twice a Day for a further 5 Days. All rats were premedicated with a dose of morphine 0.1ml/100g, 60 minutes prior to wound induction. Rats were anaesthetised in an Isofor gas chamber and an L-Block local anaesthesia using Xylotox® was induced once before creating the burn wound as indicated in Figure 8.3. (Ramli and Wong, 2007; Dr. Chetan Patel, Plastic surgeon in private practice running a study under the department of surgery, University of the Witwatersrand. Clearance certificate No.2010/48/04).

8.2.5. *In vivo* Surgical Procedure: Full thickness Wound Model

The burn wound was created as depicted in Figure 8.3 by using a metal probe with a diameter of 1.5cm that was heated to 99°C by insertion into boiling water and monitored using a mercury thermometer. Burn wounds were carried over a period of 10 seconds at a point that is 1.5cm's right laterally from the back midline towards the maxillary region of the rats and then covered with simple dry dressing to prevent the rats from scratching. After 48 hours, Isofor was used as an inhalation anaesthetic agent for maintenance of anaesthetia and the resultant dry area surgically removed to create a severe burn wound model (Aoyagi et al., 2007). The shape, diameter and depth of the burn wound were determined in all animals prior to application of the test samples. All rats were given Ringers solution post procedure to

avoid a hypovolemic shock. Throughout the preparation and surgical procedure the blood pressure and temperature was monitored using a BP monitor attached to the foot of the rats as seen in Fig 8.3 for all rats to ensure normality during experimentation. Wound dressings as depicted in Figure 8.2 were applied accordingly and held into place by self-adherent medical wrap and medical tape. All rats received an analgesic Tramadol® as necessary (Dr. Chetan Patel, Plastic surgeon in private practice running a study under the department of surgery, University of the Witwatersrand. Clearance certificate No. 2010/48).

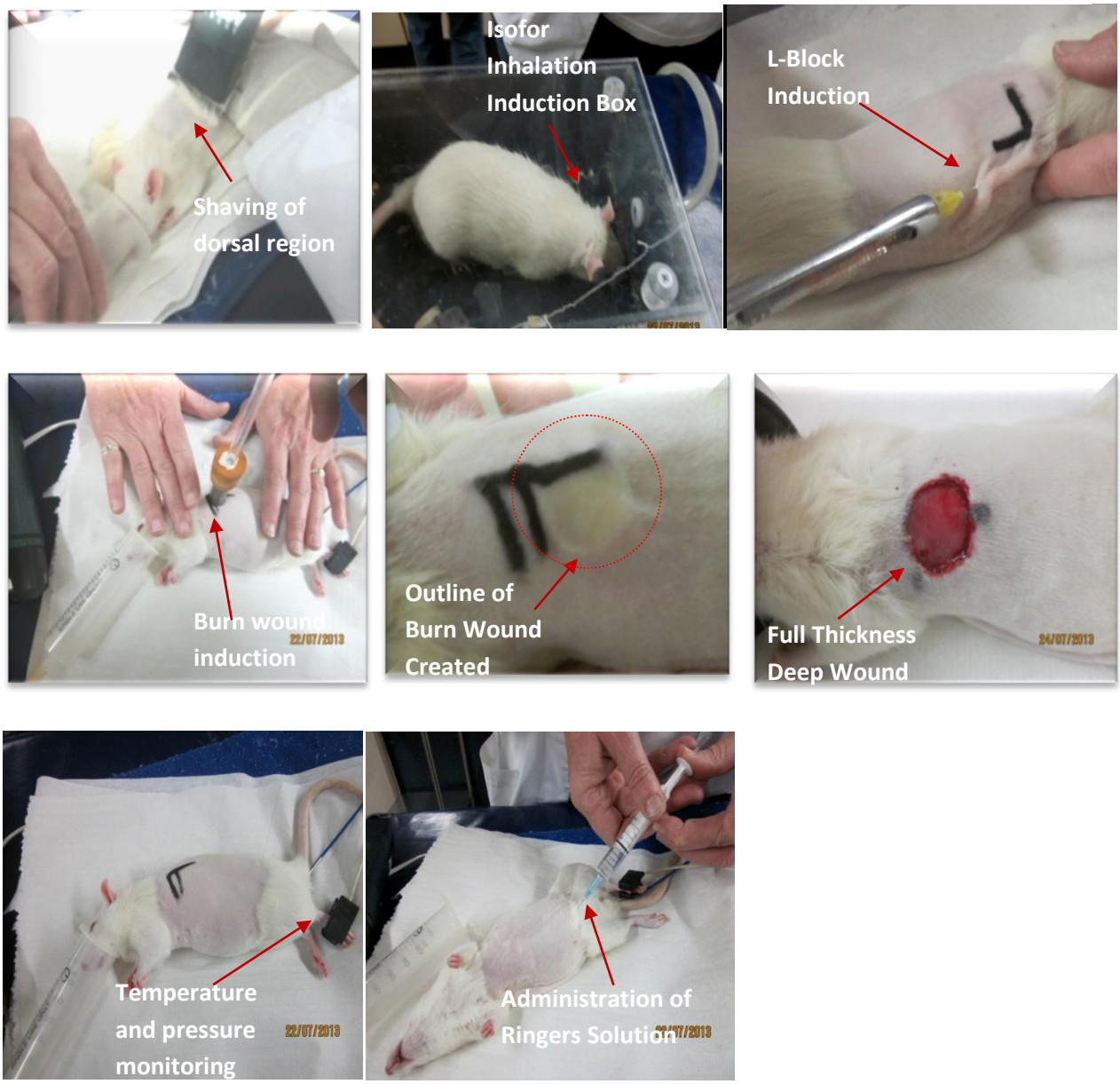

Figure 8.3: Surgical and preparatory procedure undertaken for burn wound induction

8.2.6. Macroscopic Determination by Percentage Wound Closure Evaluation

In order to determine the healing process during the experimentation period the wounds were photographed on Days 0, 5, 10, 15 and 20 post surgery. The Graphical Method was employed to determine the percentage (%) wound contraction by wound closure. This method involves the counting of the number of squares of retraced wound area or graph paper, to determine the wound

area reduction rate at different stages within the wound healing process. A ruler was used to determine the area of the wound site. The following formula was employed to determine the percentage (%) wound closure (Bindu et al., 2010).

$$\%\, Closure = 1 - \left({}^{Ad}/_{Ao}\right) \times 100 \qquad \text{[Equation 8.1]}$$

Where Ao = wound area on Day 0

Ad = wound area on the corresponding Days

8.2.7. Visual Comparative Analysis

A visual comparison was carried out whereby photography of the wound site on the dorsal region of the rat together with a indicator was undertaken to determine the wound contraction over time at the specified time intervals in order to determine the degree of wound healing on the dorsal wounded area in the control, placebo, comparative and experimental groups.

8.2.8. Histomorphological Examination to assess the Degree of Healing with the BTDS device

Experimental progress was monitored over a period of 20 Days. A rat from each group was sacrificed on Day 0, 5, 10, 15 and 20 post surgery as summarised in Figure 8.4. The wounded tissue, healthy tissue surrounding the wound including the wound bed was excised and collected for histological evaluated. The excised tissue was fixed in 10% neutral buffered solution (Siritienthong et al., 2012). From each of the formalin-fixed skin specimens a cross section area of ulcerated skin was excised and collected for histological evaluated according to standard operating procedure PTA-his-SOP-27. After tissue processing, wax blocks were produced (PTA-his-SOP-28) and sections of 5 - 6µm were cut on a microtome (PTA-his-SOP-30). The sections that were produced were stained in an automated Haematoxylin and Eosin stainer (PTA-his-SOP-205) before microscopical examination. Wound healing progression on a cellular level in terms of re-epithelisation, inflammation and granulation was determined by topographical observations.

8.2.9. Scores of Wound Healing Establishment as a Function of Time

Based on the data accumulated over the 20 Day *in vivo* test period and evaluated by H&E staining a score was set in place and in accordance with previously published data (Sariethong et al., 2012). Evaluation of the healing stages over time in terms of cell accumulation and granulation determination, variation of identified mediators and the degree of revascularization, epithelisation and keratinization was prepared (Siritienthong et al., 2012). Figure 8.4 provides a summary of the preparation and procedure methods undertaken for wound induction and healing evaluation.

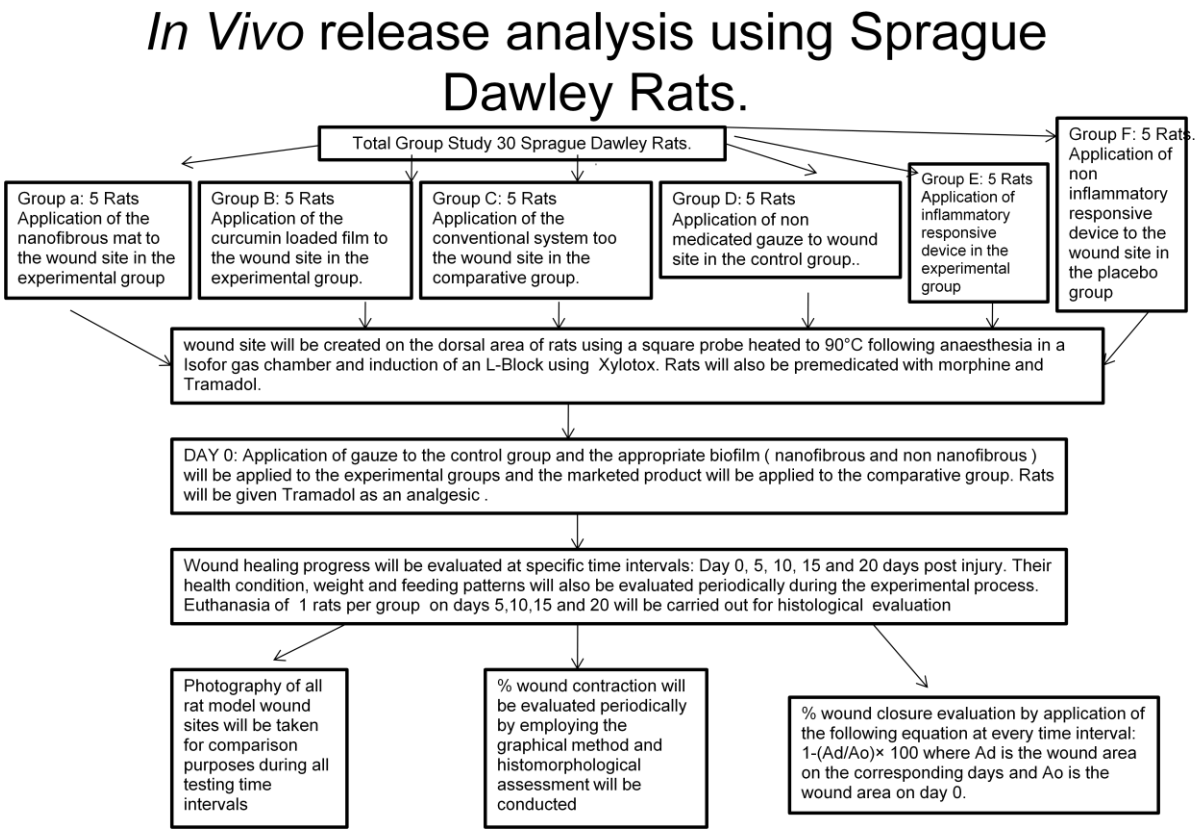

Figure 8.4: Summary of the preparation and *in vivo* surgical procedure for wound induction followed by methods undertaken to determine wound healing evaluation

8.3. Results and Discussion

8.3.1. Gross Observation of Wound by Photographic Analysis

The representative images of each group are depicted in Figure 8.5 whereby group A reveals the nanofibrous mat, group B is the film (curcumin loaded), group C is the conventional system, group D the control (non-medicated gauze), Group E is the inflammatory responsive system and Group F the “placebo” is the non inflammatory responsive device. At Day 5 post injury, the wound was still dominant in all groups however healing progression had begun by the presence of slight granulation tissue present more so in group A. Day 10 to 15 post injury clearly illustrated greater healing progression in all groups but is more prevailing in group A and group B by the process of granulation and epithelisation. On Day 20, wounds treated with nanofibrous mats revealed close to a 100% wound closure in comparison to the other groups followed by films in group B. This phenomenon is correlated to the structure of the nanofibrous mat which mimicks the natural ECM of the wound site as well as the additive and synergistic advantageous properties of the biopolymers used.

Figure 8.5 (ii) reveals digital photographic imagery of the experimental stimuli responsive device and the placebo, the non-stimuli responsive device. From the observation it was noted that wound healing activity transpired in both groups but is more dominant in the experimental stimuli

responsive group. Commencement of epithelisation can clearly be detected arising in a more rapid manner in Group E on Day 5 then in group F on Day 5 as the non-stimuli responsive device portrayed a greater degree of inflammation and slight granulation formation at this point. From an observatory point of view the healing progression was greatly advanced by Day 10 to 15 in both groups but remodelling is set in motion more notably in group E. Day 20 exhibited a close to 100% healing progression in group E and this can be attributed to the functioning of the nanofibrous mat as described above in this section as well as the enhanced function of the device attributed to its stimuli responsive nature. Furthermore the incorporation of hyaluronic acid serves as an advantageous attribute to the healing progression as it is a natural component found in the native ECM of the skin providing further healing properties which was omitted from the placebo group F.

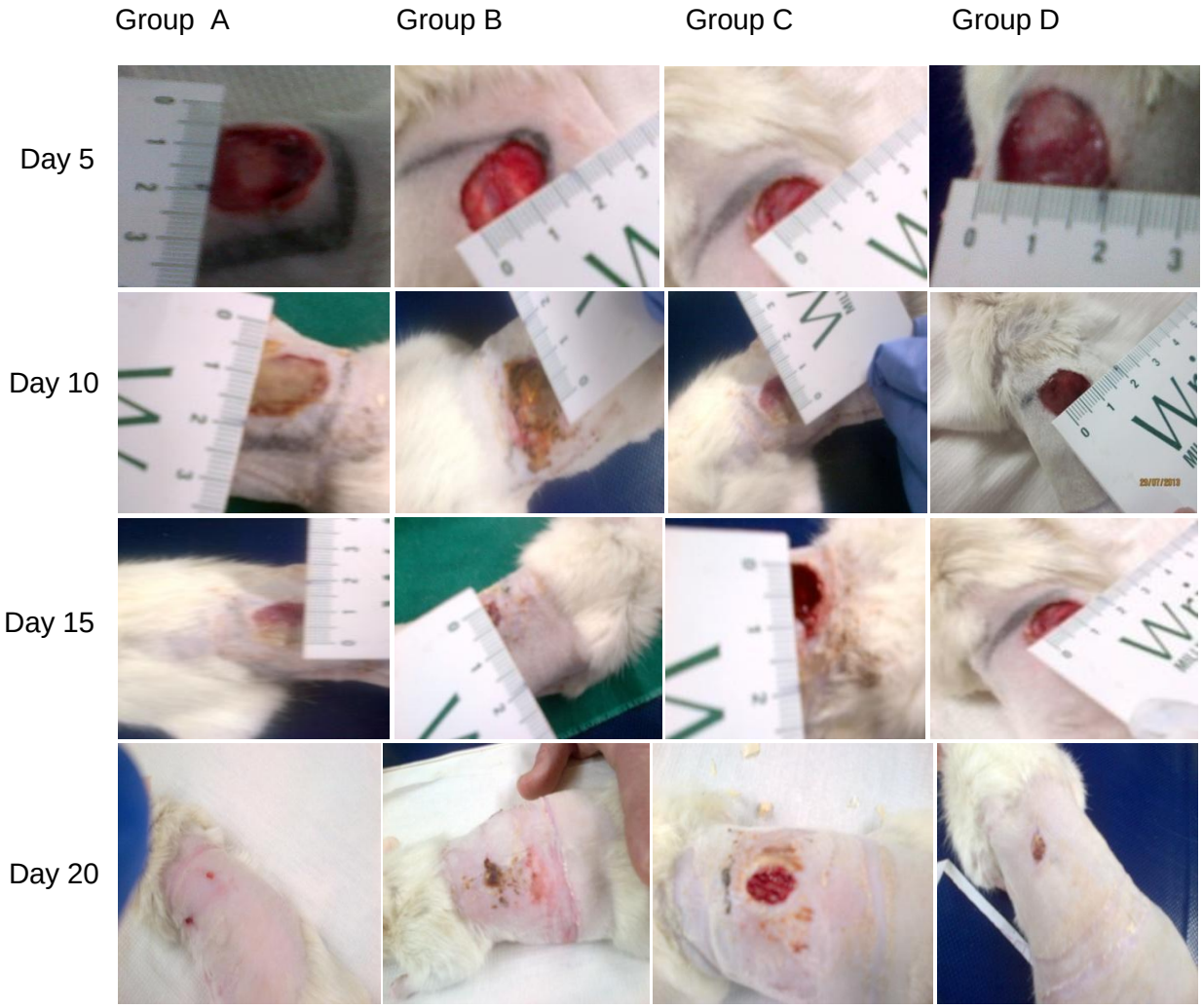

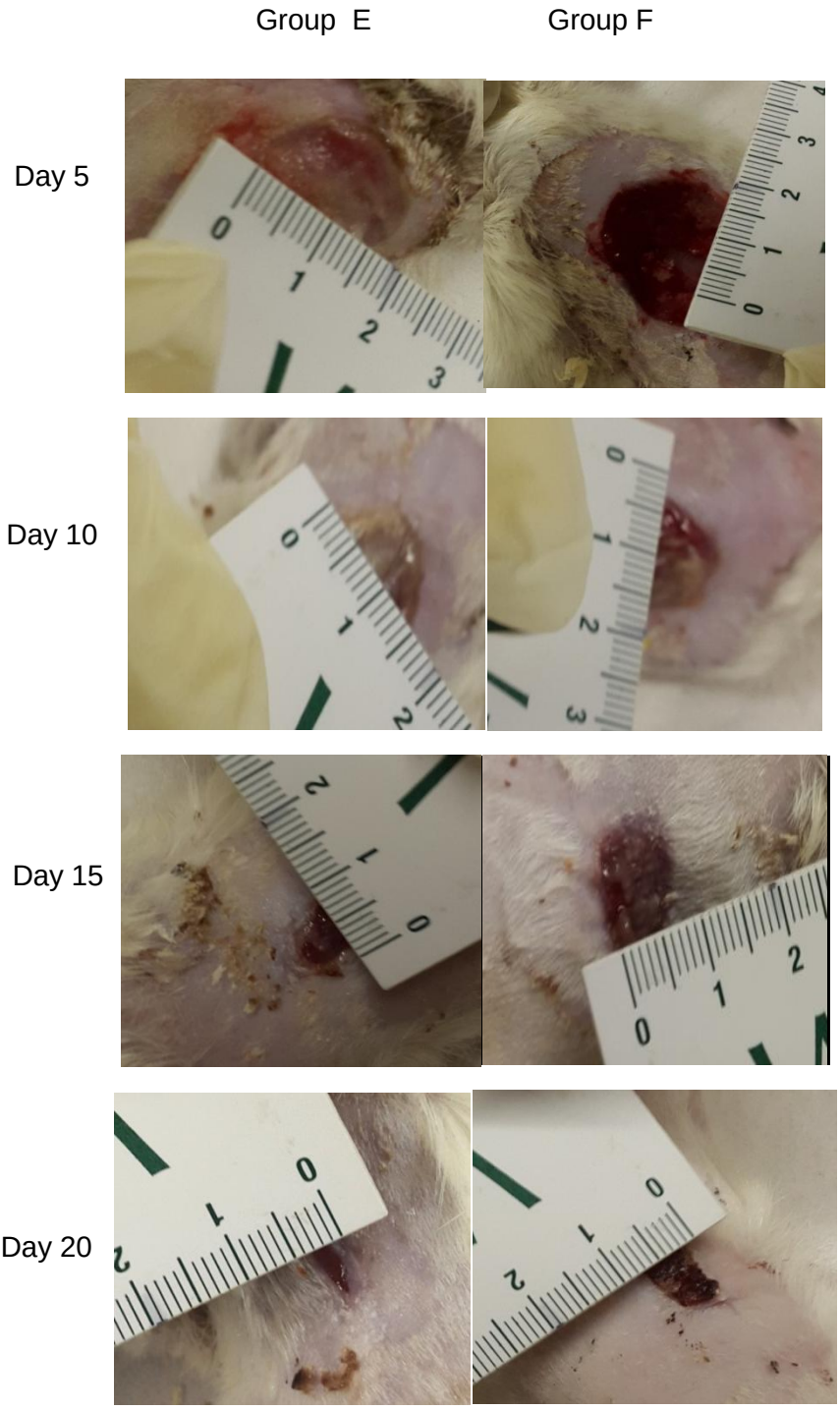

Figure 8.5: Photographic appearance of wounds (i) Group A: nanofibrous mat, Group B: Curcumin loaded film, Group C: Conventional system, Group D: Control, (ii) Group E: Stimuli responsive device, Group F: Non-stimuli responsive device

8.3.2. Wound Size Reduction Analysis by Wound Closure

Percentage wound closure was observed in all groups over the 20 Day period. Wounds treated with the nanofibrous mat disclose the greatest wound closure rate with the least scar formation in comparison to the simple non medicated gauze, conventional system and curcumin loaded films. The stimuli responsive system revealed a closure rate analogous to the nanofibrous mat though the healing progression occurs over a longer period of time as is in accordance with the phases of the wound healing cascade, thus the device will allow the

transpiration of healing over a prolonged period of time. Furthermore the rate of healing and closure rate was greater in the stimuli responsive system than the non-stimuli responsive system. Percentage wound closure rate on Day 20 revealed a wound closure rate of 99.94% for the wound healed with the nanofibrous mat, 94.88% for wounds treated with curcumin loaded films, 94.58% for wounds treated with non medicated gauze and 84.18% for wounds treated with the conventional system respectively. The stimuli and non-stimuli responsive devices depicted wound closure rates of 97.91% and 86.13% respectively. Figure 8.6 displays the wound closure rate (WCR) of the various wound healing delivery systems over the period of 20 Days (i.e.: 5, 10, 15 and 20 Days). From further observation it was noted that the nanofibrous mat adhered well to the wound site, configuring a pseudo skin structure whereby a closure rate of 99.94% was obtained with minimum scar formation. The development of a wound dressing in a nanofibrous form greatly influenced the healing progression as a subordinate wound closure rate was obtained from the curcumin loaded film at 94.88% on Day 20. Additionally throughout the healing process wound closure was dominated by treatment with the stimuli responsive device and the nanofibrous mat as demonstrated in Figure 8.6. Thus it was deduced that structuring a wound healing delivery system that configures with the natural extracellular matrix of the skin, positively influences the healing progression. Moreover, the formation of a stimuli responsive device incorporating the nanofibrous system as described provides targeted bioactive release as well as ensures the healing progression occurs over an advanced period of time. Additionally, biopolymers used such as chitosan causes a release of N-acetylglucosamine by measured depolymerisation initiating collagen deposition at the wound site by the proliferation of fibroblasts further stimulating hyaluronic acid synthesis (Archana et al., 2013). The antioxidant and antimicrobial properties of curcumin further accelerated the healing progression and hindered scar formation. The stimuli responsive system composed of hyaluronic acid as a polymeric component in the device thus directly providing advantageous properties such as tissue regeneration influencing the wound closure rate by epithelisation and fibrillogenesis.

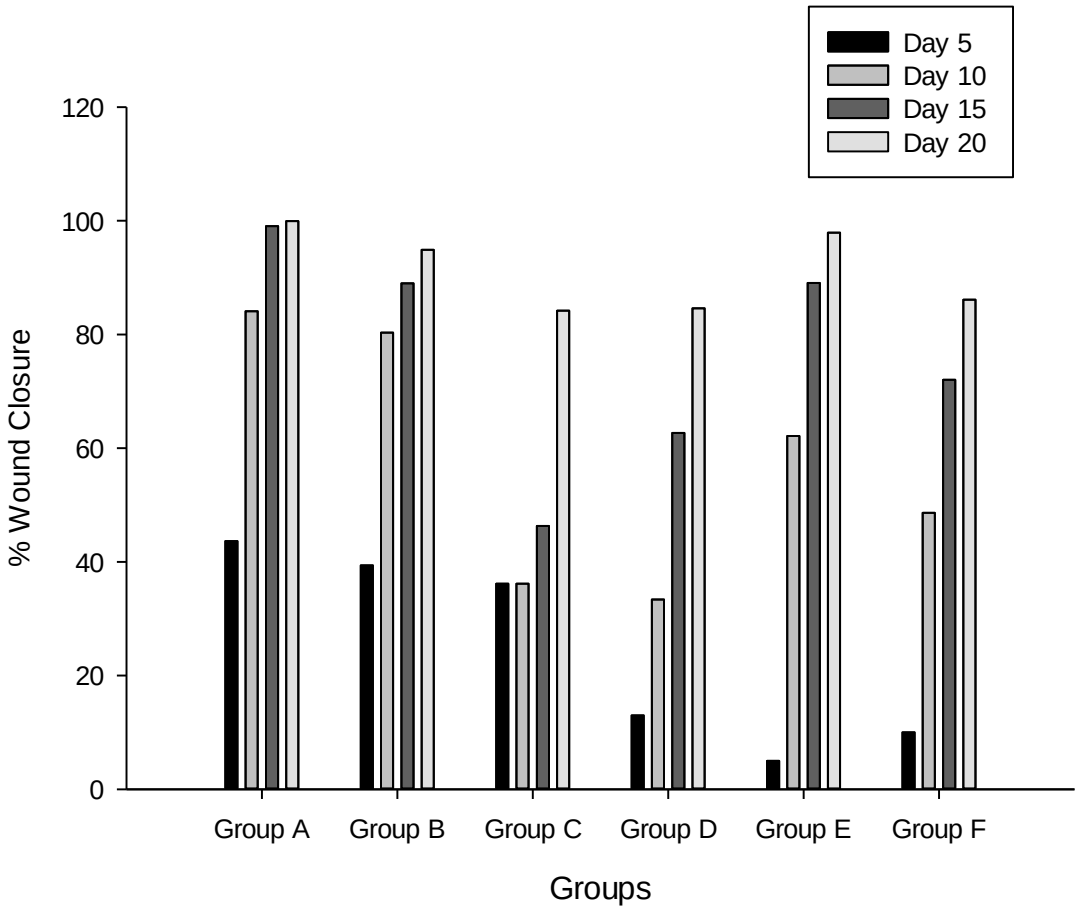

Figure 8.6: Percentage wound closure profile over the treatment 20 Day profile for Group A: Nanofibrous mat, Group B: curcumin loaded film, Group C: Conventional system, Group D: Control, Group E: Stimuli responsive system, Group F: Non-stimuli responsive system

8.3.3. Histopathological Evaluation of the Wound Site

An histological evaluation provides significant information regarding the condition of the inflicted wound site over time when topically treated with the various wound healing systems, i.e.: experimental groups (stimuli responsive system, nanofibrous mat and curcumin loaded film), control, placebo and conventional system. The H&E stained sections of healing wounds from the various groups under experimentation are illustrated in Figures 8.9-8.12 sectioned in accordance to the wound healing cascade occurring over the 20 Day period.

8.3.3.1. Ulceration and Wound Healing of the Tested Sample Specimens

Figure 8.7 reveals the presence of prominent ulcerative dermatitis in all group sections on Day 5 as depicted in Figure 8.7 a, c, d and f. This was exemplified by the presence of a hyperhaematoxylin stain showing the occurrence of thermal necrosis due to the implication of a burn wound. The stimuli and non-stimuli responsive systems revealed ulcerative dermatosis on Day 5 and Day 10 which relatively could also be experimentally induced as well. Prominent ulcerative dermatitis consisting of full-thickness ulceration with mild to minimal epithelisation has been recorded to continue throughout the 20 Day experimentation period in both the control and conventional groups including Day 15 and 20 as was seen in

the highly stained sections of Figure 8.7b and Figure 8.7g. Film application to the burn wound site resulted in the occurrence of only mild to moderate ulcerative dermatitis identified by the small ulcerated areas as demarcated in Figure 8.7e amid an advanced stage of regeneration and remodelling. Treatment with the nanofibrous mat resulted in complete re-epithelisation whereby absolute healing of the ulcer occurred by Day 15 to 20.

Figure 8.7i, 8.7j, and 8.7k depicts ulceration on Day 1 in the stimuli and non-stimuli responsive devices respectively whereby epidermal necrosis is more dominant in Figure 8.7k representative of ulceration and necrosis in the non-stimuli responsive device on Day 1. The necrotic tissue is prevalent in the image by the presence of a hyperhaematoxylin stain. The ulceration projected is referred to as epidermal necrosis and desquamation with exposure of the underlying dermis and superimposed secondary exudative inflammation. Figure 8.7h reveals the histological image of the non-stimuli responsive device on Day 20 demonstrating slight ulceration amid the epithelisation as demarcated in the figure which could possibly be experimentally induced. Severe ulcerative lesions were demonstrated in groups E and F from Day 1 to approximately Day 15 of the specimens but revealed a very mild to no grading by Day 20 of group E thus portraying an almost complete closure and healing progression in the stimuli responsive device.

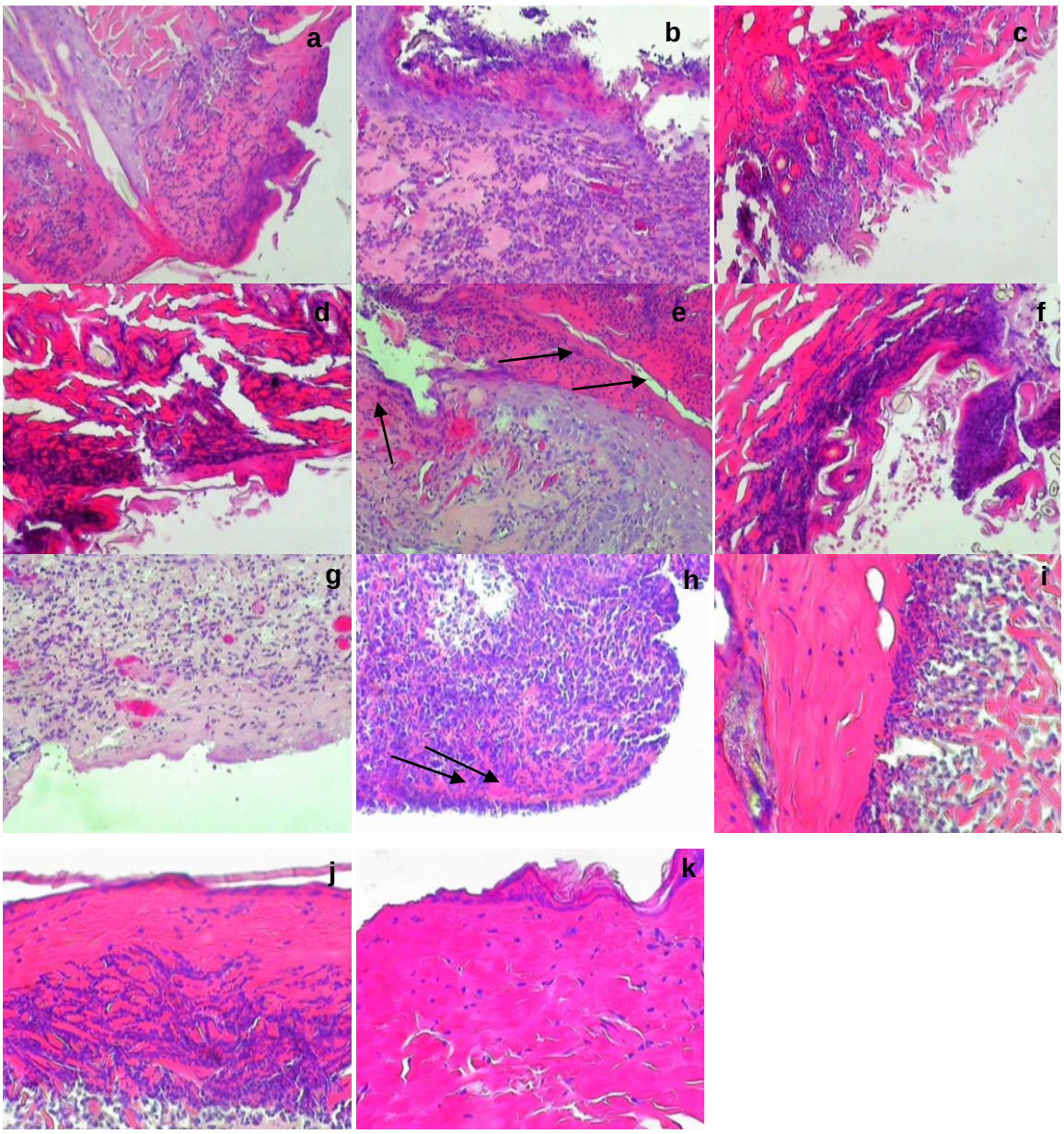

Figure 8.7: Histopathological characteristics in terms of ulcerative dermatitis of **(**a) Control Day 0, (b) control Day 20, (c) nanofibrous mat Day 0, (d) Film Day 0, (e) Film Day 20, (f) conventional Day 0, (g) Conventional Day 20, (h) non-stimuli responsive Day 20, (i) stimuli responsive Day 1, (j) and (k) non-stimuli responsive Day 1

8.3.3.2. Inflammation and Granulation of the investigated Specimens

Figure 8.8 portrays the various H&E wound sections that depict the process of granulation and inflammation. All groups revealed the commencement of the inflammatory process on Day 5. The base of the ulcer disclosed the formation of inflammatory infiltrates that was also identified at the dermal stroma. Infiltrates consisted of neovascularisation as demarcated in Figure 8.8 as well as polymorphonuclear leukocytes and mononuclear cells such as macrophages and lymphoplasma cells. On Day 5, granulating tissue appears to be more prominent in groups treated with the nanofibrous mat and curcumin loaded films whereas the control and conventional groups illustrate premature granulation formation whereby ulcerative dermatitis is still persistent in the control group on Day 5 as compared to the group

treated with the nanofibrous mat. The stimuli responsive and non-stimuli responsive device reveal the commencement of the inflammation and granulation phase by Day 5 although thin immature granulation tissue already begins to form by Day 1 of the stimuli responsive device as depicted by the image in Figure 8.8g. Slight inflammatory markers are still observed in the image of the stimuli responsive device amidst epithelisation as depicted in Figure 8.8h whereas granulation is noted on Day 15 in the non-stimuli responsive device demarcated in the figure (Figure 8.8i). Inflammation and granulation proportions appear to subdue by Day 20 in the groups treated with stimuli responsive device, nanofibrous mat and curcumin loaded films and is graded as mild, however is more dominant and persist longer (up to 20 Days) in the control categorized by the presence of thin immature granulation tissue and conventional group exhibiting inflammatory fibroplasia with moderate granulation tissue. The stimuli and non-stimuli responsive device reveal the instigation of inflammation at the base of the ulcer initially which appear to be exudative with the predominance of neutrophils in the early stages, while neovascularisation, granulation tissue development, infiltration of macrophages as well as fibroplasia are observed in the later stages. During the later stages of the healing process e.g. Day 20, the device reveals the presence of granulation tissue which is part of the normal healing process as well as extensive neovascularisation with domination of fibroblasts and collagen deposition was also noted.

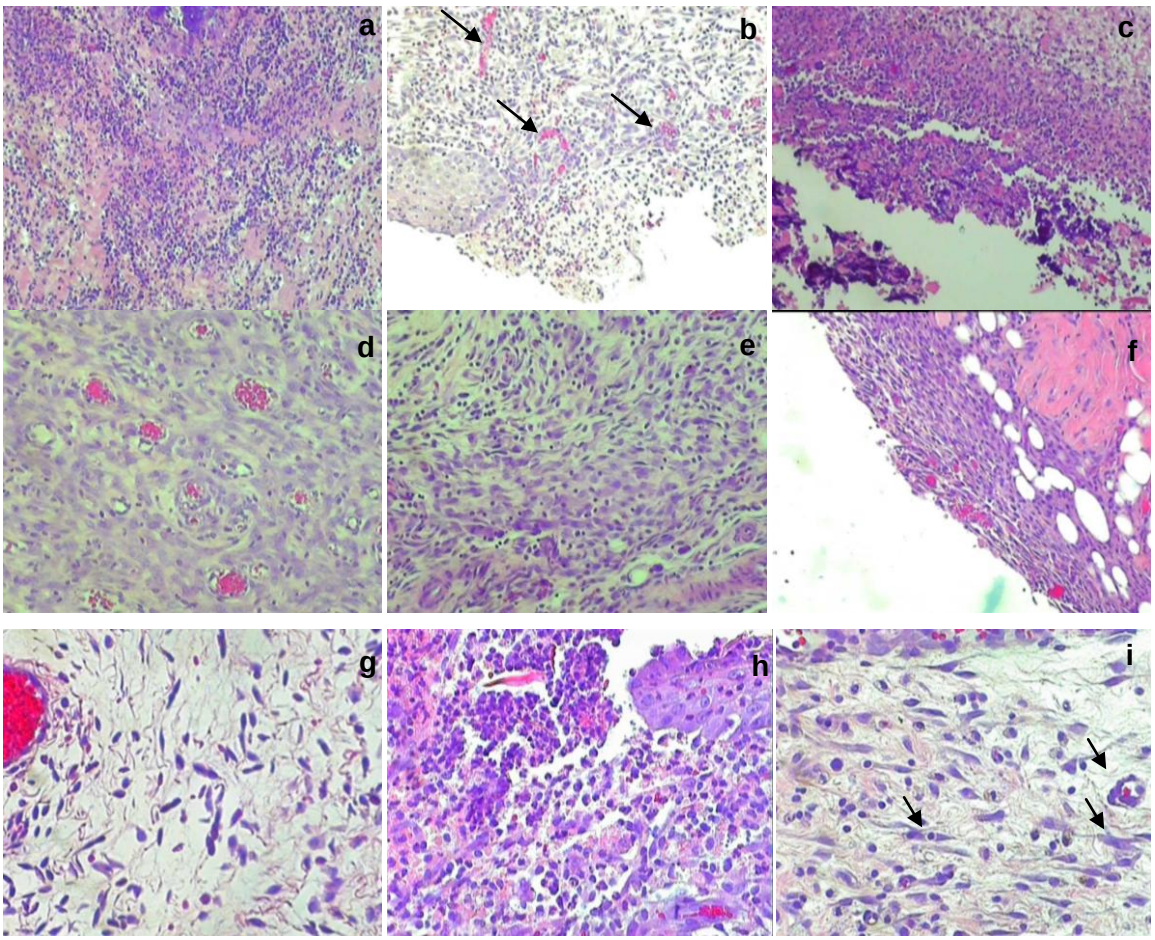

Figure 8.8: Histopathological analysis depicting inflammation in **(**a) nanofibrous mat Day 5; (b) nanofibrous mat Day 10; (c) Film Day 5; (d) conventional Day 5; (e) conventional Day 10; (f) Control Day 5, (g) stimuli responsive device Day 1, (h) stimuli responsive device Day 15, (i) non-stimuli responsive device Day 15

8.3.3.3. Epithelisation and Remodelling at the Wound Site over the 20 Day Period

Epithelisation within the healing process of an induced burn wound refers to development, by the progression of re-epithelisation of the ulcerated surface of the wound. This is characterised by proliferation whereby fibroblast and collagen deposition transpire to instigate skin regeneration by the configuration of epithelium and endothelium cells (Diegelmanns and Evans, 2004). Epithelisation starts from the periphery with growth occurring towards the centre of the ulcer. Proliferation and epithelisation dominates and occurs significantly in the group treated with the nanofibrous mat. By Day 15 to 20 complete re-epithelisation of the wound ulcerated surface occurs whereby total surface coverage of the wound prevails as seen in the figure. Epithelisation was most prominent in the group treated with the nanofibrous mat and stimuli responsive device whereby dermal collagen deposition within the extracellular matrix forming an epithelial layer prevails. Only moderately advanced epithelisation in the curcumin loaded films occur by Day 15 to 20. Epithelisation was clearly detected on the periphery of the specimen as demarcated in the histological image of the stimuli responsive device as shown in Figure 8.9i. Furthermore mild epithelisation was detected in Figure 8.9l of the non-stimuli responsive device as indicated in the figure.

Premature mild epithelium occurred at the edges of the ulcer as depicted in the figure and is detected in the control and conventional groups whereby inflammatory infiltrates still dominate.

Re-modelling refers to the final stage within the healing process whereby fibroblast activity involves the synthesis of collagen in the dermal stroma. Re-modelling entails the reorganisation of the newly synthesized collagen fibres to structure a further ordered lattice structure that has the potential to improve the tensile strength of the newly developed skin (Mackay and Miller, 2003). Siritienthong and co-workers refer to remodelling as thick vascular granulation tissue dominated by fibroblasts and extensive collagen deposition. Defects at this stage results in scarring and fibrosis. The representative images of the H&E wound sections in Figure 8.9 disclose prominent remodelling that is most pronounced in the stimuli responsive and nanofibrous group by Day 15. The results exhibit copious, compact and mature collagen type III fibres identified by the highly stained pink section on Day 15 of the nanofibrous mat treated wound. Furthermore on Day 15 curcumin loaded films reveal moderate remodelling from the granulation tissue. Mild ulceration is still present in the film treated group amidst the collagen deposition with fibroblast proliferation. Dominance of the remodelling stage was observed by the presence of collagen formation by Day 15 of the stimuli responsive device amidst the formulated granulation tissue. The haematoxylin stained fibril like structures clearly indicated the presence of collagen tissue with the occurrence of eosinically stained granulation tissue as can be seen in Figure 8.9h and 8.9j. Thus from the histomorphological image, wound healing progression was clearly detected on Day 15 of the stimuli responsive device as compared to Day 1 where apparent ulceration was noted as seen in Figure 8.6i. Prominent remodelling was surveyed by Day 20 of the stimuli responsive device as depicted in Figure 8.9k, however with the slight presence of fibrosis demarcated in the figure which is most likely to be due to an experimental error. Furthermore ulceration was also dominant in the conventional group on Day 15 to 20 which was furthermore distinguished in the photographic analysis. Re-modelling appeared to be mild to moderate by Day 20 and was graded as mild in the control group on Day 20. Interestingly, both the control and conventional groups disclose an increase in granulation and inflammatory intensity with time, however this prototype is in reverse with regards to the nanofibres and curcumin loaded films. The grading of epithelisation and remodelling intensifies with time.

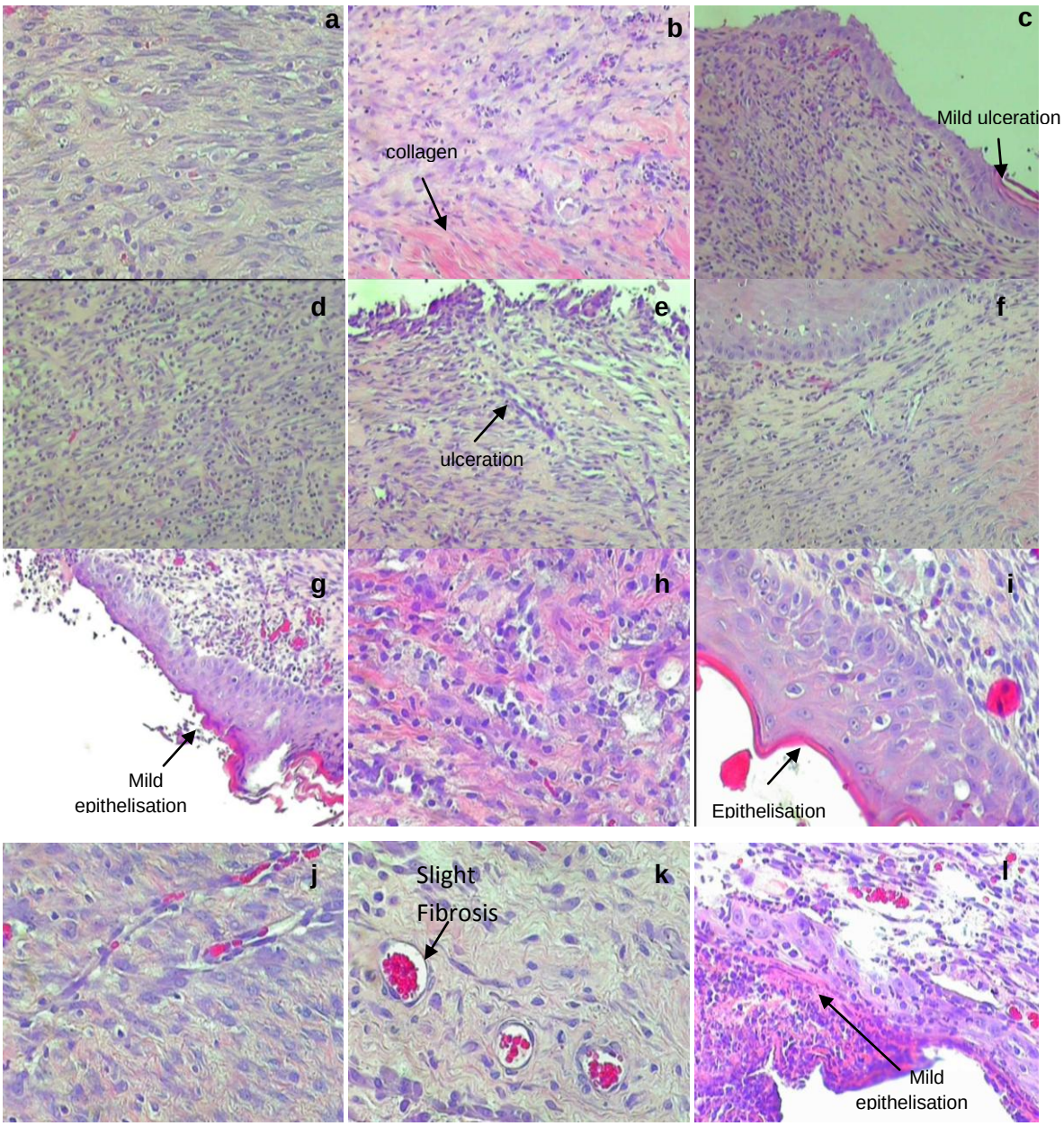

Figure 8.9: Histogram revealing rate of epithelisation and remodelling in **(**a) nanofibrous mat Day 20; (b) nanofibrous mat Day 15; (c) films Day 15; (d) films Day 10; (e) conventional Day 15; (f)control Day 15; (g) control Day 10; (h) stimuli responsive device Day 15; (i) stimuli responsive device Day 20; (j) stimuli responsive device Day 20; (k) stimuli responsive device Day 20; (l) non-stimuli responsive device Day 20

8.3.4. Wound Healing Scores

The wound healing score depicted in this chapter is designed on a score level of 8 stages depicting the various phases of healing that measures the progress of wound healing over time, whereby each score at the various stages represents wound tissue attributes produced by the applied system throughout the healing process. Table 8.1 (i), (ii), (iii) depicts the wound healing score of the wounds treated with the nanofibrous mat (group A), curcumin loaded film (group B), conventional system (group C) control (group D), stimuli responsive device (group E) and non-stimuli responsive device (group F). Significantly elevated healing

scores were obtained in the groups treated with the stimuli responsive device and the nanofibrous mat followed by the curcumin loaded film as correlates to the morphological characteristics obtained in Section 8.3.4. Subordinate scores were obtained for the conventional and control group over the 20 Day period. Scores were graded on a scale of – to 3+ whereby – signifies negative, 1+ signifies mild, 2+ signifies moderate and 3+ signifies prominent. Prominent ulceration was noted at 3+ in all groups at the commencement of the study, but was then graded low at a negative score for the stimuli responsive device and the nanofibrous mat by Day 20, but was still prevalent at 3+ in the control and conventional groups by Day 20. The films and non-stimuli responsive device revealed a mild level of ulceration by Day 20 at 1+. Severe granulation and remodelling was portrayed to be the highest at levels ranging from 10-12 (as indicated in the footnotes) in both the stimuli responsive device and the nanofibrous system from Day 10 to 20 perceiving the greatest healing effects occurring in group A and E. Inflammation and granulation was the most prominent on Day 5 of all groups at a score level of 2+ and 3+ declining in score level of group A, B, E and F over time surpassed by epithelisation and remodelling heading towards complete wound closure. However, group C and D depicted an increase in inflammatory rate over time suggesting subordinate healing closure by Day 20.

Table 8.1: Wound healing scores of the various groups where (i): Group A and B, (ii): Group B and C, (iii) Group D and E represented throughout the wound healing cascade

Groups (i)	**A: Day 0**	**A: Day 5**	**A: Day 10**	**A: Day 15**	**A: Day 20**	**B: Day 0**	**B: Day 5**	**B: Day 10**	**B: Day 15**	**B: Day 20**
Ulceration	3+	3+	2+	-	-	3+	3+	2+	1+	1+
Epithelisation	-	-	2+	3+	3+	-	-	2+	2+	2+
Inflammation/ Granulation	-	3+	2+	2+	1+	-	3+	2+	2+	1+
Remodelling	-	1+	2+	3+	3+	-	-	2+	2+	3+
Minimal Granulation										
Thin immature granulation							4			
Moderate granulation		7						9	9	
Severe granulation and collagen deposition			10	11	12					12

Groups (ii)	C: Day 0	C: Day 5	C: Day 10	C: Day 15	C: Day 20	D: Day 0	D: Day 5	D: Day 10	D: Day 15	D: Day 20
Ulceration	3+	3+	3+	3+	3+	3+	3+	3+	2+	3+
Epithelisation	-	-	-	1+	1+	-	-	2+	1+	1+
Inflammation/ Granulation	-	2+	2+	3+	2+	-	2+	3+	3+	3+
Remodelling	-	-	1+	1+	2+	-	-	1+	1+	1+
Minimal Granulation		3					3			
Thin immature granulation										6
Moderate granulation				7	9			8	8	
Severe granulation and collagen deposition										

Groups (iii)	E: Day 0	E: Day 5	E: Day 10	E: Day 15	E: Day 20	F: Day 0	F: Day 5	F: Day 10	F: Day 15	F: Day 20
Ulceration	3+	3+	2+	1+	-	3+	3+	3+	2+	1+
Epithelisation	-	-	-	2+	3+	-	-	-	1+	2+
Inflammation/ Granulation	1+	3+	2+	2+	1+	-	3+	3+	2+	2+
Remodelling	-	1+	2+	3+	3+	-	1+	1+	2+	2+
Minimal Granulation	2					1				
Thin immature granulation		5					4	4	5	6
Moderate granulation			7	9	11					
Severe granulation and collagen deposition				10	11					

Footnotes*: Scores were summarized as follows: - : Negative represents no cell accumulation, granulation or epithelisation; 1-3 represented none to minimal cell accumulation and granulation tissue; 4-6 represented thin, immature granulation dominated by inflammatory cells but with few fibroblasts, capillaries or collagen deposition; 7-9 represented moderately thick granulation tissue, ranging from being dominated by inflammatory cells to more fibroblasts and collagen deposition, extensive neovascularisation; 10-12 represented thick, vascular granulation tissue dominated by fibroblasts and extensive collagen deposition*

8.4. Concluding Remarks

In vivo morphological observations obtained indicate that treatment with nanofibrous wound dressings and more so incorporated as a stimuli responsive device achieved superlative and the fastest healing rates at a rate of 99.94% with comprehensive epithelial coverage and re-modelling indicated by the presence of mature collagen fibres that presented at an earlier stage in contrast to the other systems. Results obtained revealed that healing was superior in both group A and E, then B and F in comparison to group C and D. This can be attributed to the incorporation of biopolymers such as chitosan to the wound dressing that promote the healing process. Chitosan provides advantageous properties to the remodelling of the ECM during the healing process (Gopal et al., 2014) and simultaneously sustains exceptional healing in combination with the incorporated biopolymers. Incorporation of hyaluronic acid as

found in the stimuli responsive device favours the healing process as it is a natural component of the ECM of the native skin thus advancing regeneration. Integration of nanobiotechnology to contour nanofibres that have the ability to mimick the skin structure further endorse the healing process. Advancements by instilling bioresponsive systems prolong the healing activity of the device, ensures targeted responsive release ensuring superior healing characteristics. Furthermore the process of crosslinking with genipin provides advantageous properties to the nanofibrous system such as greater tensile strength and flexibility, resistance to decomposition, advanced nanofibre uniformity and orientation as can be seen by the characterisation results from FTIR, XRD and SEM as discussed in Chapters 6 and 7 of this thesis. Thus, the combination of nanobiotechnology, bioresponsive systems, desired biopolymers and acquaintance to the cellular and subcellular events occurring within the wound healing cascade endow vast possibilities to advance wound care and treatment.

CHAPTER 9
CONCLUSIONS, RECOMMENDATIONS AND FUTURE OUTLOOK

9.1. Conclusions

Within the African continent, thermal injuries and particularly childhood burns carry an extraordinary burden with ravaging consequences. An estimation of over a million individuals are burned annually on the African continent with an estimated mortality rate of 6 to 10% and a hospital admission rate of 18%. A survey carried out within the South African region revealed thermal injuries to be the most widespread origin of death due to external causes under the age of four years and the third universal basis for fatal injury casualties under the age of 18 (Rode et al., 2011). Within the United States it has been established that over 1.1 million burn injuries require medical attention every year, approximately 4500 deaths are been reported and 20 000 burn injuries require medical attention annually whereby burns occur involving at least 25% of their total body surface (CDC Injury Prevention, USA). Based on the statistical thermal injury rates across the globe it can be noted that prevention, adequate healing management and efficient wound care are vital criteria's that need to be put in place and implemented effectively.

Therefore, the BTDS device developed throughout this research has proven to be an efficient and effective means to manage wound care by the design of a biocompatible and biodegradable device that provides regulated bioresponsive bioactive release to the targeted wound site for the treatment and management of wounds in correspondence to the wound healing cascade. The effectiveness of the device has been exhibited through *in vivo* studies undertaken in the Sprague Dawley rat model exhibiting favourable outcomes for the stimuli responsive nanofibrous incorporated device.

Based on the aims and objectives revealed in Chapter 1 of this thesis, conclusions regarding the device are established as follows:

The study focused on the design of a topical delivery device for application on a targeted wound site in particular a wound caused by thermal injury. The most efficacious combinations of biopolymers, crosslinkers and bioactives was taken into consideration based on the pathophysiology, wound healing patterns and progressive course of injury to develop a novel conceptual device incorporating two major conceptions for wound bioactive delivery in accordance with inflammatory responsiveness.

Within the goal for establishing targeted, prolonged and controlled release for the treatment of debilitating wounds is the design of a novel polymeric device designed on a foundation based on advances in nanotechnology incorporating an intelligent mechanism that focuses

on stimuli (inflammation) responsive behaviour. This was established by means of creating a componential device as described in this thesis in a logical step-wise manner integrating the various significant functions as a novel approach delivering the various bioactive therapeutic agents that include bioactives with wound healing properties. Antibiotics, anti-inflammatory and growth factors can also be incorporated as wound healing agents. Establishment of the device in a componential manner endows the exhibition of a potentially marketable product for convenient application and consumer mobility.

Bioactive release from the BTDS on exposure to pathological (stimuli responsive) conditions and physiological (saline) conditions *in vitro* reveal a diverse pattern demonstrating prolonged bioactive release in the pathologically simulated exposed device. Under normal physiological conditions, elevated and continuous release patterns are seen irrespective of the presence on inflammatory infiltrates or not thus a greater propensity to toxicity, side-effects and inefficient therapeutic outcomes.

The research conversed throughout this thesis focused on the development of a device that exhibited characteristics mimicking the native skin and portraying a profile that is biodegradable, biocompatible, non-toxic, bioadherent and bioabsorbable. The formation of a nanofibrous mat with the use of biopolymers ensured the formation of a biostructure that mimicked the extracellular matrix (ECM) of the skin providing similar structural and physiological features as demonstrated in the *in vivo* studies of this thesis. Incorporation of hyaluronic acid, a natural component of the native ECM further enhanced this.

Determination of characteristics in terms of the physicomechanical and physicochemical nature by evaluation of the Young's modulus, storage and loss modulus, viscosity and chemical transitions provided a vast outline regarding the properties of the system. Sufficient flexibility, strength and mobility were portrayed making the device a suitable configuration for topical application.

9.2. Recommendations

The present thesis provided information and statistical data regarding the successful fabrication and implementation of the BTDS device upon *in vitro* and *in vivo* analysis. Characterisation evaluation undertaken provided significant data regarding pharmaceutical and clinical significance. However, based on the stimuli responsive behaviour of the device and its inclination to provide therapeutic properties over a longer period of time it is suggested that in future, the animal based (*in vivo*) preclinical trial study carried out be prolonged over a longer period of time, over and above the twenty day limited time phase thus providing further information regarding the healing progress to the data attained thus far.

To ascertain added precise functionality of the device as a wound healing treatment application, further analysis should be conducted in human subjects to determine the efficacy of the stimuli responsive device. It is further recommended that various other marketed products available for thermal injuries be evaluated under the same conditions employing the same techniques for comparative purposes thus establishing the advantageous healing potential of the device in comparison to those therapeutic agents already available.

Moreover, the device presented throughout this thesis can be employed for delivery of many other bioactives or potentially non-toxic drugs possessing wound healing properties, which include growth factors, mediators, antibiotics, antiseptics and inflammatories (NSAIDS). The ultimate goal for the development of the device, is to ensure marketability therefore introducing the novel system on the market. To ensure this scale-up procedures are of optimal importance. The present investigation is refined to acquisition of an optimal formulation and preclinical investigation thus it is relevant to consider product presentation and large scale manufacturing processes. Large scale manufacturing involves batch size amplification augmenting the device dimensions to fit the plant size as opposed to that produced in the laboratory, transfer of technology and integration of procedures (du Toit, 2013). Of significant importance for the production of the BTDS device is the nanofibrous mat formation. Techniques and incorporates should be put in place to ensure speedy fabrication of fibres when using deionised water as a solvent thereby enhancing the conductivity.

9.3. Future Outlook

Within the pharmaceutical field many novel opportunities can be created with regards to wound healing and application of topical systems. The development of the novel device provides many novel prospects whereby new and creative innovative technologies can be employed and incorporated to advance the therapeutic outcomes demonstrating desirable release behaviour, therapeutic efficacy and prolonged action. The device can be applied to a wide variety of bioactives that include agents which can be polymeric possessing wound healing qualities, growth factors, anti-inflammatory and antibacterials amongst others. In the interest of intellectual property protection a patent was filed and the projection of the research is aimed towards licensing of the technology with a recognised pharmaceutical company that will allow for economical growth and clinical expansion of the developed device. Introduction of this technology within the South African infrastructure will provide opportunities in the international biotechnology sector thus minimising the importation of generic products (Choonara, 2009).

10. References

Abdelrahman T and Newton H. 2011. Wound dressings: Principles and practice. Surgery (Oxford). 29,491-495

Adaramoye O.A, Anjos R.M, Almeida M.M, Veras R.C, Silvia D.F, Oliviera F.A. 2009. Hypotensive and endothelium-independent vasorelaxant effects of methanolic extract from Curcuma longa L in rats. Journal of Ethnopharmacology. 124, 457–62

Agarwal S, Wendorff J.H, Greiner A. 2008. Use of electrospinning technique for biomedical applications. Polymer 49, 5603–5621

Aggarwal B.B, Bhatt I.D, Ichikawa H, Ahn K.S, Sethi G, Sandur S.K, Natarajan C, Seeram N, Shishodia S. 2006. Curcumin — Biological and Medicinal Properties.7034, 297

Akhilender K. 2003. Vitamin C in Human Health and Disease, Nutritional Journal Review. 2, 7

Alemdaroglu C, Degim Z, Celebi N, Zor F, Ozturk S, Erdogen D. 2006. An investigation on burn wound healing in rats with chitosan gels formulation containing epidermal growth factor. Burns. 32, 319-327

Alvarez-Lorenzo C, Concheiro A. 2004. Molecularly imprinted polymers for drug delivery. Journal of Chromatography B. 804,1, 231-245

Ambrosio L , Borzacchiello A , Netti P.A, Nicolais L. 1999. Rheological study on hyaluronic

Amnuaikit C, Ikeuchi I, Ogawara K-I, Higaki K, Kimura T. 2005. Skin permeation of propranolol from polymeric film containing terpene enhancers for transdermal use. International Journal of Pharmaceutics. 289, 167– 78

Anilkumar T.V, Muhameda J, Jose A, Mohanan P.V, Lissy K, Krishnan L.K. 2011. Advantages of hyaluronic acid as a component of fibrin sheet for care of acute wounds. Wound Biologicals. 39, 81-88

Anumolu S.S, DeSantis A.S, Menjoge A.R, Hahn R.A, Beloni J.A, Gordon M.K, Sink P.J. 2010. Doxycycline loaded poly(ethylene glycol) hydrogels for healing vesicant-induced ocular wounds. Biomaterials. 31, 964–974

Aoyagi S, Onishi H, Machiba Y. 2007. Novel Chitosan Wound Dressing loaded with Minocycline for the treatment of severe burn wounds. International Journal of Pharmaceutics. 330, 2,138-145

Archana D, Dutta J, Dutta P.K. 2013. Evaluation of chitosan nano dressing for wound healing: Characterization, *in vitro* and *in vivo* studies. International Journal of Biological Macromolecules. 57, 193– 203

Asbill C.S, Mickmack B.B. 2000. Percutaneous penetration enhancers: Local versus transdermal activity. Pharmaceutical Science Technology Today 3, 36–41

Atiyeh B.S, Hayek S.N, Gunn S.W. 2005. New technologies for burn wound closure and healing- review of the literature. Burns. 31, 944-956

Atiyeh B.S, Ioannovich J, Al-Amm C.A, El-Musa K.A. 2002. Management of acute and chronic open wounds: The importance of moist environment in optimal wound healing. Current Pharmaceutical Biotechnology. 3, 179–195

Balakrishan B, Mohanty M, Fernandez A.C, Moharan P.V, Jayakrishnan A. 2006. Evaluation of the effect of incorporation of dibutyryl cyclic adenosine monophosphate in an in-situ forming hydrogel wound dressing based on oxidised alginate and gelatine. Biomaterials 27, 1355–1361

Bao P, Kodra A, Tomic-Canic M, Golinko M.S, Ehrlich H.P, Brem H. 2009. The role of vascular endothelial growth factor in wound healing. Journal of Surgical Research. 153, 347–358

Barbucci R, Rappuoli R, Borzacchiello A, Ambrosio L. 2000. Synthesis, chemical and rheological characterization of new hyaluronic acid-based hydrogels. Journal of Biomaterials Science, Polymer Edition. 11:4, 383-399, DOI: 10.1163/156856200743779

Barnes H. A, Walter K. 1985. The yield stress myth? Rheology Acta. 24, 323–6

Bawa P, Pillay V, Choonara Y.E, du Toit L.C. 2009. Topical Review. Stimuli-responsive polymers and their applications in drug delivery. Biomedical Materials. 4, 022001 (15pp)

Beppu M.M, Vieira R.S, Aimoli C.G, Santana C.C. 2007. Journal of Membrane Science. 301,126

Bharat B., (2008). Nanoscale characterization of human hair and hair conditioners. Progress in Materials Science, 53, 585-710.

Bhardwaj N, Kundu S.C. 2010. Electrospinning: A fascinating fibre fabrication technique. Research Review Paper. Biotechnology Advances. 28, 325-347

Bhuvaneshwari S, Sruthi D, Sivasubramanian V, Niranjana K, Sugunabai J. 2000. Development and characterization of chitosan films. International Journal of England Research and Applications (IJERA). 1(2), 292–9

Bhuveneshwari T, Thiyagarajan M, Geetha N, Venkatachalam P. 2014. Bioactive compound loaded stable silver nanoparticle synthesis from microwave irradiated aqueous extracellular leaf extracts of Naringi crenulata and its wound healing activity in experimental rat model. Acta Tropica. 135, 55–61

Bigi A, Cojazzi G, Panzavolta S, Roveri N, Rubini K. 2002. Stabilisation of gelatine films by crosslinking with genipin. Biomaterials. 23, 4827-4832

Bindu T.V.L, Vidyavathi M, Kavitha K, Sastry T.P, Kumar S, R.V. 2010. Preparation and evaluation of chitosan-gelatin composite films for wound healing activity. Trends in Biomaterials. Artificial Organs. 24,123–130

Biondi M, Ungaro F, Quaglia F, Netti P.A. 2008. Controlled drug delivery in tissue engineering. Advanced Drug Delivery Reviews. 60, 229–242

Bishop S.M, Griffith B, Linnane P.G, Lydon M.J, Shaw H. 2010. Patent US7759537B2

Boatang J.S, Matthews K.H, Stevens H.N.E, Eccleston G.M. 2008. Wound Healing Dressings and Drug Delivery Systems, A review. Journal of Pharmaceutical Sciences. 97, (8), 2892-2900

Boatang J.S, Pawar H.V, Tetteh J. 2013. Polyox and carrageenan based composite film dressing containing anti-microbial and anti-inflammatory drugs for effective wound healing. International Journal of Pharmaceutics. 441, 1-2, 181–191

Boateng J.S, Matthews K.H, Stevens N.E, Eccleston G.M. 2008. Wound Healing Dressings and Drug Delivery Systems: A Review. Journal of Pharmaceutical Sciences. 97, 8,2892-2923

Bolton L, Fattu A.J. 1994. Topical agents and wound healing. Clinical Dermatology. 12, 95–120

Bourke S.L, Al-Khalili U, Briggs T, Mickniak B.B, Kohn J, Poole-Warren L.A. 2003. A photo crosslinked poly(vinyl-alcohol) hydrogel growth factor release vehicle for wound healing applications. American Association of Pharmaceutical Sciences (AAPS), Pharm Sci Tech 5, E33

Bowler P.G, Davies B. 1999. The microbiology of infected and noninfected leg ulcers. International Journal of Dermatology. 38, 573–578

Branski L.K, Gauglitz G.G, Herndon D.N, Jeschke M.G. 2009. A review of gene and stem cell therapy in cutaneous wound healing. Burns 35, 171–180

Braund R, Tucker I.G, Medlicitt N.J. 2007. Hypromellose films for the delivery of growth factors for wound healing. Journal of Pharmacy and Pharmacology. 59, 367-372

Brigham P.A, McLoughlin E. 1996. Burn incidence and medical care use in United States: estimate, trends, and data sources. Journal of Burn Care and Rehabilitation. 17,95-107

Brocchini S, Duncan R. 1999. Encyclopaedia of controlled drug delivery; Mathiowitz, E, Ed. New York, NY: Wiley. pp 786–816.

Brook I. 1996. Microbilogy and management of sinusitis. Journal of Otolaryngology. 25, 249–256

Broudriot U, Dersh R, Griener A, Wendorff J.H. 2006. Electrospinning approaches toward scaffold engineering—A brief overview. Artificial Organs 30,785–792

Burns, CDC injury prevention. Department of Health and Human Services, USA. National centre for health statistics (NCHS). 1998. National vital statistics system. Hyattsville (MD): US department of health and human services. CDC, National centre for health statistics

Butler M.F, Ng Y-F, Pudney P.D.A. 2003. Mechanism and Kinetics of the Crosslinking Reaction between Biopolymers Containing Primary Amine Groups and Genipin. Journal of Polymer Science: Part A: Polymer Chemistry. 41, 3941–3953

Buyuktimkin N. 1997. Transdermal drug permeation enhancement in transdermal and topical drug delivery systems; Ghosh T, Yum S, Pfister W, Eds. Buffalo Grove, Illinois: Interpharmaceutical Press, pp 357–475

Cabane E, Zhang X, Langowska K, Palivan, Meier W. 2012. Stimuli-Responsive Polymers and Their Applications in Nanomedicine, In Focus: Nanomedicine – Review,.Biointerphases. 7,9, 1-27

Cai W, Gupta R.B. 2002. Hydrogels. Kirk-Othmer Encyclopedia of Chemical Technology. 1-20

Cairns J. 1975. Mutation selection and the natural history of cancer. Nature 255, 197–200

Canal C, Gaboriou F, Villeger S, Cvelbar U, Ricard A. 2009. Studies of antibacterial dressings obtained by fluorinated post-discharge plasma. International Journal of Pharmaceutics. 367, 155–161

Caramella C.M, Bonferoni M.C, Rossi S, Sandri G, Ferrari F, Perotti C.G, Del Fante C. 2011. Patent US2011280952 A1

Carter C.A, Jolly D.G, Worden Sr C.E, Hendren D.G, Kane C.J.M. 2003. Platelet-rich plasma gel promotes differentiation and regeneration during equine wound healing. Experimenatal and Molecular Pathology. 74, 244–255

Cevher E, Sensoy D, Taha M.A.M, Araman A. 2008. Effect of Thiolated Polymers to Textural and Mucoadhesive Properties of Vaginal Gel Formulations Prepared with Polycarbophil and Chitosan. American Association of Pharmaceutical Sciences (AAPS) PharmSciTech. 9, 3

Chambers C.W, Proctor C.M, Kabler P.W. 1962. Bactericidal effect of low concentrations of silver. Journal of American Water Works Association. 54, 208–216

Chang W.E, Chang Y, Lai P.H, Sung H.W. 2003. A genipin crosslinked gelatine membrane as a wound dressing material: *in vitro* and *in vivo* studies. Journal of Biomaterial Science. Polymer Edition. 14, 5, 481-495

Charernsriwilaiwat N, Opanasopit P, Rojanarata T, Ngawhirunpat T. 2012. Lysozyme-loaded, electrospun chitosan-based nanofiber mats for wound healing. Pharmaceutical Nanotechnology. International Journal of Pharmaceutics. 427, 379-384

Chen F.M, Zhang M, Wu Z.F. 2010. Towards delivery of multiple growth factors in tissue engineering. Biomaterials 31, 6279–6308

Chen S-C, Wu Y-C, Sung H-W. 2004. A Novel pH Sensitive Hydrogel Composed of N,O-Carboxymethyl Chitosan and Alginate Crosslinked by Genipin for Protein Drug Delivery. Journal of Controlled Release. 96(2), 285-300

Chen S-Z , Tsao C-T, Chang C-H, Lai Y-T, Wu M-F, Chuang C-N, Chou H-C, Wang C-K, Hsieh K-H. 2013. Assessment of reinforced poly (ethylene glycol) chitosan hydrogels as dressings in a mouse skin wound defect model. Materials Science and Engineering. C 33, 2584–2594

Choi J.K, Jang J.H, Jang W.H, Kim J, Bae I.H, Bae J, Park Y.H, Kim B.H, Lim K.M, Park J.W. 2012. The effect of epidermal growth factor (EGF) conjugated with ion-molecular-weight protoamine (LMWP) on wound healing of the skin. Biomaterials. 33, 8579–8590

Choi Y.S, Hong S.R, Lee Y.M, Song K.W, Park M.H, Nam Y.S. 1999. Study on gelatine containing artificial skin. I. Preparations and characteristics of novel gelatine-alginate sponge. Biomaterials. 20, 409-417

Chong E.J, Phan T.T, Lim I.J, Zhang Y.Z, Bay B.H, Ramakrishna S, Lim C.T. 2007. Evaluation of electrospun PCL/gelatin nanofibrous scaffold for wound healing and layered dermal reconstitution. Acta Biomaterialia. 3, 321–330

Choonara. Y.E. 2013**.** *In Vivo* evaluation of a novel donut-shaped minitablet for intraocular implantation. A thesis submitted to the Faculty of Health Sciences, University of the Witwatersrand, in fulfilment of the requirements for the degree of Doctor of Philosophy

Chow Y.S, Lee J.W, Lee J.S, Lee J.H, Yoon T.R, Kuroyanagi Y, Park M.H, Pyun D.G, Kim H.J. 2002. Hyaluranic acid and silver sulfadiazine impregnated polyurethane for wound dressing applications. Journal of Material Science. Material Medicals. 13, 861–865

Christian P, Von der Kammer F, Baalousha M, Hofmann T. 2008. Nanoparticles: Structure, properties, preparation and behaviour in environmental media. Ecotoxicology 17, 326–343

Chung H.J, Park T.G. 2007. Surface engineered and drug releasing pre-fabricated scaffolds for tissue engineering. Advanced Drug Delivery Review. 59, 249–262

Churochkina N.A, Staroduubstev S.G, Khokhlov A.R. 1998. Swelling and collapse of the gel composite based on neutral and slightly charged poly (acrylamide) gels containing Na-montmorrillonite. Polymer Gel Network. 6, 205–215

Coates J. 2000. Interpretation of infrared spectra, A practical approach. Encyclopedia in Analytical Chemistry. 10815-10837

Cohen S. 1983. The epidermal growth factor (EGF). Cancer 51, 1787–1791

Cooper R. 2005. A review of the evidence of the use of topical antimicrobial agents in wound care. World Wound 11, 46–52

Corkhill P.H, Hamilton C.J, Tighe B.J. 1989. Synthetic hydrogels. VI. Hydrogel composites as wound dressings and implant materials. Biomaterials. 10, 3–10

Cromack D.T, Porras- Reyes B, Mustoe T.A. 1990. Current concepts in wound healing: Growth factors and macrophage interaction. Journal of Trauma. 30, S129-S133

Cross-section of skin. Accessed June 6, 2014, at: http://www.infovisual.info/0./0.36-en.html

Crovetti G, Martinelli G, Issi M, Barone M, Guizzardi M, Campanati B, Moroni M, Carabelli A. 2004. Platelet gel for healing cutaneous chronic wounds. Transfusion and Apheresis Science. 30, 145–151

Crowder M.L, Gooding C.H. 1997. Spiral wound, hollow fibre membrane modules: a new approach to higher mass transfer efficiency. Journal of Membrane Science. 137, 17-29

Dabney S.E. 2002. The use of electrospinning technology to produce wound dressings. A thesis Submitted to the University of Akron in full requirements of a PhD dissertation. PhD Dissertation. The university of Akron.

Dagby K.B, Jalando-on K.P. 2008. Swelling and mechanical properties of genipin crosslinked chitosan (poly (ethylene glycol)) hydrogel network. Research Journal of Chemistry and Environment. 12, 24

Dao T.T, Nguyen P.H, Wonb H.K, Kim E.H, Park J, Wond B.Y. 2012. Curcuminoids from Curcuma longa and their inhibitory activities on influenza A Neuraminidases. Food Chemistry. 134(1), 21–8

Darzynkiewic Z and Balazr E.W. 1971. Effect of connective tissue intercellular matrix on lymphocyte stimulation. Experimental Cell Research. 66, 113-123

Dash M, Chiellini F, Ottenbrite R.M, Chiellini E. 2011. Chitosan- A versatile semi-synthetic polymer in biomedical applications. Progress in Polymer Science. 36, 981-1014

Datta H.S, Mitra S.K,and Partwarden B. 2011. Wound Healing Activity of Topical Application Forms Based on Ayurvedav, Evidence Based Complement Alternative Medicines.134-378

Davies D.J, Ward R.J, Heylings J.R. 2003. Multi-species assessment of electrical resistance as a skin integrity marker for *in vitro* percutaneous absorption studies. Toxicology *in vitro*. 18, 351–8

Debra J.B, Cheri O. 1998. Wound healing: Technological innovations and market overview. Technology Catalysts International Corporation. 2, 1–185

Deitzel J.M, Kosik W, McKnight S.H, Ten N.C.B, Desimone J.M, Crette S. 2002. Electrospinning of polymer nanofibers with specific surface chemistry. Polymer. 43, 3, 1025–9

Delcea M, Mo¨hwald H, Skirtach A.G. 2011. Smart polymers and their applications. Advanced Drug Delivery Review. 63, 730–747

Denuziere A, Ferrier D, Damour O, Domard A. 1998. Chitosan-chondroitin sulphate and chitosan-hyaluronate polyelectrolyte complexes: biological properties. Biomaterials. 19, 1275–1285

Deodato B, Arsic N, Zentilin L, Galeano M, Santoro D, Torre V. 2002. Recombinant AAV vector encoding human VEGF165 enhances wound healing. Gene Therapy. 9, 777–785

Dersch R, Steinhart M, Boudriot U, Greiner A, Wendorff J.H. 2005. Nanoprocessing of polymers: applications in medicine, sensors, catalysis, photonics. Polymer Advanced Technology. 16, 276–282

Diegelmann R.F, Evans M.C. 2004. Wound healing: An overview of acute, fibrotic and delayed healing. Frontier Bioscience. 9, 283–289

Diez-Sales O,Dolz M, Hernandez M.J, Casanovas A, Herraez M. 2007. Acyclovir Delivery Matrices Based on Poly (Ethylene Glycol)/ Chitosan Semi Interpenetrating Networks. Acyclovir Delivery Matrices Based on Poly (Ethylene Glycol)/ Chitosan Semi-Interpenetrating Networks. Journal of Pharmaceutical Sciences. 96, 6

Dong Y, Ruan Y, Wang H, Zhao Y, Bi D. 2004. Studies on Glass Transition Temperature of Chitosan with Four Techniques. Journal of Applied Polymer Science. 93, 1553–1558

Douglas M, Miller A.L. 2003. Review: Wound Healing, Nutritional support for wound healing. Alternative Medicine Review. 8, 4

Dr. Chetan Patel, Plastic Surgeon in Private Practice running a Study under the Department of Surgery, University of the Witwatersrand. Clearance certificate No. 2010/48/04

Du Toit L.C. 2013. A Bioresponsive Polymeric Implant for Site-Specific Prolonged Drug Delivery. A thesis submitted to the Faculty of Health Sciences, University of the Witwatersrand, in fulfilment of the requirements for the degree of Doctor of Philosophy, 2013

Duan B, Dong C, Yuan X, Yao K. 2004. Electrospinning of chitosan solutions in acetic acid with poly (ethyleneoxide). Journal of Biomaterials Science. Polymer Edition. 15, 6,797-811, DOI: 10.1163/156856204774196171

Dulmovits B.M, Herman I.M. 2012. Microvascular remodelling and wound healing: A role for pericytes. International Journal of Biochemistry. Cell Biology. 44, 1800–1812

Duncan R. 2003. The dawning era of polymer therapeutics. Nature Review Drug Discovery. 2, 347–360

Duo T, Tanaka M, Huang Y.Y, Hamblin M.R. 2011. Chitosan preparations for wounds and burns: Anti-microbial and wound healing effects. Expert Review of Anti Infective Therapy. 9, 857–879

Dupps W.J, Wilson S.E. 2006. Biomechanics and wound healing in the cornea. Experimental Eye Research. 83(4), 709-720

El-Kamel A, Sokar M, Naggar V, Gamal SA. 2002. Chitosan and sodium alginate-based bioadhesive vaginal tablets. American Association of Pharmaceutical Scientist (AAPS) Pharmaceutical Sciences. 4, 44

Eming S.A, Whitsitt J.S, He L, Krieg T, Morgan J.R, Davidson J.M. 1999. Particle-mediated gene transfer of PDGF isoforms promotes wound repair. Journal of Investigative Dermatology. 112, 297–302

Eriksson E, Yao F, Svensjo T, Winkler T, Slama J, Macklin M.D. 1998. In vivo gene transfer to skin and wound by microseeding. Journal of Surgical Research. 78, 85–91

Evan N.D, Oreffo R.O.C, Healy E, Thurner P.J, Man Y.H. 2013. Epithelial mechanobiology, skin wound healing, and the stem cell niche. Journal of Mechanical Behaviour of Biomedical Materials. 28, 397-409

Falabella A.F. 2006. Debridgement and wound bed preparation. Dermatology Therapy 19, 317–325

Falanga V. 2005. Evaluation of bilayered cell therapy for full thickness excision wounds: A multicenter, prospective, randomized, controlled trial. Wound Repair Regeneration. 13, A4-A27

Falanga V.1988. Occlusive wound dressings: Why, when, which? Architecture in Dermatology. 124, 872–877

Fan L, Du Y, Zhang B, Yang J, Zhou J, Kennedy J.F. 2006. Preparation and properties of alginate/carboxymethyl chitosan blend fibers. Carbohydrate Polymers. 65,447–452

Felgner P.L, Ringold G.M. 1989. Cationic liposome-mediated transfection. Nature 337, 387–388

Flemming R.G, Murphy C.J, Abrams G.A, Goodman S.L, Nealey P.F. 1999. Effects of synthetic micro- and nano-structured surfaces on cell behaviour. Biomaterials 20, 573–588

Flowers M.E. 1990. Long-term transplantation of canine keratinocytes made resistant to G418 through retrovirus-mediated gene transfer. Proc Natural Academy Sciences. USA 87, 2349–2353

Fong H, Chun I, Reneker DH.1999. Beaded nanofibers formed during electrospinning. Polymer. 40, 4585–4592

Galeano M, Deodato B, Altavilla D, Squadrito G, Seminara P, Marini H. 2003. Effect of recombinant adeno-associated virus vector-mediated vascular endothelial growth factor gene transfer on wound healing after burn injury. Critical Care Medicine. 31, 1017–1025

Gallant-Behm C.L, Hildebrand K.A, Hart D.A. 2008. The mast cell stabiliser ketotifen prevents development of excessive skin wound contraction and fibrosis in red Duroc pigs. Wound Repair Regeneration. 16, 226–233

Gao D, Heimann R.B. 1993. Structural and mechanical properties of superabsorbent poly (acrylamide) montmorrilonite composite hydrogels. Polymer Gel Network. 1, 225–246

Gao L, Gan H, Meng Z, Gu R, Wu Z, Zhang L, et al. 2014. Effects of genipin cross-linking of chitosan hydrogels on cellular adhesion and viability. Colloids Surfactant B: Biointerfaces. 117, 398–405

Gathin G. 2007. The significance of surface pH in chronic wounds. Wounds UK, Wound Healing Science. 3, 3, 53-56

George M, Abraham T.E. 2006. Polyionic hydrocolloids for the intestinal delivery of protein drugs: Alginate and chitosan — a review. Journal of Controlled Release. 114, 1-14

Gil E.S, Hudson S.M. 2004. Stimuli responsive polymers and their bioconjugates. Progression in Polymer Science. 29, 1173–1222

Giovino C, Ayensu I, Tetteh J, Boateng J.S. 2012. Development and characterisation of chitosan films impregnated with insulin loaded PEG-b PLA nanoparticles (NPs): a potential approach for buccal delivery of macromolecules. International Journal of Pharmaceutics. 428, 143–51

Goldberg M, Langer R, Xinqiao J. 2007. Nanostructured materials for applications in drug delivery and tissue engineering. Journal of Biomaterial Science Polymer. 18, 241–268

Goliger J.A, Paul D.L. 1995. Wounding alters epidermal connexin expression and gap junction-mediated intercellular communication. Molecular Biology Cell 6, 1491–1501

Gopal A, Kant V, Gopalakrishnan A, Tandan S.K, Kumar D. 2014. Molecular and cellular pharmacology: Chitosan-based copper nanocomposite accelerates healing in excision wound model in rats. European Journal of Pharmacology. 731, 8–19

Gopinath D, Ahmed M.R, Gomathi K, Chitra K, Srhgal P.K, Jayakumar R. 2004. Dermal wound healing processes with curcumin incorporated collagen films. Biomaterials. 25, 1911-1917

Govindjee S, Sackman J.L. 1999. On the use of continuum mechanics to estimate the properties of Nanotubes. Solid State Communications. 110, 227–230

Granick M, Boykin J, Gamelli R, Schultz G, Tenenhaus M. 2006. Toward a common language: Surgical wound bed preparation and debridgement. Wound Repair Regeneration. 14, S1–S10.

Green I.S, Jansen J.A, van der Waerden J.P, von Recum A.F. 1994. Fibroblast response to microtextured silicone surfaces: Texture orientation into or out of the surface. Journal of Biomedical Material Research. 28, 647–653

Gu J.M, Robinson J.R., Leung S.H.S. 1988. Binding of acrylic polymers to mucin/epithelial surfaces: structure property relationships, Critical Review of Thermal Drug Carrier Systems. 5, 21–67

Gu S.Y, Wang Z.M, Ren J, Zhang C.Y. 2009. Electrospinning of gelatine and gelatine/poly (L-Lactide) blend and its characteristics for wound dressings. Material Science and Engineering. 29, 1822-1828

Guncem G, Cigdem A.O, Sibel E, Fikret S, Djunsun K, Birgul S. 2009. Polyurethane films for wound dressing applications. Journal of Material Science. Material Medicals. 20, 421–431

Gurtner G.C, Werner S, Barrandon Y, Longaker M.T. 2008. Wound repair and regeneration. Insight Review. Nature. 453, doi: 10.1038/nature07039

Haghi A.K, Akbari M. 2007. Trends in electrospinning of natural nanofibres. Physical state solutions (a). 204, 6, 1830–1834

Hahn S.K, Park J.K, Tomimatsu T, Shimoboji T. 2007. Synthesis and degradation test of hyaluronic acid hydrogels. International Journal of Biological Macromolecules. 40,374–380

Hamman J.H. 2010. Review. Chitosan based polyelectrolyte complexes as potential carrier materials in drug delivery systems. Marine Drugs. 8, 1305-1322

Han S.K. 2005. Potential of human bone marrow stromal cells to accelerate wound healing in vitro. Annals in Plastic Surgery. 55, 414–419

Han X, Chen S, Hu X. 2009. Controlled-release fertilizer encapsulated by starch/polyvinyl alcohol coating. Desalination. 240, 21-26

Hardwicke J, Schmaljohann D, Boyce D, Thomas D. 2008. Epidermal growth factor therapy and wound healing- fast, present and future perspectives. Surgeon. 6, 172–177

Hashimoto T, Suzuki Y, Tanihara M, Kakimara Y, Suzuki K. 2004. Development of alginate wound dressings linked with hybrid peptides derived from laminin and elastin. Biomaterials. 25, 1407-1414

Hazel D. 2011. Prolonged Drug Delivery from a Polymeric Fibre Device for the Treatment ofacid and its derivative solutions. Journal of Macromolecular Science, Part A: Pure and Applied Chemistry. 36, 7-8, 991-1000, DOI: 10.1080/10601329908951195

Hein S, Wang K, Stevens W.F, Kjems J. 2008. Chitosan composites for biomedical applications: status, challenges and perspectives. Material Science Technology. 24, 1053–1061

Hendi A. 2011. Silver nanoparticles mediate differential responses in some of liver and kidney functions during skin wound healing. Journal of King Saudi University (Sci). 23, 47–52

Hettiaratchy S, Dziewulski P. 2004. Pathophysiology and types of burns. British Medical Journal. 328(7453), 1427-1429

Higham A.K, Landry A.M, Andrady A.L, Khan S.A. 2014. Nanofibers of Water-Soluble Polymers *via* Foam ElectrospinningDepartment of Chemical and Biomolecular Engineering, North Carolina State University. Journal of Physics and Chemical Solids. 60, 4.

Hoffman A.S, Stayton P.S, Bulmus V, Chen G, Chen J, Cheung C, Chilkoti A, Ding Z, Dong L, Fong R, Lackey C.A, Long C.J, Miura M, Morris J.E, Murthy N, Nabeshima Y, Park T.G, Press O.W, Shimoboji T, Shoemaker S, Yang H.J, Monji N, Nowinski R.C, Cole C.A, Priest J.H, Harris J.M, Nakamae K, Nishino T, Miyata T. 2013. Journal of Biomedical Material Research. 52,577–586

Horber J.K.H, Miles M.J. 2003. Scanning probe evolution in biology. Science 302:1002–1005

Howling G.I, Dettmor P.N, Goddard P.A, Hampson F.C, Dornish M, Wood A.J. 2001. The effect of chitin and chitosan on the proliferation of human skin fibroblasts and keratinocytes in vitro. Biomaterials. 2959-66

Huang L.L.H, Sung H.W, Tsai C.C, Huang D.M. 1998. Biocompatibility studies of a biological tissue fixed with a naturally occurring crosslinking reagent. Journal of Biomedical Material Research. 42, 568– 76

Huang Z.M, Zhang Y.Z, Kotaki M, Ramakrishna S. 2003. A review on polymer nanofibers by electrospinning and their applications in nanocomposites. Composites Science and Technology. 63, 2223–2253

Hutmatcher D.N. 2000. Scaffolds in tissue engineering bone and cartilage. Biomaterials 21, 2529–2543

Hwang J.J, Stupp S.I. 2000. Poly (amino acid) bioadhesives for tissue repair. Journal of Biomaterials Science. Polymer. 11, 1023-1038

Ikeda S, Nishinari K. 2001. "Weak Gel"-Type Rheological Properties of Aqueous Dispersions of Nonaggregated K-Carrageenan Helices. Journal of Agriculture. Food Chemistry. *49,* 4436-4441

Ishihara M, Nakanishi K, Ono K, Sato M, Kikuchi M, Saito Y. 2002. Photocrosslinkable chitosan as addressing for wound occlusion and acceleration in healing processes. Biomaterials. 23, 833-840

Ishihara M, Ono K, Sato M, Nakanishi K, Saito Y, Yura H. 2001. Acceleration of wound contraction and healing with a photocrosslinkable chitosan hydrogel. Wound Repair Regeneration. 9, 6, 513-21

Jannesari M, Varshosaz J, Morshed M, Zamani M. 2011. Composite poly (vinyl alcohol) /poly (vinyl acetate) electrospun nanofibrous mats as a novel wound dressing matrix for controlled release of drugs. International Journal of Nanomedicine. 6, 993–1003

Jayakumar R, Prabaharan M, Kumar P.T.S, Nair S.V, Tamura H. 2011. Biomaterials based on chitin and chitosan in wound dressing applications. Biotechnology Advances. 29, 322-337

Jeschke M.G, Barrow R.E, Hawkins H.K, Tao Z, Perez-Polo J.R, Herndon D.N. 2000. Biodistribution and feasibility of non-viral IGF-I gene transfers in thermally injured skin. Laboratory Investigation. 80, 151–158

Joe B, Vijaykumar M, Lokesh B.R. 2004. Biological Properties of Curcumin-Cellular and Molecular Mechanisms of Action. Critical Reviews in Food Science and Nutrition. 44, 2, 97-111

Jones V, Grey J.E, Harding K.G. 2006. ABC of wound healing: Wound dressings. British Medical Journal. 332, 777–780

Judith R, Nithya M, Rose C, Mandal A.B. 2010. Application of a PDGF-containing novel gel for cutaneous wound healing. Life Sciences. 87, 1–8

Kallaiinen L.K, Gordillo G.M, Schlanger R.K, Sen C. 2003. Topical oxygen as adjunct to wound healing, a clinical case series. Pathophysiology. 9, 208–216

Kanokpanont S, Damrongsakkeel S, Ratanavaraporn J, Aramwit P. 2012. An innovative bi-layered wound dressing made of silk and gelatine for accelerated wound healing. International Journal of Pharmaceutics. 436,141-153

Kapoor M. 2005. Possible anti-inflammatory role of COX-2- derived prostaglandins: Implications for inflammation research. Currunt Opinions in Investigative Drugs 6, 461–466

Kato Y, Onishi H, Mashida Y. 2003. Application for chitin and chitosan derivatives in the pharmaceutical field. Biotechnology. 4, 303-309

Kazakos K, Lyras D.N, Verettas D, Tilkeridis K, Tryfonidis M. 2009. The use of autologous PRP gel as an aid in the management of acute trauma wounds. Injury 40, 801–805

Kenawy R, Bowlin G.L, Mansfield K, Laymann J, Simpson D.G, Sanders E.H, Wnek G.E. 2002. Release of tetracycline hydrochloride from electrospin poly(ethylene-co-vinylacetate) poly(lactic acid) and a blend. Journal of Control Release. 81, 57–64

Khavari P.A, Rollman O, Vahlquist A. 2002. Cutaneous gene transfer for skin and systemic diseases. Journal of Internal Medicine. 252, 1–10

Khil M.S, Cha D.I, Kim H.Y, Kim I.S, Battaria N. 2003. Electrospun nanofibrous polyurethane membranes as wound dressings. Journal of Biomedical Materials Research B Applied Biomedicals. 67, 675–679

Kikuchi A, Okano T. 2002. Stimuli responsive polymers and their bioconjugates. Progression in Polymer Science. 27, 1165–1193

Kim B.S, Gao H, Argum A.A, Matyjaszewski K, Hammond P. 2009. All star polymer multilayers as pH responsive nanofilms. Macromolecules. 42, 368–75

Kim H.J, Choi E.J, Oh J.S, Lee H.C, Park S.S, Cho C.S. 2000. Possibility of wound dressing using poly(L-Leucin)/poly(ethylene glycol)/ poly(L-Leucin) triblock copolymer. Biomaterials. 21,131– 41

Kim I.Y, Yoo M.K, Seo J.H, Park S.S, Na H, Lee H.C. 2007. Evaluation of semi-interpenetrating polymer networks composed of chitosan and polyxamer for wound dressing applications. International Journal of Pharmaceutics. 341, 35–43

Kim J.O, Park J.K, Kim J.H, Jin S.G, Yong C.S, Li D.X, ChoI J.Y, Woo J.S, Yoo B.K, Lyoo W.S, Kim J,Choi H. 2008. Development of polyvinyl alcohol–sodium alginate gel-matrix-based wound dressing system containing nitrofurazone. International Journal of Pharmaceutics. 359, 79–86

Kim M.R, Park T.G. 2002. Temperature-responsive and degradable hyaluronic acid/ Pluronic composite hydrogels for controlled release of human growth hormone. Journal of Controlled Release. 80, 69–77

Kim T.G, Park T.G. 2006. Biomimicking extracellular matrix: Cell adhesive RGD peptide modified electrospun poly (D, L-lactic-co-glycolic acid) nanofiber mesh. Tissue Engineering. 12, 221–233

Kiwanuka E, Junker J, Eriksson E. 2012. Harnessing growth factors to influence wound healing. Clinical Plastic Surgery. 39, 239–248

Kokabi M, Sirousazar M, Hassan Z.M. 2007. PVA-clay nanocomposite hydrogels for wound dressings. European Polymer Journal. 43, 773–781

Kootstra N.A, Verma I.M. 2003. Gene therapy with viral vectors. Annual Review in Pharmacological Toxicology. 43, 413-39

Kowalewski T.A, Błon´ Ski S, Barral S. 2005. Experiments and modelling of electrospinning process. bulletin of the polish academy of sciences. Technical Sciences. 53, 4

Kreger S.T, Voytik-Harbin S.L. 2009. Hyaluronan concentration within a 3D collagen matrix modulates matrix viscoelasticity, but not fibroblast response. Matrix Biology. 28, 336–346

Kretz M. 2004. Expression and function of connexins in the epidermis, analyzed with transgenic mouse mutants. European Journal of Cell Biology. 83, 647–654

Kumar P, Choonara Y.E, Modi G, Naidoo D, Pillay V. 2014. Nanoparticulate strategies for the 5 R's of traumatic spinal cord injury intervention: restriction, repair, regeneration, restoration and reorganization. Nanomedicine 9, 331–348

Kurup V.P, Barrios C.S. 2008. Immunomodulatory effects of curcumin in allergy. Molecular Nutrition and Food Research. 52, 1031–9

Langer R, Vacanti J.P. 1993. Tissue engineering. Science. 280, 920–926

Lansown A.B.G, Jensen K, Jensen M.Q. 2003. Contreet foam and contreet hydrocolloid, an insight into two new silver-containing dressings. Journal of Wound Care. 12, 205–210

Lawrence J.C. 1994. Dressings and wound infections. American Journal of Surgery. 167, 21S-24S

Lee A.C, Moon H.K. 2003. Effect of topically applied silver sulfadiazine on fibroblast cell proliferation and biomechanical properties of the wound. Archives in Pharmaceutical Research. 26, 10,855-860

Lee K.Y, Mooney D.J. 2001. Hydrogels for tissue engineering. Chemical Review. 101, 1869–1879

Lee P.Y, Chesnoy S, Huang L. 2004. Electroporatic delivery of TGFbeta1 gene works synergistically with electric therapy to enhance diabetic wound healing in db/db mice. Journal of Investigative Dermatology. 123, 791–798

Lee Y-H, Chang J.J, Yang M-C, Chien C-T, Lai W-F. 2012. Acceleration of wound healing in diabetic rats by layered hydrogel dressings. Carbohydrate Polymer. 88, 809–819

Leitner V.M, Marschu¨tz M.K, Bernkop-Schnu¨rch A. 2003. Mucoadhesive and cohesive properties of poly (acrylic acid)-cysteine conjugates with regard to their molecular mass. European Journal of Pharmaceutical Sciences. 18, 89–96

Li X, Chen S, Zhang B, Li M, Diao K, Zhang Z, Li J, Xu Y, Wang X, Chen H. 2012. In situ injectable nano-composite hydrogel composed of curcumin, N,O-carboxymethyl chitosan and oxidized alginate for wound healing application. International Journal of Pharmaceutics, Pharmaceutical Nanotechnology.

Li J, Chen J, Kirsner R. 2007. Pathophysiology of acute wound healing. Clinics in Dermatology. 25, 1, 9-18

Li W.J, Laurencin C.T, Caterson E.J, Tuan R.S, Ko F.K. 2002. Electrospun nanofibrous structure: A novel scaffold for tissue engineering. Journal of Biomedical Material Research. 60, 613–621

Li X, Chen S, Zhang B, Li M, Diao K, Zhang Z, Li J, Xu Y, Wang X, Chen H. 2012. In-Situ injectable nanocomposite hydrogel composed of curcumin, N, O-carboxymethyl chitosan and

oxidised alginate for wound healing applications. International Journal of Pharmaceutics. 1,437(1-2), 110-9

Li X, Nan K, Li L, Zhang Z, Chen H. 2011. In vivo evaluation of curcumin nanoformulation loaded methoxy poly(ethylene glycol)-graft chitosan film for wound healing applications. Carbohydrate Polymers. 88, 84–90

Liechty K.W, Nesbit M, Herlyn M, Radu A, Adzick N.S, Crombleholme T.M. 1999. Adenoviral-mediated overexpression of platelet-derived growth factor-B corrects ischemic impaired wound healing. Journal of Investigative Dermatology. 113, 375–383

Liu F, Urban M.W. 2010. Recent advances and challenges in designing stimuli-responsive polymers. Progress in Polymer Science. 35, 3–23

Liu L, Liu L, Wang M, Du G, Chen J. 2007. Preparation and characterization of sponge-like composites by cross-linking hyaluronic acid and carboxymethylcellulose sodium with adipic dihydrazide. European Polymer Journal. 43, 2672–2681

Liu Y, Duan L.J, Kim M.J, Kim J-H, Chung D.J. 2014. *In situ* Sodium Alginate-Hyaluronic Acid Hydrogel Coating Method for Clinical Applications. Macromolecular Research. 22, 3, 240-247

Liu Y.Y, Fan X.D, Wei B.R, Si Q.F, Chen W.X, Sun L. 2006. Ph responsive amphillic hydrogel networks with IPN structure: a strategy for controlled drug release. International Journal of Pharmaceutics. 308, 205–9

Livesey S.A, Herndon D.N, Hollyoak M.A, Atkinson Y.H, Nag A. 1995. Transplanted acellular allograft dermal matrix. Potential as a template for the reconstruction of a viable dermis.. Transplantation. 60, 1–9

Lloyd A.W. 2002. Interfacial bioengineering to enhance surface biocompatibility. Medical Device Technology. 13, 18–21

Lloyd L.L, Kennedy J.F, Methacanon P, Paterson M, Knill C.J. 1998. Carbohydrate polymers as wound management aids. Carbohydrate Polymer. 37, 315–322.

Lock P.M, La L, Walderslade P, Chatham K, Webb D.R. and Way L. 1980. Wound Dressing Materials. United States Patent. Patent No.4233969, 1

Losi P, Briganti E, Errico C, Lisella A, Sanguinetti E, Chiellini F, Soldani G. 2013. Fibrin-based scaffold incorporating VEGF- and bFGF-loaded nanoparticles stimulates wound healing in diabetic mice. Acta Biomaterilia. 9, 7814–7821

Luoa Y, Kirkerb K.R, Prestwich G.D. 2000. Cross-linked hyaluronic acid hydrogel films: new biomaterials for drug delivery. Journal of Controlled Release. 69,169–184

Lutolf M.P, Hubbell J.A. 2005. Synthetic biomaterials as instructive extracellular microenvironment for morphogenesis in tissue engineering. Nature Biotechnology. 23, 47–55

Luu Y.K, Kim K, Hsiao B.S, Chu B, Hadijiargyrou M. 2003. Development of a nanostructured DNA delivery scaffold via electrospinning of PLGA and PLA-PEG block copolymer. Journal of Control Release. 289, 341–353

Ma L, Gao C, MaO Z, Zhou J, Shen J, Hu X, Han C. 2003. Collagen/chitosan porous scaffolds with improvised biostability for skin tissue engineering. Biomaterials. 24, 4833-4841

Machado M.O, Lopes E.C.N, Sousa K.S, Airoldi C. 2009. Immobilisation of ethylene sulphide in animated cellulose for removal of divalent cations. Carbohydrate Polymer. 77,760

Mackay D., Miller AL. 2003. Nutritional support for wound healing. Alternative Medicine Review, a Journal of Clinical Therapeutics. 8 (4), 359-377.

Madhumathi K, Kumar P.T.S, Apilash S, Sreeja V, Tamura H, Manzoor K, Nair S.V, Jayakumar R. 2010. Development of novel chitin nanosilver composite scaffolds for wound dressing applications. Journal of Material Science. Material Medicine. 21, 807–813.

Maheshwari R.K, Singh A.K, Gaddipathi J, Srimal R.C. 2006. Multiple biological activities of curcumin. A short Review. Life Sciences. 78, 2081-2087

Malafaya P.B, Silver G.A, Reis R.L. 2007. Natural origin polymers as carriers and scaffolds for biomolecules and all delivery in tissue engineering applications. Advanced Drug Delivery Review. 59, 207–233

Mallefet P, Dweck A.C. 2008. Mechanism involved in wound healing. Focusing on injuries. The Biomedical Scientist. 609-615

Mani H, Sidhu G.S, Kumari R, Gaddipati J.P, Seth P, Maheshwari R.K. 2002. Curcumin differentially regulates TGF-β1, its receptors and nitric oxide synthase during impaired wound healing. Biofactors. 16, 29–43

Mansour H.M, Sohn M, Al-Ghaneem A and Deluca P.P. 2010. Materials for Pharmaceutical Dosage form, Molecular Pharmaceutics and Controlled Release Drug Delivery Aspects. International Journal of Molecular Sciences. 3298

Martien A, Stuart C, Huck W.T.S, Genzer J, Müller M, Ober C, Stamm M, Sukhorukov G.B, Szleifer I, Tsukruk V.V, Urban M, Winnik F, Zauscher S, Luzinov I, Minko S. 2010. Emerging applications of stimuli responsive polymer materials. Review article. Nature materials. 9, 101-113. doi: 10.1038/nmat2614

Martindale D. 2000. Next generation applications for polymeric nanofibres. Scientific America. 34-36. Smith D and Reneker D

Mattews J.A, Wnek G.E, Simpson D.G, Bowlin G.L. 2002. Electrospinning of collagen nanofibers. Biomacromolecules 3, 232–238

Matthews K.H, Stevens H.N.E, Auffret A.D, Humphrey M.J, Eccleston G.M. 2005. Lyophillised wafers as a drug delivery system for wound healing containing methylcellulose as a viscosity enhancer. International Journal of Pharmaceutics. 289, 51–62

Mayet N, Choonara Y.E, Kumar P, Tomar L.K, Tyagi C, DuToit L.C, Pillay V. 2014. Review: A comprehensive review of advanced biopolymeric wound systems. Journal of Pharmaceutical Sciences. 103, 8, 2211-2230

Mayet N, Kumar P, Choonara Y.E, Tomar L.K, Tyagi C, Du Toit L.C, Pillay V. 2014. Synthesis of a semi-interpenetrating polymer network as a bioactive curcumin film. American Association of Pharmaceutical Sciences. (AAPS) Pharm Sci Tech. DOI: 10.1208/s12249-014-0170-3

McConell E.E. 1995. Advantages and limits of *in vivo* screening tests. The Annals of Occupational Hygiene. 39(5), 727-735

Melcalfe A.D, Ferguson M.W.J. 2007. Tissue engineering of replacement skin: The crossroads of biomaterials, wound healing, embryonic development, stem cells and regeneration. Journal of the Royal Society Interface. 4, 413–437

Mercandetti M. 2011. Wound Healing and Repair. Medscape Reference: Drug Disease and Procedures (an overview). 1298129

Mi F.L, Shyu S-S, Peng C-K. 2005. Characterization of Ring Opening Polymerization of Genipin and pH Dependent Cross-Linking Reactions between Chitosan and Genipin. Journal of Polymer Science Part A: Polymer Chemistry. 43, 10, 1985-2000

Mi F.L, Sung H.W, Shyu S.S. 2002. Drug release from chitosan–alginate complex beads reinforced by a naturally occurring cross-linking agent. Carbohydrate Polymers. 48, 1, 61-72

Mi F.L, Tan Y.C, Liang H.F, Sung H.W. 2002. In vivo biocompatibility and degradability of a novel injectable-chitosan-based-implant. Biomaterials. 23, 181–91

Mihm M.C, Soter N.A, Dvorak H.F, Austen K.F. 1976. The structure of normal skin and the morphology of atopic eczema. The Journal of Investigative Dermatology. 67, 3, 305-312.

Miller M.S. 2009. Use of topical recombinant human platelet-derived growth factor-BB (becaplermin) in healing of chronic mixed arteriovenous lower extremity diabetic ulcers. Journal of Foot Ankle Surgery. 38, 227–231

Miyoshi M, Kavaizoe T, Igawa H.H, Tabata Y, Ikada Y, Suzuki S. 2006. Effects of bFGF incorporated into a gelatin sheet on wound healing. Journal of Biomaterials Science Polymer. 16, 893–907

Moira L.I.F, Dias A.M.A, Carvalho E, Sousa H.C. 2013. Recent advances on the development of wound dressings for diabetic foot ulcer treatment- A review. Acta Biomaterialia. 9, 7, 7093-114

Morghimi H.R, Makmalzadeh B.S, Manoti A. 2009. Enhancement effect of terpenes on silver sulphadiazine permeation through third degree burn eschar. Burn. 35, 1165–1170

Morin R.J, Tomaselli N.L. 2007. Interactive dressings and topical agents. Clinical Plastic Surgery. 34, 643-658.

Moura L.I.F, Dias A.M.A, Carvalho E, de Sousa H.C. 2013. Recent advances on the development of wound dressing s for diabetic foot ulcer treatment—A review. Acta Biomaterialia. 9, 7093–7114

Mustoe T.A, Pierce G.F, Morishima C, Deuel T.F. 1991. Growth factor induced acceleration of tissue repair through direct and inductive activities in a rabbit dermal ulcer model. Journal of Clinical Investigation. 87, 694–703

Muzarelli R.A, Guerrieri M, Goteri G, Muzarelli C, Armeni T, Ghiselli R, Coenelissen M. 2005. The biocompatibility of dibutyryl chitin in the context of wound dressings. Biomaterials. 26, 5844-5854

Muzarelli R.A. 2009. A genipin crosslinked chitosan hydrogel as biomedical and pharmaceutical airs. Review. Carbohydrate Polymers. 77, 1-9

Nair L.S, Laurencin C.T. 2007. Biodegradable polymers as biomaterials. Progression in Polymer Science. 32, 762–798

Nakajimaa N.Y, Mukai K, Rahayub H.S.E, Nur M, Ishijima T, Enomoto H, Uesugi Y, Sugama J, Nakatani T. 2014. Cold plasma on full-thickness cutaneous wound accelerates healing through promoting inflammation, re-epithelialization and wound contraction. Clinical Plasma Medicine. 2, 1,28-35, doi: 10.1016/j.cpme.2014.01.001

Nam S.Y, Lee Y.M. 1997. Pervaporation and properties of chitosan-poly (acrylic acid) complex membranes. Journal of Membrane Science. 135, 161-171

Naqoba B.S, Gandhi R.C, Wadner B.J, Rao A.K, Hortalkar A.R, Selkas S.P. 2010. A simple and effective approach for the treatment of diabetic foot ulcers with different Wagner grades. International Wound Journal. 7, 153-158

Naqoba B.S, Wadher B.J, Deshmukh S.R, Mahabaleshwar L, Gandhi R.C, Kulkarni P.B, Mane V.A, Deshmukh J.S. 1998. Treatment of superficial pseudomonal infections with citric acid- an effective and economical approach. Journal of Hospital Infections. 40,155-157

Naqoba B.S, Wadher B.J, Selkar S.P. 2011. Citric acid treatment for chronic wounds in animals. International Journal of Animal and Veterinary Advances. 3, 1, 26-28

Niemeyer C.M. 2006. Nanobiotechnology. Encyclopedia of Molecular Cell Biology and Molecular Medicine. DOI: 10.1002/3527600906

Ortiz-Urda S, Thyagarajan B, Keene D.R. 2002. Stable nonviral genetic correction of inherited human skin disease. Natural Medicine. 8, 1166–1170

Pachence J.M. 1996. Collagen based device for soft tissue repair. Journal of Biomedical Material Research (Applied Biomaterial). 33, 35-40

Pachence J.M. 1996. Collagen based device for soft tissue repair. Journal of Biomedical Materials Research (Applied Biomaterial). 33, 35-40

Pakravan M.P, Heuzey M.C, Ajji A. 2011. A fundamental study of Chitosan/PEO electrospinning. Polymer. 52, 4813–24

Panchatcharam M,Miriyala S, Gayathri V.S, Suguna L. 2006. Curcumin improves wound healingby modulating collagen and decreasing reactive oxygen species. Molecular and Cellular Biochemistry. 290, 87–96

Park H, Robinson J.R. 1987. Research Article: Mechanism of mucoadhesion of Poly (Acrylic Acid) Hydrogels. Pharmaceutical Research. 4, 6

Park Y.J, Chang L.C, Liong J.F, Moon C, Chung C.P, Yang V.C. 2005. Nontoxic membrane translocation peptide from protamine, low molecular weight protamine (LMWP), for enhanced intracellular protein delivery: In vitro and in vivo study. Federation of American Societies for Experimaental Biology. J 19, 1555–1557

Parsons D, Bowler P.G, Myles V, Jones S. 2005. Silver antimicrobial dressings in wound management, a comparison of anti-bacterial physical and chemical characteristics. Wounds 17, 222–232

Patzke G.R, Krumeich F, Nesper R. 2002. Oxidic nanotubes and nanorods—Anisotropic modules for a future nanotechnology. Angewandte Chemie International Edition. 41, 2446–2461

Paul W, Sharma C.P. 2004. Chitosan and alginate wound dressings: A short review. Trends in Biomaterials. Artificial Organs. 18, 18–23

Pauliukaite R, Ghica M.E, Fatibello-Filho O, Brett C.M.A. 2009. Nanobioelectrochemistry: From implantable biosensors to green power generation. Analytical Chemistry. 81, 5364

Pawar H.V, Tetteh J, Boatang J.S. 2013. Preparation, optimisation and characterisation of novel wound healing film dressings loaded with streptomycin and diclofenac. Colloid Surfactant B: Biointerface. 102,102–110

Perez R.A, Won J, Khowles J.C, Kim H. 2012. Naturally and synthetic smart composite biomaterials for tissue regeneration. Advanced Drug Delivery Review. 65, 471–496

Perttila J, Salo M, Peltola O. 1990. Periodontal Disease. A thesis submitted to the faculty of Health Sciences, University of the Witwatersrand, in fulfilment of the requirements for the degree of Master of Pharmacy

Peter S.J, Miller M.J, Yasko A.W, Yazemski M.J, Mikos A.G. 1998. Polymer concepts in tissue engineering. Journal of Biomedical Material Research B Applied Biomaterials. 43, 422–427

Pham Q.P, Sharma U, Mikos A.G. 2006. Electrospinning of Polymeric Nanofibers for Tissue Engineering Applications: A Review. Tissue Engineering. 12, 5

Pierce G.F, Vandeberg J, Rudolph R, Tarpley S, Mustoe T.A. 1991. Platelet derived growth factor-BB and transforming growth factor beta-1 selectively moderate glycoaminoglycans, collagens and myofibroblasts in excisional wounds. American Journal of Pathology. 138, 629–646

Pillay V, Dott C, Choonara Y.E, Tyagi C, Tomar L, Kumar P, du Toit L.C, Ndesendo VMK. 2013. A review of the effect of processing variables on the fabrication of electrospun nanofibers for drug delivery applications. Journal of Nanomaterials. 789289

Pinho E.D, Martins A, Araujo J.V, Reis R.L, Neves N.M. 2009. Degradable particulate composite reinforced with nanofibres for biomedical applications. Acta Biomaterialia. 5, 1104-1114

Plasma fibronectin concentrations in blood products. Intensive Care Medicine. 16,41,e3

Ponnusamy S, Zinjarde S, Bhargava S, Rajamohanan P.R, Ravikumar A. 2012. Discovering bisdemethoxycurcumin from Curcuma longa rhizome as a potent small molecule inhibitor of human pancreatic a-amylase, a target for type-2 diabetes. Food Chemistry. 135, 2638–42

Pourjavadi A, Ghasemzadeh H, Soleyman R. 2007. Synthesis, Characterization, and Swelling Behaviour of Alginate-g-Poly (sodium acrylate)/Kaolin Superabsorbent Hydrogel Composites. Journal of Polymer Science. 105, 5

Pourjavadi A, Mahdavinia G.R. Chem T.J. 2006. Superabsorbency, pH-Sensitivity and Swelling Kinetics of Partially Hydrolyzed Chitosan-g-poly (Acrylamide) Hydrogels @ TUBITAK. 30, 595 – 608.

Prestwicha G.D, Marecaka D.M, Marecekb J.F, Vercruyssea K.P, Ziebell M.R. 1998. Controlled chemical modification of hyaluronic acid: synthesis, applications, and biodegradation of hydrazide derivatives. Journal of Controlled Release. 53, 93–103

Price R.D, Berry M.G, Navsaria H.A. 2007. Review: Hyaluronic acid: the scientific and clinical Evidence. Journal of Plastic, Reconstructive & Aesthetic Surgery. 60, 1110-1119

Pujana M.A, Perez-Alverez L, Iturbe L.C.C, Katime I. 2013. Biodegradible chitosan nanogels crosslinked with genipin. Carbohydrate Polymer. 94(2), 836–42

Purner S.K, Babu M. 2000. Collagen based dressings—A review. Burns 26, 54–62

Qiu C, Coutinho P, Frank S, Franke S, Law L.Y, Martin P, Green C.R, Becker D.L. 2003. Targeting connexin43 expression accelerates the rate of wound repair. Current Biologicals. 13, 1697–1703

Qiu L.Y, Bae Y.H. 2006. Polymer architecture and drug delivery. Pharmaceutical Research. 23, 1–30

Queen D, Evans J.H, Gaylor J.D.S, Courthey J.M, Reid W.H. 1987. Burn wound dressings—A review. Burns 13, 218–228

Queen D, Gaylor J.D.S, Evans J.H, Courtney J.M, Reid W.H. 1987. The preclinical evaluation of the water vapour transmission rate through burn wound dressings. Biomaterials. 8, 367–71

Queen D, Orsted H, Sanada H, Sussman G. 2004. A dressing history. International Wound Journal. 1, 59–77

Quintero J.A. 2003. Patent US6547467B2

Ramli N.A and Wong T.W. 2011. Sodium carboxymethylcellulose scaffolds and their physicochemical effects on partial thickness wound healing. International Journal of Pharmaceutics. 403, 73-82

Rana V, Babita K, Goyal D, Tiwary A. 2005. Sodium citrate crosslinked chitosan films: Optimization as substitute for human/ rat/ rabbit epidermal sheets. Journal of Pharmacy and Pharmaceutical Sciences. 8, 1, 10-17

Rayment E.A, Dargaville T.R, Shooter G.K, George G.A, Upton Z. 2008. Attenuation of protease activity in chronic wound fluid with biophonate functionalised hydrogels. Biomaterials. 29, 1785–1795

Reneker D.H and Chun I. 1996. Nanometre diameter fibres of polymer, produced by electrospinning. Nanotechnology.7,216

Reneker D.H, Yarin A.L, Fong H, Koombhongse S.2000. Bending instability of electrically charged liquid jets of polymer solution in electrospinning. Journal of Applied Physics. 87,4531e47

Rhett J.M, Ghatnekar G.S, Palatinus J.A, O'Quinn M, Yost M.J, Gourdie R.G. 2008. Novel therapies for scar reduction and regenerative healing of skin wounds. Trends in Biotechnology. 26, 4

Richards T.S. 2004. Protein kinase C spatially and temporally regulates gap junctional communication during human wound repair via phosphorylation of connexin43 on serine368. Journal of Cell Biology. 167, 555–562

Robson M.C. 1991. Growth factors as wound healing agents. Current Optical Biotechnology. 2, 863–867

Rode H, Berg A.M, Rogers A. 2011. Burn care in South Africa. Annals of Burns and fire disasters. Euro-Mediterranean Council for Burns and Fire Disasters. 24(1), 7-8

Rohindra D.R, Nand A.V, Khurma J.R. 2004. Swelling properties of chitosan hydrogels. The South Pacific Journal of Natural and Applied Sciences. 22, 1, 32 – 35

Rosiak J, Rucinska-Rybus A, Pekala W. 1989. Patent US4871490

Rossi S, Faccendini A, Bonferoni M.C, Ferrari F, Sandri G, Del Fante C, Perotti C, Caramella C.M. 2013. “Sponge-like” dressings based on biopolymers for the delivery of platelet lysate to skin chronic wounds. International Journal of Pharmaceutics. 440, 207–215

Roy D, Cambre J.N, Sumerlin B.S. 2010. Future perspectives and recent advances in stimuli-responsive Materials. Progress in Polymer Science. 35, 278–301

Ruszczak Z. 2003. Effect of collagen matrices on dermal wound healing. Advanced Drug Delivery Review. 55, 1595–1611

Saak A.W, Jennings H.M, Shah S.P. 2001. The influence of wall slip on yield stress and viscoelastic measurements of cement paste. Cement and Concrete Research 31, 205-212

Said S.S, Aloufy A.K, El-Halfawy O.M, Boraei N.A, El-Khordagui L.K. 2011. Antimicrobial PLGA ultrafine fibres: Interaction with wound bacteria. European Journal of Pharmaceutics. 79, 108-118

Saimani S, Dal-Cin M.M, Kumar A, Kingston D.M. 2010. Separation performance of asymmetric membranes based on PEGDa/PEI semi interpenetrating polymer network in pure and binary gas mixtures of CO_2, N_2 and CH_2. Journal of Membrane Science. 362, 353–9

Saltzmann W.M, Olbricht W.L. 2002. Building drug delivery into tissue engineering. Nature Review Drug Discovery. 1, 177–186

Sandri G, Bonferoni M.C, Autilia F.D, Rossi S, FerrarI F, Grisoli P, Sorrenti M, Catenacci L, Fante C.D, Perotti C, Caramella C. 2013. Wound dressings based on silver sulfadiazine solid lipid nanoparticles for tissue repairing. European Journal of Pharmaceutics and Biopharmaceutics. 84, 84–90

Sandri G, Bonferoni M.C, Rossi S, Ferrari F, Mori M, Fante C.D, Perotti C, Scudeller L Caramella C. 2011. Platelet lysate formulations based on mucoadhesive polymers for the treatment of corneal lesions. Journal of Pharmacy and Pharmacology. 63,189–198

Sarasam A, Madihally S.V. 2005. Characterisation of chitosan polycaprolactone blends for tissue engineering applications. Biomaterials. 26(27), 5500–8

Sarkar K, Gomez C, Zambrano S, Ramirez M, de Hoyos E, Vasquez H, Lozano K. 2010. Electrospinning to Forcespinning. Materials Today. 13, 11

Scheuplein R.J. 2011. Permeability of the skin. Handbook of physiology, Reactions to environmental agents. Comprehensive Physiology. doi: 10.1002/ cphy.cp090119

Schnaare R, Block L, Rohan L. 2005. Rheology. In: Hendrickson, R. (ed.) Remington's the Science and Practice of Pharmacy,21st edn. Lippincott, Williams and Wilkins, Philadelphia

Schultz G.S, Barillo D.J, Mozingo D.W, Chin G.A. 2004. Wound bed preparations and a brief history of time. International Wound Journal. 1, 19–32.

Schultz G.S, Sibbald G.R, Falanga V, Yello E.E.A, Dowsett C, Harding K, Romanelli M, Stacey M.C, Teot L, Vanscheidt W. 2003. Wound bed preparation, a systemic approach to wound management. Wound Repair Regeneration 11, 1–28.

Seetharaman S, Natesan S, Stowers R.S, Mullens C, Baer D.G, Suggs L.G. 2011. A PEGylated fibrin-based wound dressing with antimicrobial and angiogenic activity. Acta Biomaterialia. 7, 2787–96

Sell S.A, Wolfe P.S, Garg K, McCool J.M, Rodiguez I.A, Bowlin G.L. 2010. The use of natural polymers in tissue engineering: A focus on electrospun extracellular matrix analogues. Polymer Advanced Technology. 2, 522–553

Senet P. 2004. Becaplermin gel (Regranex gel). Annual Dermatology Venereol. 13, 351–358

Shah V.P. 1994. Skin penetration enhancers: Scientific perspectives. In: Drug permeation enhancement: Theory and applications; Hsieh, DS, Ed. New York, NY: Marcel Dekker, pp 19–23

Shaikh R.P, Kumar P, Choonara Y.E, du Toit L.C Pillay V. 2012.Crosslinked electrospun PVA nanofibrous membranes: elucidation of their physicochemical, physicomechanical and molecular disposition. Biofabrication.4, 025002, 21pp

Shanmagasundaram N, Sundaraseelan J, Uma S, Selvaraj D, Babu M. 2005. Design and delivery of silver sulphadiazine from alginate microspheres impregnated collagen scaffolds. Journal of Biomedical Material Research. Applied Biomaterials. 77B, 278–388

Shi J, Alexandra R, Votruba S, Omid C, Farokhzad S, Langer R. 2010. Nanotechnology in drug delivery and tissue engineering: From discovery to applications. Nano Letters. 10, 3223–3230

Shin Y.M, Hohman M.M, Brenner, M.P, and Rutledge, G.C. 2001. Electrospinning: a whipping fluid jet generates submicron polymer fibers. Applied Physical Letters.78, 1149
Shin Y.M, Hohman M.M., Brenner, M.P., and Rutledge, G.C. 2001. Experimental characterization of electrospinning: the electrically forced jet and instabilities. Polymer.42, 9955

Sibbald G.R, Orsted H, Schultz G.S, Coutts P, Keast D. 2003. Preparing the wound bed 2003, Focus on infection and inflammation. Ostomy Wound Management. 49, 24–51.

Sidhu G.S, Singh A.K, Thaloor D, Banaudha K.K, Pathaik G.K, Srimal R.C. 1998. Enhancement of wound healing by curcumin in animals. Wound Repair Regeneration. 16(2), 167–77

Sill T.J, von Rectum H.A. 2006. Electrospinning: Applications in drug and tissue engineering. Biomaterials. 29, 1989–2006

Singer A, Richard AF, Clark MD. 1999. Cutaneous wound healing. New England Journal of Medicine. 341, 738–746

Singer A.J and Dagum A.B. 2008. Current management of acute cutaneous wounds. New England Journal of.Medicine. 359, 1037-1046

Singer A.J, Clark R.A.F. 1999. Cutaneous wound healing, mechanism of disease, Review Article. The New England Journal of Medicine. 341,10,738-746

Singer A.J, Clark R.A.F. 1999. Mechanisms of Disease. Review Article. The New England Journal of Medicine. 738-746

Singh, A., Narvi, S. S, Dutta P .K., Pandey, N .D . 2006. External stimuli response on a novel chitosan hydrogel crosslinked with formaldehyde. Bulletin Material Science. 29(3), 233–238

Siritienthong T, Ratanavaraporn J, Aramwit P. 2012. Development of ethyl alcohol-precipitated silk sericin/polyvinyl alcohol scaffolds for accelerated healing of full-thickness wounds. International Journal of Pharmaceutics. 439, 175–186

Slaughter B.V, Shahana S.K, Fisher O.Z, Khademhasseini A, Peppas N.A. 2009. Hydrogels in regenerative medicine. Advanced Materials. 21, 3307–3329

Smart J.D. 2005. The basics and underlying mechanisms of mucoadhesion. Advanced Drug Delivery Reviews. 57, 1556-1568

Sprugel K.H, McPherson J.M, Clowes A.W, Ross R. 1987. Effects of growth factors in vivo. I. Cell in growth into porous subcutaneous chambers. American Journal of Pathology. 129, 601–613

Steffansen B, Herping S.P.K. 2008. Novel wound models for characterising ibuprofen release from foam dressings. International Journal of Pharmaceutics. 364, 150–155

Stein C, Kuchler S. 2013. Targeting inflammation and wound healing by opioids. Trends in Pharmacology Sciences. 34, 303–312

Steven T.B. 1996. Cultured skin substitutes: A review. Tissue Engineering. 2, 255–266

Stuart M.A.C, Huck W.T.S, Genzer J, Müller M, Ober C, Stamm M, Sukhorukov G.B, Szleifer I, Tsukruk V.V, Urban M, Winnik F, Zauscher S, Luzinov I and Minko S. 2010. Emerging applications of stimuli responsive polymer materials. Nature Materials. 9, 101-113.

Su Rho K, Jeong L, Lee G, Seo B-M, Park Y.J, Hong S-B, Roh S, Cho J.J, Park W.H, Min B-M. 2006. Electrospinning of collagen nanofibres: Effects on the behaviour of normal keratinocytes and early stage wound healing. Biomaterials 27, 1452–1461

Su W-Y, Chen Y-C, Lin F-H. 2010. Injectable oxidized hyaluronic acid/adipic acid dihydrazide hydrogel for nucleus pulposus regeneration. Acta Biomaterialia. 6, 3044–3055

Su Y.L, Wang J, Liu H.Z. 2002. FTIR Spectroscopic Study on Effects of Temperature and Polymer Composition on the Structural Properties of PEO-PPO-PEO Block Copolymer Micelles. Langmuir. 18, 5370-5374

Sung H.W, Hsincha T.W, Tu H. 2003. Drug loaded biological material chemically treated with genipin. United States Patent. Patent No. US 6, 624 138 BH

Sung J.H, Hwang M.R, Kim J.O, Lee J.H, Kim Y.I, Kim J.H. 2010. Gel characterisation and in vivo evaluation of minocycline-loaded wound dressing with enhanced wound healing using polyvinyl alcohol and chitosan. International Journal of Pharmaceutics. 392, 232–40

Sussman G. 2010. Understanding wound films. Wound Internationals. 1, 4

Suzuki Y, Tanihara M, Nishmura Y, Suzuki K, Kakimara Y, Shimizu Y. 1997. A novel wound dressing with an antibiotic delivery system stimulated by microbial infection. ASA10 J.43, 854-857

Tabata Y. 2009. Biomaterial technology for tissue engineering applications. Journal of the Royal Society Interface. 6, S311-S24

Tanihara Y, Suzuki Y, Nishmura Y, Suzuki K, Kakimara Y. 1998. Thrombin sensitive peptide linkers for biological signal responsive drug release systems. Peptides. 19, 421-425

Taylor G.I. 1969. Electrically Driven Jets. Proceedings of the Royal Society of London. Series A, Mathematical and Physical Science. 313, 1515, 453-475.AB13

Thakur R.A, Florek C.A, Kohn J, Michniak B.B. 2008. Electrospun nanofibre scaffold with targeted drug release profiles for potential applications as wound dressings. International Journal of Pharmaceutics. 364, 87–93

Thompson C.J, Chase G.G, Yarin A.L, Reneker D.H. 2007. Effects of parameters on nanofiber diameter determined from electrospinning model. Polymer. 48, 6913-6922

Thu H-E, Zulfakar M.H, Ng S-F. 2012. Alginate based bilayer hydrocolloid films as potential slow release modern wound dressings. International Journal of Pharmaceutics. 434, 375-383

Tolino M.A, Black E.R, Klarland J.K. 2011. Brief treatment with heparin binding EGF-like growth factor, but not with EGF is sufficient to accelerate epithelial wound healing. Biochemical Biophysics Acta. 1810, 875–878

Topham J. 2002. Why do some cavity wounds treated with honey or sugar paste heal without scarring? Journal of Wound Care. 11, 2, 53-5

Topham J. 2002. Why do some cavity wounds treated with honey or sugar paste heal without scarring? Journal of Wound Care. 11, 2, 53-5

Tsao C.T, Chang C.H, Lin Y.Y, Wu M.F, Wang J.L, Young T.H, Han J.L, Hsieh K.H. 2011. Evaluation of chitosan poly (glutamic acid) polyelectrolyte complex for wound dressing materials. Carbohydrate Polymers. 84, 812–819

Ueno H, Mori T, Fuginaga T. 2001. Topical formulations and wound healing applications of chitosan. Advanced Drug Delivery Review. 52,105-115

Ueno H, Yamada H, Tanaka I, Kaba N, Matsuura M, Okumara M. 1999. Accelerating effects of chitosan for healing at early phase of experimental open wounds in dogs. Biomaterials. 20, 1407-14

Vachon D.J, Yager D.R. 2006. Novel sulphonated hydrogel composite with the ability to inhibit proteases and bacterial growth. Journal of Biomedical Materials. 76A, 35–43

Valence M.K.N, Pillay V, Choonara Y.E, du Toit L.C, Buchmann E, Meyer L.C.R, Khan R.A, Rosin U. 2010. Investigation of the Physicochemical and Physicomechanical Properties of a Novel Intravaginal Bioadhesive Polymeric Device in the Pig Model. American association of Pharmaceutical Scientist (AAPS) PharmSciTech. 11, 2, DOI: 10.1208/s12249-010-9439-3

Van Rijswijk L. 2006. Ingredient based wound dressing classification, A paradigm shift that is passé and in need of replacement's wound care 15, 11–14

Venus M, Waterman J, Mc Nab I. 2010. Basic Physiology of the skin. Basic Science. Surgery. 28,10.

Vogel J.C. 2000. Nonviral skin gene therapy. Human Gene Therapy. 11, 2253–2259

Wei C.J. 2004. Connexins and cell signaling in development and disease. Annual Review in Cell and Development Biology. 20, 811–838

Weller C, Sussman G. 2006. Wound dressings update. Journal of Pharmaceutical Practical Research. 36, 318–324

Wolf N.B, Küchler S, Radowski M.R, Blaschke T, Kramer K.D, Weindl G, Kleuser B, Haag R, Schäfer-Korting M. 2009. Influences of opioids and nanoparticles on in vitro wound healing models. European Journal of Pharmaceutical and Biopharmacy. 73, 34–42

Wu J, Zheng Y, Song W, Luan J, Wen X, Wu Z, Chen X, Wang Q, Guo S. 2014. In situ synthesis of silver-nanoparticles/bacterial cellulose composites for slow-released antimicrobial wound dressing. Carbohydrate Polymer. 102, 762–771

Yan L.P, Wang Y.J, Ren L, Wu G, Caridade S.G, Fan J.B. 2010. Genipin crosslinked collagen/chitosan biomimetic scaffolds for articular cartilage tissue engineering applications. Journal of Biomedical Materials Research Part A. 95A,2

Yao F, Xu L.Q, Fu G.D, Lin B.P. 2010. Sliding graft interpenetrating polymer network from simultaneous “click chemistry” and atom transfer radical polymerisation. Macromolecules. 43, 9761– 70

Yarin AL, Zussman E. 2004.Upward needleless electrospinning of multiple nanofibers. Polymer. 45,2977e80

Yoshimoto H, Shin Y.M, Terai H, Vacanti J.P. 2003. A biodegradable nanofiber scaffold by electrospinning and its potential for bone tissue engineering. Biomaterials. 27, 2077–2082

Yui N, Nihira J, Okano T, Sakurai Y. 1993. Regulated release of drug microspheres from inflammation responsive degradable matrices of crosslinked hyaluronic acid. Journal of Controlled Release. 25,133-143

Yui N, Okano T, Sakurai Y. 1992. Inflammation responsive degradation of crosslinked hyaluronic acid gels. Journal of Controlled Release.22, 105-116

Zahedi P, Rezaeian I, Ranaei-Siadat S.O, Jafari S.H, Supaphol P. 2011. A review on wound dressings with an emphasis on electrospun nanofibrous polymeric bandages. Polymer Advanced Technologies. 21, 77-95

Zhang J.T, Huang S.W, Zhuo R.X. 2004. Temperature sensitive polyamidoamine dendrimer/poly (N-isopropyl/acrylamide) hydrogels with improved responsive properties. Macromolecules, Bioscience. 4, 575–8

Zhang L, Li K, Xiao W, Zheng L, Xiao Y, Fan H, Zhang X. 2011. Preparation of collagen–chondroitin sulfate–hyaluronic acid hybrid hydrogel scaffolds and cell compatibility in vitro. Carbohydrate Polymers. 84, 118–125

Zhang Y, Lim C.T, Ramakrishna S, Huang Z.M. 2005. Recent development of polymer nanofibres for biomedical and biotechnological applications. Journal of Material Science. Material Medicals. 16 (10), 933-46

Zhang Y.Z, Venugopal J, Huang Z-M, Lim C.T, Ramakrishna S. 2006. Crosslinking of the electrospun gelatin nanofibres. Polymer. 47, 8, 2911-2917.

Zhao Q.S, Ji Q.X, Xing K, Li X.Y, Liu C.S, Chen X.G. 2009. Preparation and characteristics of novel porous hydrogel films based on chitosan and glycerophosphate. Carbohydrate Polymer. 76, 410–6

Zhao Y.S, Lu C.T, Zhang Y, Xiao J, Zhao Y.P, Tian J.L. 2013. Selection of high efficient transdermal lipid vesicle for curcumin skin delivery. International Journal of Pharmaceutics. 454, 302–9

Zhong S.P, Zhang Y.Z, Lim C.T. 2010. Tissue scaffolds for skin wound healing and dermal reconstruction. Nanomedicine Nanobiotechnology. 2, 510–525

11. Appendices

11.1 Doctoral Publications

11.1.1. Review Paper

REVIEW

A Comprehensive Review of Advanced Biopolymeric Wound Healing Systems

NAEEMA MAYET, YAHYA E. CHOONARA, PRADEEP KUMAR, LOMAS K. TOMAR, CHARU TYAGI, LISA C. DU TOIT, VINESS PILLAY

Wits Advanced Drug Delivery Platform Research Unit, Department of Pharmacy and Pharmacology, School of Therapeutic Sciences, Faculty of Health Sciences, University of the Witwatersrand Johannesburg, Parktown 2193, South Africa

Received 28 February 2014; revised 28 May 2014; accepted 29 May 2014

Published online 1 July 2014 in Wiley Online Library (wileyonlinelibrary.com). DOI 10.1002/jps.24068

ABSTRACT: Wound healing is a complex and dynamic process that involves the mediation of many initiators effective during the healing process such as cytokines, macrophages and fibroblasts. In addition, the defence mechanism of the body undergoes a step-by-step but continuous process known as the wound healing cascade to ensure optimal healing. Thus, when designing a wound healing system or dressing, it is pivotal that key factors such as optimal gaseous exchange, a moist wound environment, prevention of microbial activity and absorption of exudates are considered. A variety of wound dressings are available, however, not all meet the specific requirements of an ideal wound healing system to consider every aspect within the wound healing cascade. Recent research has focussed on the development of smart polymeric materials. Combining biopolymers that are crucial for wound healing may provide opportunities to synthesise matrices that are inductive to cells and that stimulate and trigger target cell responses crucial to the wound healing process. This review therefore outlines the processes involved in skin regeneration, optimal management and care required for wound treatment. It also assimilates, explores and discusses wound healing drug-delivery systems and nanotechnologies utilised for enhanced wound healing applications. © 2014 Wiley Periodicals, Inc. and the American Pharmacists Association J. Pharm. Sci. 103:2211–2230, 2014

Keywords: wound healing; skin; wound dressings; bioactive agents; nanotechnology; extracellular matrix (ECM); polymeric biomaterials; tissue engineering; hydrogels

INTRODUCTION

The formation of creative ideas for the use and modification of delivery systems which will influence complex wound healing behaviours, such as proliferation, migration and differentiation of cells will promote novel opportunities for tissue regeneration and repair in the wound healing process. Many agents are pivotal and multifunctional, that is they are potent within the different stages of wound healing to ensure repair and regeneration.[1] Synthetic polymer delivery systems that can control and sustain release are particularly promising as materials for enhancing tissue regeneration.[2] This review discusses the processes involved in skin regeneration and the state of the art in nanotechnology and polymer drug-delivery systems and their potential application for wound healing. The interdisciplinary field of nanobiotechnology, which combines biology, chemistry, engineering and medicine is revolutionising the development of drug-delivery systems and devices. Research in the area of drug delivery, tissue engineering and wound healing has provided unlimited potential to improve human health.[3] Within the field of tissue engineering, drug delivery and wound healing, new dimensions can be envisioned with regards to enhancing the therapeutic effect and at the same time reducing risks and adverse effects. Developments in the field of nanotechnology involving nanomedicine, nanopharmacy, production of nanofibres, nanotubes and nanorods may promote novel opportunities for delivering wound dressings with efficient drug delivery.[4,5] Nanoscale delivery vehicles can enhance the therapeutic efficacy and enable new classes of therapeutics by encouraging the promotion of biologically active new molecular entities that were previously considered underdeveloped.[1]

Correspondence to: Viness Pillay (Telephone: +27-11-717-2274; Fax: +27-11-643-4435, +27-86-553-4733; E-mail: viness.pillay@wits.ac.za)

Journal of Pharmaceutical Sciences, Vol. 103, 2211–2230 (2014)
© 2014 Wiley Periodicals, Inc. and the American Pharmacists Association

PHYSIOLOGY AND MECHANISM OF ACTION OF THE NATIVE SKIN

The skin is the largest organ of the body which comprises about 8% of the human body mass and covers the entire external body surface. The surface area varies from person to person because of the variation in weight and height; skin thickness may also range from 1.5 to 4.0 mm.[6,7] The skin plays a crucial role in many functions such as sensory detection and fluid homeostasis.[8] It serves as an effective barrier against microbial invasion, and enables formation of a self-repairing and self-renewing interface between the body and its environment. It is capable of protecting the body against thermal, chemical, mechanical and osmotic damage, and has properties which allow for adsorption, selective permeability to chemicals and excretion.[7]

The main skin components of interest for wound healing comprises of the epidermis, dermis and sub-dermal layers (Fig. 1). The epidermis has a thin and highly cellular structure that forms the superficial layer of the skin. It is the outermost barrier having high impermeability, thus controlling water loss and serving as a barrier against external harmful stimuli. Underlying and separated from the epidermis by a basement membrane is the dermis. The dermis composes of collagen-rich extracellular matrix (ECM), elastin, fibroblast and glycosaminoglycans.[8] It provides flexibility and physical strength to the skin and supports the extensive vasculature, nerve bundles and lymphatic system. Throughout the dermis is a network of nerve fibres that serve a sensory role in the

AAPS PharmSciTech, Vol. 15, No. 6, December 2014 (© 2014)
DOI: 10.1208/s12249-014-0170-3

Research Article

Synthesis of a Semi-Interpenetrating Polymer Network as a Bioactive Curcumin Film

Naeema Mayet,[1] Pradeep Kumar,[1] Yahya E. Choonara,[1] Lomas K. Tomar,[1] Charu Tyagi,[1] Lisa C. du Toit,[1] and Viness Pillay[1,2]

Received 17 February 2014; accepted 9 June 2014; published online 2 July 2014

Abstract. This study focused on the synthesis and characterization of a natural polymeric system employing the interpenetrating polymer network (IPN) comprising curcumin as a bioactive. Biopolymers and actives such as chitosan, hypromellose, citric acid, genipin, and curcumin were used to develop an effective, biodegradable, and biocompatible film employed therapeutically as a wound healing platform. The semi-IPN films were investigated for their physicochemical, physicomechanical, and biological properties by quantification by FTIR, DSC, and Young's modulus. Following characterization, an optimum candidate formulation was produced whereby further *in vitro* and *ex vivo* studies were performed. Results revealed a burst release occurring at the first hour with 1.1 mg bioactive released when in contact with the dissolution medium and 2.23 mg due to bioactive permeation through the skin, thus suggesting that the lipophilic nature of skin greatly impacted the bioactive release rate. Furthermore, chemical and mechanical characterization and tensile strength analysis revealed that the degree of crosslinking and concentration of polymeric material used significantly influenced the properties of the film.

KEY WORDS: biomaterials; crosslinker; curcumin; films; semi-interpenetrating polymer network; wound healing.

INTRODUCTION

Wound healing is a complex process and can be described as a function of the human body to replace injured and dead tissue with living cells. When the integrity of the skin structure and function is compromised, an intricate and dynamic process occurs known as the wound healing cascade which allows numerous matrix and cellular components to act together ensuring resurrection of the normal skin tissue (1). The primary target of wound care and management is to ensure that both the desirable clinical and pharmaceutical features for optimal treatment are improvised. These features would include wound closure, proliferation, debridement, absorption (2), esthetically acceptable scar, anti-bacterial and anti-inflammatory properties (3), angiogenesis, easy removal, and a moist wound environment (4). Currently, there are numerous wound healing products available for the treatment of burns, lacerations, incisions, chronic, and decubitus ulcers (5,6). However, there is a growing need for novel initiatives in the treatment of burn wounds and excessive skin loss (7). Novel wound dressing applications can be produced by the modification and synthesis of biocompatible materials. Biomaterials play a pivotal role in the wound healing process as they are biodegradable, biocompatible, bioadherent, and bioabsorbable, thus augmenting the healing process. In addition, they contribute inductive, instructive, stimulating, and triggering effects to the skin cells and tissues. Numerous synthetic and natural polymers have been used for wound dressing applications as follows: natural polymers include alginate (8), gelatin (9), collagen (10), and chitosan (11,12) and the synthetic polymers such as poly(ethylene glycol) (13), silicone rubber (14), and poly(amino acid) (15) have also shown to be useful for wound healing applications.

Chitosan (CS) is a natural polymer and a derivative of chitin which has many positive facets in the wound healing process such as biodegradability and excellent biocompatibility properties that are native to the body constituents (11,16). In addition, it is nontoxic and plays an imperative role in the wound healing process due to its versatile biological activity which includes the induction of the healing process within the regenerative and inflammatory phase and its ability to promote tissue growth and differentiation within skin tissue (17). Throughout the tropical regions such as South East Asia, Africa, India, and china, the cultivation of *Curcuma longa* has been widely established. *C. longa* also known as turmeric belongs to the *Zingiberace* family and is a perennial herb known to humankind for over 6,000 years (18). Within the biological and medical field, of particular interest are the phytochemical constituents such as curcuminoids and curcumin for their wide spectrum of biological activities. "Tumeric" or curcumin is a yellow rhizome which is extensively used in the food industry as a coloring and flavoring

[1] Wits Advanced Drug Delivery Platform Research Unit, Department of Pharmacy and Pharmacology, School of Therapeutic Sciences, Faculty of Health Sciences, University of the Witwatersrand, 7 York Road, Parktown, Johannesburg, 2193, South Africa.
[2] To whom correspondence should be addressed. (e-mail: Viness.Pillay@wits.ac.za)

Crosslinked Electrospun Chitosan Nanofibre Mats as a Potential Application for Wound Healing:Exposition of the Physicomechanical and Physicochemical Nature of Electrospun Mats

Naeema Mayet, Pradeep Kumar, Lisa C. du Toit, Yahya E. Choonara and Viness Pillay

Abstract

This paper explores the electrospinning of chitosan nanofibres and the effect of crosslinking by genipin. Various concentrations of chitosan and Hypromellose containing the bioactive curcumin were crosslinked with varying concentrations of genipin and thereafter electrospun using deionised water as a solvent. Chitosan nanofibres demonstrated prolonged release of bioactive when crosslinked to a higher degree. Furthermore tensile attributes, molecular vibrational transitions and surface morphology were characterised and analysed to verify the effects of crosslinking. Results at 12h indicated that release rates were significantly lower when crosslinked to a higher degree at concentrations of 0.208mg/ml and 0.085mg/ml when 0.01%w/v and 0.025%w/v of genipin is used. Textural profiles revealed an increase in the Ultimate Strength and Young's Modulus when the degree of crosslinking was enhanced, due to crosslink formations occurring between nanofibres and can clearly be seen in the structural morphology revealed through scanning electron microscopic evaluation. Differential Scanning Calorimetry and Fourier Transform Infrared Analysis were elucidated to further support the conceptualisation and mode of crosslinking.

KEYWORDS: Biomaterials, Nanofibre, Pseudoskin, Bioactive Release, Extracellular Matrix

11.1.4. Research Paper 3

Advanced and Accelerated in Vivo Full Thickness Wound Healing by the Development of Crosslinked Nanofibrous Wound Healing Mats

Naeema Mayet, Pradeep Kumar, Lisa C, du Toit, Yahya E. Choonara and Viness Pillay

Nanofibres have become an advanced and intelligent form of drug delivery and tissue engineering. The present study focused on fabricating an optimal nanofibrous wound healing delivery system that is bioactive, non-toxic and mimicks the architecture of the native extracellular matrix (ECM) outlining 'pseudoskin'. Biopolymers such as chitosan and hypromellose loaded with curcumin were used synergistically providing healing properties in terms of angiogenesis and proliferation, antioxidant and antimicrobial effects. Crosslinking with genipin enhanced the physicomechanical, physicochemical and biological properties. We established that the nanofibrous mat revealed exceptional wound healing closure, epithelisation as well as type III collagen deposition in contrast to the other systems investigated. Application of the systems were applied to a burn wound model whereby wound progression was evaluated on days 5, 10, 15 and 20 after wound induction. Results obtained revealed a significantly elevated rate in the nanofibrous treated group whereby the closure rate on day 20 disclosed a rate of 99.94% in contrast to 84.18% and 94.88%. The absence of ulceration and inflammation with severe collagen and granulation deposition is noted. Crosslinking lead to the formation of a uniform and denser structure with improved mechanical properties, stability and bioactive release whereby a permeated release rate of 2.1016% was noted in contrast to normal release rate of 0.9457% of bioactive at 2 hours. The accelerated healing of the crosslinked nanofibrous mat can be directly attributed to its impersonation of the native skin structure, employment of bioactive polymers, biodegradability and biocompatibility. Thus the study conducted revealed that the nanofibrous mat serves as an optimal candidate for advanced wound care and management.

Keywords: nanofibres, crosslinking, bioactive, optimised, epithelisation, granulation

Boehringer Ingelheim Young Scientist Competition, 35TH Conference of the Acedemy of Pharmaceutical Sciences Publication

Naeema Mayet, Pradeep Kumar, Yayha E. Choonara, Lisa C. du Toit, and Viness Pillay

Synthesis of a Semi-Interpenetrating Polymer Network as a Bioactive Curcumin Film for Wound Healing

Purpose: Wound healing and management has been proven to be challenging due to the fact that various extrinsic and intrinsic factors govern significant roles during the healing process. complex sequential cascade of events. Wounds occur on a daily basis and can result in a declined quality of life depending on the severity. The purpose of this study was to focus on the synthesis and characterisation of a natural polymeric system employing techniques such as the interpenetrating polymer network, cast and electrospinning.

Methods: Using a statistically derived Box-Behnken Design Template, the paramount concentration of biopolymers was generated to produce 14 various formulations to fabricate wound healing films and nanofibrous mats. These were then investigated in terms of their physicochemical, physicomechanical and biological properties by quantification by FTIR, DSC, Young's Modulus, *In Vivo* and *In Vitro* characterisation.

Results: Chemical analysis by FTIR revealed greater shifts in wavelengths from 3260.11cm^{-1} to 3278.79cm^{-1} when enhancements in crosslinking bridges is endorsed. Degradation of all systems occur between a temperature spectrum of 230 and 300°C upon thermodynamic evaluation revealing the presence of both crystalline and semi-crystalline behaviour. Structural morphological analysis illustrate relatively smooth, non porous and homogonous surface texture and nanofibres of varying diameters dependent upon the polymeric solution viscosity. Upon nanotensile mapping, variation in Young's Modulus was observed at 4.25MPa providing flexibility whereas a higher Young's Modulus provides rigidity and stiffness. Further studies undertaken in terms of *in vivo* and *in vitro* reveal successful release of the bioactive compound curcumin, whereby an initial burst release was observed occurring within the first hour at 1.1mg *in vivo* and 2.23mg *in vitro*. Interestingly these results relate that the bioactive release rate from the system is greatly affected by the Lipophillic nature of the skin. Thus when exposed to the skin a superior release rate is seen improving the system performance.

Conclusion: The novel semi-IPN film and nanofibres formulated, crosslinked and incorporated with a bioactive (curcumin) was developed in view to create an advanced, innovative novel delivery system with the potential of wound healing that stimulates proliferation, differentiation and remodelling at the targeted sites.

Naeema Mayet, Viness Pillay, Yahya Choonara, Pradeep Kumar, Lisa C. du Toit

An Inflammatory Bioresponsive Transdermal Delivery System as an Application for Wound Healing

Novel prototype development and characteristic analysis of a complete prototyped device for wound healing incorporating a nanofibrous mat as well as a bioresponsive component to inflammation known as the 'bioresponsive transdermal delivery system' (BTDS). The method utilised various natural biopolymers specific to the significant component of the device thereby employing a statistically derived Box-Behnken Design Template in order to implement optimisation of the predetermined pharmaceutical and therapeutic parameters to establish the optimal formula for fabrication. In vitro evaluation by determination of the bioresponsive nature was carried out in a stimulated inflammatory environment by utilisation of the Fentons reagent: $Fe^{2+} + H_2O_2 \rightarrow Fe^{3+} + OH\cdot + OH^-$ whereby bioactive release rates were noted to be dependent upon the breakdown of the matrix by hydroxyl radicals. MDT for the bioactive release of curcumin depicted a value at 42.39 at a higher hyaluronic concentration and degree of crosslinkage whereas at lower concentrations MDT values at 33.21 and 35.76 was depicted. Further evaluation in terms of chemical and mechanical characteristics indicates that the formulatory design meets the requirements for adequate wound healing. *In vivo* histological examination on the Sprague Dawley rat model revealed the healing progression whereby the presence of the nanofibrous mat elucidated a close to complete reepithelisation and remodelling of the wound site represented by thick, vascular granulation tissue dominated by fibroblasts and extensive collagen deposition. Therefore prototype device fabrication is exhibited in view to create an advanced, innovative novel delivery system with the potential of wound healing.

Keywords: Wound healing, Bioactives, Stimuli Responsive

Conference of the Academy of Pharmaceutical Sciences, APSSA/SAAPI conference, "Today's Solutions for Tomorrow's Needs".

Naeema Mayet, Lisa C du Toit, Pradeep Kumar, Yahya E Choonara, Viness Pillay

Synthesis of a Bioactive Nanofibrous Mat as an Application for Wound Healing

Purpose: Nanofibres have become an advanced and intelligent form of drug delivery and tissue engineering. The present study focused on fabricating an optimal nanofibrous wound healing delivery device that is bioactive, non-toxic and mimicks the architecture of the native extracellular matrix (ECM) outlining 'pseudoskin'.

Methods: Biopolymers such as chitosan and hypromellose loaded with curcumin were used synergistically providing healing properties in terms of angiogenesis and proliferation, antioxidant and antimicrobial effects. Crosslinking with genipin enhanced the physicomechanical, physicochemical and biological properties. Fibres were formulated employing the electrospinning technique and thereafter determination of the various parameters was carried out in terms of the various device characteristics.

Results: We established that the nanofibrous mat revealed exceptional wound healing closure, epithelisation as well as type lll collagen deposition in contrast to the other systems investigated. Application of the systems were applied to a burn wound model whereby wound progression was evaluated on days 5, 10, 15 and 20 after wound induction. Results obtained revealed a significantly elevated rate in the nanofibrous treated group whereby the closure rate on day 20 disclosed a rate of 99.94% in contrast to 84.18% and 94.88%. The absence of ulceration and inflammation with severe collagen and granulation deposition is noted. Crosslinking lead to the formation of a uniform and denser structure with improved mechanical properties, stability and bioactive release whereby a permeated release rate of 2.1016% was noted in contrast to normal release rate of 0.9457% of bioactive at 2 hours.

Conclusions: The accelerated healing of the crosslinked nanofibrous mat can be directly attributed to its impersonation of the native skin structure, employment of bioactive polymers, biodegradability and biocompatibility. Thus the study conducted revealed that the nanofibrous mat serves as an optimal candidate for advanced wound care and management.

Naeema Mayet, Lisa C.du Toit, Pradeep Kumar, Yahya E. Choonara and Viness Pillay

A Bioresponsive Transdermal Delivery System (BTDS) for Wound Healing

Purpose: Development and characteristic analysis of a complete prototyped device for wound healing incorporating a nanofibrous mat as well as a bioresponsive component to inflammation. First novel prototype developed as an inflammation bioresponsive device for superior wound healing incorporating a nanofibrous mat

Methods: The method utilised various natural biopolymers specific to the significant component of the device. Using a statistically derived Box-Behnken Design Template, the paramount concentration of biopolymers was generated to produce 15 various formulations each to fabricate wound healing nanofibrous mats as well as the lyophilised inflammatory dependent matrix. The technique entailed the process of electrospinning for nanofiber formation as well as blending and lyophilisation for the inflammatory responsive component. Prototype component characteristics were then determined in terms of morphological analysis, mechanical, chemical, *in vitro* and *in vivo* analysis.

Results: Elucidation of the various polymeric and crosslinker concentrations greatly influenced the properties and characteristics of the system. An endorsement in intensity and conjugation is noted by the FTIR spectra whereby greater shifts in wavelengths from 3260.11cm^{-1} to 3278.79cm^{-1} is noted when enhancements in crosslinking bridges is undertaken. Structural morphological analysis revealed the synthesis of smooth, cylindrical, uniformly aligned nanofibres without the presence of nanobeads as well as the formation of a lyophilised matrix having a tough backbone structure at higher concentrations. Upon nanotensile mapping, variation in Young's Modulus was observed at 4.25MPa providing flexibility whereas a higher Young's Modulus provides rigidity and stiffness to the structure. Determination of the bioresponsive nature was carried out in a stimulated inflammatory environment by utilisation of the fentons reagent: $Fe^{2+} + H_2O_2 \rightarrow Fe^{3+} + OH\cdot + OH^-$. Results amongst the experimentally derived formulations revealed the reliance of bioactive release on the hyaluronic acid concentration and degradation by hydroxyl radicals present. MDT results obtained depicted a value at 42.39 at a higher hyaluronic concentration and degree of crosslinkage whereas at lower concentrations MDT values at 33.21 and 35.76 was depicted. *In vivo* histological examination revealed the healing progression whereby the presence of the nanofibrous mat illucidated a close to complete reepithelisation and remodelling of the wound site represented by thick, vascular granulation tissue dominated by fibroblasts and extensive collagen deposition.

Conclusions: A validated fabrication of the prototype device providing the necessary therapeutic, physical, chemical and biological requirements in view to create an advanced, innovative novel delivery system with the potential of wound healing that stimulates proliferation, differentiation and remodelling at the targeted sites.

11.4. Animal Ethics Clearance Certificate

STRICTLY CONFIDENTIAL

ANIMAL ETHICS SCREENING COMMITTEE (AESC)

CLEARANCE CERTIFICATE NO. 2013/24/05

APPLICANT: Ms N Mayet

SCHOOL: Therapeutic Sciences
DEPARTMENT: Pharmacy
LOCATION:

PROJECT TITLE: Fabrication of a novel nanofibrous multilayered biofilm as a wound healing platform in Sprague Dawley rats

Number and Species

60 Sprague-Dawley rats

Approval was given for to the use of animals for the project described above at an AESC meeting held on 20130430. This approval remains valid until 20150429.

The use of these animals is subject to AESC guidelines for the use and care of animals, is limited to the procedures described in the application form and is subject to any additional conditions listed below:

1. A score sheet on the animals must be kept

Signed: _____ (Chairperson, AESC) Date: 6/5/13

I am satisfied that the persons listed in this application are competent to perform the procedures therein, in terms of Section 23 (1) (c) of the Veterinary and Para-Veterinary Professions Act (19 of 1982)

Signed: _____ (Registered Veterinarian) Date: 6/5/13

cc: Supervisor: Professor V Pillay
Director: CAS

Works 2000/lain0015/AESCCert.wps